Optimal Material Design based on Variational Sensitivity Analysis

Dissertation

Wojciech Kijanski

Optimal Material Design based on Variational Sensitivity Analysis

von der Fakultät Architektur und Bauingenieurwesen
der Technischen Universität Dortmund
zur Verleihung des akademischen Grades
Doktor-Ingenieur (Dr.-Ing.)
genehmigte Dissertation

von
Dipl.-Ing. Wojciech Kijanski

Dortmund, Dezember 2018

Kontakt

Dipl.-Ing. Wojciech Kijanski
Lehrstuhl Baumechanik
Fakultät Architektur und Bauingenieurwesen
Technische Universität Dortmund
August-Schmidt-Str. 8, D-44227 Dortmund
Email: wojciech.kijanski@tu-dortmund.de
URL: *http://www.bauwesen.tu-dortmund.de/bm*

Prüfungskommission

Erster Referent (first referee):	Prof. Dr.-Ing. habil. Franz-Joseph Barthold
Zweiter Referent (second referee):	Prof. Dr.-Ing. habil. Jörg Schröder
Vorsitz (committee chair):	Jun.-Prof. Dr. nat. techn. Panagiotis Spyridis

Tag der Einreichung (thesis submission):	31.08.2018
Tag der mündlichen Prüfung (thesis defense):	18.12.2018

Vorwort

„Wer immer tut, was er schon kann,
bleibt immer das, was er schon ist.“

Henry Ford

Die vorliegende Arbeit entstand während meiner Tätigkeit am Lehrstuhl Baumechanik (ehemals Numerische Methoden und Informationsverarbeitung) der Fakultät Architektur und Bauingenieurwesen der Technischen Universität Dortmund. Für die finanzielle Unterstützung im Rahmen des geförderten Forschungsprojektes BA 1828/6-1 möchte ich der Deutschen Forschungsgemeinschaft (DFG) danken.

In erster Linie gilt mein persönlicher Dank meinem geschätzten Doktorvater Professor Franz-Joseph Barthold für die Möglichkeit zur Promotion unter seiner Leitung. Danke für die inspirierenden Diskussionen, für die Förderung und die Freiheiten in jeglicher Hinsicht und das damit verbundene entgegengebrachte Vertrauen. Ein großer Dank gilt auch Professor Jörg Schröder für die Übernahme des Korreferates. Weiterhin möchte ich meinen ehemaligen und derzeitigen Kollegen am Lehrstuhl Baumechanik für den regen Austausch sowie die entspannte und unkomplizierte Arbeitsatmosphäre danken.

Meinen Eltern Bozena und Paul, meinem Bruder Thomas sowie meiner gesamten Familie gilt ein großer Dank für ihren Rat und ihre Unterstützung in jeglicher Lebenslage. Danke an Arun für sein offenes Ohr und das immer entgegengebrachte Verständnis.
Abschließend möchte ich mich bei meiner Frau Nadine für ihren Rückhalt, ihre Geduld, ihr bedingungsloses Verständnis und die damit eingeräumten Freiheiten bedanken. Danke.

Dortmund, Dezember 2018 Wojciech Kijanski

Kurzfassung

Der heutige Industriestandard erfordert den Einsatz effizienter und performanter Werkstoffe, die im Sinne der Gesamt- und Produktionskosten, der Materialersparnis, des Kraftstoffverbrauchs oder des mechanischen Verhaltens optimal ausgelegt sind. In vielen Fällen leistet die richtige Materialwahl für die betrachteten Bauteile einen erheblichen Beitrag zur Gesamtleistung. Moderne Materialien sind nicht als homogen anzusehen, sondern setzen sich aus diversen Bestandteilen zusammen. Oft reicht daher die Betrachtung auf Strukturebene nicht mehr aus und Untersuchungen auf einer niederen Längenskala, der sogenannten Material- oder Mikroskala, werden erforderlich.

Der verantwortliche Entwicklungsingenieur hat basierend auf Versuchsergebnissen, Erfahrungen aus seiner Praxis sowie den verfügbaren Methoden für die computergestützte Simulation und Analyse zu entscheiden, welche Materialien und Materialbestandteile für eine zielorientierte Komposition in Frage kommen. Die Beurteilung der getroffenen Wahl kann basierend auf so genannten Mehrskalen-Methoden für die Strukturanalyse erfolgen. Hierzu gehört auch die FE^2 Methode, welche durch eine numerische Homogenisierung der mikroskopischen Materialstruktur eine kombinierte Analyse des makroskopischen Strukturverhaltens und des mikroskopischen Materialverhaltens ermöglicht.

Für den beschriebenen Anspruch der Strukturanalyse wird im Rahmen der vorliegenden Arbeit eine Weiterentwicklung realisiert, die neben der numerischen mehrskaligen Simulation des physikalischen Bauteilverhaltens eine Verbesserung definierter Eigenschaften ermöglicht. Diese Erweiterung führt zum Forschungsbereich der Strukturoptimierung, der sich neben der Dimensionierung von Bauteilkomponenten mit der optimalen Auslegung der Bauteile im Sinne der topologischen Zusammensetzung sowie der Formfindung befasst. Die klassische Aufgabe der Strukturoptimierung setzt sich zusammen aus der Definition von Zielen, Restriktionen und Designvariablen sowie der Wahl von mathematischen Optimierungsalgorithmen. Es wird eine Methode entwickelt, die eine Erweiterung der einskaligen Optimierungsaufgabe darstellt und eine Wahl von Zielfunktionen, Nebenbedingungen und Designparametern wie Material, Anzahl und Position von Löchern und Einschlüssen sowie Geometrieparametern auf mehreren Skalen ermöglicht. Da der numerische Aufwand bereits für die Methoden der Strukturanalyse erheblich werden kann, empfiehlt es sich effiziente Methoden im Rahmen der Strukturoptimierung zu verwenden. Zu dieser Klasse der Methoden zählen die sogenannten gradientenbasierten Optimierungsverfahren. Im Rahmen der vorliegenden Arbeit werden die erforderlichen Gradienten- bzw. Sensitivitätsinformationen basierend auf dem variationellen Ansatz hergeleitet und bereitgestellt. Anhand geeigneter Beispiele und numerischer Untersuchungen wird gezeigt, dass dieser Ansatz von Natur aus als *performant* klassifiziert werden kann.

Schlagwörter: Materialentwurf, FEM, Mehrskalen-Methoden (FE^2) und Homogenisierung, Variationelle Sensitivitätsanalyse, Struktur- und Formoptimierung.

Abstract

Today's state of the art within industrial applications requires the usage of efficient and high-performance materials, which are optimally designed in terms of production costs, material savings, fuel consumption or their mechanical behaviour. In many cases, a useful choice of materials of components contributes to the overall performance significantly. Modern materials can not be classified as homogeneous, but are composed of various ingredients. Often, considerations at the structural level are no longer sufficient and investigations on a lower length scale, the so-called material- or microscale, become necessary.

Based on experimental data and results, practical experience and available methods for computer-aided simulation and analysis, the responsible design engineer has to decide which ingredients are suitable for a goal-oriented composition of materials. The evaluation of the choice made can be performed based on so-called multiscale methods for structural analysis. These also include the FE^2 method, which allows a combined analysis of the macroscopic structural behaviour and the microscopic material behaviour by a numerical homogenisation scheme applied to the microscopic material structure.

The work at hand provides an enhancement of methods for the numerical multiscale simulation of the physical behaviour and enables improvements of characteristic properties. This extension leads to the research field of structural optimisation. Apart from sizing, it deals with the optimal design of components in the sense of optimal topological distribution of material as well as shape optimisation. The classical sequence of steps within a structural optimisation process contains the definition of goals, restrictions and design variables as well as the choice of algorithms for mathematical optimisation. The proposed method extends the formulation of a single-scale optimisation task and allows choices of objective functions, constraints and design parameters on multiple scales. Design parameters are for instance characteristic material properties, number and location of holes and inclusions, and geometrical parameters in general. Since the numerical effort within methods for multiscale structural analysis raises with the complexity of referred problems, it is useful to apply efficient methods in the context of structural optimisation. This class of methods includes the so-called gradient based optimisation methods. Within the present work, the required gradient and sensitivity information are derived and provided based on the variational approach for sensitivity analysis. By means of suitable examples and numerical investigations, it is shown that this approach can be classified as *performant* by nature.

Keywords: material design, FEM, multiscale methods (FE^2) and homogenisation, variational sensitivity analysis, structural optimisation, shape optimisation.

Contents

Nomenclature v

1 Introduction 1
- 1.1 Motivation . . . 1
- 1.2 Scope and goals . . . 4
- 1.3 Outline . . . 5

2 Preliminaries and notations 7
- 2.1 Notation . . . 7
- 2.2 Variations and derivatives . . . 9
- 2.3 Software environment . . . 11

3 Optimisation setup and choice of design parameters 15
- 3.1 General formulation of the optimisation problem . . . 15
- 3.2 Objective functions, constraints and design parameters . . . 19
- 3.3 Verification of derivatives and sensitivity information . . . 20
- 3.4 Choice of design parameters for optimisation . . . 21
  - 3.4.1 Design parametrisation based on CAGD models . . . 22
  - 3.4.2 Design parametrisation based on morphing . . . 23
- 3.5 Summary and concluding remarks . . . 24

4 Structural analysis on multiple scales 25
- 4.1 Introduction . . . 25
- 4.2 Mechanical two-scale problems . . . 27
- 4.3 Homogenisation methods and FE^2 techniques . . . 29
  - 4.3.1 Representative volume element (RVE) . . . 29
  - 4.3.2 Effective field variables . . . 29
  - 4.3.3 Boundary conditions for homogenisation methods . . . 30
  - 4.3.4 General setup and solution of homogenisation problems . . . 31
- 4.4 Computational homogenisation . . . 32
  - 4.4.1 Discrete relations for homogenisation . . . 33
  - 4.4.2 General form of discrete boundary conditions . . . 36
  - 4.4.3 Solution of the discrete minimisation problem of homogenisation 36
  - 4.4.4 Numerical implementation . . . 37
- 4.5 Summary and concluding remarks . . . 40

5 Variations of physical quantities on single scales 41
5.1 Introduction . . . 41
5.2 Kinematics and variations of kinematical quantities . . . 43
5.3 Basic sensitivity relations . . . 46
5.3.1 Weak form of equilibrium and its variation . . . 48
5.3.2 Sensitivity of the physical state . . . 48
5.3.3 Variations of arbitrary functionals . . . 49
5.3.4 Variations of stresses . . . 49
5.4 Discrete sensitivity relations . . . 51
5.4.1 Discrete weak form of equilibrium and its variation . . . 51
5.4.2 Discrete sensitivity of the physical state . . . 51
5.4.3 Discrete form of the variation of arbitrary functionals . . . 52
5.4.4 Discrete form of the variation of stresses . . . 52
5.5 Partitioning of discrete sensitivity relations . . . 52
5.6 Finite element approximation and explicit formulations . . . 55
5.7 Sensitivity relations for selected objectives and constraints . . . 60
5.7.1 Volume . . . 61
5.7.2 Energy and compliance . . . 61
5.7.3 Physical reaction forces . . . 63
5.8 Numerical investigations on single scales . . . 67
5.8.1 Structural optimisation of a cube-like structure of multi-material 67
Studies for different scaling factors of material properties . . . 69
Compliance minimisation and reduction of forces . . . 70
Volume minimisation and reduction of forces . . . 73
Remarks on numerical performance and accuracy . . . 74
5.8.2 Structural optimisation of RVE-like domains . . . 76
Square domain with a circular hole . . . 78
Square domain with a circular inclusion . . . 81
Square domain with rectangular stripe . . . 84
Conclusion . . . 85
5.9 Summary and concluding remarks . . . 86

6 Material design based on variational sensitivity information 89
6.1 Introduction . . . 89
6.2 Sensitivity relations for problems on multiple scales . . . 93
6.2.1 Macroscopic weak form of equilibrium and its variation . . . 94
6.2.2 Sensitivity of the macroscopic physical state . . . 95
6.2.3 Variations of arbitrary macroscopic functionals . . . 96
6.3 Discrete sensitivity relations for multiscale problems . . . 96
6.3.1 Discrete sensitivity of the macroscopic physical state . . . 97
6.3.2 Discrete form of the variation of arbitrary functionals . . . 98
6.4 Explicit formulations for multiscale sensitivity analysis . . . 100
6.4.1 Sensitivity analysis on the microscale . . . 100
Sensitivity of the microscopic physical state for periodic materials 102
6.4.2 Sensitivity analysis on the macroscale . . . 104
6.4.3 Sensitivity analysis of effective parameters . . . 109

6.5 Optimisation setup for problems on multiple scales 112
6.5.1 General formulation of the optimisation problem 112
6.5.2 Discrete form of the optimisation problem 112
6.5.3 Numerical environment for optimisation on multiple scales . . . 113
6.5.4 Design parameters and possible combinations 114
6.6 Summary and concluding remarks 117

7 Numerical investigations 119
7.1 Macroscopic tension test 120
7.2 Multiscale application for the design of microstructures 126
7.2.1 Evaluation of load case L.1: uniaxial tension 129
7.2.2 Evaluation of load case L.2: biaxial tension 134
7.3 Multiscale optimisation of a bracket 139
7.4 Observations concerning numerical behaviour 145
7.5 Summary and concluding remarks 147

8 Summary and outlook 149
8.1 Summary 149
8.2 Future work 151

List of Figures 156

List of Algorithms 156

List of Tables 157

List of Problems 158

List of Remarks 158

Bibliography 159

Nomenclature and list of symbols

All mathematical operators and short forms are explained in corresponding paragraphs. Nevertheless, a list of frequently and repetitively used symbols and abbreviations is given below and allows a quick lookup. In the scope of multiscale formulations and computational homogenisation, the term macroscopic is connected with the upper length scale and corresponding quantities are indicated by overlines. The term microscale is associated with the lower length scale and the characteristic dimensions of representative volume elements. The corresponding quantities are represented without any markers.

Abbreviations

BC	boundary conditions
BESO	bidirectional evolutionary structural optimisation
BFGS	Broyden-Fletcher-Goldfarb-Shanno update formula
BVP	boundary value problem
CAE	computer aided engineering
CAGD	computer aided geometric design
CMD	computational material design
CMMS	computational mechanics of materials and structures
CON	constraints
CUDA	compute unified device architecture
DP	design parameters or design variables
DSA	design sensitivity analysis
FDM	finite difference method
FE	finite element
FEA	finite element analysis
FEAP	finite element analysis program
FEM	finite element method
FE^2	multiscale finite element method (FE squared)
GPU	graphics processing unit
HPC	high performance computing
INA-OPT	inelastic analysis and optimisation
IVP	initial value problem

MAnO	multiscale analysis and optimisation
MOO	multiobjective optimisation
MPI	message passing interface
MSA	part of MAnO for structural analysis purposes
MSE	material science and engineering
MSO	part of MAnO for structural optimisation purposes
NLP	non-linear programming
NTFA	non-uniform transformation field analysis
OF	objective function
OpenMP	open multi-processing
POD	proper orthogonal decomposition
pRBMOR	potential-based reduced basis model order reduction
RVE	representative volume element
SA	structural analysis
SCON	side constraints
SMO	structural and multidisciplinary optimisation
SO	structural optimisation
SQP	sequential quadratic programming
SSRVE	statistically similar representative volume element
SVD	singular value decomposition
XFEM	extended finite element method
YFEM	modified extended finite element method

Notation, mathematical operators and subscripts

f	general placeholder for an arbitrary functional
$(\cdot)$	general placeholder for an arbitrary quantity
$\overline{(\cdot)}$	macroscopic or effective quantity in terms of FE^2
$\underline{(\cdot)}$	quantity in Voigt notation
$\delta(\cdot)$, $(\cdot)'$	total variation of a quantity $(\cdot)$
$\delta_*(\cdot)$, $(\cdot)'_*$	partial variation of a quantity $(\cdot)$ with respect to $*$
$\delta_{**}(\cdot)$, $(\cdot)''_*$	second partial variation of a quantity $(\cdot)$ with respect to $*$
$\delta_{\mathsf{mic}}(\cdot)$, $(\cdot)'_{\mathsf{mic}}$	variation of a quantity $(\cdot)$ with respect to microscopic state and design parameters
$(\cdot)_{\mathrm{D}}, (\cdot)_{\mathrm{N}}$	Dirichlet and Neumann domain
$(\cdot)_{\mathrm{a}}$	free domain for state
$(\cdot)_{\mathrm{b}}$	boundary domain for state
$(\cdot)_{\mathrm{A}}$	free domain for design
$(\cdot)_{\mathrm{B}}$	boundary domain for design
$(\cdot)_{\mathrm{i}}$	inner domain in terms of FE^2
$(\cdot)_{\mathrm{I}}$	general identifier for boundary conditions on microscale
$(\cdot)_{\mathrm{D}}$	identifier for linear displacement boundary conditions
$(\cdot)_{\mathrm{P}}$	identifier for periodic displacement boundary conditions
$(\cdot)_{\mathrm{S}}$	identifier for uniform traction boundary conditions

$(\cdot)^{\mathrm{ini}}, (\cdot)^{\mathrm{opt}}$	identifiers for initial and optimised state of a quantity
$(\cdot)^{\mathrm{l}}, (\cdot)^{\mathrm{u}}$	identifiers for lower and upper bounds of a quantity

Domains and boundaries

$\overline{\mathcal{K}},\ \mathcal{K}$	macro- and microscopic referential domain (Lagrange)
$\overline{\mathcal{M}},\ \mathcal{M}$	macro- and microscopic current domain (Euler)
$\overline{\mathcal{R}},\ \mathcal{R}$	macro- and microscopic local domain
$\partial\overline{\mathcal{K}}, \partial\mathcal{K}$	boundary of macro- and microscopic referential domain
$\partial\overline{\mathcal{M}}, \partial\mathcal{M}$	boundary of macro- and microscopic current domain
$\partial\overline{\mathcal{R}}, \partial\mathcal{R}$	boundary of macro- and microscopic local domain
$\partial\mathcal{K}^{+}, \partial\mathcal{K}^{-}$	positive and negative parts of referential boundary domain

Continuous quantities for structural and sensitivity analysis

$\overline{\boldsymbol{v}}, \boldsymbol{v}$	macro- and microscopic state
$\delta\overline{\boldsymbol{v}}, \delta\boldsymbol{v}$	macro- and microscopic state variation
$\overline{\boldsymbol{s}}, \boldsymbol{s}$	macro- and microscopic design
$\delta\overline{\boldsymbol{s}}, \delta\boldsymbol{s}$	macro- and microscopic design variation
$\overline{\boldsymbol{\varphi}}, \boldsymbol{\varphi}$	macro- and microscopic deformation mapping
$\overline{\boldsymbol{\kappa}}, \boldsymbol{\kappa}$	macro- and microscopic local geometry mapping
$\overline{\boldsymbol{\mu}}, \boldsymbol{\mu}$	macro- and microscopic local deformation mapping
$\overline{\mathbf{F}}, \mathbf{F}$	macro- and microscopic deformation gradient
$\underline{\overline{\boldsymbol{F}}}$	macroscopic deformation gradient in Voigt notation
$\overline{\mathbf{K}}, \mathbf{K}$	macro- and microscopic local geometry gradient
$\overline{\mathbf{M}}, \mathbf{M}$	macro- and microscopic local deformation gradient
R	microscopic physical residual (also valid for single scales)
$\overline{R}$	macroscopic physical residual
k	microscopic physical stiffness operator (also valid for single scales)
$\overline{k}$	macroscopic physical stiffness operator
$\widetilde{k}$	multilevel physical stiffness operator
p	microscopic pseudo load operator (also valid for single scales)
$\overline{p}$	macroscopic pseudo load operator
$\widetilde{p}$	multilevel pseudo load operator
s	sensitivity of microscopic state (exclusively) (also valid for single scales)
$\overline{s}$	sensitivity of macroscopic state (exclusively)
$\widetilde{s}$	sensitivity of macroscopic state caused by micro-changes (multilevel)
$\widehat{s}$	effective sensitivity of macroscopic state caused by macro- and micro-changes
$\boldsymbol{\lambda}_{\mathrm{I}}$	Lagrange multiplier for microscopic boundary conditions I, i.e. $\boldsymbol{\lambda}_{\mathrm{D}}, \boldsymbol{\lambda}_{\mathrm{P}}, \boldsymbol{\lambda}_{\mathrm{S}}$
$\overline{\mathbf{P}}_{\mathrm{I}}$	effective stress tensor for boundary conditions I, i.e. $\overline{\mathbf{P}}_{\mathrm{D}}, \overline{\mathbf{P}}_{\mathrm{P}}, \overline{\mathbf{P}}_{\mathrm{S}}$
$\overline{\mathbb{A}}_{\mathrm{I}}$	effective material tensor for boundary conditions I, i.e. $\overline{\mathbb{A}}_{\mathrm{D}}, \overline{\mathbb{A}}_{\mathrm{P}}, \overline{\mathbb{A}}_{\mathrm{S}}$
E, ν	Young's modulus and Poisson's ratio

Discrete quantities for structural and sensitivity analysis

$\overline{\boldsymbol{v}}, \boldsymbol{v}$	macro- and microscopic state
$\delta\overline{\boldsymbol{v}}, \delta\boldsymbol{v}$	macro- and microscopic state variation
$\overline{\boldsymbol{s}}, \boldsymbol{s}$	macro- and microscopic design
$\delta\overline{\boldsymbol{s}}, \delta\boldsymbol{s}$	macro- and microscopic design variation
$\boldsymbol{R}$	microscopic physical residual (also valid for single scales)
$\overline{\boldsymbol{R}}$	macroscopic physical residual
$\boldsymbol{K}$	microscopic physical stiffness operator (also valid for single scales)
$\overline{\boldsymbol{K}}$	macroscopic physical stiffness operator
$\widetilde{\boldsymbol{K}}$	multilevel physical stiffness operator
$\boldsymbol{P}$	microscopic pseudo load operator (also valid for single scales)
$\overline{\boldsymbol{P}}$	macroscopic pseudo load operator
$\widetilde{\boldsymbol{P}}$	multilevel pseudo load operator
$\breve{\boldsymbol{P}}$	total multilevel pseudo load operator
$\boldsymbol{S}$	sensitivity of microscopic state (exclusively) (also valid for single scales)
$\overline{\boldsymbol{S}}$	sensitivity of macroscopic state (exclusively)
$\widetilde{\boldsymbol{S}}$	sensitivity of macroscopic state caused by micro-changes (multilevel)
$\widehat{\boldsymbol{S}}$	effective sensitivity of macroscopic state caused by macro- and micro-changes
$\overline{\boldsymbol{P}_{\mathrm{K,I}}}$	effective stress matrix for boundary conditions I, i.e. $\overline{\boldsymbol{P}_{\mathrm{K,D}}}, \overline{\boldsymbol{P}_{\mathrm{K,P}}}, \overline{\boldsymbol{P}_{\mathrm{K,S}}}$
$\underline{\overline{\boldsymbol{P}}}_{\mathrm{K,I}}$	effective stress in Voigt notation for boundary conditions I, i.e. $\underline{\overline{\boldsymbol{P}}}_{\mathrm{K,D}}, \underline{\overline{\boldsymbol{P}}}_{\mathrm{K,P}}, \underline{\overline{\boldsymbol{P}}}_{\mathrm{K,S}}$
$\overline{\boldsymbol{A}}_{\mathrm{I}}$	effective material matrix for boundary conditions I, i.e. $\overline{\boldsymbol{A}}_{\mathrm{D}}, \overline{\boldsymbol{A}}_{\mathrm{P}}, \overline{\boldsymbol{A}}_{\mathrm{S}}$

Structural optimisation

f	arbitrary function as placeholder for an objective or constraint
J	objective function
$h,\ \boldsymbol{h},\ \boldsymbol{h}$	microscopic equality constraint as scalar, vector, matrix (also on single scale)
$g,\ \boldsymbol{g},\ \boldsymbol{g}$	microscopic inequality constraint as scalar, vector, matrix (also on single scale)
$\overline{h},\ \overline{\boldsymbol{h}},\ \overline{\boldsymbol{h}}$	macroscopic equality constraint as scalar, vector, matrix
$\overline{g},\ \overline{\boldsymbol{g}},\ \overline{\boldsymbol{g}}$	macroscopic inequality constraint as scalar, vector, matrix
$\overline{\boldsymbol{s}}^{\mathrm{l}},\ \boldsymbol{s}^{\mathrm{l}}$	macro- and microscopic lower bound for design parameters
$\overline{\boldsymbol{s}}^{\mathrm{u}},\ \boldsymbol{s}^{\mathrm{u}}$	macro- and microscopic upper bound for design parameters
$\Delta\overline{\boldsymbol{s}}, \Delta\boldsymbol{s}$	macro- and microscopic design increment
$\mathcal{L}$	Lagrange functional
$\lambda,\ \boldsymbol{\lambda}$	Lagrange multiplier for equality constraints as scalar and vector
$\mu,\ \boldsymbol{\mu}$	Lagrange multiplier for inequality constraints as scalar and vector
$\widetilde{J}$	quadratic approximation of objective function
$\widetilde{\boldsymbol{h}}$	linear approximation of equality constraints
$\widetilde{\boldsymbol{g}}$	linear approximation of inequality constraints
C	compliance
V	volume

Quantities within numerical investigations

$\overline{n}_v,\ n_v$	overall number of macro- and microscopic degrees of freedom
$\overline{n}_s,\ n_s$	overall number of macro- and microscopic design parameters
$\overline{n}_{el}, n_{el}$	overall number of macro- and microscopic elements
n_{IP}	overall number of integration points
n_{cp}	overall number of control points (CAGD)
n_X	overall number of nodal design parameters (FE mesh)
n_{IT}	number of iterations
n_{F}	number of function evaluations
$n_{\mathrm{F}}^{\mathrm{c}}$	number of function evaluations for central FDM scheme
$n_{\mathrm{F}}^{\mathrm{f,b}}$	number of function evaluations for forward/backward FDM scheme
t	time variable
t_{a}	time for structural analysis
t_{s}	time for sensitivity analysis
$t_{\mathrm{s,num}}$	time for numerical sensitivity analysis
$t_{\mathrm{s,num}}^{\mathrm{c}}$	time for numerical sensitivity analysis: central FDM scheme
$t_{\mathrm{s,num}}^{\mathrm{f,b}}$	time for numerical sensitivity analysis: forward/backward FDM scheme
$t_{\mathrm{s}}{}^{\mathrm{cp}}$	time for sensitivity analysis on geometrical basis
$t_{\mathrm{s}}{}^{\mathrm{X}}$	time for sensitivity analysis on nodal basis
t_{o}	time for optimisation
$t_{\mathrm{o,num}}$	time for numerical optimisation

Chapter 1

Introduction

This chapter aims to introduce and to motivate the work at hand. A brief classification of the combined research fields, i.e. computational homogenisation and structural optimisation with variational design sensitivity analysis, is given. Detailed reviews on the state of the art and published literature are given in corresponding chapters. The scope as well as the goals of the present work are outlined and put into the context of the overall computational material design process.

1.1 Motivation

Nowadays, *performant constructions* are of major interest in for example automotive or aerospace industries. The usage of these efficient components allows the saving of resources in all respects, e.g. in the sense of saving the total production or material costs, the weight savings or the fuel economy. The development of performant structures requires the knowledge about the material properties and its behaviour, also on different length scales. After a successful design process, these real-world mechanical structures are labelled *efficient* or *performant* and belong to the class of high performance constructions.

Reflecting the past decades, many engineers and researchers developed analytical and computational methods for the analysis of complex materials with heterogeneous microstructures. They investigated the topological composition with different microscopic constituents as well as the overall behaviour on different length scales, cf. Fig. 1.1 for few illustrative examples for microstructures. The physical behaviour and performance of modern structures from mechanical, civil or electrical engineering usually are analysed by the widespread and well-known *finite element method* (FEM). This method allows investigation of a broad field of problem formulations, e.g. non-linear hyperelasticity, instability, fluid dynamics, inelastic and non-linear materials in general or micromechanics.

In parallel and adjacent to the development of methods for *the understanding* of given structures, engineers and researchers from the field of structural optimisation concentrated on strategies for *the improvement* of structures. Optimal designs in terms of mechanical behaviour of stated problems can be achieved by incorporating the finite element method, methods for design sensitivity analysis and methods for mathematical optimisation into

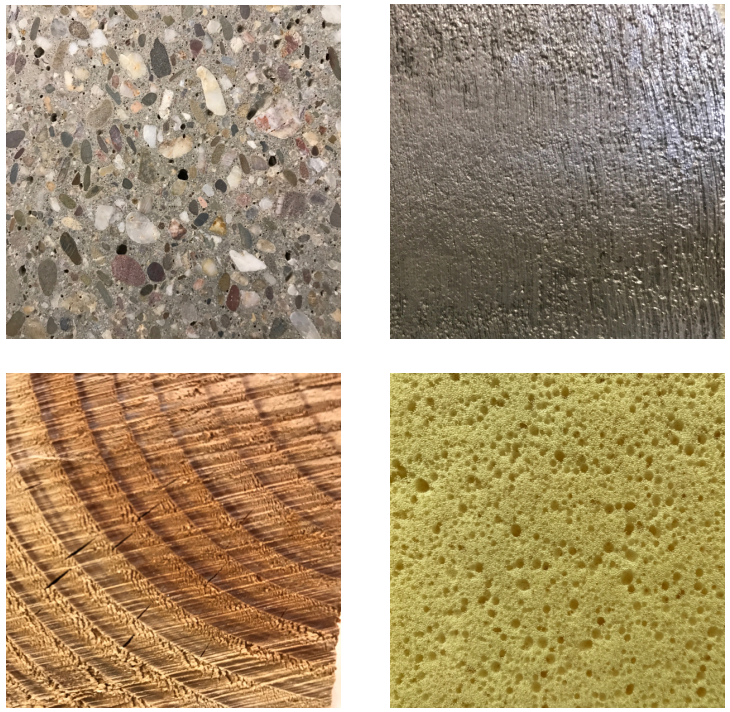

Figure 1.1: Examples for microstructures: concrete with a cement matrix and aggregated grains (top left), steel (top right), wood (bottom left), foam structure (bottom right), *(photographs taken by W. Kijanski, 2018).*

an overall environment for structural optimisation. Besides modifications of the topology of microscopic domains, this field deals with the size and shape of individual constituents and is usable for the generation of mechanical structures with desirable material properties. The research and development in mentioned disciplines is an ongoing process.

The combination of both fields of research and the corresponding methods, i.e. of the finite element method and methods for structural optimisation with the integrated design sensitivity analysis, provides an efficient framework for the development of advanced designs and optimised layouts of mechanical structures and systems for several problem formulations. These problems can be related to the overall performance in terms of weight or stiffness, and as a consequence also to the overall manufacturing or material costs, to name a few. Especially nowadays, when it comes to manufacturing processes involving 3D printing technologies and additive manufacturing, methods for analysis and optimisation gain an eminent importance. Overall and among all disciplines, the focus lies on finding solutions for optimal designs based on systematic strategies using algorithms and methods for mathematical optimisation and *non-linear programming* (NLP) and on avoiding *trial and error methods* in general. In this sense, the design sensitivity analysis plays an integral role because it is responsible for the accuracy and efficiency of incorporated solution strategies. Especially the variational approach, which is fully integrated into the scope of the general layout of continuum mechanics, promises good and efficient solutions.

The major goal is to *"Formulate a method for the determination of optimal design layouts of macroscopic structures and microscopic materials"* and it can be put into the context of *Computational Material Design* (CMD), which is briefly outlined in Fig. 1.2.

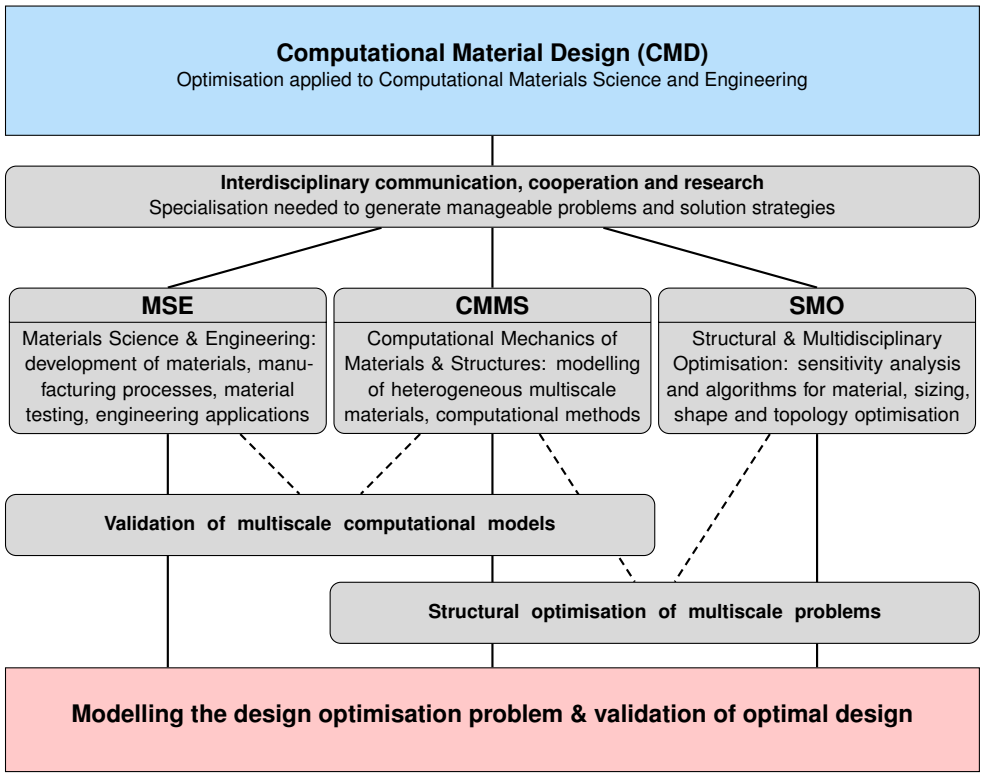

Figure 1.2: Materials Engineering and Computational Material Design (CMD).

This illustration explains how structural optimisation can be applied to research fields in computational materials science and engineering. The success of any interdisciplinary collaboration is characterised by an interdisciplinary communication, cooperation and research. Therefore, results of each individual research field, i.e. the field of *Material Science and Engineering* (MSE), the field of *Computational Mechanics of Materials and Structures* (CMMS) and the field of *Structural and Multidisciplinary Optimisation* (SMO), have to be collected and evaluated for the formulation of the overall design optimisation problem. This task deals with the optimal layout and design of structures and materials from theoretical, practical and numerical points of view. Within the mentioned process, CMMS plays the role of the facilitator. It requires the support of researchers from MSE for the validation of computational models on one hand, and on the other hand this group has to support researchers from SMO to set up feasible and correct optimisation problems with a proper formulation of objectives, constraints and design parameters.

The idea for Computational Material Design is motivated from the practical relevance of real-world applications and the flexibility of manufacturing processes with the characteristic

affinity for the generation of high performance materials. The available manufacturing technologies allow the designing engineers to consider the overall profitability and efficiency of applications and to tailor them to their special requirements. The ability to produce *new materials*, for instance using 3D printers, additionally supports this design process. Modern applications in automotive, aerospace or aircraft industries often make use of cellular materials. In general, this kind of materials is classified as ultra-lightweight and rank among high performance materials due to their high strength-to-weight ratio. Therefore, it is of special interest to figure out the best possible layouts for this kind of constructions using automated software solutions. All mentioned disciplines and research fields have one goal in common; they all intend to promote positive and to reduce or even neglect negative properties of structures and mechanical systems.

1.2 Scope and goals

The major goal of the thesis at hand, which is referred throughout the entire work is to

"Formulate a method for the determination of optimal design layouts of macroscopic structures and microscopic materials!"

The achievement of the articulated goal requires the formulation of multiscale sensitivity relations and the development of a numerical optimisation environment for an automatical design and layout generation of mechanical structures with heterogeneous microscale material representations. The formulation takes characteristic mechanical properties over multiple scales into account and allows the definition of objective functions, constraints and design parameters on different scales. This work promotes established methods for computational homogenisation within the structural analysis part in combination with the variational approach for the derivation of sensitivity information for the integrated design sensitivity analysis, especially in the scope of shape optimisation problems.

Based on hyperelastic material behaviour of constituents on the microscale without any time and history dependent effects, established computational homogenisation techniques are used for the determination of the structural response. These results constitute the basis for the design sensitivity analysis, which is used for predictions about the physical multiscale behaviour of the defined structure. Sensitivity relations for the design sensitivity analysis are derived on the continuous level prior to any discretisation steps. The major focus lies on the derivation of the design sensitivity information of the homogenisation condition, which bridges the macro- and the microscale. In general, homogenised or effective parameters can be formulated in terms of resulting quantities on the boundary of the investigated microscopic domain. Within techniques for numerical homogenisation based on the Lagrange formalism, the Lagrange parameter represents forces (or stresses) on the boundary of the domain, which enforce the formulated boundary conditions on the microscale. In this scope, understanding physical reaction forces and especially the sensitivity of physical reaction forces on the boundary of a single-scale domain with respect to design parameters is essential. This principles and insights can be transferred and adapted for the mentioned homogenisation condition.

Obtained quantities and analytical derivatives, especially for objectives and constraints within the optimisation problem, are verified using methods for the computation of numerical derivatives, i.e. the *finite difference method* (FDM). To demonstrate the flexibility

of the developed optimisation environment based on the introduced sensitivity relations, different geometry parametrisation techniques are introduced and used throughout the illustrative examples and numerical investigations.

1.3 Outline

The outline of the work reflects the described scope and goals mentioned above and is divided into eight chapters. In the following paragraphs the topics of chapters 2 to 8 are briefly emphasised.

Chapter 2 compiles the notation and some basic relations and conventions, which are used throughout this work. Moreover, the notation used for variations and derivatives is introduced and a brief overview of the developed and used software is given.

Chapter 3 details the abstract setting of a general non-linear optimisation problem and its solution based on algorithms for mathematical optimisation. A list for the choice of objective functions and constraints as well as their combinations is given. Some remarks on the verification of obtained sensitivity relations and on the choice of design parameters with corresponding parametrisation techniques accomplish the compilation.

Chapter 4 outlines a brief review of relations used for the numerical homogenisation and FE^2 methods in terms of the Lagrange formalism. Based on remarks for the choice of a representative volume element and the definition of effective field variables, solution strategies for structural problems over multiple scales in terms of computational homogenisation are discussed.

Chapter 5 provides principles for the variational approach for design sensitivity analysis on single scales. A summary of essential quantities, their variations and their discretisation can also be found in this chapter. The partitioning of relevant relations and the necessary steps for obtaining the sensitivity of physical reaction forces are discussed. This information is necessary for the formulation of sensitivity relations for multiscale optimisation problems. Some examples demonstrate the applicability of the sensitivity of physical reaction forces as constraints within applications on single scales.

Chapter 6 tackles the major purpose of this thesis and explains the necessary sequence of steps for the formulation of multiscale optimisation problems and therefore, of the computational material design task. Sensitivity relations in their continuous and discrete form are derived for the numerical homogenisation problem and are used for the formulation and the set up of the overall multiscale optimisation problem. Remarks on the numerical implementation and on possible combinations of objective functions, constraints and design parameters on multiple scales are given.

Chapter 7 demonstrates the applicability of derived formulations using three numerical examples with different design parametrisation techniques for the description of investigated geometrical domains on the macro- and the microscale. Observations concerning the numerical behaviour and performance of derived relations are discussed and compared with methods based on the numerical determination of required sensitivity information.

Chapter 8 closes the work by a summary and highlights the goals and achieved results once more. Moreover, it offers an outlook on future work and activities in the presented field of research.

Chapter 2

Preliminaries and notations

To simplify the understanding of following chapters, the subsequent sections aim to introduce fundamental and frequently used notations, mathematical operations and conventions, products, derivatives and variations. Moreover, some introductory remarks on numerical investigations in terms of implementation and software are given.

2.1 Notation

The convention presented in Table 2.1 is used and allows to distinguish between scalar quantities, vectors, tensors of different order and different types of matrices throughout this work. Relevant deviations and exceptions will be emphasised by corresponding remarks, when needed. For instance, scalars and scalar functions are represented by non-bold symbols in italic shape, e.g. A,b or using the Greek alphabet α, β, γ, respectively. With a given basis $\{\boldsymbol{g}_1, \boldsymbol{g}_2, \ldots, \boldsymbol{g}_n\}$ for a given vector space, vectors are represented by boldface letters in italic shape, e.g. $\boldsymbol{A} = A^i \boldsymbol{g}_i$ or $\boldsymbol{b} = b^i \boldsymbol{g}_i$ with the components A^i and b^i, respectively. Greek vectors $\boldsymbol{\varepsilon} = \varepsilon^i \boldsymbol{g}_i$ with corresponding components ε^i are used in the same manner. Second order tensors, e.g. $\mathbf{A} = A^{ij} \boldsymbol{g}_i \otimes \boldsymbol{g}_j$ or $\mathbf{b} = b^{ij} \boldsymbol{g}_i \otimes \boldsymbol{g}_j$, are written with bold-faced Roman letters with the components A^{ij} and b^{ij}. Greek tensors are represented by bold-faced Roman letters in a similar fashion, i.e. $\boldsymbol{\sigma} = \sigma^{ij} \boldsymbol{g}_i \otimes \boldsymbol{g}_j$ and the components σ^{ij}. Fourth order tensors are represented with a hollowed Roman font, i.e. $\mathbb{A} = A^{ijkl} \boldsymbol{g}_i \otimes \boldsymbol{g}_j \otimes \boldsymbol{g}_k \otimes \boldsymbol{g}_l$. Bold-faced sans-serif letters in italic shape are used for matrices, e.g. $\boldsymbol{\mathsf{A}} = [A_{ij}]$ or for a column matrix $\boldsymbol{\mathsf{b}} = [b_i]$, respectively. This kind of notation corresponds to the notation presented in [99], but similar conventions can also be found in standard literature on tensor algebra, tensor analysis and on continuum mechanics, see for instance [19, 45, 74, 77, 168] to name a few. Bold-face calligraphic letters are used for special and not common operators, i.e. $\mathcal{A}, \mathcal{B}, \mathcal{C}$.

To obtain a practical numerical method, the transformation of the general tensorial notation into a matrix notation is necessary. Due to efficiency aspects, the principles of the *Voigt notation* are often applied to several quantities given in matrix form and reduce their order. In the general case, an arbitrary matrix $\boldsymbol{\mathsf{A}}$ and a symmetric matrix $\boldsymbol{\mathsf{B}}$, both with components A_{ij} or B_{ij} and $(i, j = 1, 2)$, can be transformed to the following vector or

Table 2.1: Notation and topography.

Quantity	Topographic style	Example
scalar	non-bold, italic	$A, b, \alpha, \beta, \gamma$
vector	bold, italic	$\boldsymbol{A}, \boldsymbol{b}, \boldsymbol{\varepsilon}, \boldsymbol{\sigma}$
tensor, 2nd-order	bold	$\mathbf{A}, \mathbf{b}, \boldsymbol{\varepsilon}, \boldsymbol{\sigma}$
tensor, 4th-order	hollowed Roman (blackboard)	$\mathbb{A}, \mathbb{B}, \mathbb{C}$
matrix, column matrix	bold, italic, sans-serif	$\mathsf{A}, \mathsf{b}, \boldsymbol{\eta}, \boldsymbol{\mu}$
special operators	bold, calligraphic	$\mathcal{A}, \mathcal{B}, \mathcal{C}$
Voigt notation	bold, italic, sans-serif, underlined	$\underline{\mathsf{A}}, \underline{\mathsf{B}}, \underline{\mathsf{a}}, \underline{\mathsf{b}}, \underline{\boldsymbol{\alpha}}$

column matrix representations

$$\underline{\mathsf{A}} = \begin{bmatrix} \mathsf{A}_{11} & \mathsf{A}_{22} & \mathsf{A}_{12} & \mathsf{A}_{21} \end{bmatrix}^T \qquad \text{and} \qquad \underline{\mathsf{B}} = \begin{bmatrix} \mathsf{B}_{11} & \mathsf{B}_{22} & 2\mathsf{B}_{12} \end{bmatrix}^T . \tag{2.1}$$

Although the Voigt notation and the corresponding representations in Eq. (2.1) are established in standard techniques for FEM, cf. [168] for instance, the introduced notation serves for explanations of not common quantities within formulations for multiscale methods and computational homogenisation.

Standard mathematical operations and tensorial products for vectors and tensors of different order listed above, which are known from literature on tensor algebra, tensor analysis and on continuum mechanics, and which are used throughout this work, are summarised in Table 2.2. Any deviations in subsequent chapters will be emphasised, when needed, by corresponding remarks.

Table 2.2: Mathematical operations and tensorial products.

Description	Operation	
Scalar product	$c = \boldsymbol{a} \cdot \boldsymbol{b}$	
Vectorial (cross) product	$\boldsymbol{c} = \boldsymbol{a} \times \boldsymbol{b}$	
Tensorial (dyadic) product	$\mathbf{C} = \boldsymbol{a} \otimes \boldsymbol{b},$	$\mathbb{C} = \mathbf{A} \otimes \mathbf{B},$
Simple contraction	$\boldsymbol{c} = \mathbf{A} \cdot \boldsymbol{b},$	$\mathbf{C} = \mathbf{A} \cdot \mathbf{B}$
Double contraction	$c = \mathbf{A} : \mathbf{B},$	$\mathbf{C} = \mathbb{A} : \mathbf{B}$

2.2 Variations and derivatives

Several textbooks and publications, like [23, 58, 92] for instance, serve as a valuable reference and detailed introduction to fundamental principles of variational calculus. Therefore, only some important terms and relations for this work are briefly outlined.

In general physical or mechanical problems, a non-linear state variable $\boldsymbol{v}$ is often the quantity of interest. It represents the solution of stated *boundary value problems* (BVP) or *initial value problems* (IVP), e.g. the deformation state of a fixed referential configuration under prescribed loads in terms of structural analysis. When it comes to modifications of the referential (also called initial, material or Lagrangian) configuration, which are referred to as problems from design sensitivity analysis or more general from structural optimisation, an additional parameter is necessary for the description of the design under investigation. Therefore, a non-linear design parameter or design variable $\boldsymbol{s}$ is introduced. Both variables can be used for the evaluation of any arbitrary scalar valued and differentiable functional $J(\cdot)$ in several combinations depending on the stated problem formulation. For instance, $J(\cdot)$ can be one of the following forms $J(\boldsymbol{v})$, $J(\boldsymbol{s})$, $J(\boldsymbol{v},\boldsymbol{s})$ or $J(\boldsymbol{v}(\boldsymbol{s}),\boldsymbol{s})$ with an implicit dependency of the state on the design parameter $\boldsymbol{v}(\boldsymbol{s})$.

Remark 2.1 (Definition of parameters) *All introduced variables and functionals in the previous paragraph are defined on appropriate functional spaces $\mathcal{V}$ or $\mathcal{S}$. Therefore,*

$$\boldsymbol{v} \in \mathcal{V}, \quad \boldsymbol{s} \in \mathcal{S}, \qquad J(\boldsymbol{v}) : \mathcal{V} \to \mathbb{R}, \quad J(\boldsymbol{s}) : \mathcal{S} \to \mathbb{R}, \quad J(\boldsymbol{v},\boldsymbol{s}) : \mathcal{V} \times \mathcal{S} \to \mathbb{R}. \tag{2.2}$$

Variational solution strategies based on weak formulations of stated BVPs or IVPs require variations with respect to the state variable $\boldsymbol{v}$ in the physical space (also known as current, actual, deformed or Eulerian configuration) for structural analysis and variations with respect to the design parameter $\boldsymbol{s}$ in the referential configuration for the design sensitivity analysis. In general, a variation of an arbitrary functional $J(\cdot)$ is related to the directional derivative explained in Remark 2.2.

Remark 2.2 (Gâteaux or directional derivative) *In general, the first and second Gâteaux or directional derivatives of any arbitrary and at least twice continuously differentiable functional J with respect to a variable of choice, e.g. the state parameter $\boldsymbol{v}$, in directions $\{\boldsymbol{\eta}, \boldsymbol{\mu}\} \in \mathcal{V}$ are defined by*

$$\begin{aligned} J'_v(\boldsymbol{v};\boldsymbol{\eta}) &:= \lim_{\varepsilon \to 0} \ \frac{1}{\varepsilon} \ [J(\boldsymbol{v} + \varepsilon\, \boldsymbol{\eta}) - J(\boldsymbol{v})] = \frac{\mathrm{d}}{\mathrm{d}\varepsilon} \ J(\boldsymbol{v} + \varepsilon\, \boldsymbol{\eta})\Big|_{\varepsilon=0}, \\ J''_{vv}(\boldsymbol{v};\boldsymbol{\eta},\boldsymbol{\mu}) &:= \lim_{\varepsilon \to 0} \ \frac{1}{\varepsilon} \ [J'_v(\boldsymbol{v} + \varepsilon\, \boldsymbol{\mu},\boldsymbol{\eta}) - J'_v(\boldsymbol{v};\boldsymbol{\eta})] = \frac{\mathrm{d}}{\mathrm{d}\varepsilon} \ J'_v(\boldsymbol{v} + \varepsilon\, \boldsymbol{\mu};\boldsymbol{\eta})\Big|_{\varepsilon=0}. \end{aligned} \tag{2.3}$$

As a consequence, the variation of a quantity of interest $J(\cdot)$ with respect to a parameter of choice, e.g. state variable $\boldsymbol{v}$, is equal to its directional derivative in direction $\delta\boldsymbol{v} = \varepsilon\, \boldsymbol{\eta}$

$$\delta_v J(\boldsymbol{v};\delta\boldsymbol{v}) = J'_v(\boldsymbol{v};\delta\boldsymbol{v}) \tag{2.4}$$

and is valid for all upcoming investigations. In this work, major focus lies on functionals of the form $(\cdot)(\boldsymbol{v},\boldsymbol{s})$. Therefore, the total variation of this arbitrary quantity $(\cdot)(\boldsymbol{v},\boldsymbol{s})$ that depends on a general state variable $\boldsymbol{v}$ and a general design parameter $\boldsymbol{s}$, is given by the partial variation with respect to $\boldsymbol{v}$ and a fixed design $\hat{\boldsymbol{s}}$ as well as the partial variation with respect to $\boldsymbol{s}$ and a fixed state $\hat{\boldsymbol{v}}$. Therefore, the partial variations appear as

$$\begin{aligned} &\delta_v(\cdot) = \delta_v(\cdot)(\boldsymbol{v},\hat{\boldsymbol{s}}) = (\cdot)'_v(\boldsymbol{v},\hat{\boldsymbol{s}}) = (\cdot)'_v \quad \text{and} \\ &\delta_s(\cdot) = \delta_s(\cdot)(\hat{\boldsymbol{v}},\boldsymbol{s}) = (\cdot)'_s(\hat{\boldsymbol{v}},\boldsymbol{s}) = (\cdot)'_s. \end{aligned} \tag{2.5}$$

In comparison to the introduced Gâteaux derivative from Remark 2.2, the partial variations can also be expressed by

$$(\cdot)'_v(\boldsymbol{v},\boldsymbol{s};\boldsymbol{\eta}) = \frac{\mathrm{d}}{\mathrm{d}\varepsilon}\,(\cdot)(\boldsymbol{v}+\varepsilon\,\boldsymbol{\eta},\boldsymbol{s})\Big|_{\varepsilon=0} \qquad \text{and} \qquad (\cdot)'_s(\boldsymbol{v},\boldsymbol{s};\boldsymbol{\mu}) = \frac{\mathrm{d}}{\mathrm{d}\varepsilon}\,(\cdot)(\boldsymbol{v},\boldsymbol{s}+\varepsilon\,\boldsymbol{\mu})\Big|_{\varepsilon=0}. \tag{2.6}$$

Finally, the total variation of a quantity of interest is given by

$$\delta(\cdot)(\boldsymbol{v},\boldsymbol{s}) = \delta_v(\cdot)(\boldsymbol{v},\hat{\boldsymbol{s}}) + \delta_s(\cdot)(\hat{\boldsymbol{v}},\boldsymbol{s}) = (\cdot)'_v(\boldsymbol{v},\hat{\boldsymbol{s}}) + (\cdot)'_s(\hat{\boldsymbol{v}},\boldsymbol{s}) = (\cdot)'(\boldsymbol{v},\boldsymbol{s}). \tag{2.7}$$

When it comes to higher order variations, which are required in the scope of several solution strategies for structural analysis and structural optimisation based on linearisation techniques, a similar notation can be introduced, i.e. $(\cdot)''_{vv}, (\cdot)''_{ss}$, $(\cdot)''_{vs}$ and $(\cdot)''_{sv}$ represent second and mixed variations with respect to state and design parameters.

In cases with state variables which directly depend on design parameters, i.e. $\boldsymbol{v}(\boldsymbol{s})$ and therefore for arbitrary functionals $(\cdot)(\boldsymbol{v}(\boldsymbol{s}),\boldsymbol{s})$, the total derivative is given by

$$\frac{\mathrm{d}(\cdot)}{\mathrm{d}\boldsymbol{s}} = \frac{\mathrm{d}}{\mathrm{d}\boldsymbol{s}}(\cdot)(\boldsymbol{v}(\boldsymbol{s}),\boldsymbol{s}) = \frac{\partial(\cdot)}{\partial\boldsymbol{v}}\frac{\mathrm{d}\boldsymbol{v}}{\mathrm{d}\boldsymbol{s}} + \frac{\partial(\cdot)}{\partial\boldsymbol{s}}. \tag{2.8}$$

Here, explicit partial derivatives $\partial(\cdot)/\partial\boldsymbol{v}$ and $\partial(\cdot)/\partial\boldsymbol{s}$ of the quantity of interest $(\cdot)$ with respect to the general state variable $\boldsymbol{v}$ and design parameter $\boldsymbol{s}$ are included.

Remark 2.3 (Type of arguments) *The introduced notation using commas and semicolons allows to distinguish between linear and non-linear arguments in functionals and tangent forms, when needed. For instance, a functional $(\cdot)(\cdot;\cdot,\cdot)$, which has a similar form to the variations in Eq.* (2.6)*, is non-linear in arguments on the left hand side of the semicolon, and linear in arguments on the right hand side of the semicolon, respectively.*

2.3 Software environment

The following section gives a brief overview on the software environment and hardware components, which are used within the presented work. All presented topics, numerical calculations and investigations of this thesis are realised within a MATLAB in-house code. The development process of the past years involved implementations using versions of MATLAB in chronological order, but the final state of the implemented software is available in MATLAB R2018a. In all subsequent chapters, the developed main program is referred to as **M**ultiscale **A**nalysis a**n**d **O**ptimisation (MANO). As can be deduced from the given name, MANO can be utilised for structural analysis and structural optimisation on different scales. For instance, single scale structural analysis is performed using MANO.SA, single scale optimisation using MANO.SO and consequently, multiscale structural analysis and optimisation are carried out by MANO.MSA and MANO.MSO, respectively. Only some of its basic features are introduced and summarised here.

Several geometrical features, like methods from *Computer Aided Geometric Design* (CAGD) or morphing techniques, which are explained in Section 3.4, are implemented to initialise the investigated model problems and BVPs and to handle changes in design parameters induced from applied mathematical optimisation. General hyperelastic or Green elastic constitutive models, like the St. Venant–Kirchhoff or Neo-Hookean model, are available. Besides one-scale constitutive formulations, methods for numerical homogenisation in terms of FE^2 techniques, with different type of boundary conditions on the lower scale, are available as well and can be seen as surrogate material models for the macro scale structural analysis. The major purpose of MANO is the variational design sensitivity analysis and structural optimisation. The non-linear optimisation problems are basically solved using the *Sequential Quadratic Programming method* (SQP). In this scope, the MATLAB routine `quadprog` is applied to solve occurring quadratic subproblems. Some more details on SQP are presented in Chapter 3. Due to the fact that SQP is a gradient based optimisation technique, several derivatives of objectives, constraints and quantities from continuum mechanics are implemented. For the verification of mentioned sensitivity information, environments based on *finite difference method* (FDM), which is introduced in Section 3.3, are provided and allow evaluations of numerical gradients for comparison.

Remark 2.4 (Structure of argument list) *For a given objective or constraint functional of the form* $(\cdot)(\overline{\boldsymbol{s}}, \overline{\boldsymbol{v}}, \boldsymbol{s}, \boldsymbol{v})$*, explicit variations* $(\cdot)'_{\overline{s}}, (\cdot)'_{\overline{v}}, (\cdot)'_{s}$ *and* $(\cdot)'_{v}$ *are required for tangent forms and are derived analytically. Verification of obtained gradients is realised using finite difference quotients in terms of FDM. Let the index* 0*, i.e.* $(\cdot)_0$*, represent the initial values of referred quantities, i.e.* $(\cdot)_0 = (\cdot)(\overline{\boldsymbol{s}}_0, \overline{\boldsymbol{v}}_0, \boldsymbol{s}_0, \boldsymbol{v}_0)$ *being the function value for the initial set of parameters. Perturbations of referred terms are indicated by the index* c *(c for changed), i.e.* $(\cdot)_c$ *with* $(\cdot)_c = (\cdot)_0 + \Delta(\cdot)$*. With this convention at hand, perturbed output values of given functionals can be evaluated, i.e.* $\tilde{(\cdot)} = (\cdot)(\overline{\boldsymbol{s}}_c, \overline{\boldsymbol{v}}_0, \boldsymbol{s}_0, \boldsymbol{v}_0)$ *for the computation of numerical derivatives with respect to the first input variable* $\overline{\boldsymbol{s}}$ *or* $\hat{(\cdot)} = (\cdot)(\overline{\boldsymbol{s}}_0, \overline{\boldsymbol{v}}_c, \boldsymbol{s}_0, \boldsymbol{v}_0)$ *with respect to the second input* $\overline{\boldsymbol{v}}$*.*

According to Remark 2.4, it can be shown, that the following structure of argument list of a function is advantageous and is applied in most of the implemented routines.

```
funValue = funName(stateMacro, designMacro, stateMicro, designMicro)
```

On the one hand, for computations on single scales the last two input arguments are optional and can be replaced by some dummy arguments. On the other hand, perturbation of any quantity in the input argument list to obtain perturbed output values `funValue` is straightforward. This convention is useful for testing partial derivatives and variations, where a perturbation of a single input has an influence on the output.

Post-processing steps, like plots of the model problem under investigation, the optimisation model with available design parameters, deformed shapes after structural analysis, displacement or stress contour plots or plots with diagrams and graphs with optimisation results, are realised using MATLAB in-house routines. In some cases, obtained results are exported as `vtk`-files and are investigated in the open-source and cross-platform application PARAVIEW, see [80] for further details. The advantage of PARAVIEW is an efficient handling and fast visualisation of large datasets, which is often useful for quick look-up and access of results.

Several required routines for the solution of stated structural analysis and structural optimisation problems are provided by MATLAB R2018a toolboxes listed in Table 2.3. The non-linear optimisation problem, introduced in Problem 3.1 in Chapter 3 on optimisation, is solved using routines provided by the Optimization Toolbox. For efficient computations, the abilities of the Parallel Computing Toolbox are used for the assembly of global system matrices and vectors. Certain routines and functions can be transferred to C++ code and pre-compiled using the MATLAB coder and MATLAB compiler toolbox. This step, which includes calls of external, pre-compiled and so-called `mex`-files or `mex`-functions, provides an efficient method to fasten the overall runtime of the program. For numerous derivations, the Symbolic Math Toolbox provides useful routines at different stages of the development procedure. Finally, the documentation of the implemented code is realised using the MATLAB Report Generator.

Table 2.3: List of utilised MATLAB R2018a toolboxes.

Toolbox	**Version**
MATLAB Compiler	6.6
Optimization Toolbox	8.1
Parallel Computing Toolbox	6.12

(a) Essential numerical toolboxes.

Toolbox	**Version**
MATLAB Coder	4.0
MATLAB Report Generator	5.4
Symbolic Math Toolbox	8.1

(b) Optional numerical toolboxes.

In general, there are barely restrictions of the usage of the presented methodology in any commercial or non-commercial simulation software for structural analysis and structural optimisation. Adaptions for software like ANSYS, ABAQUS, COMSOL MULTIPHYSICS, FEAP, see [5, 43, 44, 152] for further information on mentioned software, or any other individual in-house simulation software like INA-OPT (Inelastic Analysis and Optimisation), developed and used in [11] and [12], can be realised and managed with respect to individual restrictions. Altogether, the best conditions are given if developers have access to the sourcecode directly and therefore, to quantities on the element level to formulate and to evaluate necessary sensitivity relations. Additionally, access to assembled system quantities for the formulation of global sensitivity relations is beneficial. It is also useful, if manipulations of input-output argument lists are possible, cf. Remark 2.4.

The flexibility of the presented methodology allows the application to a wide range of applications, like linear and non-linear elasticity, plasticity and damage, dynamics, theory of porous media or to take influence on several processes during manufacturing. Therefore, extensions of MAnO are straight forward and only a matter of time and diligence.

Remark 2.5 (Element library and controls on element level) *So far, the element library and therefore, the implemented element routines within* MAnO *have a comparable structure to* FEAP *and* INA-OPT. *Several switches on the element level are introduced to control parts of the code and therefore, to control the computation procedure. This gives the ability to deliver required outputs for structural analysis and structural optimisation at different stages of the overall program.*

Development, testing and debugging of the presented software MAnO took place on a Linux based operating system. It was extensively tested on hardware environments listed in Table 2.4, which run Linux based operating systems. Nevertheless, Matlab is a platform independent environment and the software was also tested on Windows based operating systems and can be adopted to any further user requirements. When it comes to numerical investigations in terms of time, number of function evaluations or overall performance measurements, the results are identified by the corresponding label of the affiliated hardware environment, which is also given in Table 2.4. Every type of evaluated quantity is marked by $^{\mathtt{m}}(\cdot)$ or $^{\mathtt{d}}(\cdot)$, e.g. run times for one structural analysis on different types of presented hardware are distinguished by $^{\mathtt{m}}t_{\mathrm{a}}$ or $^{\mathtt{d}}t_{\mathrm{a}}$. The number of corresponding function evaluations is tagged by n_{F}.

Table 2.4: Hardware environments and labels for numerical investigations.

Label **Description**	**RAM**	**CPU**
m Dell Precision M4800 (mobile workstation)	32 GB	1× Intel® Core™ i7-4800MQ (quad-core @ 2.70GHz)
d Fujitsu CELSIUS R920 (desktop workstation)	64 GB	2× Intel® Xeon® E5-2690 (octa-core @ 2.90GHz)

Chapter 3

Optimisation setup and choice of design parameters

In this chapter, the general setup for optimisation problems considering objective functions, constraints and design parameters as well as iterative methods for computing their solutions are presented. Remarks on the verification of obtained sensitivity information and on the choice of design parameters for optimisation are given.

The major purpose of the presented work is to suggest possible approaches for the combination of known frameworks for structural analysis (SA), e.g. in the scope of numerical homogenisation and FE^2 techniques, and known frameworks for structural optimisation (SO), like shape and topology optimisation. The focus lies on formulations of possible concepts for the numerical treatment of design processes of new structures and to improve the overall performance of given mechanical parts and components.

In this section, the basic notation for structural optimisation problems is introduced. An extensive introduction on topics from design sensitivity analysis (DSA) and structural optimisation is provided on sensitivity analysis in Chapter 5 and on material design in Chapter 6. In the mentioned chapters, topics from several publications, standard books and papers on structural optimisation, like [7, 22, 38, 39, 40, 67, 133], will be introduced, discussed and tailored to the stated optimisation problems. Prior to any statements, it has to be mentioned that all appearing optimisation problems are solved using first order mathematical optimisation methods, which all require Fréchet derivatives or gradient information of the objective function and constraints with respect to the full space of available design parameters as inputs. As a consequence, each obtained optimum or each optimal solution can be characterised as a local optimum and is never unique. Inherently, different initial parameters lead to different optimisation results. Nevertheless, the obtained solutions represent remarkable improvements compared to initial shapes and design configurations.

3.1 General formulation of the optimisation problem

The general optimisation problem with an arbitrary objective functional J, various equality and inequality constraints $(\boldsymbol{h}, \boldsymbol{g})$, several lower and upper side constraints $(\boldsymbol{s}^{\mathrm{l}}, \boldsymbol{s}^{\mathrm{u}})$ for design parameters can be introduced in the following abstract way.

Problem 3.1 (General optimisation problem) *Find* $\{\boldsymbol{v}, \boldsymbol{s}\} \in \mathcal{V} \times \mathcal{S}$ *of the objective functional* $J : \mathcal{V} \times \mathcal{S} \to \mathbb{R}$ *such that*

$$\min_{\boldsymbol{v},\, \boldsymbol{s} \in \mathcal{V} \times \mathcal{S}} J(\boldsymbol{v}, \boldsymbol{s}) \tag{3.1}$$

subject to the constraints

$$\boldsymbol{h}(\boldsymbol{v}, \boldsymbol{s}) = \boldsymbol{0}, \qquad \boldsymbol{g}(\boldsymbol{v}, \boldsymbol{s}) \leq \boldsymbol{0}, \qquad \boldsymbol{s}^l \leq \boldsymbol{s} \leq \boldsymbol{s}^u, \tag{3.2}$$

with the vector notation $\boldsymbol{h}(\boldsymbol{v}, \boldsymbol{s})$ *for introduced equality constraints* $h_i(\boldsymbol{v}, \boldsymbol{s}) = 0$, $i \in \mathcal{E}$, *and also the vector notation* $\boldsymbol{g}(\boldsymbol{v}, \boldsymbol{s})$ *for introduced inequality constraints* $g_j(\boldsymbol{v}, \boldsymbol{s}) \leq 0$, $j \in \mathcal{I}$. *The sets of indices for equality and inequality constraints are denoted by* $\mathcal{E}$ *and* $\mathcal{I}$.

This abstract setting of a general optimisation problem is presented in several standard publications on structural and numerical optimisation and design sensitivity analysis, see [7, 38, 39, 67, 111] and references therein for further details. According to the continuous formulation of the general optimisation Problem 3.1, the discrete form can be obtained by using discretised values for objectives, constraints and design parameters.

Problem 3.2 (Discrete form of the optimisation problem) *Find* $\{\boldsymbol{v}, \boldsymbol{s}\} \in \mathcal{V}_h \times \mathcal{S}_h$ *of the discrete objective functional* $J : \mathcal{V}_h \times \mathcal{S}_h \to \mathbb{R}$ *such that*

$$\min_{\boldsymbol{v},\, \boldsymbol{s} \in \mathcal{V}_h \times \mathcal{S}_h} J(\boldsymbol{v}, \boldsymbol{s}) \tag{3.3}$$

subject to the constraints

$$\boldsymbol{h}(\boldsymbol{v}, \boldsymbol{s}) = \boldsymbol{0}, \qquad \boldsymbol{g}(\boldsymbol{v}, \boldsymbol{s}) \leq \boldsymbol{0}, \qquad \boldsymbol{s}^l \leq \boldsymbol{s} \leq \boldsymbol{s}^u, \tag{3.4}$$

with a matrix notation $\boldsymbol{h}(\boldsymbol{v}, \boldsymbol{s})$ *of introduced equality constraints* $h_i(\boldsymbol{v}, \boldsymbol{s}) = 0$, $i \in \mathcal{E}_h$, *and a matrix representation* $\boldsymbol{g}(\boldsymbol{v}, \boldsymbol{s})$ *of introduced inequality constraints* $g_j(\boldsymbol{v}, \boldsymbol{s}) \leq 0$, $j \in \mathcal{I}_h$. *The sets of indices for equality and inequality constraints are denoted by* $\mathcal{E}_h$ *and* $\mathcal{I}_h$.

The treatment of Problem 3.1 or Problem 3.2, respectively, requires an iterative process with some essential and recurring steps, which are briefly outlined in Fig. 3.1. The definition of the initial structural design in terms of a physical model with appropriate boundary conditions, a geometry and/or CAE-FEM model, the definition of the mathematical optimisation model, which includes the definition of an objective function (OF) J, equality and/or inequality constraints (CON) $(\boldsymbol{h}, \boldsymbol{g})$, some side constraints (SCON) $(\boldsymbol{s}^{\mathrm{l}}, \boldsymbol{s}^{\mathrm{u}})$ and design parameters (DP) $\boldsymbol{s}$, is followed by a first structural analysis for the initial design using FEM. The obtained results for the equilibrium state can be used for the evaluation of required design responses, in terms of objective functions and constraints and the design sensitivity analysis for the stated optimisation problem. The provided sensitivity information and therefore all available gradient information, serve as input for algorithms for mathematical optimisation and *non-linear programming* (NLP) and are essential quantities to seek for a new and updated design description. Final optimisation results can be provided as drafts to designers and design engineers. The explicit solution of the abstract optimisation Problem 3.1 is investigated in [94, 95, 97]. The authors choose the

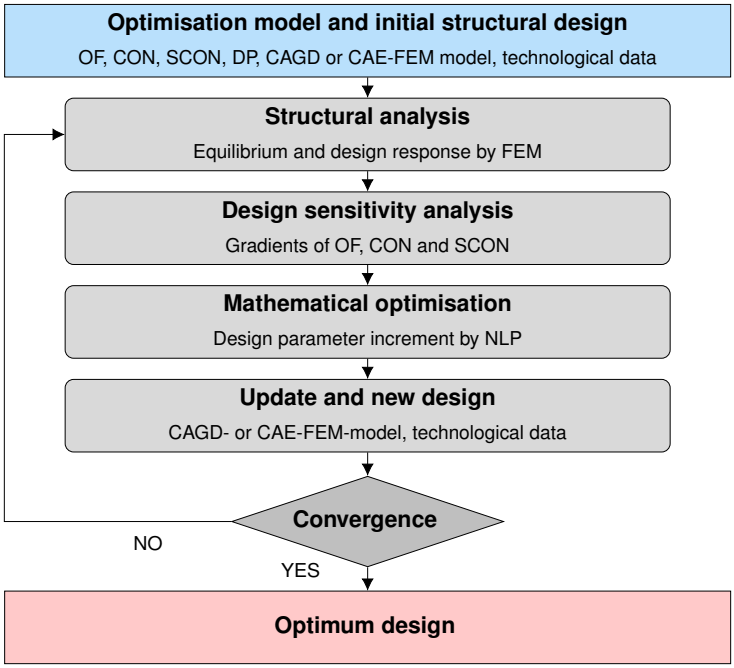

Figure 3.1: Principle framework for structural optimisation.

total potential energy of a hyperelastic body as a special objective functional, consider only the non-linear residual (introduced in Eq. (5.28)) as the equality constraint, i.e. inequality constraints are neglected and therefore $\mathcal{I} = \emptyset$, and discuss solution strategies using the *steepest descent method*, the *full Newton* or a *staggered solution method* in detail. A more general and more versatile approach, which also guarantees solutions in feasible regions with respect to stated constraints, is the SQP method. Its application allows the solution of the full non-linear optimisation problem with all possible constraints, i.e. equality and inequality ($\mathcal{E} \neq \emptyset$ and $\mathcal{I} \neq \emptyset$) as well as side constraints ($\boldsymbol{s}^{\mathrm{l}}, \boldsymbol{s}^{\mathrm{u}}$). The basic idea of the incorporated Lagrange formalism in the scope of SQP is briefly summarised in Problem 3.3 and will be investigated in this form throughout this work. Further explanations and details on this method can be found for instance in [25, 63, 111, 128, 129] and in several references therein.

Problem 3.3 (Lagrange formalism in the scope of SQP) *Several types of solution strategies for constrained optimisation problems are often based on reformulations of stated optimisation problems using the* ***Lagrange formalism***

$$\mathcal{L}(\boldsymbol{s}, \boldsymbol{\lambda}, \boldsymbol{\mu}) = J(\boldsymbol{s}) + \sum_{i=1}^{n_h} \lambda_i \, h_i(\boldsymbol{s}) + \sum_{j=1}^{n_g} \mu_j \, g_j(\boldsymbol{s}) = J(\boldsymbol{s}) + \boldsymbol{\lambda}^T \, \boldsymbol{h}(\boldsymbol{s}) + \boldsymbol{\mu}^T \, \boldsymbol{g}(\boldsymbol{s}). \tag{3.5}$$

Here, the original objective function $J(\boldsymbol{s})$ is additively manipulated by scaled equality and inequality constraints $(h_i(\boldsymbol{s}), g_j(\boldsymbol{s}))$ using Lagrange multipliers (λ_i, μ_j), also known

as adjoint or dual variables, and results in the so-called Lagrange function $\mathcal{L}(\boldsymbol{s}, \boldsymbol{\lambda}, \boldsymbol{\mu})$. *The solution of the obtained objective functional* $\mathcal{L}(\boldsymbol{s}, \boldsymbol{\lambda}, \boldsymbol{\mu})$, *in terms of minimisation or maximisation, requires the* ***optimality criteria*** *to be fulfilled*

$$\nabla \mathcal{L}(\boldsymbol{s},\boldsymbol{\lambda},\boldsymbol{\mu}) = \mathbf{0}. \tag{3.6}$$

The approach of SQP for the solution of general non-linear optimisation problems is based on the solution of sequential subproblems with a quadratic approximation of the objective functional $J(\boldsymbol{v}, \boldsymbol{s})$ *and the linearisation of constraints* $(\boldsymbol{h}(\boldsymbol{v}, \boldsymbol{s}), \boldsymbol{g}(\boldsymbol{v}, \boldsymbol{s}))$. *Therefore, for each subproblem* k *and each iteration point* (s^k, λ^k, μ^k) *the resulting system of equations for the* ***quadratic subproblem*** *results in the form*

$$\min_{\Delta \boldsymbol{s} \in \mathcal{S}} \widetilde{J}^k \;=\; \min_{\Delta \boldsymbol{s} \in \mathcal{S}} \; \frac{1}{2}\, \Delta \boldsymbol{s}^T \, \nabla^2_{\boldsymbol{ss}} \mathcal{L}(\boldsymbol{s}^k, \boldsymbol{\lambda}^k, \boldsymbol{\mu}^k)\, \Delta \boldsymbol{s} + \nabla J(\boldsymbol{s}^k)^T \, \Delta \boldsymbol{s} \tag{3.7}$$

subject to the constraints

$$\begin{aligned} \widetilde{\boldsymbol{h}}^k(\Delta \boldsymbol{s}) = \boldsymbol{h}(\boldsymbol{s}^k) + \nabla \boldsymbol{h}(\boldsymbol{s}^k)^T \, \Delta \boldsymbol{s} \;&=\; \mathbf{0}, \\ \widetilde{\boldsymbol{g}}^k(\Delta \boldsymbol{s}) = \boldsymbol{g}(\boldsymbol{s}^k) + \nabla \boldsymbol{g}(\boldsymbol{s}^k)^T \, \Delta \boldsymbol{s} \;&\leq\; \mathbf{0}, \\ (\boldsymbol{s}^l - \boldsymbol{s}^k) \;\leq\; \Delta \boldsymbol{s} \;&\leq\; (\boldsymbol{s}^u - \boldsymbol{s}^k). \end{aligned} \tag{3.8}$$

The quadratic subproblem, i.e. the functional $\widetilde{J}^k$ *is quadratic in* $\Delta \boldsymbol{s}$, *and its solution provides incremental design updates by*

$$\boldsymbol{s}^{k+1} = \boldsymbol{s}^k + \Delta \boldsymbol{s}^k. \tag{3.9}$$

Altogether, derivatives or variations, especially partial variations of the objective functional J and constraints h_i, g_j with respect to the state variables $\boldsymbol{v}$ and design parameters $\boldsymbol{s}$, are essential for first order optimisation strategies. The fundamental relations for design sensitivity analysis in the scope of finite element formulations and especially of optimisation of problems from structural mechanics are provided in Chapter 5. The formulation of the quadratic subproblem in Problem 3.3 requires the provision of second order derivatives, i.e. the Hessian matrix of the Lagrange functional $\nabla^2_{\boldsymbol{ss}} \mathcal{L}(\boldsymbol{s}^k, \boldsymbol{\lambda}^k, \boldsymbol{\mu}^k)$. In addition to the numerical effort for its computation, the demand for positive definiteness of $\nabla^2_{\boldsymbol{ss}} \mathcal{L}$ is not guaranteed to be fulfilled and therefore, in many cases, it is sufficient to chose appropriate approximations of second order derivatives. For instance, the well known *Broyden-Fletcher-Goldfarb-Shanno* update formula (BFGS) provides a positive definite approximation of the Hessian matrix, see [30, 50, 62, 136] for details on this method. This approximation is used in following numerical investigations in all subsequent chapters.

Remark 3.1 (Multiobjective optimisation) *Improvements of many mechanical systems with practical relevance and of real world problems often require the solution of optimisation problems in terms of minimisation or maximisation of more than one objective function, i.e.* $\min_{\boldsymbol{s}} \; (f_1(\boldsymbol{s}), f_2(\boldsymbol{s}), \ldots, f_n(\boldsymbol{s}))$ *with respect to certain equality and/or inequality constraints and the design parameters* $\boldsymbol{s}$. *This kind of optimisation problem is termed multiobjective optimisation* (MOO) *or vector optimisation, respectively.*

MOO *problems might contain different combinations of following goals: overall or operating cost, profit, quality, efficiency, safety or performance in general. Usually, most of the goals are conflicting and non-commensurable, e.g. it might be impossible to measure performance in monetary units. Consequently, an appropriate priorising of goals is required but it often leads to arbitrary and subjective optimal solutions, which are not unique. Within the mentioned problem formulation the target is to find a solution that satisfies each objective function at the best. In general, no single best solution exist, but a set of feasible solutions, that are all characterised as equally good solutions. The points in this solution set are the so-called Pareto optimums. They stand out due to the balance in the trade-off of solutions, which means, that a solution cannot improve any objective without degrading one or more of the other objectives. The authors in [37] compile and compare four solution strategies for this kind of problem formulations, i.e. the global criterion method, the linear combination of weights method, the ε-constrained method and the multiobjective genetic algorithm. Further details can also be found in [48] or [46] for instance.* MOO *is a standalone research field and therefore, a detailed review on theory and available methods is beyond the scope of this work. In the work at hand no* MOO *problems are solved but one solution strategy is considered and adapted for the solution of multiscale optimisation problems, i.e. the linear combination of weights method or the weighted sum method. It requires a construction of a weighted sum of objectives, i.e.*

$$\boldsymbol{F}(\boldsymbol{s}) = \sum_{i=1}^{k} w_i \, f_i(\boldsymbol{s}) \tag{3.10}$$

including individual weight factors w_i. The optimisation is performed in terms of the objective function $\boldsymbol{F}(\boldsymbol{s})$, i.e. $\min_{\boldsymbol{s}} \boldsymbol{F}(\boldsymbol{s})$. Within multiscale optimisation problems, the approach of a weighted sum of functions is applied to constraints and allows a formulation of a well-posed optimisation problem.

Example: For a solid square domain with inclusions and different material properties but no voids and a side length of 1, the volume results to 1. A constant volume constraint requires the volume of the domain not to change. In that case, the gradient of the constraint vanishes and a computation of incremental design parameters is not possible. To force a modification of the design, the contribution of each individual constituent is weighted, i.e. the overall volume is computed by $V = \sum_{i=1}^{k} w_i V_i$. The weight factors w_i can be related to the importance, overall costs or valency of each constituent in an abstract sense.

3.2 Objective functions, constraints and design parameters

The challenge within the presented work is to find appropriate mathematical formulations for the modelling of multiscale optimisation problems. Beside the necessity of sensitivity relations for the coupling conditions of different scales, the choice of appropriate objective functionals and constraints in combination with useful design parameters is essential. Table 3.1 lists possible sets for objectives, constraints and design parameters, which are common and often used in standard publications on structural optimisation, see [7, 22, 40, 67, 133] to name a few. Within presented numerical investigations, a special choice will be made and embedded in Problem 3.1 and Problem 3.2 formulation, respectively.

Table 3.1: Possible sets for objectives (OF) in terms of goal setting, constraints (CON) in terms of restrictions and design parameters (DP) in the design space.

Goals *Cost functions*	**Restrictions** *Failure & manufacturing*	**Design space** *Geometry & material*
stiffness, compliance	volume fractions	shape parameters
volume, mass	stresses, strains	material distribution
displacements, frequencies	damage criteria	thickness, cross-sections
costs of constructions	manufacturing parameters	technological data

3.3 Verification of derivatives and sensitivity information

Gradient based mathematical optimisation methods require correct sensitivity information to guarantee an efficient optimisation process and to find feasible solutions. Throughout the entire work, all variations of mechanical quantities, derivatives and gradients of objective functions and constraints are verified using the *finite difference method* (FDM) with either forward, backward or central differences. FDM is a reliable and well-known tool from computer algebra and can be applied to prove the accuracy of provided sensitivity information up to a certain numerical precision. Useful suggestions for the computation of numerical derivatives are given in Remark 2.4. Actually, the numerical sensitivity information obtained by FDM can be used for optimisation, but in the practical sense the numerical effort depends on the investigated model problem and perhaps it might become enormous. Here, some hints on the number of function evaluations and on the resulting time consumption are briefly outlined. In general, it is necessary to distinguish which gradients need to be computed.

1. *Gradients on nodal basis*, i.e. gradients with respect to nodal design parameters $\boldsymbol{X}$.
2. *Gradients on geometrical basis*, i.e. gradients with respect to design parameters $\boldsymbol{s}$.
   a) In the case where a geometry description is used, the obtained gradient has to be multiplied by a design velocity fields matrix $\boldsymbol{V}$, as explained in Section 3.4.
   b) Gradients with respect to a subset of geometrical design parameters $\boldsymbol{s}$, i.e. gradients with respect to the final design variables. These gradients are equal to a subset of the gradients from Item 2a.

Numerical derivation of gradients are, for a typical forward or backward difference quotient, $n_{\mathrm{F}}^{\mathrm{f,b}} = n + 1$ and a for central difference quotient, $n_{\mathrm{F}}^{\mathrm{c}} = 2n$ function evaluations, with n being a general and replaceable number of design variables and therefore, of n necessary perturbations and structural analyses. Thus, the resulting computation times for numerical gradients result to

$$\begin{aligned} t_{\mathrm{s,num}}^{\mathrm{f,b}} &= n_{\mathrm{F}}^{\mathrm{f,b}} \cdot t_{\mathrm{a}} \quad \text{(forward/backward FDM scheme)}, \\ t_{\mathrm{s,num}}^{\mathrm{c}} &= n_{\mathrm{F}}^{\mathrm{c}} \cdot t_{\mathrm{a}} \qquad\qquad \text{(central FDM scheme)}. \end{aligned} \tag{3.11}$$

3.4 Choice of design parameters for optimisation

Using finite element techniques, the structural analysis of given mechanical systems is based on discrete nodal state variables $\boldsymbol{v}$ and nodal coordinates $\boldsymbol{X}$ of the underlying finite element mesh. Details on finite element approximations follow in subsequent sections. Together with element incidences, the nodal coordinates $\boldsymbol{X}$ represent the approximation of the referred and subdivided continuous domain and can also be tackled as design parameters within structural optimisation procedures, cf. publications on parameter free or FEM node based optimisation investigated in [24, 88] and [127] for example. In this case, design sensitivity analysis has to be performed with respect to nodal coordinates $\boldsymbol{X}$ of the chosen discretisation and finite element mesh, i.e. the discrete design parameter $\boldsymbol{s}$ is set to $\boldsymbol{s} = \boldsymbol{X}$. As a consequence, the residual R (later in Eq. (5.28)) depends on discrete coordinates $\boldsymbol{X}$ and its variation R'_X in direction $\delta\boldsymbol{X}$ is the necessary variation of the residual to obtain the sought tangent pseudo load operator. The final result is the discrete pseudo load matrix $\boldsymbol{P} \in \mathbb{R}^{n_v \times n_X}$, with n_X being the overall number of finite element nodal coordinates. Same holds true for the design variation of any arbitrary objective or constraint functional f (later in Eq. (5.33)) and means that f'_X is the variation in request.

Within parameter free optimisation procedures, often some intensively discussed drawbacks occur. Drawbacks like jagged boundaries, mesh distortions and the necessity of filtering or regularisation techniques during the optimisation processes to avoid non-physical results for different kinds of physical problems are described in [66] for instance. Although the mentioned aspects are investigated in several publications, see [24, 60, 88, 127] to name a few, and several solution strategies, like the fictitious energy approach or several filtering techniques, are proposed, utilisation of parametrisation techniques for the control of geometrical properties of given structures comes along with several advantages. For instance, any of the following parametrisations comes with an enormous reduction of design variables and allows avoiding jagged boundaries in advance due to the characteristic smoothness of included mappings. Several *computer aided engineering* (CAE) techniques and applications for structural analysis in most cases involve an underlying geometry description. Here for instance, *computer aided geometric design* (CAGD) is an established and widely spread technique. Its main advantage within the structural optimisation process is, that the chosen and modified (by several optimisation steps) geometry can be handled in every step of the design and the prototype manufacturing process. The obtained analysis and optimisation results can directly be transferred to responsible engineers and product designers and can be used for subsequent virtual and physical test scenarios. In contrast, parameter free optimisation requires intensive post processing steps to construct manufacturable geometry data. The geometry description is realised using Bézier curves, *basis splines* (B-splines) or even *non-uniform rational B-Splines* (NURBS), see for example [49] for elementary details and explanations. The coordinates of the control points of the control polygon can be chosen as design variables and are identified by the design parameter $\boldsymbol{s}$. The design parameters $\boldsymbol{X}$ of the underlying finite element mesh depend on the newly introduced design variables $\boldsymbol{s}$, i.e. $\boldsymbol{X}(\boldsymbol{s})$. Therefore, the sensitivities with respect to $\boldsymbol{X}$, mentioned in the prior paragraph, have to be transformed via a design velocity fields matrix $\boldsymbol{V} = \partial\boldsymbol{X}/\partial\boldsymbol{s}$ into the chosen design space. The final discrete variation of a

continuous functional $f(\boldsymbol{v}, \boldsymbol{X}(\boldsymbol{s}))$ reads

$$f' = \frac{\partial f}{\partial \boldsymbol{v}} \delta \boldsymbol{v} + \frac{\partial f}{\partial \boldsymbol{X}} \frac{\partial \boldsymbol{X}}{\partial \boldsymbol{s}} \delta \boldsymbol{s} = \left(\frac{\partial f}{\partial \boldsymbol{v}} \, \boldsymbol{S} + \frac{\partial f}{\partial \boldsymbol{X}} \right) \boldsymbol{V} \delta \boldsymbol{s}, \tag{3.12}$$

with $\boldsymbol{S}$ being the total derivative of the state $\boldsymbol{v}$ with respect to the nodal coordinates $\boldsymbol{X}$ of the finite element mesh, i.e. $\boldsymbol{S} = \mathrm{d}\boldsymbol{v}/\mathrm{d}\boldsymbol{X}$. For further explanations on design velocity fields see [38, 39, 94]. Generally in both cases, i.e. within parameter free optimisation and within parametrised optimisation, the kernel task is to compute the sensitivities of quantities of interest with respect to nodal coordinates $\boldsymbol{X}$ first. Therefore, nodal coordinates of the finite element mesh are chosen as design variables to determine the necessary tangent operators $\boldsymbol{K}$ and $\boldsymbol{P}$ as well as the sensitivity matrix $\boldsymbol{S}$. If dependencies change or a different choice for the design parameter $\boldsymbol{s}$ is made, explicit hints and remarks are given. The derivatives of objectives and constraints with respect to nodal coordinates have to be transformed into the design space of interest using the design velocity matrix $\boldsymbol{V}$. In the following, two approaches for design parametrisation, i.e. design description based on CAGD models and design parametrisation based on morphing, which are used within the work in hand, are briefly introduced and illustrated by two simple examples pictured in Fig. 3.2. Here, for the upcoming investigations a simple domain with a hole represents the first setup and a simple domain with an inclusion represents the second setup. Both sets are parametrised using CAGD models on the one hand and morphing techniques on the other hand. The differences between both approaches are pointed out in the following two sections.

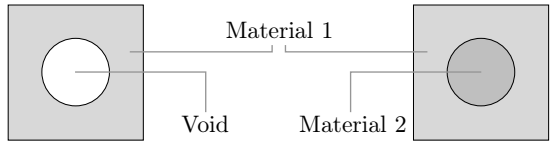

Figure 3.2: Design parametrisation techniques: example with two different setups: setup 1 - domain with a hole (left), setup 2 - domain with an inclusion (right).

3.4.1 Design parametrisation based on CAGD models

As already mentioned in prior section, the description of underlying structures using CAGD models is basically realised using Bézier curves and the corresponding evaluation of Bernstein polynomials. This kind of mathematical formulation allows the description of geometrical elements and forms like lines, areas and volumes, see [49] for extensive details on this topic. Due to the fact that the complete description of investigated domains is realised using CAGD objects and geometrical forms, algorithms for mesh generations are required to be able to perform structural analysis of the stated problem using FEM for instance. For this purpose, publications [47] and [51] on mesh generation can be referred.

Illustrations in Fig. 3.3 consider CAGD representations of already introduced setups from Fig. 3.2. The blue markers represent the control points of Bézier patches, which itself are illustrated by the blue lines. The definition of the geometry and the corresponding mesh generation algorithms result in grey coloured finite element meshes. Depending

on mesh generation algorithms, different kinds of element formulations are available, e.g. setup 1 in Fig. 3.3 is represented by a mesh with triangular elements and setup 2 in Fig. 3.3 is represented by a mesh with rectangular elements. Possible design parameters, which are identified by the discrete design parameter $\boldsymbol{s}$, are control points of Bézier curves of lines or areas, denoted by the blue markers, radii of holes or inclusions, here the initial parameters a_0, b_0, the angle of the hole or inclusion, indicated by α_0, or lengths of lines (not pictured). For several investigations and examples see [38, 39, 40, 133] to name a few. Modifications of initial design parameters $\boldsymbol{s}_0 = \{a_0, b_0, \alpha_0\}$ lead to geometries represented by the parameters $\boldsymbol{s}_1 = \{a_1, b_1, \alpha_1\}$ for both setups in Fig. 3.3. The consequence of the dependence of the finite element mesh on the geometry description and the positions of the defined control points is that any modification $\delta\boldsymbol{s}$ results in a modification of the discrete parameters $\delta\boldsymbol{X}$, i.e. the positions of finite element nodes change due to changes in design parameters and have to be recalculated after obtained updates of $\boldsymbol{s}$. Within optimisation procedures, gradients of objectives and constraints with respect to design parameters $\boldsymbol{s}$ are required. Therefore, the calculated gradients on nodal basis, i.e. the gradients with respect to $\boldsymbol{X}$, have to be transformed using design velocity fields $\boldsymbol{V}$.

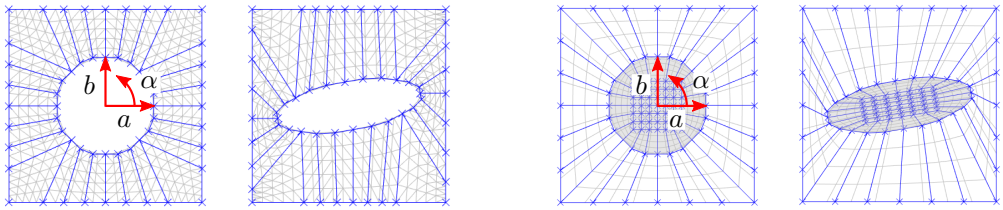

Set 1: a_0, b_0, α_0 a_1, b_1, α_1 Set 2: a_0, b_0, α_0 a_1, b_1, α_1

Figure 3.3: Design parametrisation based on CAGD model: introduced design variables are radii a, b of the hole/inclusion and angle α (0=initial, 1=modified)(red).

The ability for direct manufacturing and low number of design variables can be seen as an advantage compared to parameter free optimisation techniques, but the enormous effort for the generation of CAGD models and the extension of existing software environments by tools and routines for sensitivity analysis represent arguable drawbacks.

3.4.2 Design parametrisation based on morphing

Design parametrisation based on morphing is useful to handle forms and geometries without explicit geometrical properties, like diameters, positions and angles. This technique is basically established and known from image processing and is based on smooth and continuous transformations of target objects into other objects of interest. A review on different aspects and approaches can be found in [167] and extensions to three-dimensional investigations are presented in [146, 166]. Overall, morphing techniques within structural optimisation procedures can be classified as a combination of parameter free and CAGD based optimisation techniques. So-called morphing boxes are defined by general B-Spline tensor products with arbitrary number of control points $\boldsymbol{C}_i$ and arbitrary degree of basis splines, see [29, 49, 123] for details on this topics. Algorithms scan the domains within defined morphing boxes for existing nodes of finite element meshes and collect

the corresponding nodal coordinates. Due to the fact that only finite element nodes are involved, this technique is valid for arbitrary element formulations and element types. Coordinates C_i of control points of defined morphing boxes, summarised in the column matrix $\boldsymbol{C}$, are used as design parameters, i.e. $\boldsymbol{s} = \boldsymbol{C}$, and control positions of depending finite element nodes $\boldsymbol{X}$ within the morphing box. This procedure is pictured in Fig. 3.4 referring to already introduced setups from Fig. 3.2. The modification $\delta\boldsymbol{s}$ results in a modification of the discrete parameters $\delta\boldsymbol{X}$, i.e. the positions of FEM nodes change due to changes in design parameters. Gradients of objectives and constraints with respect to design parameters $\boldsymbol{s}$ are required within the optimisation process. Therefore, the calculated gradients on nodal basis, i.e. the gradients with respect to $\boldsymbol{X}$, have to be transformed into the design space of interest using design velocity fields $\boldsymbol{V}$. Using this technique for design parametrisation, costly remeshing can be avoided, see [121] for details.

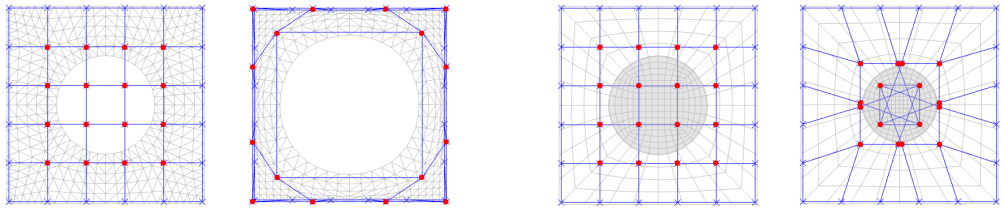

Figure 3.4: Design parametrisation based on morphing: introduced design variables are coordinates $\boldsymbol{C}$ (0=initial, 1=modified) of control points of the morphing box (red).

The main advantage of a morphing based approach for design descriptions is that, beside the manageable implementation effort, it is valid for all types of finite element meshes. In other words, meshes can be generated in any pre-processing environment of choice and than imported to the optimisation program to be controlled by defined morphing boxes. The ability to consider and investigate some subdomains of a given structure defining morphing boxes only in relevant domains, can be seen as an additional feature. Several details on mesh generation, analytical design velocity fields and overall morphing controlled FEM and general mesh handling can be found in [59].

3.5 Summary and concluding remarks

In this chapter the abstract layout of a general non-linear optimisation problem in continuous and discrete form is stated. A flow chart is used to introduce the iterative solution procedure for structural optimisation problems in terms of the gradient based SQP method. Beside remarks on the verification of obtained sensitivity information using FDM, a list of possible objective functions, constraints and design parameters is outlined. After a brief review on the choice of design parameters, two explicit parametrisation techniques based on a square domain with two different setups are presented.

Chapter 4

Structural analysis on multiple scales

This chapter constitutes a concise introduction to basic principles for structural analysis on multiple scales and the treatment of microheterogeneous materials. Basically, the class of two-scale problems in terms of homogenisation methods and FE^2 techniques is considered. Necessary relations as well as aspects for the numerical realisation for the application within structural optimisation problems are stated.

4.1 Introduction

Beside efficient and reliable structural performance (on so-called macroscale), in recent years, modern engineering applications from several fields require also high performance behaviour on the material level (on so-called meso-/microscale). In general, the degree of utilisation has to be maximised on different levels. Here, heterogeneous multiphase and composite materials with different constituents come into play due to their ability to adjust their behaviour and overall characteristic properties to stated requirements, like optimal strength-to-weight ratios. The spatial distribution of individual and so-called microscale constituents on the so-called mesoscale, the individual properties of each constituent as well as their size and shape have a strong influence on the overall mechanical behaviour on the macroscopic structural level. The schematic layout of scale nomenclature is pictured in Fig. 4.1. To be able to postulate reliable predictions about the overall behaviour or possible failure scenarios, fundamental knowledge about the physical behaviour on lower scales is required. This requirement represents an enormous challenge, namely to find formulations for the analysis of the interaction between referred scales. Using FEM as the analysis tool of choice, a direct modelling of the microstructure within the coarse macroscale model of the stated problem is a possible strategy. The drawback is the enormous computational effort and the enormous memory consumption with the consequence that this approach is practically not realisable in many cases. Instead, homogenisation techniques are usually applied and act like a bridging approach for the coupling of structural and material scales. One major prerequisite for such homogenisation approaches is the existence of different length scales, i.e. the physical dimensions of referred scales have to be distinguishable. The principle of scale separation, which states $L_{\text{micro}} < L_{\text{meso}} \ll L_{\text{macro}}$ and is presented in Fig. 4.1, has to be fulfilled. Furthermore, to be able to derive phenomenological

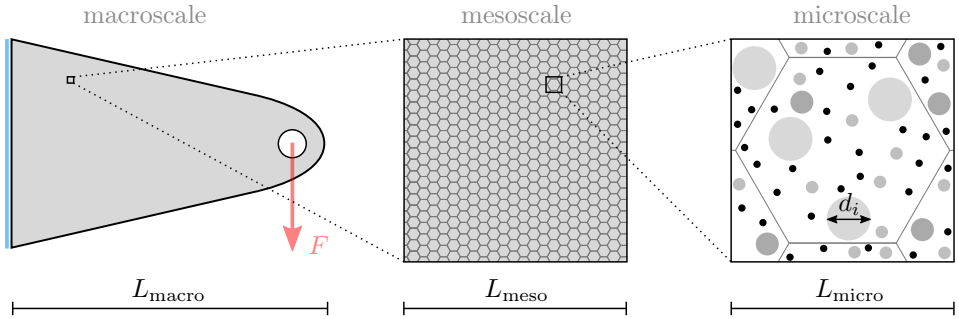

Figure 4.1: Principle of scale separation: macro-, meso- and microscale.

descriptions of the material behaviour on the macroscale, knowledge about mechanical properties, shape and orientation of each constituent on the microscale is required.

So far and over past decades, several groups and researchers developed a variety of theories, formulations and numerical realisations for aforementioned homogenisation of microheterogeneous materials and so-called multiscale methods. For instance, a basic introduction on numerical two-scale homogenisation methods is given in [183] or [130]. In the latter publication, based on the approach for micro to macro transitions, boundary value problems on both scales are formulated and enhanced by several details. Remarks on so-called effective parameters are also discussed. Extensive explanations on effective quantities in terms of upper and lower bounds for the effective response of underlying microstructures, i.e. in terms of Voigt and Reuss bounds, are given in [162] and [124] and also in [70, 71, 72, 73]. A general discussion on the well-known Hill-Mandel condition can be found in [70] and [69]. The Hill-Mandel condition postulates the equality of the stress power between upper and lower scales and is a fundamental principle for homogenisation approaches and discussions on moduli of mixtures. non-linear formulations in terms of geometrical non-linearities are investigated in [157] and [159] and are supplemented by frameworks for physical non-linearities in the works [102, 105, 106, 107]. A discussion on heterogeneous, non-linear and history dependent material behaviour, like elastoplasticity, can be found in [86] and [120], and especially on elastoviscoplastic materials in [145] for instance. Investigations on the convergence behaviour of microscopic stress values and elastoplastic mechanical responses on different scales are presented in [155]. Within the deformation driven context and deformation driven microstructures, solution strategies based on the Lagrange multiplier methods are discussed in [104]. On the other hand, solution strategies based on penalty methods can be found in [153]. Explanations on numerical implementations, algorithms and matrix representations of obtained formulations are summarised in [101] and [103] and several mathematical aspects within numerical homogenisation techniques are given in [151]. In all presented formulations and approaches, the choice of so-called unit cells or *representative volume elements* (RVE) is essential for reliable solutions. The authors in [8] and [9] investigated several aspects for the generation of such RVEs and suggested approaches for the construction of *statistically similar representative volume elements* (SSRVE) in two- and three-dimensional cases with much less complexity than the real microstructures. Based on minimisation of least-square functionals they were able to find simplified unit cell descriptions compared to

real microstructure morphology but with similar characteristics and mechanical behaviour. Aforementioned SSRVEs are also investigated in terms of heterogeneous materials in the context of linear and non-linear elasticity in [154]. The explanation of a possible numerical implementation of the computational homogenisation technique into an existing environment for structural analysis on single scales, i.e. into the structural analysis program FEAP, can be found in [83]. The authors extended their application of inverse analysis for an identification of material parameters of non-linear composites and viscoelastic heterogeneous materials by the application of the Levenberg–Marquardt method in [82] and [84]. Several extensions of the field of applications are proposed in several publications. For instance, the authors in [131] extended the basis formulation for electromechanically coupled boundary value problems, in [132] for magneto-electro-mechanically coupled boundary value problems or in [148] for ferromagnetic materials, which are characterized by a heterogeneous microstructure, that can be altered by external magnetic and mechanical stimuli. The enormous numerical effort and the enormous amount of data resulting from the solution of the mentioned complex BVPs on multiple scales is predestinated for developments of efficient formulations and solutions of described multiscale problems. The authors in [52] and [53] developed reduced order models based on *Nonuniform Transformation Field Analysis* (NTFA), which is an order reduction technique specifically designed for homogenization problems, and investigated thermo-mechanical properties of microheterogeneous materials in terms of polycrystalline aggregates, porous metals and particle reinforced composite materials as well as the non-linear behaviour of the interface between constituents.

A discussion on computational homogenisation, a general overview and a summary of developments is given in [149] and [100]. A variety of methods is presented in [109], and especially the article [57] reviews the state-of-the-art of computational homogenisation, discusses trends and upcoming challenges in this field and contains a historical overview and key principles on first-order computational homogenisation, which is used within the work at hand.

4.2 Mechanical two-scale problems

The aforementioned principle of scale separation is a fundamental prerequisite for any application of homogenisation techniques. Nevertheless, in literature there are differences in labelling the lower scales, i.e. the meso- and the microscale. In most cases where two-scale problems are considered, the microscale is directly identified with the so-called unit cell or *representative volume element* (RVE) and is used within numerical realisations. The mesoscale can be seen as an intermediate scale and is often omitted within numerical investigations. This is also the case in the presented work, i.e. the term *coupling the scales* is interpreted as the coupling of the macro- with the microscale. Based on the existence of different length-scales and the knowledge about physical properties of involved constituents, a solution strategy based on the direct modelling of the stated problem is expensive and impossible in most cases. The large amount of variables and the large amount of data obtained is often hardy interpretable. Therefore, solution strategies based on substitution of real material properties by effective or homogenised models are more attractive and are part of so-called multiscale or FE^2 problem formulations. Such approaches are still

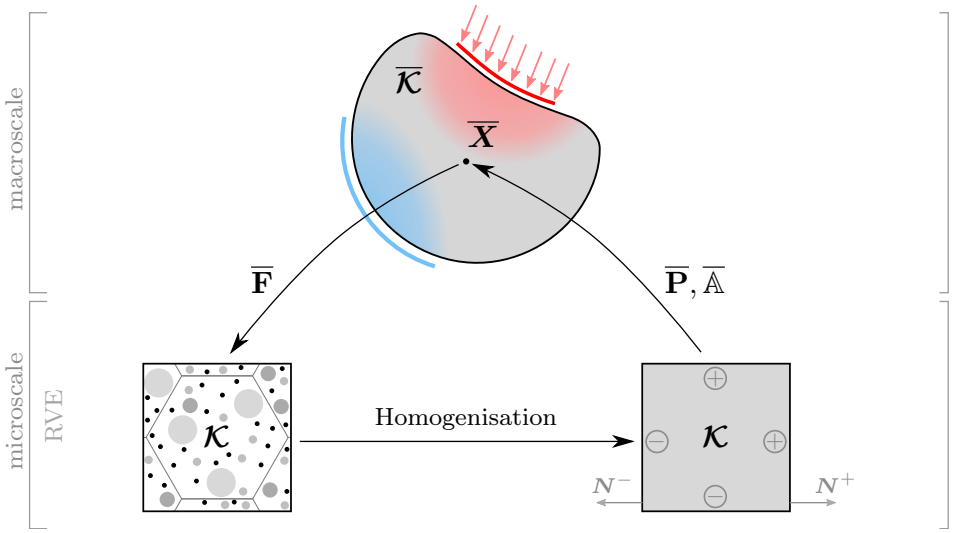

Figure 4.2: Basic homogenisation scheme.

expensive but the effort is not comparable to the direct solution of the real problem. Furthermore, a lot of formulations for the solution of mentioned two-scale problems are predestinated for parallel computing techniques on high performance computing clusters. This chapter's goal is to sample relations for mechanical two-scale problems and to obtain homogenised models for the material based on the solution of several BVPs on underlying microscales, which all contribute to the solution of the stated BVP on the macroscale.

Remark 4.1 (Macro and micro notation) *Throughout this work, all frequently used quantities connected to the macroscale are identified by overlines, i.e.* $\overline{(\cdot)}$*, and quantities connected to the microscale are represented without additional markers, i.e.* $(\cdot)$*.*

The basic concept of the homogenisation scheme is pictured in Fig. 4.2. The underlying RVE with the domain $\mathcal{K}$ is associated with each macroscopic referential point $\overline{\boldsymbol{X}}$ in the macroscopic domain $\overline{\mathcal{K}}$. The macroscopic deformation gradient $\overline{\mathbf{F}}$ in $\overline{\boldsymbol{X}}$ is the necessary driving factor for the formulation of boundary conditions for the microscopic BVP. The solution investigated within homogenisation approaches results in so-called effective stress and material parameters, i.e. $\overline{\mathbf{P}}$ and $\overline{\mathbb{A}}$. The effective response $\overline{\mathbf{P}}$ and $\overline{\mathbb{A}}$ of the microscale is finally involved in the solution of the macroscopic BVP. Most concepts presented in several books and publications basically include a similar sequence of following sub-tasks for a closed formulation of the solution of the BVP on the upper scale.

- **Representative volume element.** Choice or definition of an RVE on the microscale, where the physical properties of each microscopic constituent are known.
- **Coupling the scales.** Definition of physically useful effective variables on the macroscale (according to macro to micro context) for the formulation of microscopic boundary conditions and solution of the microscopic boundary value problem.

- **Homogenisation.** Application of useful homogenisation schemes and computation of effective quantities in terms of the microscopic deformation state and the effective response of the microscale.
- **Solution of stated BVP.** Solution of the stated macroscopic boundary value problem in terms of effective microscopic response and effective parameters.

4.3 Homogenisation methods and FE^2 techniques

Heterogeneities are part of most natural and non-natural materials and often cause anisotropic effects in stress and strain fields. Homogenisation methods and so-called FE^2 techniques allow to include these effects into overall investigations. Therefore, in this section the aforementioned aspects on mechanical two-scale problems are discussed. After some remarks on the choice of representative volume elements, averaging theorems and effective parameters, the formulation of boundary conditions on the microscale, the necessary setup for computational homogenisation schemes based on the continuous setup for multiscale problems are presented. The notation of following descriptions is related to the formulations in [21], [103], [101] and [107]. A lot of extensive details and explanations can be found in the cited literature in the beginning of this chapter.

4.3.1 Representative volume element (RVE)

As already mentioned, most homogenisation techniques are based on so-called *unit cells* or *representative volume elements* (RVE). The whole material distribution within the stated BVP has to be statistically represented by the chosen RVE. Unit cells have to represent the smallest sample of the overall material distribution. For the representation of typical, structural properties of interest on average, they have to contain enough microscopic heterogeneities. Simultaneously, their physical size has to comply with the principle of scale separation, which is pictured in Fig. 4.1 and explicitly reads

$$L_{\mathrm{micro}} < \; L_{\mathrm{meso}} \ll L_{\mathrm{macro}}. \tag{4.1}$$

Furthermore, the representative choice has to be independent of its placement in the context of the macrostructure and the macroscopic domain $\overline{\boldsymbol{\mathcal{K}}}$. In general, details concerning the size and shape of RVEs cannot be specified, except in some special cases.

4.3.2 Effective field variables

Regarding the macroscopic referential point $\overline{\boldsymbol{X}}$ in the macroscopic domain $\overline{\boldsymbol{\mathcal{K}}}$, two different kinds of field variables can be identified:

- **local variables,** connected with the underlying RVE and
- **effective variables,** resulting from the homogenised microscopic domain $\boldsymbol{\mathcal{K}}$.

For coupling the referred scales, it is necessary to define macroscopic effective variables in terms of local microscopic variables, which are exclusively formulated on the boundary of the microscopic domain $\partial\boldsymbol{\mathcal{K}}$. For this purpose, it is useful to take the deformation gradient

$\mathbf{F}$ as the central kinematic variable due to its advantage of being valid for domains with and without discontinuities. Together with its work-conjugated quantity, i.e. with the first Piola-Kirchhoff stress tensor $\mathbf{P}$, both represent well-suited effective parameters.

For the representation of effective parameters or of volume averaged quantities, the following notation is used throughout the work

$$\overline{(\cdot)} = \langle (\cdot) \rangle = \frac{1}{V} \int_{\boldsymbol{\mathcal{K}}} (\cdot) \, \mathrm{d}V. \tag{4.2}$$

Considering the averaging theorem in Eq. (4.2), the macroscopic deformation gradient can be formulated as the volume average of the microscopic deformation gradient, i.e.

$$\overline{\mathbf{F}} = \frac{1}{V} \int_{\boldsymbol{\mathcal{K}}} \mathbf{F} \, \mathrm{d}V = \frac{1}{V} \int_{\partial \boldsymbol{\mathcal{K}}} \boldsymbol{\varphi} \otimes \boldsymbol{N} \, \mathrm{d}A, \tag{4.3}$$

where the divergence theorem is used to obtain an expression in terms of the surface integral of the micro domain. In a similar fashion, effective first Piola-Kirchhoff stresses can be obtained from the volume average of microscopic first Piola-Kirchhoff stresses and the relation $\boldsymbol{t} = \mathbf{P}\boldsymbol{N}$ for the surface traction vector on the boundary of the underlying domain by

$$\overline{\mathbf{P}} = \frac{1}{V} \int_{\boldsymbol{\mathcal{K}}} \mathbf{P} \, \mathrm{d}V = \frac{1}{V} \int_{\partial \boldsymbol{\mathcal{K}}} \boldsymbol{t} \otimes \boldsymbol{X} \, \mathrm{d}A. \tag{4.4}$$

Using the effective deformation gradient $\overline{\mathbf{F}}$, the effective first Piola-Kirchhoff stress tensor $\overline{\mathbf{P}}$ and the Jacobian $J_F = \mathrm{d}v/\mathrm{d}V$, further effective stress measurements can be obtained, e.g. the Kirchhoff, Cauchy or second Piola-Kirchhoff stress tensors read

$$\overline{\boldsymbol{\tau}} = \overline{\mathbf{P}} \, \overline{\mathbf{F}}^T, \qquad \overline{\mathbf{T}} = \frac{1}{J_F} \overline{\mathbf{P}} \, \overline{\mathbf{F}}^T, \qquad \overline{\mathbf{S}} = \overline{\mathbf{F}}^{-1} \overline{\mathbf{P}}. \tag{4.5}$$

Finally, the fundamental principle within multiscale and homogenisation approaches, i.e. the aforementioned and well-known Hill-Mandel condition, see [70], can be formulated

$$\overline{\mathbf{P}} : \dot{\overline{\mathbf{F}}} = \frac{1}{V} \int_{\boldsymbol{\mathcal{K}}} \mathbf{P} : \dot{\mathbf{F}} \, \mathrm{d}V = \frac{1}{V} \int_{\partial \boldsymbol{\mathcal{K}}} \boldsymbol{t} \cdot \dot{\boldsymbol{\varphi}} \, \mathrm{d}A. \tag{4.6}$$

It postulates, that the local stress power on the macro scale (first term in Eq. (4.6)) has to be equal to the volume average of the microscopic stress power in the RVE.

4.3.3 Boundary conditions for homogenisation methods

The aforementioned Hill-Mandel condition in Eq. (4.6) and following boundary conditions in Eq. (4.7) formulated on the surface $\partial \boldsymbol{\mathcal{K}}$ of the RVE, which satisfy the stated relation (4.6) a priori, are subject of many investigations, for instance in the work [149]. Within the deformation driven context, all boundary conditions have to be formulated in terms of

the macroscopic deformation gradient $\overline{\mathbf{F}}$.

$$\begin{aligned} &\text{(D)} && \text{Linear displacements} && \boldsymbol{\varphi} = \overline{\mathbf{F}}\boldsymbol{X}, \\ &\text{(P)} && \text{Periodic displacements} && [\![\boldsymbol{\varphi}]\!] = \overline{\mathbf{F}}[\![\boldsymbol{X}]\!] \quad \text{and} \quad \boldsymbol{t}^+ = -\boldsymbol{t}^-, \\ &\text{(S)} && \text{Uniform tractions} && \boldsymbol{t} = \overline{\mathbf{P}}\boldsymbol{N}. \end{aligned} \tag{4.7}$$

Here, $[\![(\cdot)]\!] = (\cdot)^+ - (\cdot)^-$ indicates the jump of the field $(\cdot)$ and the quantities $(\cdot)^+$ and $(\cdot)^-$ can be identified as elements of the periodic point sets $\partial\boldsymbol{\mathcal{K}}^+$ and $\partial\boldsymbol{\mathcal{K}}^-$ on the surface $\partial\boldsymbol{\mathcal{K}}$ of the underlying RVE, cf. Fig. 4.2 or Fig. 4.3. For materials with periodically distributed properties, the periodic displacement formulation (P) is expected to deliver best results.

4.3.4 General setup and solution of homogenisation problems

Definition of the aforementioned micro to macro transition as an energy minimisation problem for microstructures with constituents of standard materials is possible and is presented by the authors in [101, 102] and [105]. Therefore, an exact geometrical resolution of the referred microscale has to be possible and a non-linear elastic material behaviour is considered within this work. The relation in Eq. (4.8), which depends on the microscopic deformation $\boldsymbol{\varphi}$, which itself is induced by the macroscopic deformation $\overline{\mathbf{F}}$,

$$\overline{W}(\overline{\mathbf{F}}) = \inf_{\boldsymbol{\varphi}} \; \tilde{W}(\boldsymbol{\varphi}), \qquad \text{with} \qquad \widetilde{W}(\boldsymbol{\varphi}) = \frac{1}{V}\int_{\boldsymbol{\mathcal{K}}} W(\nabla\boldsymbol{\varphi}; \boldsymbol{X}) \, \mathrm{d}V, \tag{4.8}$$

minimises the average energy of the microstructure after enforcement of introduced boundary conditions from Eq. (4.7) on the microscale, i.e. after enforcement of linear displacements (D), periodic displacements (P) or uniform tractions (S). Note that $V \cdot \widetilde{W}(\boldsymbol{\varphi})$ can be identified with the total energy of the microstructure. The boundary conditions $\{\mathrm{D}, \mathrm{P}, \mathrm{S}\}$ can be applied using the standard Lagrange formalism, which is already presented in Problem 3.3, and allows to recast Eq. (4.8) into the following saddle point problem

$$\overline{W}_{\mathrm{I}}^{\lambda}(\overline{\mathbf{F}}; \overline{\boldsymbol{X}}) = \inf_{\boldsymbol{\varphi}} \sup_{\lambda_{\mathrm{I}}} \left\{ \frac{1}{V}\int_{\boldsymbol{\mathcal{K}}} W(\nabla\boldsymbol{\varphi}; \boldsymbol{X}) \, \mathrm{d}V - c_{\mathrm{I}}(\boldsymbol{\varphi}, \boldsymbol{\lambda}_{\mathrm{I}}; \overline{\mathbf{F}}) \right\}. \tag{4.9}$$

Here, a general form of enforced constraints c_{I} and a general description of the necessary Lagrange multiplier $\boldsymbol{\lambda}_{\mathrm{I}}$ for introduced classes of boundary conditions $\mathrm{I} = \{\mathrm{D}, \mathrm{P}, \mathrm{S}\}$ is used. The explicit formulations for all three types are given by

$$\begin{aligned} c_{\mathrm{D}}(\boldsymbol{\varphi}, \boldsymbol{\lambda}_{\mathrm{D}}; \overline{\mathbf{F}}) &:= \frac{1}{V}\int_{\partial\boldsymbol{\mathcal{K}}} \boldsymbol{\lambda}_{\mathrm{D}} \cdot (\boldsymbol{\varphi} - \overline{\mathbf{F}}\boldsymbol{X}) \, \mathrm{d}A, \\ c_{\mathrm{P}}(\boldsymbol{\varphi}, \boldsymbol{\lambda}_{\mathrm{P}}; \overline{\mathbf{F}}) &:= \frac{1}{V}\int_{\partial\boldsymbol{\mathcal{K}}^+} \boldsymbol{\lambda}_{\mathrm{P}} \cdot ([\![\boldsymbol{\varphi}]\!] - \overline{\mathbf{F}}[\![\boldsymbol{X}]\!]) \, \mathrm{d}A, \\ c_{\mathrm{S}}(\boldsymbol{\varphi}, \boldsymbol{\lambda}_{\mathrm{S}}; \overline{\mathbf{F}}) &:= \frac{1}{V}\int_{\partial\boldsymbol{\mathcal{K}}} (\boldsymbol{\lambda}_{\mathrm{S}}\boldsymbol{N}) \cdot \boldsymbol{\varphi} \, \mathrm{d}A - \boldsymbol{\lambda}_{\mathrm{S}} : \overline{\mathbf{F}}. \end{aligned} \tag{4.10}$$

Finally, the Lagrange functionals for minimisation with respect to the deformation $\boldsymbol{\varphi}$ in terms of the deformation driven context and with explicit constraints on the boundary of

the microstructure can be formulated by

$$
\begin{aligned}
&\text{(D)} \qquad \overline{W}^{\lambda}_{\mathrm{D}}(\overline{\mathbf{F}};\overline{\boldsymbol{X}}) = \inf_{\boldsymbol{\varphi}} \sup_{\lambda_{\mathrm{D}}} \left\{ \widetilde{W}(\boldsymbol{\varphi}) - \frac{1}{V}\int_{\partial\boldsymbol{\mathcal{K}}} \boldsymbol{\lambda}_{\mathrm{D}} \cdot (\boldsymbol{\varphi} - \overline{\mathbf{F}}\boldsymbol{X})\, \mathrm{d}A \right\},\\
&\text{(P)} \qquad \overline{W}^{\lambda}_{\mathrm{P}}(\overline{\mathbf{F}};\overline{\boldsymbol{X}}) = \inf_{\boldsymbol{\varphi}} \sup_{\lambda_{\mathrm{P}}} \left\{ \widetilde{W}(\boldsymbol{\varphi}) - \frac{1}{V}\int_{\partial\boldsymbol{\mathcal{K}}^{+}} \boldsymbol{\lambda}_{\mathrm{P}} \cdot (\llbracket\boldsymbol{\varphi}\rrbracket - \overline{\mathbf{F}}\llbracket\boldsymbol{X}\rrbracket)\, \mathrm{d}A \right\},\\
&\text{(S)} \qquad \overline{W}^{\lambda}_{\mathrm{S}}(\overline{\mathbf{F}};\overline{\boldsymbol{X}}) = \inf_{\boldsymbol{\varphi}} \sup_{\lambda_{\mathrm{S}}} \left\{ \widetilde{W}(\boldsymbol{\varphi}) - \frac{1}{V}\int_{\partial\boldsymbol{\mathcal{K}}} (\boldsymbol{\lambda}_{\mathrm{S}}\boldsymbol{N}) \cdot \boldsymbol{\varphi}\, \mathrm{d}A - \boldsymbol{\lambda}_{\mathrm{S}} : \overline{\mathbf{F}} \right\}.
\end{aligned}
\tag{4.11}
$$

The effective stress and material parameters can be obtained directly from Eq. (4.9) by

$$
\overline{\mathbf{P}}_{\mathrm{I}} = \partial_{\overline{\mathbf{F}}}\, \overline{W}^{\lambda}_{\mathrm{I}} \qquad \text{and} \qquad \overline{\mathbb{A}}_{\mathrm{I}} = \partial_{\overline{\mathbf{F}}}\, \overline{\mathbf{P}}_{\mathrm{I}} = \partial^{2}_{\overline{\mathbf{F}}\overline{\mathbf{F}}}\, \overline{W}^{\lambda}_{\mathrm{I}}. \tag{4.12}
$$

Eq. (4.9) indicates that only constraints c_{I} depend on the macroscopic deformation gradient $\overline{\mathbf{F}}$ and therefore, the explicit homogenised stresses can be obtained from

$$
\begin{aligned}
&\text{(D)} \qquad \overline{\mathbf{P}}_{\mathrm{D}} = \partial_{\overline{\mathbf{F}}}\, c_{\mathrm{D}} = \frac{1}{V}\int_{\partial\boldsymbol{\mathcal{K}}} \boldsymbol{\lambda}_{\mathrm{D}} \otimes \boldsymbol{X}\, \mathrm{d}A,\\
&\text{(P)} \qquad \overline{\mathbf{P}}_{\mathrm{P}} = \partial_{\overline{\mathbf{F}}}\, c_{\mathrm{P}} = \frac{1}{V}\int_{\partial\boldsymbol{\mathcal{K}}^{+}} \boldsymbol{\lambda}_{\mathrm{P}} \otimes \llbracket\boldsymbol{X}\rrbracket\, \mathrm{d}A,\\
&\text{(S)} \qquad \overline{\mathbf{P}}_{\mathrm{S}} = \partial_{\overline{\mathbf{F}}}\, c_{\mathrm{S}} = \boldsymbol{\lambda}_{\mathrm{S}}.
\end{aligned}
\tag{4.13}
$$

Within the chosen homogenisation approach it is possible to derive homogenised quantities exclusively from surface terms of the microstructure. It can be observed that in Eq. (4.13) the Lagrange multipliers $\boldsymbol{\lambda}_{\mathrm{D}}$ and $\boldsymbol{\lambda}_{\mathrm{P}}$ for linear and periodic displacements, respectively, can be identified as traction vectors on the boundary of the microstructure. Whereas the Lagrange multiplier $\boldsymbol{\lambda}_{\mathrm{S}}$ corresponds to homogenised stresses directly. Extended details and derivations of all presented relations can be found in [21, 101, 102, 105] and [103]. The used notation is also adopted from mentioned publications.

4.4 Computational homogenisation

For a numerical implementation of the general homogenisation approach and the micro to macro transition, introduced relations in previous sections have to be transferred to their discretised counterparts. For this purpose, standard finite element techniques and approximations, which are known from standard text books and are briefly summarised in Section 5.4 and Section 5.6, respectively, can be utilised. One point, which has to be mentioned is, that due to the principle of scale separation, RVEs representing the microstructure are coupled point-wise with the upper scale. The consequence within the application of FEM is, that the chosen discretised RVE is connected individually to each integration point or Gaussian point of the discretised upper scale. Therefore, a series of microscopic BVPs with several test loadings induced by the macroscopic deformation gradient $\overline{\mathbf{F}}$ in each macroscopic integration point have to be solved, to be able to search for the solution of one macroscopic BVP. Available analytical approaches are restricted in many ways. Most of them are usable only for linear elastic material behaviour and are

related to representative microstructures with simple and not changing geometry models. Therefore, the upcoming formulations for numerical investigations present a versatile extension to existing and so far widely spread analytical approaches.

After a spatial FE discretisation of the energy minimisation problem of homogenisation in Eq. (4.8), the following finite-dimensional minimisation problem is obtained

$$\overline{W}(\overline{\boldsymbol{F}}) = \inf_{\boldsymbol{v}} \widetilde{W}(\boldsymbol{v}) \qquad \text{with} \qquad \widetilde{W}(\boldsymbol{v}) = \frac{1}{V}\int_{\mathcal{K}} W(\boldsymbol{F};\boldsymbol{X})\,\mathrm{d}V. \tag{4.14}$$

According to its continuous form, the total energy of the microstructure reads $V \cdot \widetilde{W}(\boldsymbol{v})$. Referring explanations in Section 5.3 and Section 5.3.1, the physical residual and the physical stiffness tangent operator in the context of homogenisation can be derived in a similar fashion. The partial derivative of the discrete energy functional from Eq. (4.14) with respect to the state variable $\boldsymbol{v}$ yields

$$\begin{aligned} &\text{Physical residual vector:} && \boldsymbol{R}(\boldsymbol{v}) = V \cdot \partial_{\boldsymbol{v}}\, \widetilde{W}(\boldsymbol{v}), && \text{with} \quad \boldsymbol{R} \in \mathbb{R}^{n_v}, \\ &\text{Physical stiffness matrix:} && \boldsymbol{K}(\boldsymbol{v}) = V \cdot \partial^2_{\boldsymbol{v}\boldsymbol{v}}\, \widetilde{W}(\boldsymbol{v}), && \text{with} \quad \boldsymbol{K} \in \mathbb{R}^{n_v \times n_v}. \end{aligned} \tag{4.15}$$

The dimension n_v represents the overall number of discrete state variables or degrees of freedom, which results from the overall number of FE nodes n_N and the number of degrees of freedom per node n_d, i.e. $n_v = n_N \cdot n_d$.

Remark 4.2 (Contribution of external loads to microscopic energy) *Due to the existence of different length scales and the associated principle of scale separation, contributions of external loads, in terms of physical body forces* $\boldsymbol{b}$ *per unit volume and prescribed surface tractions* $\bar{\boldsymbol{t}}$*, can be neglected on the lower scale. The loading situation of the microstructure is induced by the macroscopic deformation gradient* $\overline{\boldsymbol{F}}$ *and therefore, the deformation of the surface of the microstructure is the present loading scenario. A further consequence is, that the defined relation in Eq.* (5.98) *for the overall energy potential coincides with the internal strain energy and necessary variations and linearisations for physical residual and tangent operators include only contributions of internal parts.*

4.4.1 Discrete relations for homogenisation

The authors in [21] and [103] presented a very elegant tactic for the numerical solution of the above introduced homogenisation problem. Their approach and their notation are adopted in the following and useful preparations for the usage within frameworks for structural optimisation and material design in upcoming Chapter 6 are made. After partitioning of contributions of degrees of freedom, discretised relations for explicit boundary conditions are presented, which are finally used within the discrete setup for the minimisation problem of homogenisation. The solution scheme follows a process similar to a classical Newton iteration procedure.

The very first step is the partitioning of nodes of the underlying FE mesh of the discretised domain $\mathcal{K}$. Two sets of nodes can be distinguished: the nodes in the interior of the domain $\mathcal{K}$, i.e. nodes indicated by the (i), and nodes on the boundary $\partial\mathcal{K}$ of the RVE, i.e. nodes indicated by the index (b). Fig. 4.3 can be referred for a schematic

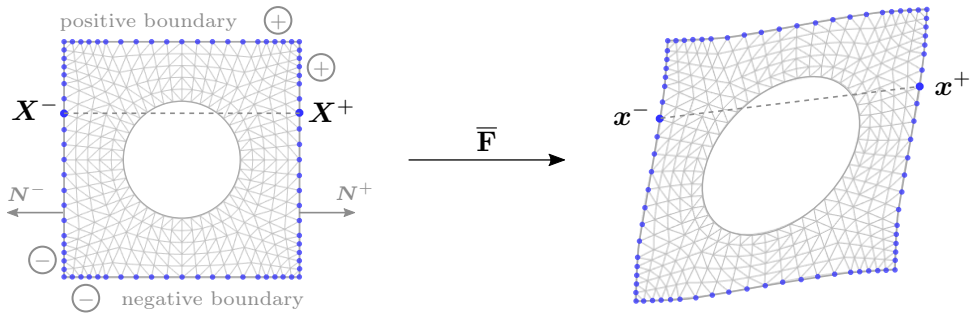

Figure 4.3: Separation of nodes on boundary (blue).

clarification. The introduction of the set (i, b) has a similar fashion to the partitioning of discrete sensitivity relations, which is explained and extended with a partitioning of design parameters in Section 5.5. The number of quantities in set (i) is given by n_i and the number of quantities in set (b) is given by n_b. The partitioning of physical quantities is realised by so-called projection matrices

$$\mathbb{P}_\mathrm{i} \in \mathbb{R}^{n_d \cdot (n_N - n_B) \times n_d \cdot n_N} \qquad \text{and} \qquad \mathbb{P}_\mathrm{b} \in \mathbb{R}^{n_d \cdot n_B \times n_d \cdot n_N}. \tag{4.16}$$

The projection matrix $\mathbb{P}_\mathrm{i}$ defines the interior contribution and the projection matrix $\mathbb{P}_\mathrm{b}$ defines the contribution on the boundary. Here, n_N corresponds to the overall number of nodes of the FE mesh, n_B is the number of nodes on the boundary and $n_B \leq n_N$, and n_d indicates the number of degrees of freedom per node. With this notation at hand and similar to the partitioned relations in Section 5.5, a partitioning of state variables, the physical residual vector and the physical stiffness matrices are presented in Eq. (4.17).

$$\begin{aligned} \boldsymbol{v} = \begin{bmatrix} \boldsymbol{v}_\mathrm{i} \\ \boldsymbol{v}_\mathrm{b} \end{bmatrix} &:= \begin{bmatrix} \mathbb{P}_\mathrm{i}\, \boldsymbol{v} \\ \mathbb{P}_\mathrm{b}\, \boldsymbol{v} \end{bmatrix}, \quad \boldsymbol{R} = \begin{bmatrix} \boldsymbol{R}_\mathrm{i} \\ \boldsymbol{R}_\mathrm{b} \end{bmatrix} := \begin{bmatrix} \mathbb{P}_\mathrm{i}\, \boldsymbol{R} \\ \mathbb{P}_\mathrm{b}\, \boldsymbol{R} \end{bmatrix}, \\ \boldsymbol{K} = \begin{bmatrix} \boldsymbol{K}_\mathrm{ii} & \boldsymbol{K}_\mathrm{ib} \\ \boldsymbol{K}_\mathrm{bi} & \boldsymbol{K}_\mathrm{bb} \end{bmatrix} &:= \begin{bmatrix} \mathbb{P}_\mathrm{i}\, \boldsymbol{K}\, \mathbb{P}_\mathrm{i}^T & \mathbb{P}_\mathrm{i}\, \boldsymbol{K}\, \mathbb{P}_\mathrm{b}^T \\ \mathbb{P}_\mathrm{b}\, \boldsymbol{K}\, \mathbb{P}_\mathrm{i}^T & \mathbb{P}_\mathrm{b}\, \boldsymbol{K}\, \mathbb{P}_\mathrm{b}^T \end{bmatrix}. \end{aligned} \tag{4.17}$$

After the prerequisite of decomposition of contributions, discrete formulations for the boundary conditions in Eq. (4.11) on the microscale are required. In the following, the three introduced classes of constraints are discussed, i.e. linear displacements (D), periodic displacements (P) or uniform tractions (S). All formulations are based on the macroscopic deformation gradient $\overline{\mathbf{F}}$. Within the numerical realisation, $\overline{\mathbf{F}}$ is used in its matrix representation obtained from the explanations on the Voigt notation in Chapter 2, i.e. for the two-dimensional case $\overline{\boldsymbol{F}}$ reads $\underline{\overline{\boldsymbol{F}}} = \begin{bmatrix} \overline{F}_{11} & \overline{F}_{22} & \overline{F}_{12} & \overline{F}_{21} \end{bmatrix}^T$ and for completeness, the three-dimensional case reads $\underline{\overline{\boldsymbol{F}}} = \begin{bmatrix} \overline{F}_{11} & \overline{F}_{22} & \overline{F}_{33} & \overline{F}_{23} & \overline{F}_{32} & \overline{F}_{13} & \overline{F}_{31} & \overline{F}_{12} & \overline{F}_{21} \end{bmatrix}^T$. For notational simplicity, here, only the two-dimensional case is considered, i.e. $d = 2$, and therefore, $\boldsymbol{X}_q = \begin{bmatrix} X_1 & X_2 \end{bmatrix}_q^T$ as position vector of node q on the surface of the RVE

in the reference configuration and $\boldsymbol{x}_q = \begin{bmatrix} x_1 & x_2 \end{bmatrix}_q^T$ as position vector of same node q in deformed configuration is assumed.

Linear displacements. All linear displacement constraints (D) of nodes on the surface of the RVE in terms of partitioned state variables $\boldsymbol{v}_\mathrm{b}$ can be represented by the relation

$$\boldsymbol{v}_\mathrm{b} - \mathcal{D}^T(\underline{\overline{\boldsymbol{F}}} - \underline{\boldsymbol{I}}) = \boldsymbol{0}, \tag{4.18}$$

with $\underline{\boldsymbol{I}} = \begin{bmatrix} 1 & 1 & 0 & 0 \end{bmatrix}^T$ being the column matrix representation of the identity matrix $\boldsymbol{I}$. Furthermore, a global coordinate matrix $\mathcal{D} \in \mathbb{R}^{d^2 \times n_B}$ is considered, i.e.

$$\mathcal{D} = \begin{bmatrix} \mathcal{D}_1 & \mathcal{D}_2 & \dots & \mathcal{D}_{n_B} \end{bmatrix}. \tag{4.19}$$

The matrix $\mathcal{D}$ contains coordinates of each node $\boldsymbol{X}_q$ with $q = 1, \dots, n_B$ on the surface of the underlying RVE in terms of matrices $\mathcal{D}_q \in \mathbb{R}^{d^2 \times d}$. Each matrix $\mathcal{D}_q$ has the following explicit form

$$\mathcal{D}_q := \begin{bmatrix} X_1 & 0 \\ 0 & X_2 \\ X_2 & 0 \\ 0 & X_1 \end{bmatrix}_q . \tag{4.20}$$

Periodic displacements. To obtain a suitable formulation of periodic boundary conditions (P) for the numerical implementation, it is important to define pairs of nodal coordinates $\boldsymbol{X}_q^+$ and $\boldsymbol{X}_q^-$ associated with positive and negative boundaries $\partial\boldsymbol{\mathcal{K}}^+$ and $\partial\boldsymbol{\mathcal{K}}^-$, respectively, as indicated in Fig. 4.3. In the presented scheme, $n_P = n_B/2 + 2$ couples of nodes can be identified. For each pair, the periodicity condition $[\![\boldsymbol{v}_\mathrm{b}]\!] = (\underline{\overline{\boldsymbol{F}}} - \underline{\boldsymbol{I}})[\![\boldsymbol{X}_q]\!]$ with already introduced jump notation $[\![\boldsymbol{v}_\mathrm{b}]\!] = \boldsymbol{v}_\mathrm{b}^+ - \boldsymbol{v}_\mathrm{b}^-$ and $[\![\boldsymbol{X}_q]\!] = \boldsymbol{X}_q^+ - \boldsymbol{X}_q^-$ is used. To reformulate the periodicity condition to a representation similar to linear displacement condition, the coordinate matrix in Eq. (4.20) can be referred and yields $\boldsymbol{v}_\mathrm{b}^+ - \boldsymbol{v}_\mathrm{b}^- = (\mathcal{D}_q^{+T} - \mathcal{D}_q^{-T})(\underline{\overline{\boldsymbol{F}}} - \underline{\boldsymbol{I}})$ for the nodes $q = 1, \dots, n_P$. The discretised form of all constraints in terms of partitioned state variables $\boldsymbol{v}_\mathrm{b}$ reads

$$\mathcal{P}\,\boldsymbol{v}_\mathrm{b} - \mathcal{P}\,\mathcal{D}^T(\underline{\overline{\boldsymbol{F}}} - \underline{\boldsymbol{I}}) = \boldsymbol{0}, \tag{4.21}$$

with the topology matrix $\mathcal{P} \in \mathbb{R}^{n_P \times n_B}$ including only values $\{0, 1, -1\}$. The entries of the matrix $\mathcal{P}$ can be constructed using following cases

$$\mathcal{P}_{ij} = \begin{cases} 1 & \text{for } i = j, \\ -1 & \text{for coupled nodes on surface, i.e. } i \neq j, \\ 0 & \text{otherwise.} \end{cases} \tag{4.22}$$

Uniform tractions. The discrete formulation of the boundary constraint (S) for uniform tractions on the surface of the RVE in its final form reads

$$\mathcal{A}\,\boldsymbol{v}_{\mathrm{b}} - V(\overline{\underline{\boldsymbol{F}}} - \underline{\boldsymbol{I}}) = \boldsymbol{0}. \tag{4.23}$$

Here, a global matrix $\mathcal{A} \in \mathbb{R}^{d^2 \times n_B}$ is used and contains components $\mathcal{A}_q \in \mathbb{R}^{d^2 \times d}$, i.e.

$$\mathcal{A} = \begin{bmatrix} \mathcal{A}_1 & \mathcal{A}_2 & \dots & \mathcal{A}_{n_B} \end{bmatrix}, \qquad \text{and} \qquad \mathcal{A}_q := \begin{bmatrix} \boldsymbol{A}_1 & 0 \\ 0 & \boldsymbol{A}_2 \\ \boldsymbol{A}_2 & 0 \\ 0 & \boldsymbol{A}_1 \end{bmatrix}_q . \tag{4.24}$$

Components ($\boldsymbol{A}_1$,$\boldsymbol{A}_2$) in $\mathcal{A}_q$ represent entries of the discrete normal area vector $\boldsymbol{A}_q$ at node q in the referential configuration. It results from the limit of its continuous counterpart $\boldsymbol{N}\,\mathrm{d}A \to \boldsymbol{A}_q$, with outward normal $\boldsymbol{N}$, and is connected to the discretised surface integral.

4.4.2 General form of discrete boundary conditions

The chosen structure of introduced boundary conditions {D, P, S} in Eq. (4.18), Eq. (4.21) and Eq. (4.24), respectively, and their obvious similarity, allows to find a general formulation for the representation of boundary conditions and to use this unique and compact notation for further purposes and investigations. This general form is defined by

$$\mathcal{S}_1\,\boldsymbol{v}_{\mathrm{b}} - \mathcal{S}_2\,(\overline{\underline{\boldsymbol{F}}} - \underline{\boldsymbol{I}}) = \boldsymbol{0} \tag{4.25}$$

for introduced classes of boundary conditions I = {D, P, S} and the corresponding coefficient matrices $\mathcal{S}_1$ and $\mathcal{S}_2$ of following forms

$$\mathcal{S}_1 := \begin{cases} \mathcal{I} \in \mathbb{R}^{n_B \times n_B} & \text{(D)} \\ \mathcal{P} \in \mathbb{R}^{n_P \times n_B} & \text{(P)} \\ \mathcal{A} \in \mathbb{R}^{d^2 \times n_B} & \text{(S)} \end{cases} \qquad \text{and} \qquad \mathcal{S}_2 := \begin{cases} \mathcal{D}^T \in \mathbb{R}^{n_B \times d^2} & \text{(D)} \\ \mathcal{P}\,\mathcal{D}^T \in \mathbb{R}^{n_P \times d^2} & \text{(P)} \\ V\mathcal{I} \in \mathbb{R}^{d^2 \times d^2} & \text{(S)} \end{cases} \tag{4.26}$$

with $\mathcal{I}$ being an identity matrix. Further derivations, extended explanations and details in terms of the chosen notation can be found in [103] and [21].

4.4.3 Solution of the discrete minimisation problem of homogenisation

After the partitioning of contributions and the specification of boundary conditions in their discrete form, the discrete Lagrange functional as the basis for the solution procedure of the discrete minimisation problem of homogenisation can be stated in a general form

$$\overline{W}_{\mathrm{I}}^{\lambda}(\overline{\mathbf{F}}; \overline{\boldsymbol{X}}) = \inf_{\boldsymbol{v}} \sup_{\boldsymbol{\lambda}_{\mathrm{I}}} \left\{ \tilde{W}(\boldsymbol{v}) - \boldsymbol{\lambda}_{\mathrm{I}}^T \left[\mathcal{S}_1\,\boldsymbol{v}_{\mathrm{b}} - \mathcal{S}_2\,(\overline{\underline{\boldsymbol{F}}} - \underline{\boldsymbol{I}}) \right] \right\} \tag{4.27}$$

for introduced classes of boundary conditions I = {D, P, S}. To solve this problem in terms of minimisation, variations with respect to partitioned state variables $\boldsymbol{v}_{\mathrm{i}}$ and $\boldsymbol{v}_{\mathrm{b}}$ and with respect to the Lagrange multiplier $\boldsymbol{\lambda}_{\mathrm{I}}$ are necessary. The first variation yields

the Euler-Lagrange equations in Eq. (4.28), which are subsequently defined as residuals $\boldsymbol{R} = \begin{bmatrix}\boldsymbol{R}_\mathrm{i} & \boldsymbol{R}_\mathrm{b} & \boldsymbol{R}_\lambda\end{bmatrix}^T$ for the upcoming solution using a standard Newton scheme

$$\begin{aligned}
\boldsymbol{R}_\mathrm{i} &:= \boldsymbol{0} = \boldsymbol{R}_\mathrm{i}^\mathrm{int},\\
\boldsymbol{R}_\mathrm{b} &:= \boldsymbol{0} = \boldsymbol{R}_\mathrm{b}^\mathrm{int} - V\mathcal{S}_1^T\boldsymbol{\lambda}_\mathrm{I},\\
\boldsymbol{R}_\lambda &:= \boldsymbol{0} = \mathcal{S}_1\,\boldsymbol{v}_\mathrm{b} - \mathcal{S}_2\,(\underline{\overline{\boldsymbol{F}}} - \underline{\boldsymbol{I}}).
\end{aligned} \tag{4.28}$$

Typical Newton iterations require a linearisation of the residual in $\begin{bmatrix}\boldsymbol{v}_\mathrm{i} & \boldsymbol{v}_\mathrm{b} & \boldsymbol{\lambda}_\mathrm{I}\end{bmatrix}^T$, i.e.

$$\begin{aligned}
\boldsymbol{0} &= \boldsymbol{R}_\mathrm{i} + \boldsymbol{K}_\mathrm{ii}\Delta\boldsymbol{v}_\mathrm{i} + \boldsymbol{K}_\mathrm{ib}\Delta\boldsymbol{v}_\mathrm{b},\\
\boldsymbol{0} &= \boldsymbol{R}_\mathrm{i} + \boldsymbol{K}_\mathrm{bi}\Delta\boldsymbol{v}_\mathrm{i} + \boldsymbol{K}_\mathrm{bb}\Delta\boldsymbol{v}_\mathrm{b} - V\mathcal{S}_1^T\Delta\boldsymbol{\lambda}_\mathrm{I},\\
\boldsymbol{0} &= \boldsymbol{R}_\lambda + \mathcal{S}_1^T\Delta\boldsymbol{v}_\mathrm{b},
\end{aligned} \tag{4.29}$$

and an incremental update of state and Lagrange parameters

$$\boldsymbol{v} \Leftarrow \boldsymbol{v} + \Delta\boldsymbol{v} \qquad \text{and} \qquad \boldsymbol{\lambda}_\mathrm{I} \Leftarrow \boldsymbol{\lambda}_\mathrm{I} + \Delta\boldsymbol{\lambda}_\mathrm{I}. \tag{4.30}$$

Aforementioned sequence of steps and a detailed solution procedure is summarised in Algorithm 4.1 and is performed until a defined convergence criteria is fulfilled, e.g. in terms of the residual $|\boldsymbol{R}| < TOL_v$. In the solution point, i.e. in equilibrium state, effective quantities can be computed. Homogenised stresses and the overall tangent moduli can be obtained by the evaluation of Eq. (4.12) and result to

$$\overline{\underline{\boldsymbol{P}}}_{\mathrm{K,I}} := \partial_{\overline{\mathbf{F}}}\,\overline{W}_\mathrm{I}^\lambda = \mathcal{S}_2^T\boldsymbol{\lambda}_\mathrm{I} \quad \text{and} \quad \overline{\boldsymbol{A}}_\mathrm{I} := \partial^2_{\overline{\mathbf{F}}\overline{\mathbf{F}}}\overline{W}_\mathrm{I}^\lambda = \partial_{\overline{\mathbf{F}}}\,\overline{\underline{\boldsymbol{P}}}_{\mathrm{K,I}} = \mathcal{S}_2^T\frac{\partial\boldsymbol{\lambda}_\mathrm{I}}{\partial\overline{\mathbf{F}}} = \mathcal{S}_2^T\bar{\boldsymbol{K}}_\mathrm{I}\mathcal{S}_2. \tag{4.31}$$

It can be observed that effective stresses depend only on the Lagrange multiplier $\boldsymbol{\lambda}_\mathrm{I}$, i.e. on terms defined on the surface of the RVE, and the homogenised tangent moduli can be evaluated in terms of the condensed matrix $\bar{\boldsymbol{K}}_\mathrm{I}$ introduced and utilised in Algorithm 4.1.

4.4.4 Numerical implementation

Here, some hints and remarks on the numerical implementation are given. First, according to arguments and explanations in Remark 2.4, most routines in the implemented structural analysis and optimisation program MANO have the following form

$$f := f(\mathsf{M}, \overline{\boldsymbol{v}}, \mathsf{m}, \boldsymbol{v}). \tag{4.32}$$

Here, $\overline{\boldsymbol{v}}$ and $\boldsymbol{v}$ are macroscopic and microscopic displacement vectors, respectively. The variables M and m represent structure data types of models on the macro- and the microscale, respectively. Both contain geometrical model and technology data of stated BVPs. This structure of argument list allows perturbations of any kind of input variable and therefore, it is also useful for the verification of any linearised quantity or especially, of any derived sensitivity relation using numerical derivatives. For instance, with the notation $(\cdot)_c$ and the index c for changed or modified input quantities, perturbed function

Algorithm 4.1 Solution procedure for minimisation problem of homogenisation. Proposed solution schemes in [21, 101] and [103] are adopted to introduced notation to suit frameworks for structural optimisation.

Input: Model structure m with geometrical and technological data of stated BVP
Input: Macroscopic deformation gradient $\overline{\underline{F}}$ in column matrix form
Output: Effective stresses $\overline{\underline{P}}_{\mathrm{K,I}}$ and tangent moduli $\overline{\boldsymbol{A}}_{\mathrm{I}}$

procedure SOLVE HOMOGENISATION PROBLEM($\mathsf{m}, \overline{\underline{F}}$)
  `eval` $\{\mathcal{S}_1, \mathcal{S}_2\} \leftarrow$ Eq. (4.26) ▷ evaluate boundary conditions
  `eval` V ▷ evaluate volume of RVE
  `set` $\boldsymbol{v} = \boldsymbol{0}$, $\boldsymbol{\lambda}_{\mathrm{I}} = \boldsymbol{0}$ ▷ set initial values

  while $|\boldsymbol{R}| < TOL_v$ **do**
    // Assemble vector of internal forces and tangent of discretised RVE
    $\boldsymbol{R}^{\mathrm{int}}(\boldsymbol{v}) \leftarrow V \cdot \partial_{\boldsymbol{v}} \tilde{W}(\boldsymbol{v})$ and $\boldsymbol{K}(\boldsymbol{v}) \leftarrow V \cdot \partial^2_{\boldsymbol{vv}} \tilde{W}(\boldsymbol{v})$

    // Get partitioned contributions in terms of $(\cdot)_{\mathrm{i}} \in \mathcal{K}$ *and* $(\cdot)_{\mathrm{b}} \in \partial\mathcal{K}$
    $\boldsymbol{R}^{\mathrm{int}} = \begin{bmatrix} \boldsymbol{R}^{\mathrm{int}}_{\mathrm{i}} \\ \boldsymbol{R}^{\mathrm{int}}_{\mathrm{b}} \end{bmatrix}$ and $\boldsymbol{K} = \begin{bmatrix} \boldsymbol{K}_{\mathrm{ii}} & \boldsymbol{K}_{\mathrm{ib}} \\ \boldsymbol{K}_{\mathrm{bi}} & \boldsymbol{K}_{\mathrm{bb}} \end{bmatrix}$

    // Compute residuals
    $\boldsymbol{R}_{\mathrm{i}} = \boldsymbol{R}^{\mathrm{int}}_{\mathrm{i}}$
    $\boldsymbol{R}_{\mathrm{b}} = \boldsymbol{R}^{\mathrm{int}}_{\mathrm{b}} - V\mathcal{S}_1^T \boldsymbol{\lambda}_{\mathrm{I}}$
    $\boldsymbol{R}_{\lambda} = \mathcal{S}_1 \, \boldsymbol{v}_{\mathrm{b}} - \mathcal{S}_2 \, (\overline{\underline{F}} - \underline{\boldsymbol{I}})$

    $\boldsymbol{R} = \begin{bmatrix} \boldsymbol{R}_{\mathrm{i}} & \boldsymbol{R}_{\mathrm{b}} & \boldsymbol{R}_{\lambda} \end{bmatrix}^T$ ▷ residual for evaluation of convergence criteria

    // Compute condensed matrices
    $\tilde{\boldsymbol{R}}_{\mathrm{b}} = \boldsymbol{R}_{\mathrm{b}} - \boldsymbol{K}_{\mathrm{bb}} \boldsymbol{K}_{\mathrm{ii}}^{-1} \boldsymbol{R}_{\mathrm{i}}$ and $\tilde{\boldsymbol{K}}_{\mathrm{bb}} = \boldsymbol{K}_{\mathrm{bb}} - \boldsymbol{K}_{\mathrm{bb}} \boldsymbol{K}_{\mathrm{ii}}^{-1} \boldsymbol{K}_{\mathrm{ib}}$
    $\tilde{\boldsymbol{R}}_{\lambda} = \boldsymbol{R}_{\lambda} - \mathcal{S}_1 \tilde{\boldsymbol{K}}_{\mathrm{bb}}^{-1} \tilde{\boldsymbol{R}}_{\mathrm{b}}$ and $\bar{\boldsymbol{K}}_{\mathrm{I}} = \frac{1}{V} (\mathcal{S}_1 \tilde{\boldsymbol{K}}_{\mathrm{bb}}^{-1} \mathcal{S}_1^T)^{-1}$

    // Compute increments
    $\Delta\boldsymbol{\lambda}_{\mathrm{I}} = -\bar{\boldsymbol{K}}_{\mathrm{I}} \tilde{\boldsymbol{R}}_{\lambda}$
    $\Delta\boldsymbol{v}_{\mathrm{b}} = \tilde{\boldsymbol{K}}_{\mathrm{bb}}^{-1} (V\mathcal{S}_1^T \Delta\boldsymbol{\lambda}_{\mathrm{I}} - \tilde{\boldsymbol{R}}_{\mathrm{b}})$
    $\Delta\boldsymbol{v}_{\mathrm{i}} = -\boldsymbol{K}_{\mathrm{ii}}^{-1} (\boldsymbol{K}_{\mathrm{ib}} \Delta\boldsymbol{v}_{\mathrm{b}} + \boldsymbol{R}_{\mathrm{i}})$

    // Update state variable and Lagrange parameter
    $\boldsymbol{v} \leftarrow \boldsymbol{v} + \Delta\boldsymbol{v}$ and $\boldsymbol{\lambda}_{\mathrm{I}} \leftarrow \boldsymbol{\lambda}_{\mathrm{I}} + \Delta\boldsymbol{\lambda}_{\mathrm{I}}$
  end while

  // Compute homogenised values
  $\overline{\underline{P}}_{\mathrm{K,I}} = \mathcal{S}_2^T \boldsymbol{\lambda}_{\mathrm{I}}$ and $\overline{\boldsymbol{A}}_{\mathrm{I}} = \mathcal{S}_2^T \bar{\boldsymbol{K}}_{\mathrm{I}} \mathcal{S}_2$ ▷ effective stresses and tangent moduli
end procedure

values for computations of numerical derivatives can be obtained from

$$\begin{aligned} &\text{perturbed state:} && \tilde{f} = f(\mathsf{M}, \overline{\boldsymbol{v}}_c, \mathsf{m}, \boldsymbol{v}) \quad \text{or} \quad \tilde{f} = f(\mathsf{M}, \overline{\boldsymbol{v}}, \mathsf{m}, \boldsymbol{v}_c), \\ &\text{perturbed model data:} && \tilde{f} = f(\mathsf{M}_c, \overline{\boldsymbol{v}}, \mathsf{m}, \boldsymbol{v}) \quad \text{or} \quad \tilde{f} = f(\mathsf{M}, \overline{\boldsymbol{v}}, \mathsf{m}_c, \boldsymbol{v}). \end{aligned} \tag{4.33}$$

The overall structure and organisation of the program MANO for the structural analysis part is presented in the flowchart in Fig. 4.4 schematically. Using a material card, it can be distinguished between solution procedures based on single scale constitutive laws or based on solution of microscopic homogenisation problems in the integration points. The first case requires no definition of microscopic BVPs and therefore, the microscopic structure field with microscopic model data is set empty. Within the macroscopic BVP, the assembly process of global residual and tangent forms depends on homogenised parameters.

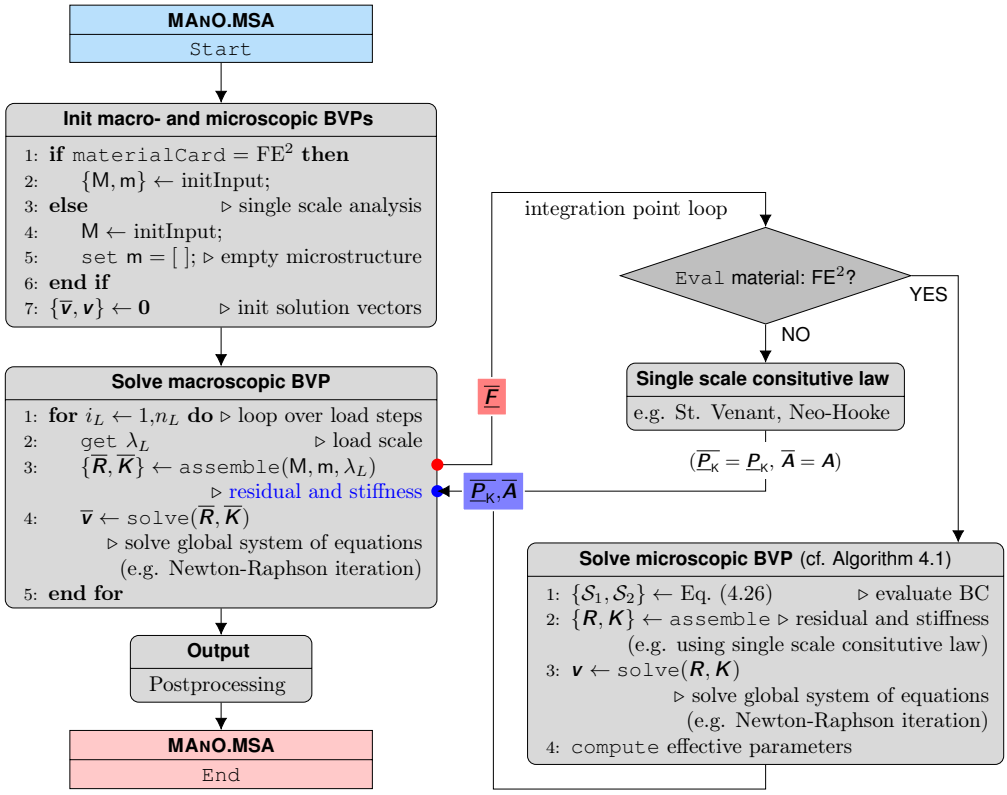

Figure 4.4: Principle framework for multiscale structural analysis (MANO.MSA)

4.5 Summary and concluding remarks

After a short overview on literature and relevant publications for the work at hand, a brief introduction to mechanical two-scale problems is given. The approach used for homogenisation based on the choice of effective field variables, representative volume elements (RVE) and the formulation of appropriate boundary conditions, here linear (D) and periodic (P) displacements as well as uniform tractions (S), is presented. A numerical solution procedure based on the general Lagrange formalism in terms of discretised relations is adapted from literature and implemented in the framework of the simulation program MAnO. Hints on the numerical implementation and the overall structure of the program, especially on the structural analysis part, are given.

The development of the software has been a work over past years. Different strategies for the determination of solutions have been implemented, tested and compared. Nevertheless, the presented approach appears to be the most promising method, especially when it comes to the solution of multiscale optimisation problems. Here, the multiscale structural analysis problem or FE^2 problem has to be solved many times in many optimisation iterations. Besides necessary adaptions for the availability of pre-compiled functions (so-called *mex-files* in MATLAB), the assembly routines for structural analysis are organised in a similar fashion to assembly routines for sensitivity analysis. The element routines are extended by additional options, which allow an efficient evaluation of sensitivity information on element level with regard to quantities, which are already available for structural analysis. The overall simulation and optimisation environment MAnO provides pre-conceived placeholders for different types of objective functions, constraints and design parameters, but also for extensions for a broad field of problem formulations from structural mechanics.

Chapter 5

Variations of physical quantities on single scales

In this chapter, the strategies and fundamental principles for variational sensitivity analysis based on known relations from continuum mechanics are outlined. Beside references on basic publications, essential coherences for this work are introduced. Relevant physical and mechanical quantities as well as their corresponding variations are discussed. The explicit discretised relations for the numerical treatment are summarised. Characteristic features are emphasised by some additional remarks.

5.1 Introduction

In general physical or mechanical problems, a non-linear state variable $\boldsymbol{v}$ is often the quantity of interest and represents the solution of stated *boundary value problems* (BVP) or *initial value problems* (IVP). In other words, seeked quantities are often the deformation state of a fixed referential configuration under prescribed loads or the distribution of a temperature field. In contrast to structural analysis (SA), where changes in the so-called current, spatial or physical configuration are observed, structural optimisation (SO) focuses on changes in the referential (initial or material) configuration. The major purpose of structural optimisation is to improve given structural systems in some proper sense and to propose reliable environments for predictions of the physical behaviour due to changes of initial design parameters. Basically, the field of structural optimisation and especially the design sensitivity analysis is driven by the following central question:

"How do resulting quantities change if input parameters are modified?"

The essential statements for answering this question can be deduced from the so-called design sensitivity analysis (DSA), which plays the key role within frameworks for structural optimisation and is an important prerequisite for the success of mathematical optimisation algorithms. This integrated design sensitivity analysis leads to insights about impacts and significant effects of design modifications on the physical properties and the resulting physical behaviour. Design modifications are often characterised by changes in cross-sections, material parameters, and changes in shape and topology or by modifications of the referential configuration to be more general. DSA is a powerful and efficient tool to make predictions and to examine changes of objectives and constraints due to changes

of design parameters. Moreover, it is investigated for several years and in several fields of applications, all in parallel to the progress of methods for structural analysis. The methodology of its theoretical derivation and of its numerical realisation is responsible for the accuracy and the overall performance of numerical algorithms. This contribution is based on a variational approach for design sensitivity analysis, and especially on the enhanced intrinsic formulation proposed by [18] and [10, 12]. In contrast to a variety of further variational techniques, like the *material derivative approach* (MDA), which performs sensitivity analysis analogous to the *material time derivative*, see [6, 38, 39, 85], or the *domain parametrisation approach* (DPA), which is based on the introduction of a design independent global reference configuration (ALE), see [34, 65, 122, 161], the intrinsic formulation is fully integrated into the classical framework for continuum mechanics by the introduction of enhanced kinematics with a decomposition of geometrical and physical properties. Beside a *state* (function), which describes changes in the physical configuration and is primarily used for structural analysis, a *design* (function) is introduced and allows modifications in the referential configuration. If solution methods of choice are based on variational formulations and on variational principles, variations of several quantities of interest, especially of quantities from continuum mechanics, in corresponding physical and referential configurations are required. Variations in the physical space are connected with problems from structural analysis, while variations in the referential space are connected to problems from design sensitivity analysis or from structural optimisation. The variational approach according to [85] and [38, 39] appears to be a particularly promising approach to design sensitivity analysis. Especially the enhanced intrinsic formulation proposed in [18] and [10, 12] provides many beneficial advantages. Compared to different established methods, see [12, 16] and [10] for a short overview, it is the most sophisticated approach to design sensitivity analysis in theory but with the gain of accuracy of necessary derivatives and enormous numerical efficiency. Both aspects as well as an intensive discussion on further advantages and on the numerical realisation can be found in [13]. Using this approach, variations with respect to the state and design on the continuous level can be performed prior to any discretisation. This order of steps leads to an increasing efficiency of the presented approach within modern methods in computational mechanics. When it comes to numerical computations, following approaches can be distinguished.

- *Finite differences approach* requires almost no theoretical knowledge and is widely used, but it has a high numerical effort due to many function evaluations.
- *Semi-analytical approach* is used for the computation of numerical derivatives with respect to design parameters based on exact analytical formulations.
- *Discrete analytical approach* can be classified by exact derivatives of discrete formulations with respect to some given design parameters.
- *Continuous variational approach* is based on design variations of continuous problems. Discretisation takes place after derivation of exact analytical variations.

All mentioned strategies yield finally a useful sensitivity information in a proper sense and can be utilised within schemes for structural optimisation, but they differ in their computational behaviour. Overall, only analytical methods provide correct and exact sensitivity information in contrast to approximations in terms of numerical derivatives.

5.2 Kinematics and variations of kinematical quantities

The content of the following sections on fundamental principles for sensitivity analysis can be basically related to the works [10, 12, 113] and [18]. The initial approach based on an intrinsic formulation in convective coordinates in [113] is extended in [10, 12] and [18], where the authors presented an enhanced kinematical framework based on an intrinsic formulation in local coordinates. Especially the continuum mechanics point of view leads to very deep insights on mechanical problem formulations and allows a full embedding of a framework for variational sensitivity analysis due to its fundamental methodology into the classical layout of continuum mechanics. The basic idea behind this concept is the introduction of an arbitrary but fixed local convective configuration $\mathcal{R}$ with defined local coordinates $\boldsymbol{\theta}$ and is schematically pictured in Fig. 5.1. It allows the decomposition of

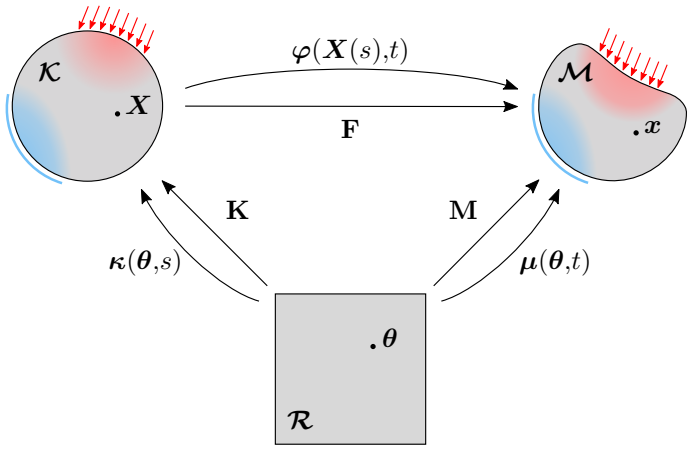

Figure 5.1: Concept of enhanced kinematics: referential configuration $\mathcal{K}$, physical configuration $\mathcal{M}$ and introduction of a local convective configuration $\mathcal{R}$, deformation mapping $\boldsymbol{\varphi}$ and introduction of a local geometry mapping $\boldsymbol{\kappa}$ and local motion mapping $\boldsymbol{\mu}$.

the classical kinematical concept, with the time (t) and design (s) dependent deformation mapping $\boldsymbol{\varphi}(\boldsymbol{X}(s),t)$, into two additional mappings, i.e. into a local referential or local geometry mapping $\boldsymbol{\kappa}(\boldsymbol{\theta},s)$ and into a local current or local motion mapping $\boldsymbol{\mu}(\boldsymbol{\theta},t)$ and therefore, a separation of geometrical and physical properties is possible. The well known deformation mapping $\boldsymbol{x} = \boldsymbol{\varphi}(\boldsymbol{X}(s),t)$ can be rewritten by the composition of the local geometry and the local motion mapping in the following way

$$\boldsymbol{\varphi} = \boldsymbol{\mu} \circ \boldsymbol{\kappa}^{-1}. \tag{5.1}$$

Besides the classical deformation gradient $\mathbf{F}$, two additional tangent forms $\mathbf{K}$ and $\mathbf{M}$ are introduced in Eq. (5.2) and are used to perform pull-back and push-forward operations between the configurations $\mathcal{K}, \mathcal{M}$ and $\mathcal{R}$ for quantities from continuum mechanics and for corresponding variations.

$$\mathbf{F} = \operatorname{Grad} \boldsymbol{\varphi}, \qquad \mathbf{K} = \operatorname{GRAD} \boldsymbol{\kappa}, \qquad \text{and} \qquad \mathbf{M} = \operatorname{GRAD} \boldsymbol{\mu}. \tag{5.2}$$

The Jacobians of introduced tangent mappings in Eq. (5.2) can be identified by

$$J_F = \det \mathbf{F}, \qquad J_K = \det \mathbf{K}, \qquad \text{and} \qquad J_M = \det \mathbf{M}. \tag{5.3}$$

Remark 5.1 (Gradient and divergence operators) *The following notation with respect to corresponding coordinates* $\{\boldsymbol{\theta}, \boldsymbol{X}, \boldsymbol{x}\}$ *for gradient operators and divergence operators is used throughout this work*

$$\text{referential}: \quad \mathrm{Grad}(\cdot) = \mathrm{grad}_X(\cdot) = \nabla_X(\cdot) \quad \text{and} \quad \mathrm{Div}(\cdot) = \nabla_X \cdot (\cdot), \tag{5.4}$$

$$\text{physical}: \quad \mathrm{grad}(\cdot) = \mathrm{grad}_x(\cdot) = \nabla_x(\cdot) \quad \text{and} \quad \mathrm{div}(\cdot) = \nabla_x \cdot (\cdot), \tag{5.5}$$

$$\text{local}: \quad \mathrm{GRAD}(\cdot) = \mathrm{grad}_\theta(\cdot) = \nabla_\theta(\cdot) \quad \text{and} \quad \mathrm{DIV}(\cdot) = \nabla_\theta \cdot (\cdot). \tag{5.6}$$

Remark 5.2 (Variation of determinants) *Variations of determinants of second order tensors* $\mathbf{A}$ *are performed by the application of* $\delta(\det \mathbf{A}) = \det \mathbf{A}\mathbf{A}^{-T} : \delta\mathbf{A}$.

Following the main approach for the decomposition of the deformation mapping $\boldsymbol{\varphi}$ in Eq. (5.1), the deformation gradient $\mathbf{F}$ in Eq. (5.2) consequently can be obtained from the multiplicative decomposition

$$\mathbf{F} = \mathbf{M}\mathbf{K}^{-1}. \tag{5.7}$$

The displacements are defined as the difference vector between the coordinates of the current and referential placements, i.e. between the referential points $\boldsymbol{x}$ and $\boldsymbol{X}$, respectively. The explicit displacements known from continuum mechanics can also be formulated in terms of the local mappings $\boldsymbol{\kappa}$ and $\boldsymbol{\mu}$, with $\boldsymbol{x} = \boldsymbol{\varphi}(\boldsymbol{X},t) = \boldsymbol{\mu}(\boldsymbol{\theta},t)$ and $\boldsymbol{X} = \boldsymbol{\kappa}(\boldsymbol{\theta},s)$, and therefore the displacement vector field $\boldsymbol{u}$ is given as

$$\boldsymbol{u} = \boldsymbol{x} - \boldsymbol{X} = \boldsymbol{\varphi}(\boldsymbol{X},t) - \boldsymbol{X} = \boldsymbol{\mu}(\boldsymbol{\theta},t) - \boldsymbol{\kappa}(\boldsymbol{\theta},s). \tag{5.8}$$

As a consequence from the presented approach, the referential gradient $\mathbf{H}$ of displacements $\boldsymbol{u}$ can be split into a local displacement gradient $\mathbf{H}_\theta$ and the inverse geometry gradient

$$\mathbf{H} = \mathrm{Grad}\,\boldsymbol{u} = \mathrm{GRAD}\,\boldsymbol{u}\,\mathbf{K}^{-1} = \mathbf{H}_\theta\,\mathbf{K}^{-1}. \tag{5.9}$$

The beneficial advantage of the introduced local configuration $\boldsymbol{\mathcal{R}}$ is, that after transformation to $\boldsymbol{\mathcal{R}}$, variations in this configuration can be performed additively in one single step due to the independence of geometrical and physical properties. Therefore, Eq. (5.10) is an elegant way to obtain the total variation of the deformation gradient

$$\delta\mathbf{F} = \delta\mathbf{M}\mathbf{K}^{-1} + \mathbf{M}\delta\mathbf{K}^{-1}. \tag{5.10}$$

Here, the variation $\delta\mathbf{M}$ can be identified as variation in the physical space, and the variation $\delta\mathbf{K}^{-1}$ can be identified as variation in the referential space.

Remark 5.3 (Variation of inverse tensors) *The total variation of the inverse tensor* $\mathbf{A}^{-1}$ *can be obtained using the identity* $\mathbf{A}\mathbf{A}^{-1} = \mathbf{I}$. *Its total variation* $\delta(\mathbf{A}\mathbf{A}^{-1}) = \delta\mathbf{A}\mathbf{A}^{-1} + \mathbf{A}\delta\mathbf{A}^{-1} = \delta\mathbf{I} = \mathbf{0}$ *yields finally* $\delta\mathbf{A}^{-1} = -\mathbf{A}^{-1}\delta\mathbf{A}\mathbf{A}^{-1}$.

Remark 5.4 (Transformation of gradients) *Gradients can be transformed between introduced configurations $\mathcal{K}, \mathcal{M}$ and $\mathcal{R}$ using following relations*

$$\mathrm{Grad}(\cdot) = \mathrm{grad}(\cdot)\mathbf{F} = \mathrm{GRAD}(\cdot)\mathbf{K}^{-1}, \qquad \mathrm{grad}(\cdot) = \mathrm{Grad}(\cdot)\mathbf{F}^{-1} = \mathrm{GRAD}(\cdot)\mathbf{M}^{-1}. \tag{5.11}$$

Using Remark 5.3, the total variation of the deformation gradient can be obtained using $\delta\mathbf{K}^{-1} = -\mathbf{M}\mathbf{K}^{-1}\delta\mathbf{K}\mathbf{K}$ and reads

$$\delta\mathbf{F}(\boldsymbol{\varphi}, \delta\boldsymbol{\varphi}, \delta\boldsymbol{X}) = \delta\mathbf{M}\mathbf{K}^{-1} - \mathbf{M}\mathbf{K}^{-1}\delta\mathbf{K}\mathbf{K} = \mathrm{Grad}\,\delta\boldsymbol{\varphi} - \mathbf{F}\,\mathrm{Grad}\,\delta\boldsymbol{X}, \tag{5.12}$$

where the variations of the local gradients $\delta\mathbf{K} = \delta[\mathrm{GRAD}\,\boldsymbol{\kappa}] = \mathrm{GRAD}\,\delta\boldsymbol{\kappa} = \mathrm{GRAD}\,\delta\boldsymbol{X}$ and $\delta\mathbf{M} = \delta[\mathrm{GRAD}\,\boldsymbol{\mu}] = \mathrm{GRAD}\,\delta\boldsymbol{\mu} = \mathrm{GRAD}\,\delta\boldsymbol{x} = \mathrm{GRAD}\,\delta\boldsymbol{\varphi}$, and the transformation of gradients from Remark 5.4 are used. For a deformation gradient $\mathbf{F}$ given as a function of the displacement field, i.e. $\mathbf{F} = \mathbf{I} + \mathrm{Grad}\,\boldsymbol{u} = \mathbf{I} + \mathbf{H}$, it's total variation reads

$$\delta\mathbf{F}(\boldsymbol{u}, \delta\boldsymbol{u}, \delta\boldsymbol{X}) = \mathrm{Grad}\,\delta\boldsymbol{u} - \mathbf{H}\,\mathrm{Grad}\,\delta\boldsymbol{X} \tag{5.13}$$

with the relation $\delta\boldsymbol{x} = \delta\boldsymbol{X} + \delta\boldsymbol{u}$. Therefore, if modifications of the referential configuration are allowed, it is important to distinguish between formulations in terms of $\boldsymbol{\varphi}$ and $\boldsymbol{u}$. To obtain general descriptions, the generalised state variable $\boldsymbol{v}$ is introduced, and represents $\boldsymbol{\varphi}$ or $\boldsymbol{u}$ depending on stated problems. Furthermore, the variable $\boldsymbol{s}$ can be identified as a general design variable, which differs depending on the chosen design description. The presented notation is adopted from intensive explanations and discussions on the variation of kinematical quantities and mentioned distinctions presented in [12] and [99]. As a consequence, the total variation of the deformation gradient in terms of the generalised state variable $\boldsymbol{v}$ is given as

$$\delta\mathbf{F}(\boldsymbol{v}, \delta\boldsymbol{v}, \delta\boldsymbol{s}) = \mathrm{Grad}\,\delta\boldsymbol{v} - \mathrm{Grad}\,\boldsymbol{v}\,\mathrm{Grad}\,\delta\boldsymbol{s} \tag{5.14}$$

and the partial variations with respect to the state $\boldsymbol{v}$ and design $\boldsymbol{s}$ can be identified as

$$\mathbf{F}'_v = \mathrm{Grad}\,\delta\boldsymbol{v}, \qquad \mathbf{F}'_s = -\,\mathrm{Grad}\,\boldsymbol{v}\,\mathrm{Grad}\,\delta\boldsymbol{s}. \tag{5.15}$$

The deformation gradient and its decomposition in Eq. (5.7), and therefore also its variations in Eq. (5.14) and in Eq. (5.15), represent essential relations for all subsequent derivations of strain measures and of their corresponding variations. Within weak formulations of stated BVPs, in some cases also some second partial variations are needed, e.g. the mixed variation of the deformation gradient $\mathbf{F}$ with respect to $\boldsymbol{v}$ and $\boldsymbol{s}$ reads

$$\mathbf{F}''_{vs} = -\,\mathrm{Grad}\,\delta\boldsymbol{v}\,\mathrm{Grad}\,\delta\boldsymbol{s}. \tag{5.16}$$

The Green-Lagrange strain tensor $\mathbf{E}$ in Eq. (5.17) is often used for strain measurements in structural mechanics and in several applications within FEM. To obtain the full set of its variations, it is useful to formulate $\mathbf{E}$ in terms of local geometry and motion gradients

$$\mathbf{E} = \frac{1}{2}(\mathbf{F}^T\mathbf{F} - \mathbf{I}) = \frac{1}{2}(\mathbf{K}^{-T}\mathbf{M}^T\mathbf{M}\mathbf{K}^{-1} - \mathbf{I}). \tag{5.17}$$

Its variations can be obtained applying techniques similar to the variations of the deformation gradient, and therefore, the necessary partial variations read

$$\begin{aligned}
\mathbf{E}'_v(\boldsymbol{v}, \delta\boldsymbol{v}) &= \ \ \mathrm{sym}(\mathbf{F}^T \operatorname{Grad} \delta\boldsymbol{v}), \\
\mathbf{E}'_s(\boldsymbol{v}, \delta\boldsymbol{s}) &= -\mathrm{sym}(\mathbf{F}^T \operatorname{Grad} \boldsymbol{v} \operatorname{Grad} \delta\boldsymbol{s}), \\
\mathbf{E}''_{vv}(\boldsymbol{v}, \delta\boldsymbol{v}, \Delta\boldsymbol{v}) &= \ \ \mathrm{sym}(\operatorname{Grad} \delta\boldsymbol{v}^T \operatorname{Grad} \Delta\boldsymbol{v}), \\
\mathbf{E}''_{vs}(\boldsymbol{v}, \delta\boldsymbol{v}, \delta\boldsymbol{s}) &= -\mathrm{sym}(\operatorname{Grad} \delta\boldsymbol{s}^T \mathbf{H}^T \operatorname{Grad} \delta\boldsymbol{v} + \mathbf{F}^T \operatorname{Grad} \delta\boldsymbol{v} \operatorname{Grad} \delta\boldsymbol{s}).
\end{aligned} \tag{5.18}$$

Complete compilations of first and second variations of several quantities from continuum mechanics can be found in [12] and [99], and are accentuated by several details and remarks. Here, only necessary relations for this work are presented and outlined.

5.3 Basic sensitivity relations

In this work, hyperelastic materials are considered, and therefore, the existence of a strain energy function W can be assumed. Extensions to time dependent and non-linear material formulations are possible and dedicated to future work. This prerequisite allows to formulate an internal energy functional Π^{int} of a hyperelastic body in terms of W

$$\Pi^{\mathsf{int}}(\boldsymbol{v}, \boldsymbol{s}) = \int_{\boldsymbol{\mathcal{K}}} W(\mathbf{F}) \, \mathrm{d}V = \int_{\boldsymbol{\mathcal{K}}} W(\mathbf{E}) \, \mathrm{d}V = \int_{\boldsymbol{\mathcal{K}}} W(\boldsymbol{v}, \boldsymbol{s}) \, \mathrm{d}V. \tag{5.19}$$

The energy potential in Eq. (5.19) is used to derive necessary relations for structural and sensitivity analysis, structural optimisation, and especially, the strain energy W is referred for the definition of different stress measures. The first and second Piola-Kirchhoff stress tensors $\mathbf{P}$ and $\mathbf{S}$ can be derived from

$$\mathbf{P} := \frac{\partial W}{\partial \mathbf{F}} \qquad \text{and} \qquad \mathbf{S} := \frac{\partial W}{\partial \mathbf{E}}. \tag{5.20}$$

Using the deformation gradient $\mathbf{F}$ and its Jacobian J_F, several transformations of the introduced stress measures are possible, e.g. to obtain the symmetric Cauchy stress tensor

$$\mathbf{T} := J_F^{-1} \mathbf{P} \mathbf{F}^T = J_F^{-1} \mathbf{F} \mathbf{S} \mathbf{F}^T. \tag{5.21}$$

In subsequent investigations variations of the energy potential in Eq. (5.19) with respect to state variables $\boldsymbol{v}$ and design parameters $\boldsymbol{s}$ are necessary. The total variation of the overall internal energy functional Π^{int} is given by

$$(\Pi^{\mathsf{int}})'(\boldsymbol{v}, \boldsymbol{s}; \delta\boldsymbol{v}, \delta\boldsymbol{s}) = \int_{\boldsymbol{\mathcal{K}}} (W)'_v(\boldsymbol{v}, \boldsymbol{s}; \delta\boldsymbol{v}) + (W)'_s(\boldsymbol{v}, \boldsymbol{s}; \delta\boldsymbol{s}) + W \operatorname{Div} \delta\boldsymbol{s} \, \mathrm{d}V, \tag{5.22}$$

where the divergence term results from the variation of the referential configuration $\boldsymbol{\mathcal{K}}$ itself and can be replaced by $\operatorname{Div} \delta\boldsymbol{s} = \mathbf{I} : \operatorname{Grad} \delta\boldsymbol{s}$. The partial variations are identified as

$$\begin{aligned} (\mathit{\Pi}^{\text{int}})'_v &= \int_{\boldsymbol{\mathcal{K}}} (W)'_v(\boldsymbol{v},\boldsymbol{s};\delta\boldsymbol{v}) \,\mathrm{d}V, \\ (\mathit{\Pi}^{\text{int}})'_s &= \int_{\boldsymbol{\mathcal{K}}} (W)'_s(\boldsymbol{v},\boldsymbol{s};\delta\boldsymbol{s}) + W\,\mathbf{I} : \operatorname{Grad} \delta\boldsymbol{s} \,\mathrm{d}V, \end{aligned} \tag{5.23}$$

and require partial variations of the introduced strain energy W with respect to state variables $\boldsymbol{v}$ and design parameters $\boldsymbol{s}$. This partial variations can be given in terms of the deformation gradient $\mathbf{F}$ or the Green-Lagrange strains $\mathbf{E}$ and have the form

$$\begin{aligned} (W)'_v(\boldsymbol{v},\boldsymbol{s};\delta\boldsymbol{v}) &= \frac{\partial W}{\partial \mathbf{F}} : \mathbf{F}'_v(\boldsymbol{v},\delta\boldsymbol{v}) = \mathbf{P} : \operatorname{Grad} \delta\boldsymbol{v} = \mathbf{S} : \mathbf{E}'_v, \\ (W)'_s(\boldsymbol{v},\boldsymbol{s};\delta\boldsymbol{s}) &= \frac{\partial W}{\partial \mathbf{F}} : \mathbf{F}'_s(\boldsymbol{v},\delta\boldsymbol{s}) = -\mathbf{P} : \operatorname{Grad} \boldsymbol{v} \operatorname{Grad} \delta\boldsymbol{s} = \mathbf{S} : \mathbf{E}'_s. \end{aligned} \tag{5.24}$$

Finally, the partial variations of the internal energy potential are given as

$$\begin{aligned} (\mathit{\Pi}^{\text{int}})'_v = R^{\text{int}} &= \int_{\boldsymbol{\mathcal{K}}} \mathbf{P} : \operatorname{Grad} \delta\boldsymbol{v} \,\mathrm{d}V = \int_{\boldsymbol{\mathcal{K}}} \mathbf{S} : \mathbf{E}'_v(\boldsymbol{v},\delta\boldsymbol{v}) \,\mathrm{d}V, \\ (\mathit{\Pi}^{\text{int}})'_s = G^{\text{int}} &= \int_{\boldsymbol{\mathcal{K}}} -\operatorname{Grad} \boldsymbol{v}^T \mathbf{P} : \operatorname{Grad} \delta\boldsymbol{s} + W\,\mathbf{I} : \operatorname{Grad} \delta\boldsymbol{s} \,\mathrm{d}V \\ &= \int_{\boldsymbol{\mathcal{K}}} \mathbf{S} : \mathbf{E}'_s(\boldsymbol{v},\delta\boldsymbol{s}) + W\,\mathbf{I} : \operatorname{Grad} \delta\boldsymbol{s} \,\mathrm{d}V. \end{aligned} \tag{5.25}$$

Both quantities can be connected to weak formulations known from structural analysis and configurational mechanics or mechanics of configurational forces, i.e. $(\mathit{\Pi}^{\text{int}})'_v$ corresponds to the internal part of the physical residual R^{int} and $(\mathit{\Pi}^{\text{int}})'_s$ can be associated with the internal part of the material residual G^{int}, respectively. For further references and detailed explanations see [99] for instance.

A complete formulation of the overall energy requires the specification of the contribution of external loads in terms of body forces $\boldsymbol{b}$ per unit volume and stresses $\bar{\boldsymbol{t}}$ on the surface of the domain $\boldsymbol{\mathcal{K}}$, i.e. on the Neumann boundary $\partial\boldsymbol{\mathcal{K}}_{\text{N}}$. These terms are given by

$$\mathit{\Pi}^{\text{ext}}(\boldsymbol{v},\boldsymbol{s}) = \int_{\boldsymbol{\mathcal{K}}} \boldsymbol{b} \cdot \boldsymbol{v} \,\mathrm{d}V + \int_{\partial\boldsymbol{\mathcal{K}}} \bar{\boldsymbol{t}} \cdot \boldsymbol{v} \,\mathrm{d}A. \tag{5.26}$$

In subsequent steps also variations of the external part of the energy term $\mathit{\Pi}^{\text{ext}}$ are necessary. Especially, the variation with respect to state parameters $\boldsymbol{v}$ contributes to the external part of the residual and reads

$$(\mathit{\Pi}^{\text{ext}})'_v = R^{\text{ext}} = F(\boldsymbol{s};\boldsymbol{\eta}) = \int_{\boldsymbol{\mathcal{K}}} \boldsymbol{b} \cdot \boldsymbol{\eta} \,\mathrm{d}V + \int_{\partial\boldsymbol{\mathcal{K}}} \bar{\boldsymbol{t}} \cdot \boldsymbol{\eta} \,\mathrm{d}A. \tag{5.27}$$

5.3.1 Weak form of equilibrium and its variation

In solid mechanics and other fields of computational mechanics, especially in the finite element framework, the weak form of equilibrium plays a central role. Within structural optimisation, the weak form of equilibrium is of same importance for the setting of design sensitivity analysis as for structural analysis. Its variation leads to the well-known tangent stiffness operator for structural analysis as well as to the tangent pseudo load operator, which is used to formulate sensitivity relations to describe effects in the physical space due to modifications in the referential space. In accordance to methods for structural analysis, discretisation of mentioned tangent forms and an efficient solution are essentials steps for the treatment of structural optimisation problems. The required state parameter $\boldsymbol{v}$, which fulfils the equilibrium of mechanical systems, is obtained from the solution of the general non-linear residual

$$R(\boldsymbol{v}, \boldsymbol{s}; \boldsymbol{\eta}) = 0 \tag{5.28}$$

It depends on a general state variable $\boldsymbol{v} \in \mathcal{V}$, the design variable $\boldsymbol{s} \in \mathcal{S}$, and any test function $\boldsymbol{\eta} \in \mathcal{V}$. Here, all spaces of admissible states and designs are denoted by $\mathcal{V}$ and $\mathcal{S}$. In the context of structural optimisation, the weak form of equilibrium is often seen as an equality constraint within the posed optimisation problem and has to be fulfilled for any arbitrary state and design.

The variation of the weak form can be motivated in several ways, e.g. minimisation principle of overall energy, solution of an optimisation problem for an arbitrary objective function with an equilibrium constraint, or finally, that any perturbation in the design space must not violate the physical equilibrium state. Therefore, the total variation of the non-linear residual in Eq. (5.28) can be investigated

$$R' = R'_v(\boldsymbol{v}, \boldsymbol{s}; \boldsymbol{\eta}, \delta\boldsymbol{v}) + R'_s(\boldsymbol{v}, \boldsymbol{s}; \boldsymbol{\eta}, \delta\boldsymbol{s}) = k(\boldsymbol{v}, \boldsymbol{s}; \boldsymbol{\eta}, \delta\boldsymbol{v}) + p(\boldsymbol{v}, \boldsymbol{s}; \boldsymbol{\eta}, \delta\boldsymbol{s}) = 0. \tag{5.29}$$

Here, the variations of the physical residual with respect to $\boldsymbol{v}$ and $\boldsymbol{s}$ are introduced by the tangent operators k and p

$$k(\boldsymbol{v}, \boldsymbol{s}; \boldsymbol{\eta}, \delta\boldsymbol{v}) = R'_v(\boldsymbol{v}, \boldsymbol{s}; \boldsymbol{\eta}, \delta\boldsymbol{v}) \qquad \text{physical stiffness,} \tag{5.30}$$

$$p(\boldsymbol{v}, \boldsymbol{s}; \boldsymbol{\eta}, \delta\boldsymbol{s}) = R'_s(\boldsymbol{v}, \boldsymbol{s}; \boldsymbol{\eta}, \delta\boldsymbol{s}) \qquad \text{pseudo load.} \tag{5.31}$$

Both tangent operators are bilinear forms $k : \mathcal{V} \times \mathcal{V} \to \mathbb{R}$ and $p : \mathcal{V} \times \mathcal{S} \to \mathbb{R}$.

5.3.2 Sensitivity of the physical state

The solution of the sensitivity relation in Eq. (5.29) allows the derivation of the implicit sensitivity of the state in the current equilibrium point $(\boldsymbol{v}, \boldsymbol{s})$

$$\delta\boldsymbol{v} = s(\boldsymbol{v}, \boldsymbol{s}; \delta\boldsymbol{s}). \tag{5.32}$$

So far, Eq. (5.32) is an implicit representation of the sensitivity operator s. Its explicit determination is only possible after discretisation of corresponding global quantities. Explicit formulations for the residual forms, the pseudo load and also for the resulting

sensitivity operator s are given in Section 5.4 and can be found in [97, 99] and [96] with detailed descriptions, derivations and explanations.

5.3.3 Variations of arbitrary functionals

The implicit sensitivity relation of the state in Eq. (5.32) provides a possibility for the evaluation of any design variation of any arbitrary objective or constraint functional $\hat{f}(\boldsymbol{v},\boldsymbol{s}) = f(\boldsymbol{v}(\boldsymbol{s}),\boldsymbol{s})$ with respect to the chosen design parameter s

$$f' = f'_v + f'_s = \frac{\partial f}{\partial \boldsymbol{v}}\delta\boldsymbol{v} + \frac{\partial f}{\partial \boldsymbol{s}}\delta\boldsymbol{s} = \left(\frac{\partial f}{\partial \boldsymbol{v}} \circ s + \frac{\partial f}{\partial \boldsymbol{s}}\right)\delta\boldsymbol{s}. \tag{5.33}$$

5.3.4 Variations of stresses

The introduced weak form of equilibrium or physical residual and especially its variations require variations of stresses with respect to state variables $\boldsymbol{v}$ and design parameters $\boldsymbol{s}$. The explicit variations of introduced Piola-Kirchhoff stress tensors $\mathbf{P}$ and $\mathbf{S}$, respectively, deliver also known elasticity tensors $\mathbb{A}$ and $\mathbb{C}$ for hyperelastic materials, i.e.

$$\begin{aligned} \mathbf{P}'(\boldsymbol{v},\delta\boldsymbol{v},\delta\boldsymbol{s}) &= \frac{\partial \mathbf{P}}{\partial \mathbf{F}} : \mathbf{F}'(\boldsymbol{v},\delta\boldsymbol{v},\delta\boldsymbol{s}) = \mathbb{A} : \mathbf{F}'(\boldsymbol{v},\delta\boldsymbol{v},\delta\boldsymbol{s}), \qquad \text{and} \qquad \mathbb{A} = \frac{\partial \mathbf{P}}{\partial \mathbf{F}}, \\ \mathbf{S}'(\boldsymbol{v},\delta\boldsymbol{v},\delta\boldsymbol{s}) &= \frac{\partial \mathbf{S}}{\partial \mathbf{E}} : \mathbf{E}'(\boldsymbol{v},\delta\boldsymbol{v},\delta\boldsymbol{s}) = \mathbb{C} : \mathbf{E}'(\boldsymbol{v},\delta\boldsymbol{v},\delta\boldsymbol{s}), \qquad \text{and} \qquad \mathbb{C} = \frac{\partial \mathbf{S}}{\partial \mathbf{E}}. \end{aligned} \tag{5.34}$$

Referring the introduced variations of the deformation gradient $\mathbf{F}$ and the Green-Lagrange strain tensor $\mathbf{E}$, the explicit partial variations can be identified as

$$\mathbf{P}'_v(\boldsymbol{v},\delta\boldsymbol{v}) = \mathbb{A} : \operatorname{Grad}\delta\boldsymbol{v}, \qquad \mathbf{P}'_s(\boldsymbol{v},\delta\boldsymbol{s}) = -\mathbb{A} : \operatorname{Grad}\boldsymbol{v}\operatorname{Grad}\delta\boldsymbol{s}, \tag{5.35}$$

for the variation of the first Piola-Kirchhoff stress tensor and as

$$\mathbf{S}'_v(\boldsymbol{v},\delta\boldsymbol{v}) = \mathbb{C} : \mathbf{F}^T\operatorname{Grad}\delta\boldsymbol{v}, \qquad \mathbf{S}'_s(\boldsymbol{v},\delta\boldsymbol{s}) = -\mathbb{C} : \mathbf{F}^T\operatorname{Grad}\boldsymbol{v}\operatorname{Grad}\delta\boldsymbol{s}, \tag{5.36}$$

for the variation of the symmetric second Piola-Kirchhoff stress tensor. In some cases, the stated optimisation problems involve stress measures as a characteristic quantity of failure and therefore, they are used as constraints or restrictions. Common stress components under investigation are von Mises or equivalent tensile stresses σ_{eq}, which are usually formulated in terms of principal stresses or in terms of Cauchy stress components T_{ij}. In the general three-dimensional case, the von Mises stresses can be computed using relation

$$\sigma_{\mathsf{eq}}(\mathbf{T}) = \sqrt{T_{11}^2 + T_{22}^2 + T_{33}^2 - T_{11}T_{22} - T_{11}T_{33} - T_{22}T_{33} + 3(T_{12}^2 + T_{13}^2 + T_{23}^2)}. \tag{5.37}$$

The von Mises stress for the plane stress condition is computed by

$$\sigma_{\mathsf{eq}}(\mathbf{T}) = \sqrt{T_{11}^2 + T_{22}^2 - T_{11}T_{22} + 3T_{12}^2}, \tag{5.38}$$

and for the plane strain condition using the Poisson's ratio ν

$$\begin{aligned} \sigma_{\mathsf{eq}}(\mathbf{T}) &= \sqrt{(T_{11}+T_{22})^2(\nu^2-\nu+1)+T_{11}T_{22}(2\nu^2-2\nu-1)+3T_{12}^2} \qquad \text{and} \\ T_{33} &= \nu(T_{11}+T_{22}). \end{aligned} \tag{5.39}$$

The variation of von Mises stresses with respect to state variables $\boldsymbol{v}$ and design parameters $\boldsymbol{s}$ read in abstract form

$$\sigma'_{\mathsf{eq}}(\mathbf{T}) = \frac{\partial \sigma_{\mathsf{eq}}}{\partial \mathbf{T}} : \mathbf{T}'(\boldsymbol{v},\boldsymbol{s},\delta\boldsymbol{v},\delta\boldsymbol{s}) = \frac{\partial \sigma_{\mathsf{eq}}}{\partial \mathbf{T}} : \left\{ \mathbf{T}'_v(\boldsymbol{v},\boldsymbol{s},\delta\boldsymbol{v}) + \mathbf{T}'_s(\boldsymbol{v},\boldsymbol{s},\delta\boldsymbol{s}) \right\}. \tag{5.40}$$

As a consequence, the total variation of Cauchy stresses is required and reads

$$\mathbf{T}'(\boldsymbol{v},\boldsymbol{s},\delta\boldsymbol{v},\delta\boldsymbol{s}) = \mathbf{T}'_v(\boldsymbol{v},\boldsymbol{s},\delta\boldsymbol{v}) + \mathbf{T}'_s(\boldsymbol{v},\boldsymbol{s},\delta\boldsymbol{s}). \tag{5.41}$$

The partial variations in terms of the deformation gradient $\mathbf{F}$ and the first Piola-Kirchhoff stress $\mathbf{P}$, i.e. $\mathbf{T} = J_F^{-1}\mathbf{P}\mathbf{F}^T$, can be extracted to

$$\begin{aligned} \mathbf{T}'_v(\boldsymbol{v},\boldsymbol{s},\delta\boldsymbol{v}) &= -(J_F^{-1}\mathbf{F}^{-T} : \mathbf{F}'_v)\ \mathbf{P}\mathbf{F}^T + J_F(\mathbf{P}'_v\mathbf{F}^T + \mathbf{P}(\mathbf{F}^T)'_v), \\ \mathbf{T}'_s(\boldsymbol{v},\boldsymbol{s},\delta\boldsymbol{s}) &= -(J_F^{-1}\mathbf{F}^{-T} : \mathbf{F}'_s)\ \mathbf{P}\mathbf{F}^T + J_F(\mathbf{P}'_s\mathbf{F}^T + \mathbf{P}(\mathbf{F}^T)'_s). \end{aligned} \tag{5.42}$$

Here, the previously introduced variations of the deformation gradient $\mathbf{F}$ and of first Piola-Kirchhoff stresses $\mathbf{P}$ are used. In terms of the Green-Lagrange strains $\mathbf{E}$ and the second Piola-Kirchhoff stress $\mathbf{S}$, i.e. $\mathbf{T} = J_F^{-1}\mathbf{F}\mathbf{S}\mathbf{F}^T$, the partial variations of Cauchy stresses $\mathbf{T}$ are given by

$$\begin{aligned} \mathbf{T}'_v(\boldsymbol{v},\boldsymbol{s},\delta\boldsymbol{v}) &= -(J_F^{-1}\mathbf{F}^{-T} : \mathbf{F}'_v)\ \mathbf{F}\mathbf{S}\mathbf{F}^T + J_F((\mathbf{F}^T)'_v\mathbf{S}\mathbf{F}^T + \mathbf{F}\mathbf{S}'_v\mathbf{F}^T + \mathbf{F}\mathbf{S}(\mathbf{F}^T)'_v), \\ \mathbf{T}'_s(\boldsymbol{v},\boldsymbol{s},\delta\boldsymbol{s}) &= -(J_F^{-1}\mathbf{F}^{-T} : \mathbf{F}'_s)\ \mathbf{F}\mathbf{S}\mathbf{F}^T + J_F((\mathbf{F}^T)'_s\mathbf{S}\mathbf{F}^T + \mathbf{F}\mathbf{S}'_s\mathbf{F}^T + \mathbf{F}\mathbf{S}(\mathbf{F}^T)'_s). \end{aligned} \tag{5.43}$$

Here, already introduced variations of the Green-Lagrange strains $\mathbf{E}$ and of the second Piola-Kirchhoff stresses $\mathbf{S}$ are used. Furthermore, in both cases and referring Remark 5.2, the variations of the inverse Jacobian read

$$\begin{aligned} (J_F^{-1})'_v &= -J_F^{-2}(J_F)'_v = -J_F^{-2}J_F\mathbf{F}^{-T} : \mathbf{F}'_v = -J_F^{-1}\mathbf{F}^{-T} : \mathbf{F}'_v \\ (J_F^{-1})'_s &= -J_F^{-2}(J_F)'_s = -J_F^{-2}J_F\mathbf{F}^{-T} : \mathbf{F}'_s = -J_F^{-1}\mathbf{F}^{-T} : \mathbf{F}'_s. \end{aligned} \tag{5.44}$$

The last missing quantity for a complete representation of the variation of von Mises stresses, here in Voigt notation as necessary for numerical implementation, is the partial derivative of von Mises stresses with respect to the Cauchy stress and reads

$$\frac{\partial \sigma_{\mathsf{eq}}}{\partial \boldsymbol{T}} = \frac{1}{2\,\sigma_{\mathsf{eq}}} \begin{bmatrix} 2\,T_{11} - T_{22} \\ 2\,T_{22} - T_{11} \\ 6\,T_{12} \end{bmatrix}. \tag{5.45}$$

5.4 Discrete sensitivity relations

Within the variational approach to design sensitivity analysis, all quantities are fully integrated in the well-known framework of classical non-linear continuum mechanics and variations are derived on the continuous level, cf. [12] for details. This fundamental and beneficial aspect allows the discretisation of the final resulting sensitivity expressions, beside a few modifications, using standard finite element techniques known from several standard literature on finite element analysis, e.g. [20, 28, 181, 182] and [168]. In this work, the presented relations are basically referred to pure displacement finite element formulations. This type of elements can be seen as an important and widely used class of element formulations. Extensions to modified and advanced element technologies are straight forward. Remarks on design parametrisations and the choice of explicit design variables are followed by a compilation of necessary sensitivity relations, explanations on their numerical realisation in terms of FEM and on their verification. Overall, the main target is to obtain an ability to control the shape and boundary of given geometries.

5.4.1 Discrete weak form of equilibrium and its variation

After standard finite element discretisation with the discrete approximation $\boldsymbol{v}_h$ for the state and $\boldsymbol{X}_h$ for design, the discrete parameters $\boldsymbol{v} \in \mathbb{R}^{n_v}$ and $\boldsymbol{X} \in \mathbb{R}^{n_X}$ can be used to obtain the matrix description of the continuous forms, i.e. the physical residual vector in Eq. (5.46) and the tangent forms in Eq. (5.47) for the physical stiffness and in Eq. (5.48) for the pseudo load matrix. Additionally, the approximations for the corresponding variations $\delta\boldsymbol{v}_h, \delta\boldsymbol{X}_h$ and the test function $\boldsymbol{\eta}_h$ are chosen in the same manner, i.e. $\delta\boldsymbol{v} \in \mathbb{R}^{n_v}$ and $\delta\boldsymbol{X} \in \mathbb{R}^{n_X}$ as well as $\boldsymbol{\eta} \in \mathbb{R}^{n_v}$. The overall number of the discrete state variables in $\mathcal{V}_h \subset \mathcal{V}$ is given by n_v, and n_X is the number of discrete design parameters in $\mathcal{S}_h \subset \mathcal{S}$.

$$R(\boldsymbol{v}_h, \boldsymbol{X}_h; \boldsymbol{\eta}_h) = \boldsymbol{\eta}^T \boldsymbol{R}, \qquad \boldsymbol{R} \in \mathbb{R}^{n_v}, \tag{5.46}$$

$$k(\boldsymbol{v}_h, \boldsymbol{X}_h; \boldsymbol{\eta}_h, \delta\boldsymbol{v}_h) = \boldsymbol{\eta}^T \boldsymbol{K} \delta\boldsymbol{v}, \qquad \boldsymbol{K} \in \mathbb{R}^{n_v \times n_v}, \tag{5.47}$$

$$p(\boldsymbol{v}_h, \boldsymbol{X}_h; \boldsymbol{\eta}_h, \delta\boldsymbol{X}_h) = \boldsymbol{\eta}^T \boldsymbol{P} \delta\boldsymbol{X}, \qquad \boldsymbol{P} \in \mathbb{R}^{n_v \times n_X}. \tag{5.48}$$

As a consequence thereof, the discrete form of the variation of the weak form from Eq. (5.29) evaluated in $(\boldsymbol{v}_h, \boldsymbol{X}_h)$ reads

$$R' = \boldsymbol{\eta}^T \boldsymbol{R}' = \boldsymbol{\eta}^T \left[\boldsymbol{K} \delta\boldsymbol{v} + \boldsymbol{P} \delta\boldsymbol{X} \right] = 0, \tag{5.49}$$

and thus, due to the arbitrariness of the test function $\boldsymbol{\eta}$, following relation holds true

$$\boldsymbol{R}' = \boldsymbol{K} \delta\boldsymbol{v} + \boldsymbol{P} \delta\boldsymbol{X} = \boldsymbol{0}. \tag{5.50}$$

5.4.2 Discrete sensitivity of the physical state

Finally, Eq. (5.50) is utilised for the evaluation of the discrete form of the sensitivity relation from Eq. (5.32) for the state variable

$$\delta\boldsymbol{v} = \boldsymbol{S} \delta\boldsymbol{X} \quad \text{with} \quad \boldsymbol{S} = -\boldsymbol{K}^{-1} \boldsymbol{P} \quad \text{and} \quad \boldsymbol{S} \in \mathbb{R}^{n_v \times n_X} \tag{5.51}$$

for any arbitrary design variable of the discrete nodal set $\boldsymbol{X}$ and its variation $\delta\boldsymbol{X}$. The introduced matrix $\boldsymbol{S}$ is the so-called sensitivity matrix. It connects variations in the referential space with variations in the physical space and allows predictions of changes in the state $\boldsymbol{v}$ due to arbitrary design modifications $\delta\boldsymbol{X}$.

5.4.3 Discrete form of the variation of arbitrary functionals

The discrete form of the variation of any arbitrary objective or constraint functional in Eq. (5.33) with respect to any design variation $\delta\boldsymbol{X}$ can finally be specified by

$$f' = \frac{\partial f}{\partial \boldsymbol{v}}\delta\boldsymbol{v} + \frac{\partial f}{\partial \boldsymbol{X}}\delta\boldsymbol{X} = \left(\frac{\partial f}{\partial \boldsymbol{v}}\,\boldsymbol{S} + \frac{\partial f}{\partial \boldsymbol{X}}\right)\delta\boldsymbol{X}. \tag{5.52}$$

5.4.4 Discrete form of the variation of stresses

In structural optimisation, stress components and their variations play an important role. If stresses are chosen as objective functions in some appropriate manner or as constraints, especially variations with respect to design parameters $\boldsymbol{s}$ are the values of interest. The continuous total variations in terms of linearised strain measures of the first and second Piola-Kirchhoff stress tensors are given in Eq. (5.34), and the partial variations are given in Eq. (5.35) and Eq. (5.36), respectively. Variations of both stress quantities contain variations with respect to state variables $\boldsymbol{v}$ and design parameters $\boldsymbol{X}$, i.e.

$$\begin{aligned}
\mathbf{P}'(\boldsymbol{v},\delta\boldsymbol{v},\delta\boldsymbol{X}) &= \mathbf{P}'_v(\boldsymbol{v},\delta\boldsymbol{v}) + \mathbf{P}'_X(\boldsymbol{v},\delta\boldsymbol{X}) = \frac{\partial\mathbf{P}}{\partial\boldsymbol{v}}\delta\boldsymbol{v} + \frac{\partial\mathbf{P}}{\partial\boldsymbol{X}}\delta\boldsymbol{X},\\
\mathbf{S}'(\boldsymbol{v},\delta\boldsymbol{v},\delta\boldsymbol{X}) &= \mathbf{S}'_v(\boldsymbol{v},\delta\boldsymbol{v}) + \mathbf{S}'_X(\boldsymbol{v},\delta\boldsymbol{X}) = \frac{\partial\mathbf{S}}{\partial\boldsymbol{v}}\delta\boldsymbol{v} + \frac{\partial\mathbf{S}}{\partial\boldsymbol{X}}\delta\boldsymbol{X}.
\end{aligned} \tag{5.53}$$

In the discretised sense, the first and second Piola-Kirchhoff stresses are identified by $\boldsymbol{P}_{\mathrm{K}}$ and $\boldsymbol{S}_{\mathrm{K}}$, respectively. Using the discrete sensitivity relation for the state in Eq. (5.51), the discrete relation for the variation of stresses can be given similar to Eq. (5.52) as

$$\begin{aligned}
\boldsymbol{P}'_{\mathrm{K}}(\boldsymbol{v},\delta\boldsymbol{v},\delta\boldsymbol{X}) &= \frac{\partial\boldsymbol{P}_{\mathrm{K}}}{\partial\boldsymbol{v}}\delta\boldsymbol{v} + \frac{\partial\boldsymbol{P}_{\mathrm{K}}}{\partial\boldsymbol{X}}\delta\boldsymbol{X} = \left(\frac{\partial\boldsymbol{P}_{\mathrm{K}}}{\partial\boldsymbol{v}}\boldsymbol{S} + \frac{\partial\boldsymbol{P}_{\mathrm{K}}}{\partial\boldsymbol{X}}\right)\delta\boldsymbol{X},\\
\boldsymbol{S}'_{\mathrm{K}}(\boldsymbol{v},\delta\boldsymbol{v},\delta\boldsymbol{X}) &= \frac{\partial\boldsymbol{S}_{\mathrm{K}}}{\partial\boldsymbol{v}}\delta\boldsymbol{v} + \frac{\partial\boldsymbol{S}_{\mathrm{K}}}{\partial\boldsymbol{X}}\delta\boldsymbol{X} = \left(\frac{\partial\boldsymbol{S}_{\mathrm{K}}}{\partial\boldsymbol{v}}\boldsymbol{S} + \frac{\partial\boldsymbol{S}_{\mathrm{K}}}{\partial\boldsymbol{X}}\right)\delta\boldsymbol{X}.
\end{aligned} \tag{5.54}$$

5.5 Partitioning of discrete sensitivity relations

Regarding the discrete formulation of derived relations for structural and sensitivity analysis in terms of FEM, the discrete parameters, i.e. the state parameters $\boldsymbol{v}$ and the explicit design parameters $\boldsymbol{X}$, which represent the coordinates of the underlying mesh (therefore $\boldsymbol{s} = \boldsymbol{X}$ holds true), are partitioned into contributions on the Dirichlet boundary $\partial\mathcal{K}_{\mathrm{D}}$, the Neumann boundary $\partial\mathcal{K}_{\mathrm{N}}$ and into those of the inner domain $\mathcal{K}$, cf. Fig. 5.2 for clarification. Further explanations on the choice of design parameters are given in Section 3.4.

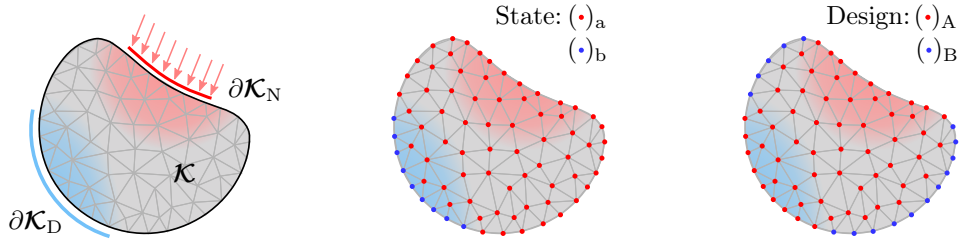

Figure 5.2: Partitioning of nodes in domains $\mathcal{K}$, $\partial\mathcal{K}_\mathrm{N}, \partial\mathcal{K}_\mathrm{D}$ and corresponding sets: set (a, b) for partitioning of state variables and set (A, B) for partitioning of design parameters.

With the overall representation of the domain $\overline{\mathcal{K}} = \mathcal{K} \cup \partial\mathcal{K}$ and the boundary $\partial\mathcal{K} = \partial\mathcal{K}_\mathrm{N} \cup \partial\mathcal{K}_\mathrm{D}$, where $\partial\mathcal{K}_\mathrm{N} \cap \partial\mathcal{K}_\mathrm{D} = \emptyset$, all emerging quantities can be identified by the following notation for

$$\begin{aligned} \text{State:} \quad & (\cdot)_\mathrm{a} \in \mathcal{K} \cup \partial\mathcal{K}_\mathrm{N} \quad \text{and} \quad (\cdot)_\mathrm{b} \in \partial\mathcal{K}_\mathrm{D}, \\ \text{Design:} \quad & (\cdot)_\mathrm{A} \in \mathcal{K} \cup \partial\mathcal{K}_\mathrm{N} \quad \text{and} \quad (\cdot)_\mathrm{B} \in \partial\mathcal{K}_\mathrm{D}, \end{aligned} \tag{5.55}$$

with the set (a, b) for the partitioning of state variables and the set (A, B) for the partitioning of design parameters. The number of state quantities $(\cdot)_\mathrm{a}$ is given by n_a, and the number of state quantities $(\cdot)_\mathrm{b}$ is given by n_b. Same holds true for the design partitioning and therefore, the number of design quantities $(\cdot)_\mathrm{A}$ is given by n_A, and the number of design quantities $(\cdot)_\mathrm{B}$ is given by n_B. It is useful to introduce these different kinds of subsets because it finally allows to define and prescribe different types of boundary conditions, i.e. explicit boundary conditions in the physical and explicit boundary conditions in the design space. In the special case the sets for state and design parameters can coincide, but in general they can be completely different.

Remark 5.5 (Nomination of sets for state parameters) *Compared to the set (i, b) introduced in Section 4.4.1 for inner and boundary nodes of an RVE, the nodes on the Dirichlet boundary given in Eq. (5.56) are also indicated by the index (b). Whereas the set identified by the index (a) introduced above contains all nodes except boundary nodes, i.e. it contains nodes in the inner domain as well as nodes on the Neumann boundary.*

Using this definition, the state $\boldsymbol{v}$, the variation of the state $\delta\boldsymbol{v}$, the chosen design parameters $\boldsymbol{X}$ and the variation of the design parameters $\delta\boldsymbol{X}$ are subdivided

$$\boldsymbol{v} = \begin{bmatrix} \boldsymbol{v}_\mathrm{a} \\ \boldsymbol{v}_\mathrm{b} \end{bmatrix}, \quad \delta\boldsymbol{v} = \begin{bmatrix} \delta\boldsymbol{v}_\mathrm{a} \\ \delta\boldsymbol{v}_\mathrm{b} \end{bmatrix}, \quad \boldsymbol{X} = \begin{bmatrix} \boldsymbol{X}_\mathrm{A} \\ \boldsymbol{X}_\mathrm{B} \end{bmatrix}, \quad \delta\boldsymbol{X} = \begin{bmatrix} \delta\boldsymbol{X}_\mathrm{A} \\ \delta\boldsymbol{X}_\mathrm{B} \end{bmatrix}, \tag{5.56}$$

with the defined dimensions $\{\boldsymbol{v}_\mathrm{a}, \delta\boldsymbol{v}_\mathrm{a}\} \in \mathbb{R}^{n_\mathrm{a}}$, $\{\boldsymbol{v}_\mathrm{b}, \delta\boldsymbol{v}_\mathrm{b}\} \in \mathbb{R}^{n_\mathrm{b}}$, $\{\boldsymbol{X}_\mathrm{A}, \delta\boldsymbol{X}_\mathrm{A}\} \in \mathbb{R}^{n_\mathrm{A}}$ and $\{\boldsymbol{X}_\mathrm{B}, \delta\boldsymbol{X}_\mathrm{B}\} \in \mathbb{R}^{n_\mathrm{B}}$. As a consequence, a similar partitioning holds true for the physical residual vector $\boldsymbol{R}$ from Eq. (5.46) as well as for its variation $\boldsymbol{R}'$ from Eq. (5.50)

$$\boldsymbol{R}(\boldsymbol{v}, \boldsymbol{X}; \boldsymbol{\eta}) = \begin{bmatrix} \boldsymbol{R}_\mathrm{a}(\boldsymbol{v}_\mathrm{a}, \boldsymbol{v}_\mathrm{b}, \boldsymbol{X}_\mathrm{A}, \boldsymbol{X}_\mathrm{B}; \boldsymbol{\eta}) \\ \boldsymbol{R}_\mathrm{b}(\boldsymbol{v}_\mathrm{a}, \boldsymbol{v}_\mathrm{b}, \boldsymbol{X}_\mathrm{A}, \boldsymbol{X}_\mathrm{B}; \boldsymbol{\eta}) \end{bmatrix} \quad \text{and} \quad \boldsymbol{R}' = \begin{bmatrix} \boldsymbol{R}'_\mathrm{a} \\ \boldsymbol{R}'_\mathrm{b} \end{bmatrix} = \begin{bmatrix} (\boldsymbol{R}_\mathrm{a})'_v + (\boldsymbol{R}_\mathrm{a})'_X \\ (\boldsymbol{R}_\mathrm{b})'_v + (\boldsymbol{R}_\mathrm{b})'_X \end{bmatrix}, \tag{5.57}$$

with the dimensions $\{\boldsymbol{R}_\mathrm{a}, \boldsymbol{R}'_\mathrm{a}\} \in \mathbb{R}^{n_\mathrm{a}}$, $\{\boldsymbol{R}_\mathrm{b}, \boldsymbol{R}'_\mathrm{b}\} \in \mathbb{R}^{n_\mathrm{b}}$. Here, the partial variations $\boldsymbol{R}'_\mathrm{a}$ and $\boldsymbol{R}'_\mathrm{b}$ of the partitioned residual $\boldsymbol{R}$, i.e. of $\boldsymbol{R}_\mathrm{a}$ and $\boldsymbol{R}_\mathrm{b}$, have to be determined with respect to the partitioned state $\boldsymbol{v}_\mathrm{a}, \boldsymbol{v}_\mathrm{b}$ and with respect to the partitioned design $\boldsymbol{X}_\mathrm{A}, \boldsymbol{X}_\mathrm{B}$. The explicit terms can be outlined as

$$\boldsymbol{R}'_v = \begin{bmatrix} (\boldsymbol{R}_\mathrm{a})'_v \\ (\boldsymbol{R}_\mathrm{b})'_v \end{bmatrix} = \begin{bmatrix} \boldsymbol{K}_\mathrm{aa} & \boldsymbol{K}_\mathrm{ab} \\ \boldsymbol{K}_\mathrm{ba} & \boldsymbol{K}_\mathrm{bb} \end{bmatrix} \begin{bmatrix} \delta\boldsymbol{v}_\mathrm{a} \\ \delta\boldsymbol{v}_\mathrm{b} \end{bmatrix}, \quad \boldsymbol{R}'_X = \begin{bmatrix} (\boldsymbol{R}_\mathrm{a})'_X \\ (\boldsymbol{R}_\mathrm{b})'_X \end{bmatrix} = \begin{bmatrix} \boldsymbol{P}_\mathrm{aA} & \boldsymbol{P}_\mathrm{aB} \\ \boldsymbol{P}_\mathrm{bA} & \boldsymbol{P}_\mathrm{bB} \end{bmatrix} \begin{bmatrix} \delta\boldsymbol{X}_\mathrm{A} \\ \delta\boldsymbol{X}_\mathrm{B} \end{bmatrix}, \tag{5.58}$$

and therefore, the partitioned explicit representation of Eq. (5.50) is of the form

$$\boldsymbol{R}' = \boldsymbol{K}\delta\boldsymbol{v} + \boldsymbol{P}\delta\boldsymbol{X} = \begin{bmatrix} \boldsymbol{K}_\mathrm{aa} & \boldsymbol{K}_\mathrm{ab} \\ \boldsymbol{K}_\mathrm{ba} & \boldsymbol{K}_\mathrm{bb} \end{bmatrix} \begin{bmatrix} \delta\boldsymbol{v}_\mathrm{a} \\ \delta\boldsymbol{v}_\mathrm{b} \end{bmatrix} + \begin{bmatrix} \boldsymbol{P}_\mathrm{aA} & \boldsymbol{P}_\mathrm{aB} \\ \boldsymbol{P}_\mathrm{bA} & \boldsymbol{P}_\mathrm{bB} \end{bmatrix} \begin{bmatrix} \delta\boldsymbol{X}_\mathrm{A} \\ \delta\boldsymbol{X}_\mathrm{B} \end{bmatrix} = \boldsymbol{0}, \tag{5.59}$$

with nodal coordinates $\boldsymbol{X}$ of the finite element nodes as design variables, as explained in Section 3.4. The resulting dimensions of the obtained submatrices can be specified for the stiffness matrix and also for the pseudo load matrix by

$$\begin{aligned} &\boldsymbol{K}_\mathrm{aa} \in \mathbb{R}^{n_\mathrm{a} \times n_\mathrm{a}}, \quad &&\boldsymbol{K}_\mathrm{ab} \in \mathbb{R}^{n_\mathrm{a} \times n_\mathrm{b}}, \quad &&\boldsymbol{K}_\mathrm{ba} \in \mathbb{R}^{n_\mathrm{b} \times n_\mathrm{a}}, \quad &&\boldsymbol{K}_\mathrm{bb} \in \mathbb{R}^{n_\mathrm{b} \times n_\mathrm{b}}, \\ &\boldsymbol{P}_\mathrm{aA} \in \mathbb{R}^{n_\mathrm{a} \times n_\mathrm{A}}, \quad &&\boldsymbol{P}_\mathrm{aB} \in \mathbb{R}^{n_\mathrm{a} \times n_\mathrm{B}}, \quad &&\boldsymbol{P}_\mathrm{bA} \in \mathbb{R}^{n_\mathrm{b} \times n_\mathrm{A}}, \quad &&\boldsymbol{P}_\mathrm{bB} \in \mathbb{R}^{n_\mathrm{b} \times n_\mathrm{B}}. \end{aligned} \tag{5.60}$$

According to explained relations, Eq. (5.59) can be rearranged and allows the explicit computation of the sensitivity of the state from Eq. (5.51)

$$\delta\boldsymbol{v}_\mathrm{a} = -\boldsymbol{K}_\mathrm{aa}^{-1} \begin{bmatrix} \boldsymbol{P}_\mathrm{aA} & \boldsymbol{P}_\mathrm{aB} \end{bmatrix} \begin{bmatrix} \delta\boldsymbol{X}_\mathrm{A} \\ \delta\boldsymbol{X}_\mathrm{B} \end{bmatrix} = -\boldsymbol{K}_\mathrm{aa}^{-1}\boldsymbol{P}_\mathrm{a}\delta\boldsymbol{X} = \boldsymbol{S}_\mathrm{a}\delta\boldsymbol{X}. \tag{5.61}$$

With $\boldsymbol{P}_\mathrm{a} = \begin{bmatrix} \boldsymbol{P}_\mathrm{aA} & \boldsymbol{P}_\mathrm{aB} \end{bmatrix}$, the resulting quantity $\boldsymbol{S}_\mathrm{a} = -\boldsymbol{K}_\mathrm{aa}^{-1}\boldsymbol{P}_\mathrm{a}$ contains the sensitivity information of the state variable in the inner domain $\mathcal{K}$ and on the Neumann boundary $\partial\mathcal{K}_\mathrm{N}$. Compared to Eq. (5.51) it can be termed reduced sensitivity matrix. The part $(\cdot)_\mathrm{b}$ in the overall sensitivity matrix $\boldsymbol{S}$, i.e. $\boldsymbol{S}_\mathrm{b}$, vanishes due to the fact that the boundary conditions for the displacements $\boldsymbol{v}_\mathrm{b}$ on the Dirichlet boundary $\partial\mathcal{K}_\mathrm{D}$ are fulfilled strongly and therefore, their variations $\delta\boldsymbol{v}_\mathrm{b}$ vanish. The submatrices of the sensitivity matrix

$$\boldsymbol{S} = \begin{bmatrix} \boldsymbol{S}_\mathrm{a} \\ \boldsymbol{S}_\mathrm{b} \end{bmatrix} = \begin{bmatrix} \dfrac{\mathrm{d}\boldsymbol{v}_\mathrm{a}}{\mathrm{d}\boldsymbol{X}} \\ \dfrac{\mathrm{d}\boldsymbol{v}_\mathrm{b}}{\mathrm{d}\boldsymbol{X}} \end{bmatrix} \tag{5.62}$$

have the dimensions $\boldsymbol{S}_\mathrm{a} \in \mathbb{R}^{n_\mathrm{a} \times n_X}$ and $\boldsymbol{S}_\mathrm{b} \in \mathbb{R}^{n_\mathrm{b} \times n_X}$. Here, $n_X = (n_\mathrm{A} + n_\mathrm{B})$ represents the overall number of possible design parameters, which corresponds to the overall number of nodal coordinates of the finite element mesh.

5.6 Finite element approximation and explicit formulations

This section focusses on some remarkable details of the numerical implementation. The target is to obtain discrete relations for the introduced residual and tangent forms. So far, relations for residual and tangent forms in terms of the Green-Lagrange strain tensor $\mathbf{E}$ and the symmetric second Piola-Kirchhoff stress tensor $\mathbf{S}$ are well known and established in literature, see especially [99] for a detailed explanations. Additionally, an alternative formulation for the residual and tangent forms in terms of the deformation gradient $\mathbf{F}$ and the first Piola-Kirchhoff stress tensor $\mathbf{P}$ is presented and is used within the scope of deformation driven schemes for numerical homogenisation, presented in Chapter 4. Without going into detail, but referring the well known and standard text books on FEM like [20, 28, 168, 181, 182], the approximation of state variables $\boldsymbol{v}_h$ and design parameters $\boldsymbol{X}_h$ follows the isoparamteric concept within the finite element method. Therefore, both quantities are approximated using same shape functions N_i, which are defined on a fixed parameter space with coordinates $\boldsymbol{\xi}$, i.e. $N_i(\boldsymbol{\xi})$. The variations $\delta\boldsymbol{v}_h, \delta\boldsymbol{X}_h$ as well as the test functions $\boldsymbol{\eta}_h$ are also approximated using shape functions N_i in accordance to the classical Bubnov-Galerkin technique. In all subsequent investigations and compilations the two-dimensional case is considered, but the extension to the third dimension is straightforward.

Approximations of all mentioned quantities in every element have the same structure and therefore, a general rule for any arbitrary variable $\boldsymbol{a}$ can be introduced

$$\boldsymbol{a}^e_{\boldsymbol{h}} = \sum_{i=1}^{nn} \boldsymbol{a}_i \, N_i, \qquad \text{with} \qquad \boldsymbol{a}_i = \begin{bmatrix} a^i_1 \\ a^i_2 \end{bmatrix}. \tag{5.63}$$

In this case, $\boldsymbol{a}^e_{\boldsymbol{h}}$ is the approximation of a continuous variable $\boldsymbol{a}$ using the discrete values $\boldsymbol{a}_i$ and the value of the shape function N_i, both at node i. The number of nodes per element is indicated by nn. The approximation $\boldsymbol{a}^i_{\boldsymbol{h}}$ can be used for any of the following variables $\{\boldsymbol{v}^e_h, \boldsymbol{X}^e_h, \delta\boldsymbol{v}^e_h, \delta\boldsymbol{X}^e_h, \boldsymbol{\eta}^e_h\}$. The coefficients of the column matrix $\boldsymbol{a}_i$ then can be replaced by any discrete parameter $\{\boldsymbol{v}_i, \boldsymbol{X}_i, \delta\boldsymbol{v}_i, \delta\boldsymbol{X}_i, \boldsymbol{\eta}_i\}$. A similar rule can be stated for gradient and divergence operators in the referential configuration, i.e. the gradient or divergence of any arbitrary variable $\boldsymbol{a}$ has the form

$$\operatorname{Grad} \boldsymbol{a}^e_{\boldsymbol{h}} = \sum_{i=1}^{nn} \boldsymbol{a}_i \, \boldsymbol{L}_i^T \qquad \text{and} \qquad \operatorname{Div} \boldsymbol{a}^e_{\boldsymbol{h}} = \sum_{i=1}^{nn} \boldsymbol{L}_i^T \, \boldsymbol{a}_i, \tag{5.64}$$

with $\boldsymbol{L}_i$ being a vector with the gradient of the shape function N_i, i.e.

$$\boldsymbol{L}_i := \operatorname{Grad} N_i = \begin{bmatrix} N_{i,1} \\ N_{i,2} \end{bmatrix}. \tag{5.65}$$

With the Voigt notation introduced in Section 2.1 at hand, non-symmetric and symmetric

strain measures can be obtained in their vector representation, i.e.

$$\begin{aligned} \text{Deformation gradient:} \quad & \boldsymbol{F} = \begin{bmatrix} F_{11} & F_{12} \\ F_{21} & F_{22} \end{bmatrix}, \qquad \underline{\boldsymbol{F}} = \begin{bmatrix} F_{11} & F_{22} & F_{12} & F_{22} \end{bmatrix}^T, \\ \text{Green-Lagrange strain:} \quad & \boldsymbol{E} = \begin{bmatrix} E_{11} & E_{12} \\ E_{21} & E_{22} \end{bmatrix}, \qquad \underline{\boldsymbol{E}} = \begin{bmatrix} E_{11} & E_{22} & 2E_{12} \end{bmatrix}^T. \end{aligned} \tag{5.66}$$

After evaluation of constitutive equations, the resulting stresses can also be transformed to their vector representation, and therefore one obtains

$$\begin{aligned} &1.\ \text{Piola-Kirchhoff stress:} \quad \boldsymbol{P}_{\mathsf{K}} = \begin{bmatrix} P_{11} & P_{12} \\ P_{21} & P_{22} \end{bmatrix}, \qquad \underline{\boldsymbol{P}}_{\mathsf{K}} = \begin{bmatrix} P_{11} & P_{22} & P_{12} & P_{22} \end{bmatrix}^T, \\ &2.\ \text{Piola-Kirchhoff stress:} \quad \boldsymbol{S}_{\mathsf{K}} = \begin{bmatrix} S_{11} & S_{12} \\ S_{21} & S_{22} \end{bmatrix}, \qquad \underline{\boldsymbol{S}}_{\mathsf{K}} = \begin{bmatrix} S_{11} & S_{22} & S_{12} \end{bmatrix}^T. \end{aligned} \tag{5.67}$$

In the following, the approximation of variations of strain measures is the last relation which is necessary for final approximations of residual and tangent forms. In [99] the author introduced a general approximation for variations of symmetric strain measures using a description with a general form of B-matrices, which can be connected to descriptions in known standard FEM approximations, i.e. the variation of an arbitrary tensor $\mathbf{T}$ with respect to a variable $\boldsymbol{v}$ and some tensor $\mathbf{A}(\boldsymbol{v})$ of the form

$$\mathbf{T}'_v(\boldsymbol{v}, \delta\boldsymbol{v}) = \frac{1}{2}\left[\operatorname{Grad}\delta\boldsymbol{v}^T\mathbf{A} + \mathbf{A}^T\operatorname{Grad}\delta\boldsymbol{v}\right] = \operatorname{sym}(\mathbf{A}^T\operatorname{Grad}\delta\boldsymbol{v}) \tag{5.68}$$

can be approximated by

$$\boldsymbol{T}'_v(\boldsymbol{v}_h, \delta\boldsymbol{v}_h) = \begin{bmatrix} (T'_v)_{11} \\ (T'_v)_{22} \\ 2(T'_v)_{12} \end{bmatrix} = \sum_{i=1}^{nn} \boldsymbol{B}_{*i}\delta\boldsymbol{v}_i, \qquad \text{with} \qquad \delta\boldsymbol{v}_i = \begin{bmatrix} \delta v_1^i \\ \delta v_2^i \end{bmatrix}, \tag{5.69}$$

using the introduced Voigt notation for symmetric strain measures. Here, the introduced matrix $\boldsymbol{B}_{*i}$ is of general form

$$\boldsymbol{B}_{*i} = \begin{bmatrix} A_*^{11}N_{i,1} & A_*^{21}N_{i,1} \\ A_*^{12}N_{i,1} & A_*^{22}N_{i,1} \\ A_*^{11}N_{i,2} + A_*^{12}N_{i,1} & A_*^{21}N_{i,2} + A_*^{22}N_{i,1} \end{bmatrix}, \tag{5.70}$$

where $*$ is a placeholder for the variation in request, e.g the obtained B-matrices for variations with respect to the state read $\boldsymbol{B}_{vi}$ and the obtained B-matrices for variations with respect to design read $\boldsymbol{B}_{si}$. The components A_*^{ij} in $\boldsymbol{B}_{*i}$, with $(i, j = 1, 2)$, are components of a general matrix $\boldsymbol{A}_*$, which varies in terms of seeked variations and will be specified for explicit variations. This description can be applied to the variation of the Green-Lagrange strain tensor. The variation of $\mathbf{E}$ with respect to the state variable

$$\mathbf{E}'_v(\boldsymbol{v}, \delta\boldsymbol{v}) = \operatorname{sym}(\mathbf{F}^T\operatorname{Grad}\delta\boldsymbol{v}) = \operatorname{sym}(\mathbf{A}_v^T\operatorname{Grad}\delta\boldsymbol{v}) \tag{5.71}$$

with $\mathbf{A}_v = \mathbf{F}$ can be approximated by

$$\boldsymbol{E}'_v(\boldsymbol{v}_h, \delta\boldsymbol{v}_h) = \begin{bmatrix} (E'_v)_{11} \\ (E'_v)_{22} \\ 2(E'_v)_{12} \end{bmatrix} = \sum_{i=1}^{nn} \boldsymbol{B}_{vi} \delta\boldsymbol{v}_i \tag{5.72}$$

and the variation of $\mathbf{E}$ with respect to the design parameter

$$\mathbf{E}'_X(\boldsymbol{v}, \delta\boldsymbol{X}) = -\mathrm{sym}(\mathbf{F}^T \operatorname{Grad} \boldsymbol{v} \operatorname{Grad} \delta\boldsymbol{X}) = \mathrm{sym}(\mathbf{A}_s^T \operatorname{Grad} \delta\boldsymbol{X}) \tag{5.73}$$

with $\mathbf{A}_s = -\mathbf{F}^T \operatorname{Grad} \boldsymbol{v}$ can be approximated by

$$\boldsymbol{E}'_s(\boldsymbol{v}_h, \delta\boldsymbol{X}_h) = \begin{bmatrix} (E'_s)_{11} \\ (E'_s)_{22} \\ 2(E'_s)_{12} \end{bmatrix} = \sum_{i=1}^{nn} \boldsymbol{B}_{si} \delta\boldsymbol{X}_i. \tag{5.74}$$

The introduced notation is also applicable to second mixed variations of the Green-Lagrange strain tensor, i.e. the variations

$$\begin{aligned} \mathbf{E}''_{vv}(\boldsymbol{v}, \delta\boldsymbol{v}, \Delta\boldsymbol{v}) &= \mathrm{sym}(\operatorname{Grad} \Delta\boldsymbol{v}^T \operatorname{Grad} \delta\boldsymbol{v}) = \mathrm{sym}(\mathbf{A}_{vv}^T \operatorname{Grad} \delta\boldsymbol{v}) \\ \mathbf{E}''_{vs}(\boldsymbol{v}, \delta\boldsymbol{v}, \delta\boldsymbol{X}) &= -\mathrm{sym}(\operatorname{Grad} \delta\boldsymbol{X}^T \mathbf{H}^T \operatorname{Grad} \delta\boldsymbol{v} + \mathbf{F}^T \operatorname{Grad} \delta\boldsymbol{v} \operatorname{Grad} \delta\boldsymbol{X}) \\ &= \mathrm{sym}(\mathbf{A}_{vs}^T \operatorname{Grad} \delta\boldsymbol{X}) \end{aligned} \tag{5.75}$$

with $\mathbf{A}_{vv} = \operatorname{Grad} \Delta\boldsymbol{v}$ and $\mathbf{A}_{vs} = -(\mathbf{H}^T \operatorname{Grad} \delta\boldsymbol{v} + \mathbf{F}^T \operatorname{Grad} \delta\boldsymbol{v})$ are approximated by

$$\boldsymbol{E}'_{vv}(\boldsymbol{v}_h, \delta\boldsymbol{v}_h) = \sum_{i=1}^{nn} \boldsymbol{B}_{vvi} \delta\boldsymbol{v}_i, \qquad \text{and} \qquad \boldsymbol{E}'_{vs}(\boldsymbol{v}_h, \delta\boldsymbol{X}_h) = \sum_{i=1}^{nn} \boldsymbol{B}_{vsi} \delta\boldsymbol{X}_i. \tag{5.76}$$

A simple modification allows to use this notation also for variations of non-symmetric measures, for instance for the variation of the deformation gradient. Therefore, the introduced B-matrix has the form

$$\boldsymbol{B}_{*i} = \begin{bmatrix} \boldsymbol{A}_{11} N_{i,1} & \boldsymbol{A}_{21} N_{i,1} \\ \boldsymbol{A}_{12} N_{i,1} & \boldsymbol{A}_{22} N_{i,1} \\ \boldsymbol{A}_{11} N_{i,2} & \boldsymbol{A}_{21} N_{i,2} \\ \boldsymbol{A}_{12} N_{i,1} & \boldsymbol{A}_{22} N_{i,1} \end{bmatrix}. \tag{5.77}$$

The variation of the deformation gradient with respect to the state variable

$$\mathbf{F}'_v = \operatorname{Grad} \delta\boldsymbol{v} = \mathbf{A}_v \operatorname{Grad} \delta\boldsymbol{v}, \qquad \text{and} \qquad \mathbf{A}_v = \mathbf{I}, \tag{5.78}$$

is approximated using the approximation for gradients

$$\boldsymbol{F}'_v(\boldsymbol{v}_h, \delta\boldsymbol{v}_h) = \sum_{i=1}^{nn} \boldsymbol{v}_i \boldsymbol{L}_i^T = \sum_{i=1}^{nn} \boldsymbol{B}_{vi} \boldsymbol{v}_i. \tag{5.79}$$

The variation of the deformation gradient with respect to the design parameter

$$\mathbf{F}'_s = -\operatorname{Grad}\boldsymbol{v}\operatorname{Grad}\delta\boldsymbol{X} = \mathbf{A}_s\operatorname{Grad}\delta\boldsymbol{X} \tag{5.80}$$

with $\mathbf{A}_s = -\operatorname{Grad}\boldsymbol{v}$ can be approximated by

$$\boldsymbol{F}'_s(\boldsymbol{v}_h, \delta\boldsymbol{X}_h) = \sum_{i=1}^{nn} \boldsymbol{B}_{si}\delta\boldsymbol{X}_i. \tag{5.81}$$

The following tangent forms also require the approximation of the second mixed variation of the deformation gradient, i.e. the approximation

$$\mathbf{F}''_{vs} = -\operatorname{Grad}\delta\boldsymbol{v}\operatorname{Grad}\delta\boldsymbol{X} = \mathbf{A}_{vs}\operatorname{Grad}\delta\boldsymbol{X}. \tag{5.82}$$

With $\mathbf{A}_{vs} = -\operatorname{Grad}\delta\boldsymbol{v}$ the finite element approximation reads

$$\boldsymbol{F}''_{vs}(\delta\boldsymbol{v}_h, \delta\boldsymbol{X}_h) = \sum_{i=1}^{nn} \boldsymbol{B}_{vsi}\delta\boldsymbol{X}_i. \tag{5.83}$$

Finally, the matrix representation of elasticity tensors is necessary for the full numerical description of required tangent forms. The fourth order elasticity tensors $\mathbb{C}$ and $\mathbb{A}$ are rearranged to the matrix forms $\boldsymbol{C}$ and $\boldsymbol{A}$, respectively, and read

$$\boldsymbol{C} = \begin{bmatrix} \mathbb{C}_{1111} & \mathbb{C}_{1122} & \mathbb{C}_{1112} \\ \mathbb{C}_{2211} & \mathbb{C}_{2222} & \mathbb{C}_{2212} \\ \mathbb{C}_{1211} & \mathbb{C}_{1222} & \mathbb{C}_{1212} \end{bmatrix} \quad \text{and} \quad \boldsymbol{A} = \begin{bmatrix} \mathbb{A}_{1111} & \mathbb{A}_{1122} & \mathbb{A}_{1112} & \mathbb{A}_{1121} \\ \mathbb{A}_{2211} & \mathbb{A}_{2222} & \mathbb{A}_{2212} & \mathbb{A}_{2221} \\ \mathbb{A}_{1211} & \mathbb{A}_{1222} & \mathbb{A}_{1212} & \mathbb{A}_{1221} \\ \mathbb{A}_{2111} & \mathbb{A}_{2122} & \mathbb{A}_{2112} & \mathbb{A}_{2121} \end{bmatrix}. \tag{5.84}$$

At this point, all necessary relations and approximations are available for the overall approximation of residual and tangent forms. After the discretisation procedure on the element level, the assembly process over all elements n_{el} has to be performed and is indicated by the operator $\bigcup$. The approximation of the physical residual in terms of the Green-Lagrange strain tensor $\mathbf{E}$ and the corresponding second Piola-Kirchhoff tensor $\mathbf{S}$ as well as in terms of the deformation gradient $\mathbf{F}$ and the first Piola-Kirchhoff tensor $\mathbf{P}$ has then the following form

$$\begin{aligned} R(\boldsymbol{v}_h,\boldsymbol{X}_h;\boldsymbol{\eta}_h) &= \bigcup_{e=1}^{n_{el}} \int_{\boldsymbol{\mathcal{K}}^e} \mathbf{S} : \mathbf{E}'_v(\boldsymbol{v}_h^e,\boldsymbol{\eta}_h^e)\,\mathrm{d}V - F(\boldsymbol{X}_h^e,\boldsymbol{\eta}_h^e) \\ &= \bigcup_{e=1}^{n_{el}} \int_{\boldsymbol{\mathcal{K}}^e} \mathbf{P} : \mathbf{F}'_v(\boldsymbol{v}_h^e,\boldsymbol{\eta}_h^e)\,\mathrm{d}V - F(\boldsymbol{X}_h^e,\boldsymbol{\eta}_h^e) \\ &= \bigcup_{e=1}^{n_{el}} \sum_{i=1}^{nn} \boldsymbol{\eta}_i^T \boldsymbol{R}_i^e = \boldsymbol{\eta}^T \boldsymbol{R}. \end{aligned} \tag{5.85}$$

The tangent forms, i.e. the stiffness and the pseudo load operator k and p, in terms of $\mathbf{E}$

and $\mathbf{S}$ or $\mathbf{F}$ and $\mathbf{P}$, respectively, are given by

$$\begin{aligned} k(\boldsymbol{v}_h,\boldsymbol{X}_h;\boldsymbol{\eta}_h,\delta\boldsymbol{v}_h) &= \bigcup_{e=1}^{n_{el}} \int_{\mathcal{K}^e} \mathbf{E}'_v(\boldsymbol{v}_h^e,\boldsymbol{\eta}_h^e) : \mathbb{C} : \mathbf{E}'_v(\boldsymbol{v}_h^e,\delta\boldsymbol{v}_h^e) + \mathbf{S} : \mathbf{E}''_{vv}(\boldsymbol{\eta}_h^e,\delta\boldsymbol{v}_h^e)\, \mathrm{d}V \\ &= \bigcup_{e=1}^{n_{el}} \int_{\mathcal{K}^e} \mathbf{F}'_v(\boldsymbol{v}_h^e,\boldsymbol{\eta}_h^e) : \mathbb{A} : \mathbf{F}'_v(\boldsymbol{v}_h^e,\delta\boldsymbol{v}_h^e)\, \mathrm{d}V \\ &= \bigcup_{e=1}^{n_{el}} \sum_{i=1}^{nn} \sum_{j=1}^{nn} \boldsymbol{\eta}_i^T \boldsymbol{K}_{ij}^e \delta\boldsymbol{v}_i = \boldsymbol{\eta}^T \boldsymbol{K} \delta\boldsymbol{v}, \end{aligned} \tag{5.86}$$

$$\begin{aligned} p(\boldsymbol{v}_h,\boldsymbol{X}_h;\boldsymbol{\eta}_h,\delta\boldsymbol{X}_h) &= \bigcup_{e=1}^{n_{el}} \int_{\mathcal{K}^e} \mathbf{S} : \mathbf{E}''_{vs}(\boldsymbol{v}_h^e,\boldsymbol{\eta}_h^e,\delta\boldsymbol{X}_h^e) + \mathbf{E}'_v(\boldsymbol{v}_h^e,\boldsymbol{\eta}_h^e) : \mathbb{C} : \mathbf{E}'_s(\boldsymbol{v}_h^e,\delta\boldsymbol{X}_h^e) \\ &\qquad + \mathbf{S} : \mathbf{E}'_v(\boldsymbol{v}_h^e,\boldsymbol{\eta}_h^e)\, \mathrm{Div}\, \delta\boldsymbol{X}_h^e\, \mathrm{d}V - F'_s(\boldsymbol{X}_h^e;\boldsymbol{\eta}_h^e,\delta\boldsymbol{X}_h^e) \\ &= \bigcup_{e=1}^{n_{el}} \int_{\mathcal{K}^e} \mathbf{P} : \mathbf{F}''_{vs}(\boldsymbol{v}_h^e,\boldsymbol{\eta}_h^e,\delta\boldsymbol{X}_h^e) + \mathbf{F}'_v(\boldsymbol{v}_h^e,\boldsymbol{\eta}_h^e) : \mathbb{A} : \mathbf{F}'_s(\boldsymbol{v}_h^e,\delta\boldsymbol{X}_h^e) \\ &\qquad + \mathbf{P} : \mathbf{F}'_v(\boldsymbol{v}_h^e,\boldsymbol{\eta}_h^e)\, \mathrm{Div}\, \delta\boldsymbol{X}_h^e\, \mathrm{d}V - F'_s(\boldsymbol{X}_h^e;\boldsymbol{\eta}_h^e,\delta\boldsymbol{X}_h^e) \\ &= \bigcup_{e=1}^{n_{el}} \sum_{i=1}^{nn} \sum_{j=1}^{nn} \boldsymbol{\eta}_i^T \boldsymbol{P}_{ij}^e \delta\boldsymbol{X}_i = \boldsymbol{\eta}^T \boldsymbol{P} \delta\boldsymbol{X}. \end{aligned} \tag{5.87}$$

The terms $\mathbf{S}'_v(\boldsymbol{v}_h,\delta\boldsymbol{v}_h) = \mathbb{C} : \mathbf{E}'_v(\boldsymbol{v}_h^e,\delta\boldsymbol{v}_h^e)$ and $\mathbf{P}'_v(\boldsymbol{v}_h,\delta\boldsymbol{v}_h) = \mathbb{A} : \mathbf{F}'_v(\boldsymbol{v}_h^e,\delta\boldsymbol{v}_h^e)$ can be identified as variations of stresses $\mathbf{S}$ and $\mathbf{P}$ with respect to state variable $\boldsymbol{v}$, respectively, and the terms $\mathbf{S}'_v(\boldsymbol{v}_h,\delta\boldsymbol{X}_h) = \mathbb{C} : \mathbf{E}'_s(\boldsymbol{v}_h^e,\delta\boldsymbol{X}_h^e)$ and $\mathbf{S}'_v(\boldsymbol{v}_h,\delta\boldsymbol{X}_h) = \mathbb{A} : \mathbf{F}'_s(\boldsymbol{v}_h^e,\delta\boldsymbol{X}_h^e)$ are the variations of stresses $\mathbf{S}$ and $\mathbf{P}$ with respect to design parameters $\boldsymbol{X}$. The design variation of the external part of the residual $R^{\mathsf{ext}} = F(\boldsymbol{X};\boldsymbol{\eta})$ in its continuous form reads

$$F'_s(\boldsymbol{X};\boldsymbol{\eta},\delta\boldsymbol{X}) = \int_{\mathcal{K}^e} \boldsymbol{b}\cdot\boldsymbol{\eta}\ \mathrm{Div}\, \delta\boldsymbol{X}\ \mathrm{d}V. \tag{5.88}$$

Finally, using the introduced approximations for strain and stress measures and their linearised forms, residual and tangent forms on element level can be specified with respect to the appropriate B-matrix for symmetric or non-symmetric quantities. The nodal contribution of the discrete residual vector $\boldsymbol{R}_i^e$ in element e at node i is realised by

$$\boldsymbol{R}_i^e = \int_{\mathcal{K}^e} \boldsymbol{B}_{vi}^T\, \underline{\boldsymbol{S}}_{\mathsf{K}}\, \mathrm{d}V - \boldsymbol{F}_i^e(\boldsymbol{X}) = \int_{\mathcal{K}^e} \boldsymbol{P}_{\mathsf{K}} \boldsymbol{L}_i\, \mathrm{d}V - \boldsymbol{F}_i^e(\boldsymbol{X}). \tag{5.89}$$

External loads $F(\boldsymbol{X}_h^e;\boldsymbol{\eta}_h^e) = R^{\mathsf{ext}}(\boldsymbol{X}_h^e;\boldsymbol{\eta}_h^e) = \boldsymbol{F}_i^e(\boldsymbol{X})$ in terms of physical body forces read

$$\boldsymbol{F}_i^e(\boldsymbol{X}) = \int_{\mathcal{K}^e} N_i \boldsymbol{b}\, \mathrm{d}V. \tag{5.90}$$

For notational simplicity, the external part of the virtual work is assumed to be deformation

independent and therefore, terms containing external stress loads are omitted. The nodal contributions to the element stiffness matrices $\boldsymbol{K}^e$ in terms of constitutive matrices $\boldsymbol{C}$ or $\boldsymbol{A}$, respectively, are discretised by

$$\boldsymbol{K}^e_{ij} = \int_{\boldsymbol{\mathcal{K}}^e} \boldsymbol{B}^T_{vi} \boldsymbol{C} \boldsymbol{B}_{vj} + \boldsymbol{L}^T_i \boldsymbol{S}_{\mathsf{K}} \boldsymbol{L}_j \boldsymbol{I} \, \mathrm{d}V = \int_{\boldsymbol{\mathcal{K}}^e} \boldsymbol{B}^T_{vi} \boldsymbol{A} \boldsymbol{B}_{vj} \, \mathrm{d}V. \tag{5.91}$$

The nodal contributions to the element pseudo load matrices $\boldsymbol{P}^e$ in terms of constitutive matrices $\boldsymbol{C}$ or $\boldsymbol{A}$, respectively, and in terms of the design variation of the external part of the residual can be computed from

$$\begin{aligned} \boldsymbol{P}^e_{ij} &= \int_{\boldsymbol{\mathcal{K}}^e} \boldsymbol{B}^T_{vi} \boldsymbol{C} \boldsymbol{B}_{sj} - \boldsymbol{L}^T_i \boldsymbol{S}_{\mathsf{K}} \boldsymbol{L}_j \operatorname{Grad} \boldsymbol{v} - \boldsymbol{F} \boldsymbol{S}_{\mathsf{K}} \boldsymbol{L}_j \boldsymbol{L}^T_i + \boldsymbol{F} \boldsymbol{S}_{\mathsf{K}} \boldsymbol{L}_i \boldsymbol{L}^T_j \, \mathrm{d}V - (\boldsymbol{F}'_X)_{ij}(\boldsymbol{X}) \\ &= \int_{\boldsymbol{\mathcal{K}}^e} \boldsymbol{B}^T_{vi} \boldsymbol{A} \boldsymbol{B}_{sj} - \boldsymbol{P}_{\mathsf{K}} \boldsymbol{L}_j \boldsymbol{L}^T_i + \boldsymbol{P}_{\mathsf{K}} \boldsymbol{L}_i \boldsymbol{L}^T_j \, \mathrm{d}V - (\boldsymbol{F}'_X)_{ij}(\boldsymbol{X}). \end{aligned} \tag{5.92}$$

For the approximation of the variation of the external part of the residual, i.e. the approximation of $(\boldsymbol{F}'_X)_{ij}$, the approximation for divergence operators is referred and yields

$$(\boldsymbol{F}'_X)_{ij}(\boldsymbol{X}) = \int_{\boldsymbol{\mathcal{K}}^e} N_i \boldsymbol{b} \, \boldsymbol{L}^T_j \, \mathrm{d}V. \tag{5.93}$$

Remark 5.6 (Structure of stiffness and pseudo load operator) *Referring the introduced discretisation it is evident that the structures of introduced stiffness and pseudo load operators are similar. Therefore, several quantities for the stiffness operator on element level can be referred to for the implementation of the pseudo load operator. In comparison, the required effort for numerical implementation as well as for the numerical performance is similar for both operators.*

5.7 Sensitivity relations for selected objectives and constraints

In structural optimisation functions and quantities can be investigated in terms of minimisation, maximisation or adaptation of applications to special requirements. In this work only the minimisation of the compliance under volume constraints or minimisation of volume under stress constraints or constraints on reaction forces on the Dirichlet boundary are considered. The necessary relations are outlined in subsequent sections.

5.7.1 Volume

The volume of a given domain $\boldsymbol{\mathcal{K}}$ is characterised by the domain itself and therefore, by its design description and is given by

$$V = \int_{\boldsymbol{\mathcal{K}}} \mathrm{d}V. \tag{5.94}$$

The variation of the volume with respect to design parameters can be obtained after transformation into the local parameter space, variation of the Jacobian and final back-transformation to the domain $\boldsymbol{\mathcal{K}}$, and therefore, the variation of V reads

$$V' = \int_{\boldsymbol{\mathcal{R}}} J'_K \, \mathrm{d}V_\theta = \int_{\boldsymbol{\mathcal{K}}} \mathrm{Div}\, \delta\boldsymbol{X} \, \mathrm{d}V. \tag{5.95}$$

Within the numerical realisation, the volume is computed as a sum of all element volumes of the underlying FEM mesh, i.e.

$$V_h = \sum_{e=1}^{n_{el}} V^e = \sum_{e=1}^{n_{el}} \int_{\boldsymbol{\mathcal{K}}^e} \mathrm{d}V. \tag{5.96}$$

The approximation of the variation of the volume can be obtained from the general approximation of divergence operators and the assembly of all elements of the underlying FEM mesh, i.e.

$$V'_h = \bigcup_{e=1}^{n_{el}} (V^{e_h})' = \bigcup_{e=1}^{n_{el}} \sum_{i=1}^{nn} \int_{\boldsymbol{\mathcal{K}}^e} \boldsymbol{L}_i^T \delta\boldsymbol{X}_i \, \mathrm{d}V. \tag{5.97}$$

5.7.2 Energy and compliance

Maximisation of structural stiffness is an often used target within applications from civil and mechanical engineering. A suitable objective function for this task is the potential energy of given system due to the fact that energy minimisation can be connected to maximisation of structural stiffness. The explicit energy terms, defined by internal and external parts, are given in Eq. (5.19) and Eq. (5.26), respectively. The overall value of the total potential energy can be evaluated from

$$\mathit{\Pi}(\boldsymbol{v}, \boldsymbol{s}) = \mathit{\Pi}^{\mathsf{int}}(\boldsymbol{v}, \boldsymbol{s}) - \mathit{\Pi}^{\mathsf{ext}}(\boldsymbol{v}, \boldsymbol{s}). \tag{5.98}$$

In many cases, the potential energy is replaced by the end- or mean structural compliance, which is related to the potential energy $\mathit{\Pi}$ by a certain factor

$$C(\boldsymbol{v}, \boldsymbol{s}) := -2\mathit{\Pi}. \tag{5.99}$$

The authors in [31, 33, 56] tackled several optimisation problems in terms of linear and non-linear elasticity and propose strategies for the stiffness design of mechanical structures undergoing large displacements and geometric and material non-linearities. Studies for

several types of elastic potentials within topology optimisation of hyperelastic bodies are discussed and compared in [81] in detail.

Overall, the maximum stiffness of a structure can be achieved by the minimisation of the compliance functional C and modifications of selected design parameters. Within gradient based optimisation techniques variations with respect to state and design parameters are necessary, i.e. the total variation

$$C'(\boldsymbol{v}, \boldsymbol{s}) = C'_v + C'_s \tag{5.100}$$

contains the partial variations

$$\begin{aligned} C'_v &= -2\Pi'_v = -2R \qquad \text{with } R \text{ in terms of } R^{\text{int}} \text{ and } R^{\text{ext}}, \\ C'_s &= -2\Pi'_s = -2G \qquad \text{with } G \text{ in terms of } G^{\text{int}} \text{ and } G^{\text{ext}}. \end{aligned} \tag{5.101}$$

The seeked equilibrium state of structural systems and the corresponding solution $\boldsymbol{v}$ allow negligence of the partial variation with respect to the state parameter v. In the case, that the residual vanishes, i.e. $R = 0$ and thus $C'_v = 0$, the total variation of the compliance reduces to

$$C'(\boldsymbol{v}, \boldsymbol{s}) = C'_s = -2G. \tag{5.102}$$

The internal part of the referential residual G is already given in Eq. (5.25) and reads

$$\begin{aligned} G^{\text{int}} &= \int_{\mathcal{K}} - \operatorname{Grad} \boldsymbol{v}^T \mathbf{P} : \operatorname{Grad} \delta\boldsymbol{s} + W\, \mathbf{I} : \operatorname{Grad} \delta\boldsymbol{s} \, \mathrm{d}V \\ &= \int_{\mathcal{K}} \mathbf{S} : \mathbf{E}'_s(\boldsymbol{v}, \delta\boldsymbol{s}) + W\, \mathbf{I} : \operatorname{Grad} \delta\boldsymbol{s} \, \mathrm{d}V. \end{aligned} \tag{5.103}$$

The external part is missing and has to be specified. It can be deduced from the formulation of the external part of the energy in Eq. (5.26) and yields

$$G^{\text{ext}} = \int_{\mathcal{K}} (\boldsymbol{b} \cdot \boldsymbol{v}) \ \operatorname{Div} \delta\boldsymbol{X} \, \mathrm{d}V = \int_{\mathcal{K}} (\boldsymbol{b} \cdot \boldsymbol{v}) \ \mathbf{I} : \operatorname{Grad} \delta\boldsymbol{X} \, \mathrm{d}V. \tag{5.104}$$

The final finite element approximation is given by

$$G(\boldsymbol{v}_h, \boldsymbol{X}_h; \boldsymbol{\eta}_h) = \bigcup_{e=1}^{n_{el}} \sum_{i=1}^{nn} \boldsymbol{\eta}_i^T \boldsymbol{G}_i^e = \boldsymbol{\eta}^T \boldsymbol{G} \tag{5.105}$$

with the nodal contribution i on element level

$$\begin{aligned} \boldsymbol{G}_i^e &= \int_{\mathcal{K}^e} \boldsymbol{B}_{si}^T \, \underline{\boldsymbol{P}}_{\mathsf{K}} + W \boldsymbol{I} \boldsymbol{L}_i \, \mathrm{d}V - \int_{\mathcal{K}^e} N_i \boldsymbol{v}_i^T \boldsymbol{b} \, \boldsymbol{I} \boldsymbol{L}_i \, \mathrm{d}V \\ &= \int_{\mathcal{K}^e} \boldsymbol{B}_{si}^T \, \underline{\boldsymbol{S}}_{\mathsf{K}} + W \boldsymbol{I} \boldsymbol{L}_i \, \mathrm{d}V - \int_{\mathcal{K}^e} N_i \boldsymbol{v}_i^T \boldsymbol{b} \, \boldsymbol{I} \boldsymbol{L}_i \, \mathrm{d}V. \end{aligned} \tag{5.106}$$

5.7.3 Physical reaction forces

In some cases, it is interesting to analyse support areas of given systems to get detailed information about the interaction between the considered structural parts and the ground. The profile of distributed forces, tractions or stresses can be investigated in order to make predictions about mechanical behaviour or even about possible failure. Using some advanced information it is also possible to improve and optimise several kinds of support areas. For instance, methods for simultaneous design of structures and supports using techniques from topology optimisation were proposed by [32]. Here, supports are introduced as a new subset of design variables within the optimisation process for minimum compliance and mechanism design with the target to find the optimal location of supports. A similar approach can be found in [180]. Studies in [115] focused on identification of optimal locations of lateral spring supports in terms of their stiffness and position as design variables for problems of maximum buckling load of Bernoulli-Euler columns. Aspects concerning optimal design of supports for beam and frame structures in general were reported by [27]. Several influences, e.g. number of supports, their position and stiffness, on total structural cost were investigated and, in a similar fashion, [26] demonstrated a method for the determination of the overall number, position and generalised forces of actuators in smart structures. The shape design of rectangular support blocks and foundations of machines in order to reduce mass is tackled in [137]. Their studies focused on external dynamic forces and loads coming from the soil. Introduced constraints are horizontal and vertical amplitudes of forces and stresses on the soil ground. The investigations in [147] can be put in a similar context. The authors presented methods for optimisation of boundary conditions subjected to maximum fundamental frequency of vibrating structures in order to find optimal locations. A variational formulation and the approach of material derivatives is the foundation in their gradient-based optimisation techniques. Another field of applications is discussed in [35], where an algorithm is proposed for shape optimisation of contact problems with desired contact traction distribution on specified contact surfaces or areas. It should be mentioned that the quantity of interest is the distribution of forces or tractions and therefore, it can be related to the presented sensitivity analysis of reaction forces. In contrast to the topic of this contribution, the influence of the position of externally applied constant loads or forces on structural response such as nodal displacements, mean compliance and stress can be investigated and is done in [163]. The common aspect is, that in both cases sensitivity of forces plays the central role, on one hand on the active side (applied force) and on the other hand on the passive side (reaction force). The author in [179] investigated shape design sensitivities with respect to kinematical boundaries, i.e. influence on structural response due to modification on the Dirichlet boundary $\partial\boldsymbol{\mathcal{K}}_{\mathrm{D}}$ (cf. Fig. 5.2). Although the contribution has a different topic and intention, the support area is the domain of interest in both cases, i.e. in terms of kinematical boundaries and in terms of sensitivity analysis of reaction forces.

The purpose of this study is to describe and examine a sensitivity relation for reaction forces based on both tangent operators and the sensitivity relation for the state. The obtained gradient information can be used to set up optimisation problems and to find optimal designs with respect to the distribution of reaction forces. The overall amplitude of maximum reaction forces can be controlled and adjusted in combination with several objective functionals, e.g. compliance or volume. The presented approach is not comparable

to previously referred works directly, but it can be seen as an extension to the variety of available methods for analysis and design of support areas. An advantage is that derived relations can be transferred to optimisation problems on multiple scales, where effective quantities of representative volume elements on the microscale are formulated in terms of tractions or forces on the boundary, see Chapter 4 and [101, 103, 130] on theoretical aspects and explanations on multiscale methods.

For the derivation of the sensitivity relation for the physical reaction forces only parts of the discrete physical residual from Eq. (5.46) have to be considered. Therefore, some arrangements are necessary in advance. The discrete relations presented in Section 5.4 have to be partitioned in internal and boundary parameters as specified in the following. In structural analysis, equilibrium is fulfilled for a state variable $\boldsymbol{v}$ and a fixed design $\boldsymbol{X}$ if the residual Eq. (5.28) and therefore its discretised form in Eq. (5.46) vanishes. Referring the partitioned residual from Eq. (5.57) and the division in internal and external contributions $\boldsymbol{R}^{\text{int}}(\boldsymbol{v}, \boldsymbol{X}; \boldsymbol{\eta})$ and $\boldsymbol{R}^{\text{ext}}(\boldsymbol{v}, \boldsymbol{X}; \boldsymbol{\eta})$ of the residual forces one obtains

$$\boldsymbol{R}(\boldsymbol{v}, \boldsymbol{X}; \boldsymbol{\eta}) = \boldsymbol{R}^{\text{int}}(\boldsymbol{v}, \boldsymbol{X}; \boldsymbol{\eta}) - \boldsymbol{R}^{\text{ext}}(\boldsymbol{v}, \boldsymbol{X}; \boldsymbol{\eta}) = \begin{bmatrix} \boldsymbol{R}_{\text{a}}^{\text{int}} \\ \boldsymbol{R}_{\text{b}}^{\text{int}} \end{bmatrix} - \begin{bmatrix} \boldsymbol{R}_{\text{a}}^{\text{ext}} \\ \boldsymbol{R}_{\text{b}}^{\text{ext}} \end{bmatrix} = \boldsymbol{0}. \tag{5.107}$$

The dimensions of the residual in Eq. (5.107) correspond to already discussed quantities

$$\left\{\boldsymbol{R}, \boldsymbol{R}^{\text{int}}, \boldsymbol{R}^{\text{ext}}\right\} \in \mathbb{R}^{n_v} \quad \text{and therefore} \quad \left\{\boldsymbol{R}_{\text{a}}^{\text{int}}, \boldsymbol{R}_{\text{a}}^{\text{ext}}\right\} \in \mathbb{R}^{n_{\text{a}}}, \ \left\{\boldsymbol{R}_{\text{b}}^{\text{int}}, \boldsymbol{R}_{\text{b}}^{\text{ext}}\right\} \in \mathbb{R}^{n_{\text{b}}}.$$

Here, $n_v = n_{\text{a}} + n_{\text{b}}$ is the overall number of state parameters, which are connected with the inner domain with n_{a} state parameters and the boundary domain with n_{b} state parameters. In the solution point $\boldsymbol{v}$, reaction forces or external forces on the Dirichlet boundary $\partial\mathcal{K}_{\text{D}}$ for a given system are equal to their internal counterparts and can be computed using

$$\boldsymbol{R}_{\text{b}}^{\text{ext}}(\boldsymbol{v}, \boldsymbol{X}; \boldsymbol{\eta}) = \boldsymbol{R}_{\text{b}}^{\text{int}}(\boldsymbol{v}, \boldsymbol{X}; \boldsymbol{\eta}). \tag{5.108}$$

Note that the relation given in Eq. (5.108) is only valid for fully converged solutions $\boldsymbol{v}$. Otherwise, errors are unavoidable and have a significant influence on following sensitivity relations. For the sensitivity relation of reaction forces, parts of already discussed sensitivity relations in Chapter 5 for continuous, and especially in Section 5.4 for discrete formulations, can be considered. The variation of an arbitrary function f is presented in Eq. (5.33) and Eq. (5.52), respectively. This principle can be transferred to the variation of reaction forces. Hence, variations with respect to the state and design are necessary

$$\left(\boldsymbol{R}_{\text{b}}^{\text{ext}}\right)' = \left(\boldsymbol{R}_{\text{b}}^{\text{int}}\right)' = \left(\boldsymbol{R}_{\text{b}}^{\text{int}}\right)_v' + \left(\boldsymbol{R}_{\text{b}}^{\text{int}}\right)_X'. \tag{5.109}$$

In contrast to the variation of the overall residual, here only variations of the internal part $\boldsymbol{R}^{\text{int}}$ are necessary. For that reason, the investigation of the sensitivity relation for the residual $\boldsymbol{R}$ in terms of internal and external parts $\boldsymbol{R}^{\text{int}}$ and $\boldsymbol{R}^{\text{ext}}$ is conducted in the following. The total variation of the partitioned residual in Eq. (5.107) reads

$$\begin{aligned} \boldsymbol{R}' &= \left(\boldsymbol{R}^{\text{int}}(\boldsymbol{v}, \boldsymbol{X}; \boldsymbol{\eta}) - \boldsymbol{R}^{\text{ext}}(\boldsymbol{v}, \boldsymbol{X}; \boldsymbol{\eta})\right)' = \left(\boldsymbol{R}^{\text{int}}\right)_v' - \left(\boldsymbol{R}^{\text{ext}}\right)_v' + \left(\boldsymbol{R}^{\text{int}}\right)_X' - \left(\boldsymbol{R}^{\text{ext}}\right)_X' \\ &= \left(\boldsymbol{K}^{\text{int}} - \boldsymbol{K}^{\text{ext}}\right) \delta\boldsymbol{v} + \left(\boldsymbol{P}^{\text{int}} - \boldsymbol{P}^{\text{ext}}\right) \delta\boldsymbol{X}. \end{aligned} \tag{5.110}$$

Using the partial variations of $\boldsymbol{R}$ with respect to the state variable $\boldsymbol{v} = \begin{bmatrix}\boldsymbol{v}_\mathrm{a} & \boldsymbol{v}_\mathrm{b}\end{bmatrix}^T$, cf. Eq. (5.56), and with respect to design $\boldsymbol{X} = \begin{bmatrix}\boldsymbol{X}_\mathrm{a} & \boldsymbol{X}_\mathrm{b}\end{bmatrix}^T$, cf. Eq. (5.56),

$$\begin{aligned}
\boldsymbol{R}'_v &= \left(\boldsymbol{R}^{\mathrm{int}}(\boldsymbol{v},\boldsymbol{X};\boldsymbol{\eta})\right)'_v - \left(\boldsymbol{R}^{\mathrm{ext}}(\boldsymbol{v},\boldsymbol{X};\boldsymbol{\eta})\right)'_v \\
&= \begin{bmatrix}\left(\boldsymbol{R}^{\mathrm{int}}_\mathrm{a}\right)'_v - \left(\boldsymbol{R}^{\mathrm{ext}}_\mathrm{a}\right)'_v \\ \left(\boldsymbol{R}^{\mathrm{int}}_\mathrm{b}\right)'_v - \left(\boldsymbol{R}^{\mathrm{ext}}_\mathrm{b}\right)'_v\end{bmatrix} = \left\{\begin{bmatrix}\boldsymbol{K}^{\mathrm{int}}_{\mathrm{aa}} & \boldsymbol{K}^{\mathrm{int}}_{\mathrm{ab}} \\ \boldsymbol{K}^{\mathrm{int}}_{\mathrm{ba}} & \boldsymbol{K}^{\mathrm{int}}_{\mathrm{bb}}\end{bmatrix} - \begin{bmatrix}\boldsymbol{K}^{\mathrm{ext}}_{\mathrm{aa}} & \boldsymbol{K}^{\mathrm{ext}}_{\mathrm{ab}} \\ \boldsymbol{K}^{\mathrm{ext}}_{\mathrm{ba}} & \boldsymbol{K}^{\mathrm{ext}}_{\mathrm{bb}}\end{bmatrix}\right\}\begin{bmatrix}\delta\boldsymbol{v}_\mathrm{a} \\ \delta\boldsymbol{v}_\mathrm{b}\end{bmatrix} \\
\boldsymbol{R}'_X &= \left(\boldsymbol{R}^{\mathrm{int}}(\boldsymbol{v},\boldsymbol{X};\boldsymbol{\eta})\right)'_X - \left(\boldsymbol{R}^{\mathrm{ext}}(\boldsymbol{v},\boldsymbol{X};\boldsymbol{\eta})\right)'_X \\
&= \begin{bmatrix}\left(\boldsymbol{R}^{\mathrm{int}}_\mathrm{a}\right)'_X - \left(\boldsymbol{R}^{\mathrm{ext}}_\mathrm{a}\right)'_X \\ \left(\boldsymbol{R}^{\mathrm{int}}_\mathrm{b}\right)'_X - \left(\boldsymbol{R}^{\mathrm{ext}}_\mathrm{b}\right)'_X\end{bmatrix} = \left\{\begin{bmatrix}\boldsymbol{P}^{\mathrm{int}}_{\mathrm{aA}} & \boldsymbol{P}^{\mathrm{int}}_{\mathrm{aB}} \\ \boldsymbol{P}^{\mathrm{int}}_{\mathrm{bA}} & \boldsymbol{P}^{\mathrm{int}}_{\mathrm{bB}}\end{bmatrix} - \begin{bmatrix}\boldsymbol{P}^{\mathrm{ext}}_{\mathrm{aA}} & \boldsymbol{P}^{\mathrm{ext}}_{\mathrm{aB}} \\ \boldsymbol{P}^{\mathrm{ext}}_{\mathrm{bA}} & \boldsymbol{P}^{\mathrm{ext}}_{\mathrm{bB}}\end{bmatrix}\right\}\begin{bmatrix}\delta\boldsymbol{X}_\mathrm{A} \\ \delta\boldsymbol{X}_\mathrm{B}\end{bmatrix},
\end{aligned} \tag{5.111}$$

the linearised form of the total discrete variation of the residual $\boldsymbol{R}$ can be represented by

$$\boldsymbol{R}' = \left(\boldsymbol{K}^{\mathrm{int}} - \boldsymbol{K}^{\mathrm{ext}}\right)\delta\boldsymbol{v} + \left(\boldsymbol{P}^{\mathrm{int}} - \boldsymbol{P}^{\mathrm{ext}}\right)\delta\boldsymbol{X}. \tag{5.112}$$

In Eq. (5.111) the partitioned stiffness matrix $\boldsymbol{K}$ is equal to the stiffness matrix introduced in Eq. (5.47) and therefore it is also equal to Eq. (5.58). The derivation of the stiffness matrix based on the internal and external part of the residual, as presented in Eq. (5.111), results in two contributions. On one hand, $\boldsymbol{K}^{\mathrm{int}}$ contains the material and geometrical contribution to the stiffness, known from the variation of the internal part of the residual. On the other hand, $\boldsymbol{K}^{\mathrm{ext}}$ is the so-called load correction matrix and results from the variation of the external part of the residual. Initially, this term is proposed by [114] and [68] and has to be considered if external forces depend on the deformation themselves. Further explanation on this topic, on theoretical background and numerical realisation can be found in [134, 135, 144, 168] and [181, 182]. The overall stiffness matrix $\boldsymbol{K} = \boldsymbol{K}^{\mathrm{int}} - \boldsymbol{K}^{\mathrm{ext}}$ from Eq. (5.47) is subdivided in Eq. (5.111) in following submatrices

$$\boldsymbol{K}^{\mathrm{int}} = \begin{bmatrix}\boldsymbol{K}^{\mathrm{int}}_{\mathrm{aA}} & \boldsymbol{K}^{\mathrm{int}}_{\mathrm{aB}} \\ \boldsymbol{K}^{\mathrm{int}}_{\mathrm{bA}} & \boldsymbol{K}^{\mathrm{int}}_{\mathrm{bB}}\end{bmatrix}, \boldsymbol{K}^{\mathrm{ext}} = \begin{bmatrix}\boldsymbol{K}^{\mathrm{ext}}_{\mathrm{aA}} & \boldsymbol{K}^{\mathrm{ext}}_{\mathrm{aB}} \\ \boldsymbol{K}^{\mathrm{ext}}_{\mathrm{bA}} & \boldsymbol{K}^{\mathrm{ext}}_{\mathrm{bB}}\end{bmatrix}. \tag{5.113}$$

The dimensions of the resulting submatrices of the stiffness matrix $\boldsymbol{K}$ finally result to

$$\begin{aligned}
&\left\{\boldsymbol{K}, \boldsymbol{K}^{\mathrm{int}}, \boldsymbol{K}^{\mathrm{ext}}\right\} \in \mathbb{R}^{n_v \times n_v} \qquad \text{and therefore} \\
&\left\{\boldsymbol{K}^{\mathrm{int}}_{\mathrm{aa}}, \boldsymbol{K}^{\mathrm{ext}}_{\mathrm{aa}}\right\} \in \mathbb{R}^{n_\mathrm{a} \times n_\mathrm{a}}, \left\{\boldsymbol{K}^{\mathrm{int}}_{\mathrm{ab}}, \boldsymbol{K}^{\mathrm{ext}}_{\mathrm{ab}}\right\} \in \mathbb{R}^{n_\mathrm{a} \times n_\mathrm{b}}, \\
&\left\{\boldsymbol{K}^{\mathrm{int}}_{\mathrm{ba}}, \boldsymbol{K}^{\mathrm{ext}}_{\mathrm{ba}}\right\} \in \mathbb{R}^{n_\mathrm{b} \times n_\mathrm{a}}, \left\{\boldsymbol{K}^{\mathrm{int}}_{\mathrm{bb}}, \boldsymbol{K}^{\mathrm{ext}}_{\mathrm{bb}}\right\} \in \mathbb{R}^{n_\mathrm{b} \times n_\mathrm{b}}.
\end{aligned} \tag{5.114}$$

Here, $n_v = n_\mathrm{a} + n_\mathrm{b}$ is the overall number of state parameters with n_a state parameters in the inner domain and with n_b state parameters on the boundary.

In Eq. (5.112) the quantities $\boldsymbol{P}^{\mathrm{int}}$ and $\boldsymbol{P}^{\mathrm{ext}}$ represent internal and external contributions to the overall pseudo load matrix $\boldsymbol{P} = \boldsymbol{P}^{\mathrm{int}} - \boldsymbol{P}^{\mathrm{ext}}$ from Eq. (5.48) and are subdivided in

Eq. (5.111) in following submatrices

$$\boldsymbol{P}^{\text{int}} = \begin{bmatrix} \boldsymbol{P}^{\text{int}}_{\text{aA}} & \boldsymbol{P}^{\text{int}}_{\text{aB}} \\ \boldsymbol{P}^{\text{int}}_{\text{bA}} & \boldsymbol{P}^{\text{int}}_{\text{bB}} \end{bmatrix}, \boldsymbol{P}^{\text{ext}} = \begin{bmatrix} \boldsymbol{P}^{\text{ext}}_{\text{aA}} & \boldsymbol{P}^{\text{ext}}_{\text{aB}} \\ \boldsymbol{P}^{\text{ext}}_{\text{bA}} & \boldsymbol{P}^{\text{ext}}_{\text{bB}} \end{bmatrix}. \tag{5.115}$$

Dimensions of the resulting submatrices of the pseudo load matrix $\boldsymbol{P}$ finally result to

$$\begin{aligned} &\left\{\boldsymbol{P}, \boldsymbol{P}^{\text{int}}, \boldsymbol{P}^{\text{ext}}\right\} \in \mathbb{R}^{n_v \times n_X} \qquad \text{and therefore} \\ &\left\{\boldsymbol{P}^{\text{int}}_{\text{aA}}, \boldsymbol{P}^{\text{ext}}_{\text{aA}}\right\} \in \mathbb{R}^{n_{\text{a}} \times n_{\text{A}}}, \left\{\boldsymbol{P}^{\text{int}}_{\text{aB}}, \boldsymbol{P}^{\text{ext}}_{\text{aB}}\right\} \in \mathbb{R}^{n_{\text{a}} \times n_{\text{B}}}, \\ &\left\{\boldsymbol{P}^{\text{int}}_{\text{bA}}, \boldsymbol{P}^{\text{ext}}_{\text{bA}}\right\} \in \mathbb{R}^{n_{\text{b}} \times n_{\text{A}}}, \left\{\boldsymbol{P}^{\text{int}}_{\text{bB}}, \boldsymbol{P}^{\text{ext}}_{\text{bB}}\right\} \in \mathbb{R}^{n_{\text{b}} \times n_{\text{B}}}, \end{aligned} \tag{5.116}$$

with $n_v = n_{\text{a}} + n_{\text{b}}$ being the overall number of state parameters and $n_X = n_{\text{A}} + n_{\text{B}}$ being the overall number of design parameters in accordance with Fig. 5.2.

With the obtained parts and submatrices, Eq. (5.109) for the sensitivity of reaction forces continues finally to

$$\left(\boldsymbol{R}^{\text{ext}}_{\text{b}}\right)' = \boldsymbol{K}^{\text{int}}_{\text{ba}}\, \delta\boldsymbol{v}_{\text{a}} + \begin{bmatrix} \boldsymbol{P}^{\text{int}}_{\text{bA}} & \boldsymbol{P}^{\text{int}}_{\text{bB}} \end{bmatrix} \begin{bmatrix} \delta\boldsymbol{X}_{\text{A}} \\ \delta\boldsymbol{X}_{\text{B}} \end{bmatrix} = \boldsymbol{K}^{\text{int}}_{\text{ba}}\, \delta\boldsymbol{v}_{\text{a}} + \boldsymbol{P}^{\text{int}}_{\text{b}} \delta\boldsymbol{X} = \begin{bmatrix} \boldsymbol{K}^{\text{int}}_{\text{ba}}\, \boldsymbol{S}_{\text{a}} + \boldsymbol{P}^{\text{int}}_{\text{b}} \end{bmatrix} \delta\boldsymbol{X} \tag{5.117}$$

where the contributions to the pseudo load matrix are summarised in $\boldsymbol{P}^{\text{int}}_{\text{b}} = \begin{bmatrix} \boldsymbol{P}^{\text{int}}_{\text{bA}} & \boldsymbol{P}^{\text{int}}_{\text{bB}} \end{bmatrix}$ and the relation from Eq. (5.61) for the sensitivity of the state variable $\delta\boldsymbol{v}_{\text{a}}$ is used.

Remarks on numerical implementation

The sensitivity relation in Eq. (5.117), particularly the quantity which corresponds to the partial derivative of the external part of the residual on $\partial\boldsymbol{\mathcal{K}}_{\text{D}}$ with respect to design

$$\frac{\partial \boldsymbol{R}^{\text{ext}}_{\text{b}}}{\partial \boldsymbol{X}} = \boldsymbol{K}^{\text{int}}_{\text{ba}}\, \boldsymbol{S}_{\text{a}} + \boldsymbol{P}^{\text{int}}_{\text{b}}, \tag{5.118}$$

can be implemented into an existing framework for structural optimisation, e.g. they are implemented and available in MAnO. The reaction forces $\boldsymbol{R}^{\text{ext}}_{\text{b}}$ as well as their sensitivities $\left(\boldsymbol{R}^{\text{ext}}_{\text{b}}\right)'$ can be used as objective or constraint functional within the posed optimisation Problem 3.1 or Problem 3.2, respectively. The introduced sensitivity relation is valid for a wide class of element formulations due to the fact that only evaluation of assembled matrices $\boldsymbol{R}, \boldsymbol{K}$ and $\boldsymbol{P}$ on global system level is necessary. The computation of contributions on the element level to global matrices can be organised internally for any triangular, quadrilateral, tetrahedral or hexahedral element formulation with linear or quadratic shape functions. The implemented element function has to provide required output quantities, i.e. $\boldsymbol{R}_e, \boldsymbol{K}_e$ and $\boldsymbol{P}_e$ as element contributions to assembled global matrices $\boldsymbol{R}, \boldsymbol{K}$ and $\boldsymbol{P}$ presented in Eq. (5.46), Eq. (5.47) and Eq. (5.48). Details on the explicit formulation for $\boldsymbol{R}$, $\boldsymbol{K}$ and $\boldsymbol{P}$ of a two-dimensional displacement element in terms of symmetric quantities like the Green-Lagrange strain tensor $\mathbf{E}$, second Piola-Kirchhoff stress tensor $\mathbf{S}$ and the resulting fourth order elasticity tensor $\mathbb{C}$ and its matrix representation $\boldsymbol{C}$, are presented in Section 5.3 and Section 5.4 and can also be found in [99], for instance.

5.8 Numerical investigations on single scales

The intention of this section is to demonstrate the abilities of the sensitivity relations for physical reaction forces introduced in Section 5.7. Obtained formulations are applied to the following two situations

- structural optimisation of a macroscopic structure and
- structural optimisation of RVE-like domains,

both with single scale constitutive laws. Therefore, the numerical studies are simulations on single scales without the application of any homogenisation technique. Special attention is paid to the maximum amplitude of physical reaction forces on Dirichlet boundaries as well as to their sensitivity information from Section 5.7.3. The latter is incorporated as a constraint into the stated structural optimisation problems.

5.8.1 Structural optimisation of a cube-like structure of multi-material

In this example close attention is paid to the sensitivity analysis of physical reaction forces, which are used as indicators for the design of support areas. This study is divided into three parts. First, the influence of the choice of material parameters on the reaction forces is examined for the compliance minimisation problem. Afterwards, computations for compliance and volume minimisation with the reduction of the resulting maximum amplitude of reaction forces to a certain prescribed maximum value using inequality constraints follow. A brief discussion on performance and numerical accuracy is the last part of this example.

A simple cube-like structure according to the sketch in Fig. 5.3 with the side length A, loaded by a surface load on the top, fixed on the ground, and two different materials, an outer shell material E_s and a kernel material E_k, is investigated. Due to symmetry, the three dimensional cube can be reduced to the mechanical system and finite element analysis model illustrated in Fig. 5.3.

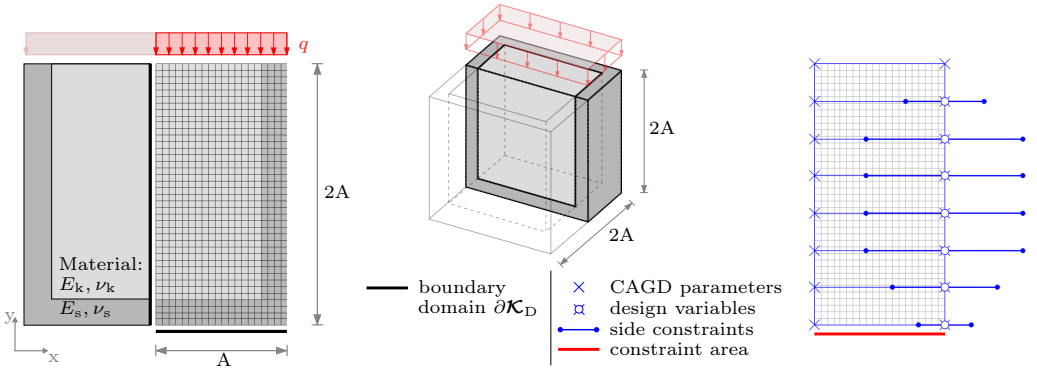

Figure 5.3: Cube of multi-material: mechanical system, FE mesh, model parameters and optimisation model (design variables and constraints area).

Table 5.1: Cube of multi-material: model parameters.

length	A	1.0
thickness	t	0.10
load	q	25.0
Young's modulus	E_{s}	25000
	E_{k}	$\gamma \cdot E_{\mathrm{s}}$
Poisson's ratio	$\nu_{\mathrm{s}} = \nu_{\mathrm{k}}$	0.20
number of elements	n_{elx} / n_{ely}	20 / 40

The overall number of elements $n_{el} = 800$ for the underling FE mesh results from the choice of the number of elements in x- and y-direction ($n_{elx} = 20, n_{ely} = 40$). For a pure displacement and geometrically non-linear element formulation based on two displacement degrees of freedom per node and Neo-Hookean constitutive law, the overall number of degrees of freedom results to $n_v = 1722$. All investigations are based on the model parameters listed in Fig. 5.3. It also contains the underling optimisation model, where a CAGD model with 16 control points assembling one Bézier patch is used for the geometry description. The number of design parameters on the nodal basis (FE mesh) amounts $n_X = 1722$ and on the geometry basis $n_{cp} = 32$. The final subset of design variables used for optimisation counts $n_s = 7$ design parameters and is reselected from the set of parameters for the described geometry model. Remarks on the choice of design variables and the differentiation between nodal and geometry design parameters are already given in Section 3.4 and Section 3.3. Referring to the formulation of an optimisation problem in Problem 3.1 or Problem 3.2, respectively, the discrete form of objectives and constraints is specified in the following subsections. Here, only lower and upper side constraints are introduced in Eq. (5.119). They are valid for all subsequent investigations and are arranged in descending order from top to bottom according to the optimisation model in Fig. 5.3.

$$\begin{bmatrix} 0.7 \\ 0.4 \\ 0.4 \\ 0.4 \\ 0.4 \\ 0.6 \\ 0.8 \end{bmatrix} = \boldsymbol{s}^{\mathrm{l}} \leq \boldsymbol{s} \leq \boldsymbol{s}^{\mathrm{u}} = \begin{bmatrix} 1.3 \\ 1.6 \\ 1.6 \\ 1.6 \\ 1.6 \\ 1.4 \\ 1.2 \end{bmatrix} . \tag{5.119}$$

The material parameter E_{k} for the kernel area is scaled by the factor γ and is related to the outer material parameter E_{s} by $E_{\mathrm{k}} = \gamma\, E_{\mathrm{s}}$. The choice of γ will be done in the following subsections explicitly. The surface load $q = 25.0$ given in Fig. 5.3 is distributed on the present 11 nodes on the top equivalently and results in nodal forces of $F_{\mathrm{n}} = 2.5$ for regular and of $F_{\mathrm{nc}} = 1.25$ for corner nodes.

Studies for different scaling factors of material properties

Eight optimisation runs are evaluated for eight different kernel material parameters E_k to examine the influence on physical reaction forces as constraints. The material scaling factor γ varies from 0.33 to 1.5 and the overall end-compliance of the system is the chosen objective, i.e. $J = C = \boldsymbol{F}^T \boldsymbol{u}$, is evaluated with the target to find a minimum. Inequality constraints $\boldsymbol{g}$ in the constraint area (cf. Fig. 5.3) are used to control the physical reaction forces $\boldsymbol{F}_\mathrm{R}$, i.e. $\boldsymbol{g} = \boldsymbol{F}_\mathrm{R}$. Compared to the initial design, the maximum amplitude of the resulting reaction force after optimisation has to remain constant for each material parameter γ, i.e. $F^{\mathrm{ini}}_{\mathrm{R,max}} = F^{\mathrm{opt}}_{\mathrm{R,max}}$. The results for all related objectives and constraints are summarised in Table 5.2. The values of the objective C can be reduced in each optimisation case. The reduction range is between approximately 5% for $\gamma = 0.33$ and 19% for $\gamma = 1.50$. Same results can be seen in Fig. 5.4, where the values of the objective decrease over iterations to a minimal value. The ratios ${}^{\mathrm{opt}}/_{\mathrm{ini}} = 1.0$ in the last column of Table 5.2 as well as the graphs in Fig. 5.4 prove, that the maximum amplitude of reaction forces remains constant for each value of γ. It is obvious how the design will change due to changes of the material parameters. For softer kernel material E_k the optimisation algorithm tends to reduce this type of material to decrease the value of compliance. For stiffer kernel material it tends to the opposite direction, i.e. the amount of stiffer material has to be increased. All design modifications, i.e. optimal distribution of the chosen control points of the Bézier patch for each value γ and the comparison of the distribution of initial reaction forces $\boldsymbol{F}^{\mathrm{ini}}_\mathrm{R}$ and the distribution of $\boldsymbol{F}^{\mathrm{opt}}_\mathrm{R}$ after optimisation are presented in Fig. 5.5 for material parameters $0.33 \leq \gamma \leq 1.5$. All design variables lie in-between prescribed side constraints $\boldsymbol{s}^{\mathrm{l}}$,$\boldsymbol{s}^{\mathrm{u}}$ and no nodal reaction force F_R exceeds the predefined maximum value $F_{\mathrm{R,max}}$. Finally, using sensitivity information of physical reaction forces allow the control of reaction forces in selected areas independent of the choice of material properties. One can observe that for softer kernel material the related area will be reduced and vice versa, i.e. that for stiffer kernel material the related area needs to be extended.

Table 5.2: Cube of multi-material: optimisation results for material parameters γ: values for objective (compliance C^{ini},C^{opt}) and constraint (reaction force $\boldsymbol{F}_\mathrm{R}$).

Material scaling factor	Objective C			Constraint $\boldsymbol{F}_\mathrm{R}$		
γ	C^{ini}	C^{opt}	${}^{\mathrm{opt}}/_{\mathrm{ini}}$	$F^{\mathrm{ini}}_{\mathrm{R,max}}$	$F^{\mathrm{opt}}_{\mathrm{R,max}}$	${}^{\mathrm{opt}}/_{\mathrm{ini}}$
0.33	4.2033	3.9847	0.99	5.0404	5.0404	1.00
0.50	3.1165	2.8864	0.93	3.9187	3.9187	1.00
0.66	2.5559	2.3114	0.90	3.2777	3.2777	1.00
0.75	2.3330	2.0853	0.89	3.0150	3.0150	1.00
1.00	1.9001	1.6680	0.88	2.5000	2.5000	1.00
1.25	1.6214	1.3534	0.83	2.6001	2.5976	1.00
1.33	1.5517	1.2822	0.83	2.6257	2.6257	1.00
1.50	1.4256	1.1554	0.81	2.6723	2.6723	1.00

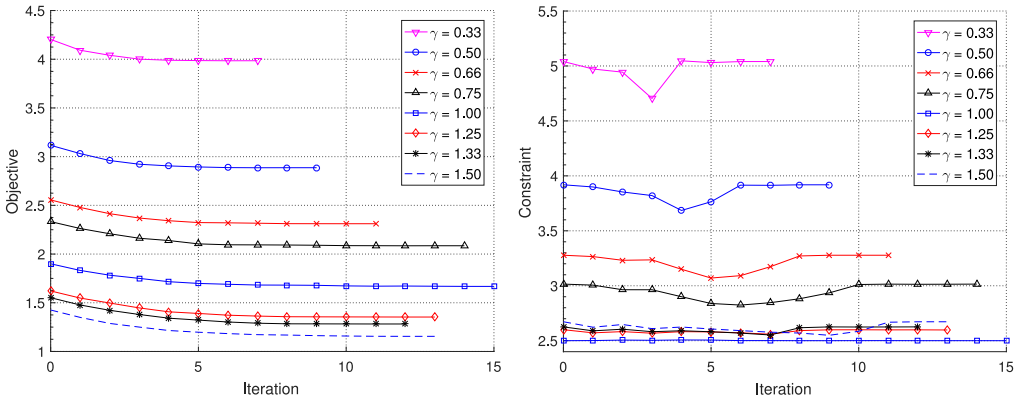

Figure 5.4: Cube of multi-material: optimisation results for material parameters γ: values for objective (compliance) and constraint (reaction force) over iterations.

Compliance minimisation and reduction of forces

In this study, the material scaling factor is fixed to the value $\gamma = 0.5$. For this explicit material distribution the compliance minimisation problem with the objective $J = C = \boldsymbol{F}^T \boldsymbol{u}$ is investigated, but different to the study in Section 5.8.1, the physical reaction forces in the constraint area (cf. Fig. 5.3) have to be reduced to the maximum amplitude of 75% compared to the amplitude of reaction force for the initial design. This can be done by the incorporation of the reaction forces as inequality constraints $\boldsymbol{g} = \boldsymbol{F}_{\mathrm{R}}$ and the definition of $F_{\mathrm{R,max}}$ as the maximum value. Used side constraints $\boldsymbol{s}^{\mathrm{l}}$,$\boldsymbol{s}^{\mathrm{u}}$ are presented in Eq. (5.119).

The mathematical optimisation algorithm used 11 iterations to obtain a minimum value for the objective, which could be reduced by approximately 6% compared to the initial design. In parallel, the incorporation of reaction forces as constraints gives the advantage and the possibility to reduce them too. Both results are presented in Fig. 5.6. The optimal distribution of design variables, which are all in the prescribed boundaries or side constraints $\boldsymbol{s}^{\mathrm{l}}$,$\boldsymbol{s}^{\mathrm{u}}$ is pictured in Fig. 5.7. Here, the contour of the initial profile of reaction forces is compared to the profile of reaction forces for the optimised design.

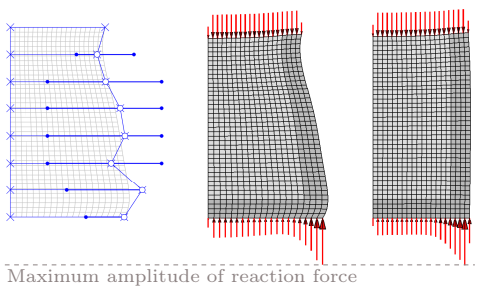

(a) $\gamma = 0.33$, amplitude $F_{\mathrm{R,max}} = 5.0404$

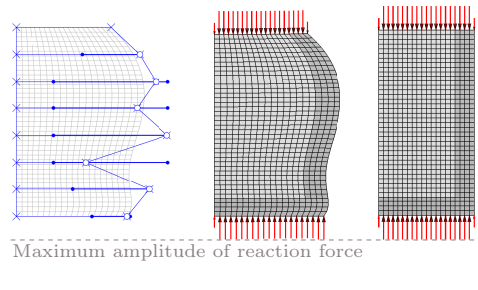

(b) $\gamma = 1.00$, amplitude $F_{\mathrm{R,max}} = 2.5000$

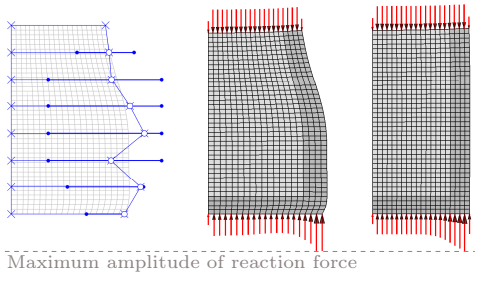

(c) $\gamma = 0.50$, amplitude $F_{\mathrm{R,max}} = 3.9187$

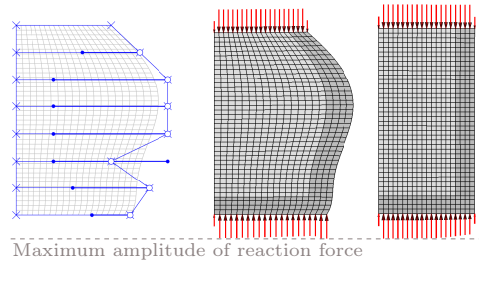

(d) $\gamma = 1.25$, amplitude $F_{\mathrm{R,max}} = 2.5976$

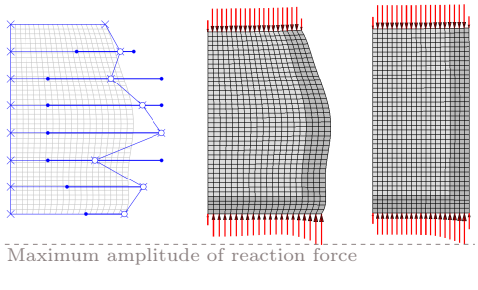

(e) $\gamma = 0.66$, amplitude $F_{\mathrm{R,max}} = 3.2777$

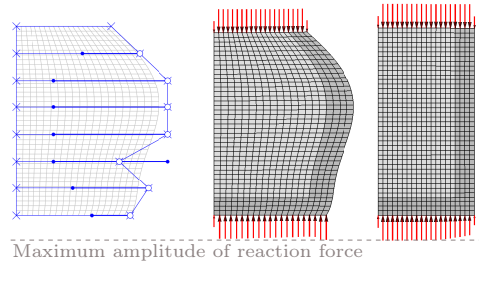

(f) $\gamma = 1.33$, amplitude $F_{\mathrm{R,max}} = 2.6257$

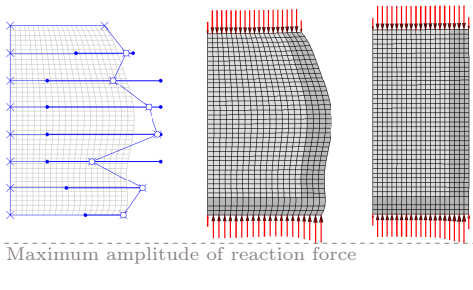

(g) $\gamma = 0.75$, amplitude $F_{\mathrm{R,max}} = 3.0150$

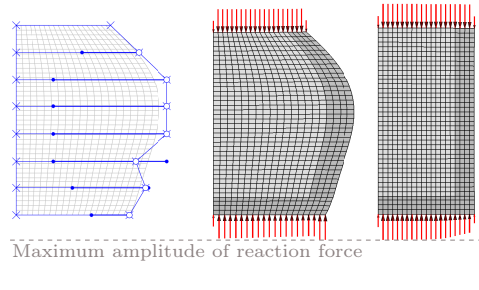

(h) $\gamma = 1.50$, amplitude $F_{\mathrm{R,max}} = 2.6723$

Figure 5.5: Cube of multi-material: optimal design (left) for material scale factors $0.33 \leq \gamma \leq 1.5$ and comparison maximum amplitude of reaction forces for optimised (middle) and initial design (right).

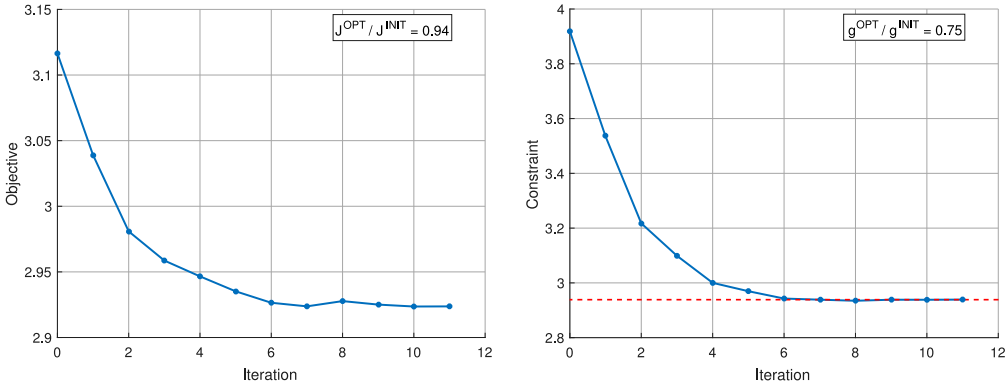

Figure 5.6: Cube of multi-material: compliance minimisation: optimisation results for objective (left) and constraint (right) over iterations.

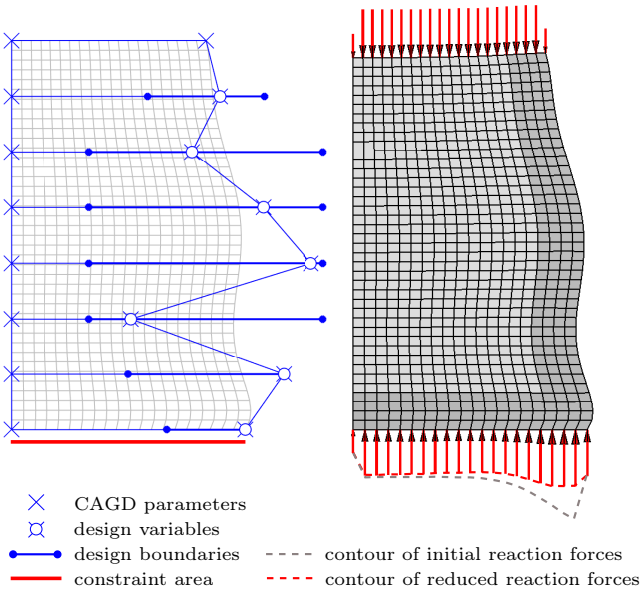

Figure 5.7: Cube of multi-material: compliance minimisation: optimal design for $\gamma = 0.50$, comparison of reaction forces for deformed system (scaling of displacements = 1).

Finally, it is the engineer's or designer's choice how to manage the balance between compliance minimisation and reduction of reaction forces. If the required maximum value for reduction of 75% is increased, the balance in the overall potential of the system between objective and constraint will change and the compliance minimisation will lead to higher reduction values than only 6%.

Volume minimisation and reduction of forces

Here, the setup for the optimisation problem is similar to the setup for the compliance minimisation presented in Section 5.8.1. The only difference is that the objective function will be exchanged and the overall volume $J = V$ of the given system has to be minimised. The material scaling factor is fixed to the value $\gamma = 0.5$ and the maximum amplitude of the reaction forces have to be reduced to 75% compared to the initial design by incorporation of inequality constraints and a maximum value $F_{\mathrm{R,max}}$. The optimisation algorithm reaches the optimum value for the objective after 11 iterations and the optimisation process is aborted. The overall volume can be reduced by approximately 37% compared to the initial design. Furthermore the constraint for the reaction forces is fulfilled and allows to reduce them by 25% compared to the initial design. These results are illustrated in Fig. 5.8. The corresponding distribution of design variables which remain in the prescribed side constraints $\boldsymbol{s}^{\mathrm{l}}$,$\boldsymbol{s}^{\mathrm{u}}$ from Eq. (5.119) as well as the contour of the initial and optimised profile of reaction forces is presented in Fig. 5.9.

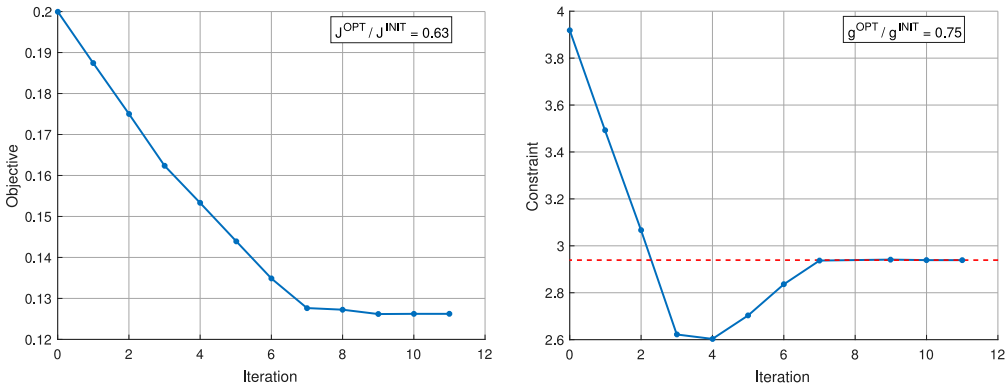

Figure 5.8: Cube of multi-material: volume minimisation: optimisation results for objective (left) and constraint (right) over iterations.

In this case, the designer or the engineer also has to decide on the balance between volume minimisation and reduction of reaction forces. For the chosen and presented optimisation setup, the large resulting displacements on the right top side of the system (cf. Fig. 5.9) are the consequence. If the system or the material is able to handle this kind of displacement amplitude, the gain is the enormous reduction of volume and the reduction of final reaction forces as pressure loads on the ground.

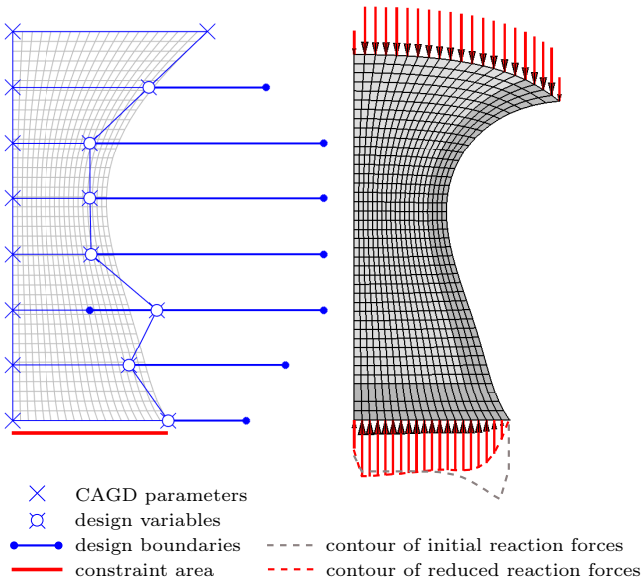

Figure 5.9: Cube of multi-material: volume minimisation: optimal design for $\gamma = 0.50$, comparison of reaction forces for deformed system (scaling of displacements = 1).

Remarks on numerical performance and accuracy

To demonstrate the time consuming differences between structural optimisation based on numerically obtained gradients in terms of FDM and on the variational approach for design sensitivity analysis, the investigated model problem in this section with the following dimensions is considered. The number of design variables on nodal basis is $n_X = 1722$ and on geometrical basis $n_{cp} = 32$. The final number for a selected subset of design variables amounts $n_s = 7$. The average computation time for one nonlinear structural analysis with Neo-Hookean constitutive law takes four Newton iterations and lasts approximately ${}^{\mathrm{m}}t_{\mathrm{a}} \approx 1.0$ second using a moderately optimised MATLAB R2018a code on the mobile workstation listed in Table 2.4 in Chapter 2. The consequences for the numerical determination of gradients lead for a typical forward or backward difference quotient $n_{\mathrm{F}}^{\mathrm{f,b}} = n + 1$ and a central difference quotient $n_{\mathrm{F}}^{\mathrm{c}} = 2\,n$ function evaluations, with n being a general and replaceable number of design variables and therefore, of n necessary perturbations and structural analyses. Thus, the resulting computation times for numerical gradients are ${}^{\mathrm{m}}t_{\mathrm{s,num}}^{\mathrm{f,b}} = n_{\mathrm{F}}^{\mathrm{f,b}} \cdot {}^{\mathrm{m}}t_{\mathrm{a}}$ (forward/backward FDM scheme) and ${}^{\mathrm{m}}t_{\mathrm{s,num}}^{\mathrm{c}} = n_{\mathrm{F}}^{\mathrm{c}} \cdot {}^{\mathrm{m}}t_{\mathrm{a}}$ (central FDM scheme). Due to the fact that one structural analysis takes approximately 1.0 second and coincides fine with one function evaluation n_{F}, the times for comparison are directly used in seconds instead of relative representations. For the given model problem the results for the numerical effort and time consumptions are summarised in Table 5.3. Compared to these results, it can be shown that the analytical gradients are characterised by a significantly improved performance. Despite the assembly of the overall pseudo load matrix from Eq. (5.48) and the solution of a global system of equations for the sensitivity

Table 5.3: Numerical effort for optimisation based on numerical gradients (FDM).

number of design parameters n	FDM computation times ${}^{\mathrm{m}}t^{\mathrm{f,b}}_{\mathrm{s,num}}$	${}^{\mathrm{m}}t^{\mathrm{c}}_{\mathrm{s,num}}$
$n_X = 1722$	1723 sec.	3444 sec.
$n_{cp} = 32$	33 sec.	64 sec.
$n_s = 7$	8 sec.	14 sec.

of the state from Eq. (5.51) to obtain the required reduced sensitivity matrix, only one structural analysis is needed and the overall run time amounts $t_{\mathrm{s}} \approx 2.0$ seconds. Thus, for $n > t_{\mathrm{s}} \;/\; t_{\mathrm{a}}$ design parameters, the analytically derived gradients will save computation time. Even in the fastest numerical test for seven design variables and only a forward FDM scheme, the ratio is ${}^{\mathrm{m}}t_{\mathrm{s}} \;/\; {}^{\mathrm{m}}t_{\mathrm{a}} = 2 \;/\; 8$ and the analytical gradient is faster. In the case of linear elastic structural analyses with St. Venant-Kirchhoff constitutive law, the computation times in Table 5.3 will be reduced by approximately 75%, but even then, the analytical gradient is more efficient if more than one design parameter is considered.

Next, the accuracy of the gradient information from Eq. (5.118) is examined. To gain the highest precision for numerical approximations of the required gradient, central finite difference approximation with perturbations $\boldsymbol{\Delta X}$ between 1×10^{-2} and 1×10^{-9} are applied. The relative error between both gradients, i.e. the numerical and analytical gradient, is evaluated by the application of the *L2-norm* (also known as the *Euclidean norm*).

Fig. 5.4: Cube of multi-material: accuracy of derived gradients.

Perturbation $\boldsymbol{\Delta X}$	$\frac{\|\nabla \boldsymbol{g}^{\mathrm{num}} - \nabla \boldsymbol{g}\|}{\|\nabla \boldsymbol{g}\|}$
1×10^{-2}	4.7892×10^{-3}
1×10^{-3}	4.7424×10^{-5}
1×10^{-4}	4.7419×10^{-7}
1×10^{-5}	4.7426×10^{-9}
1×10^{-6}	1.4128×10^{-9}
1×10^{-7}	1.4002×10^{-8}
1×10^{-8}	1.3134×10^{-7}
1×10^{-9}	1.6846×10^{-6}

The final results of this numerical test are depicted in Table 5.4. The results let conclude, that best approximations of analytically derived gradients can be achieved by using perturbations $\boldsymbol{\Delta X}$ of design parameters in the range between 1×10^{-5} and 1×10^{-7} (coloured blue) for this particular example and prove the correctness of the determination of analytical gradients at the same time. Besides the importance of accuracy, there is still potential for improvements of the numerical behaviour and numerical performance of the analytically derived sensitivity information. For instance, the factorised stiffness matrix from structural analysis, can be used at different stages in the structural analysis and the design sensitivity analysis framework.

5.8.2 Structural optimisation of RVE-like domains

The purpose of following investigations is the demonstration of the application of the sensitivity information of reaction forces introduced in Eq. (5.118) as a constraint within structural, ptimisation for different situations affiliated with characteristic microscale representations. The focus lies on the geometrical design and improvement of selected RVE-like domains illustrated in Fig. 5.10. Parametrisations of the design domain using CAGD

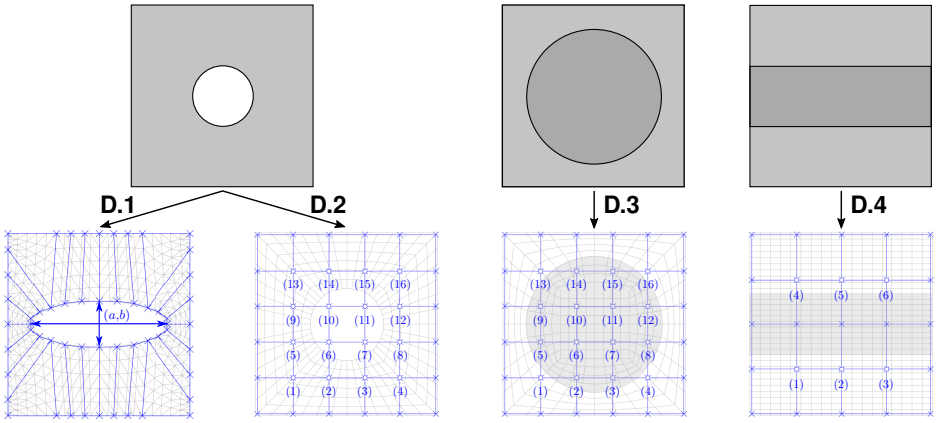

Figure 5.10: RVE-like domains: selection of samples for numerical investigations: square domain with i) a circular hole (left), ii) a circular inclusion (middle), iii) bi-material (right).

and morphing based models are applied. All studies can be connected to a microscale analysis in an individual integration point of a stated upper scale BVP according to presented homogenisation techniques in Chapter 4 and therefore, a macroscopic deformation gradient $\overline{\boldsymbol{F}}$ is used as a test loading case. The evaluation of the structural response is performed using periodic boundary conditions (P) from Eq. (4.26) for underlying St. Venant-Kirchhoff or Neo-Hookean constitutive laws. In addition, the impact on the homogenised or effective stresses $\overline{\boldsymbol{P}}_{\mathrm{K,P}}$ from Eq. (4.31) is emphasised. The upcoming investigations are organised in following four examples

- **D.1**: Square domain with a hole using CAGD model,
- **D.2**: Square domain with a hole using morphing based model,
- **D.3**: Square domain with an inclusion using morphing based model,
- **D.4**: Square domain with bi-material using morphing based model.

Each of the square domains has a characteristic side length $A = 1$ and is incorporated into the general discrete optimisation form from Problem 3.2. The origin of the coordinate system is positioned in the center of the domain and the boundaries of design parameters are referred to this position. The target of minimisation of the overall material consumption in an appropriate way is expressed by the volume objective function, i.e. $J = V$. Inequality constraints in form of reaction forces, i.e. $\boldsymbol{g} = \boldsymbol{F}_{\mathrm{R}}$, allow to control the design process in terms of specified characteristics, e.g. resulting effective stresses can be tailored to structural and materials abilities. It should be mentioned that design sensitivity information

obtained on nodal level of the FEM mesh has to be transformed via corresponding design velocity fields according to descriptions in Section 3.4. Within all examples D.1 to D.4, a transformation via the design velocity matrix $\boldsymbol{V}_C = \mathrm{d}\boldsymbol{X}/\mathrm{d}\boldsymbol{C}$ for geometrical control points of the CAGD model or of the morphing box, respectively, is required. Additionally, in D.1 control points of the CAGD model depend on the diameters $\boldsymbol{a} = \begin{bmatrix} a & b \end{bmatrix}$ of the hole, which are finally chosen as design variables. Therefore, a further transformation of obtained sensitivity information via the design velocity $\boldsymbol{V}_s = \mathrm{d}\boldsymbol{C}/\mathrm{d}\boldsymbol{s}$ for the diameters is necessary. To obtain the final sensitivity information, the following evaluations are necessary

$$\begin{aligned} \textbf{D.1}: \quad & \frac{\mathrm{d}(\cdot)}{\mathrm{d}\boldsymbol{s}} = \frac{\partial(\cdot)}{\partial \boldsymbol{X}} \frac{\mathrm{d}\boldsymbol{X}}{\mathrm{d}\boldsymbol{C}} \frac{\mathrm{d}\boldsymbol{C}}{\mathrm{d}\boldsymbol{s}} = \frac{\partial(\cdot)}{\partial \boldsymbol{X}} \boldsymbol{V}_C \boldsymbol{V}_s, \\ \textbf{D.1} \text{ to } \textbf{D.4}: \quad & \frac{\mathrm{d}(\cdot)}{\mathrm{d}\boldsymbol{s}} = \frac{\partial(\cdot)}{\partial \boldsymbol{X}} \frac{\mathrm{d}\boldsymbol{X}}{\mathrm{d}\boldsymbol{C}} = \frac{\partial(\cdot)}{\partial \boldsymbol{X}} \boldsymbol{V}_C. \end{aligned} \tag{5.120}$$

To avoid confusion, the dimensions for the number of finite element nodes n_N, for the number of finite elements n_{el}, the resulting number of degrees of freedom n_v, the number of possible design parameters on the nodal level n_X and on the geometry level n_{cp} and the final subset of chosen design variables n_s for optimisation is summarised in Table 5.5 for all examples. The underlying element technology is in all cases a pure displacement formulation with linear shape functions and two degrees of freedom per node for tri- and rectangular element types. Beside the optimisation results, all mesh and design information from Table 5.5 can be found in Fig. 5.11 to 5.14. Beside some example specific remarks, the results concerning optimisation are presented in following paragraphs.

Table 5.5: RVE-like domains: model dimensions for numerical investigations.

		CAGD	**Morphing**		
Number of ...		**D.1**	**D.2**	**D.3**	**D.4**
finite element nodes	n_N	360	336	337	608
finite elements	n_{el}	600	288	320	558
degrees of freedom	n_v	720	672	674	1216
design parameters on					
nodal level	n_X	720	672	674	1216
geometry level	n_{cp}	56	72	72	50
final design variables	n_s	2	32	32	10

Square domain with a circular hole

The first study considers situations D.1 and D.2, both square domains with a circular hole. Parametrisation of the domain is realised by a CAGD model for D.1 on one hand and using morphing techniques D.2 on the other hand. Additionally, for both cases different initial situations are defined, i.e. D.1 considers an elliptical hole as initial design and a St. Venant-Kirchhoff constitutive law, where D.2 considers a circular hole as initial design and a Neo-Hookean constitutive law. The technological data is equal for both situations and is set to $E = 1000$ for the Young's modulus, to $\nu = 0.2$ for the Poisson's ratio and to $t = 0.1$ for the thickness of both domains. Both domains are evaluated for the macroscopic deformation gradient as a loading case

$$\overline{\boldsymbol{F}} = \begin{bmatrix} 1.20 & 0.10 \\ 0.05 & 1.10 \end{bmatrix} \tag{5.121}$$

in accordance to numerical homogenisation techniques. The design parameters within the solution of the optimisation problems are the diameters (a,b) of inclusion for D.1 and therefore, the overall number of design variables is $n_s = 2$, and coordinates of control points of the inner morphing box for D.2 and therefore, the overall number of design variables is $n_s = 32$. The optimisation results for D.1 are pictured in Fig. 5.11. The distribution of design variables is listed in Section 5.8.2 .

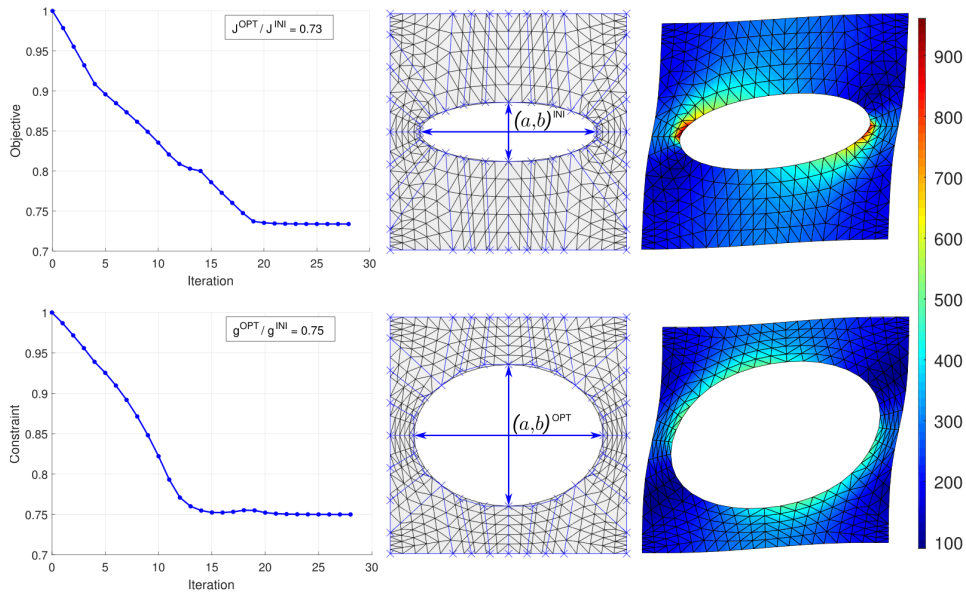

Figure 5.11: RVE-like domains: optimisation results for domain **D.1**: progress of objective and constraint (left), initial and optimised design (middle), von Mises stress disctribution for initial and optimised design (right).

The optimisation algorithm takes 28 iterations to reduce the volume objective by approximately 27%. Simultaneously, the maximum amplitude of arising reaction forces

Table 5.6: RVE-like domains: distribution of design variables for domain **D.1**: defined lower and upper design bounds $s^{\mathrm{l}}$and s^{u}, initial and optimised design values $s^{\mathrm{ini}}$and s^{opt}.

Design variable	s^{l}	s^{u}	s^{ini}	s^{opt}
a	0.1000	0.8000	0.7500	0.8000
b	0.1000	0.8000	0.2500	0.5981

on the surface of the domain can be reduced by approximately 25%. The reduction of reaction forces has an impact on the maximum value of resulting local von Mises stresses, i.e. the maximum value $\sigma_{\mathrm{eq}}^{\mathrm{ini}} = 960.85$ can be reduced to $\sigma_{\mathrm{eq}}^{\mathrm{opt}} = 509.56$. A similar impact can be observed after the evaluation of effective stresses for both states, i.e.

$$\overline{\boldsymbol{P}}_{\mathrm{K,P}}^{\mathrm{ini}} = \begin{bmatrix} 261.37 & 55.93 \\ 53.56 & 103.18 \end{bmatrix} \quad \text{and} \quad \overline{\boldsymbol{P}}_{\mathrm{K,P}}^{\mathrm{opt}} = \begin{bmatrix} 156.23 & 25.64 \\ 24.35 & 68.02 \end{bmatrix}. \tag{5.122}$$

The optimisation results for **D.2** are pictured in Fig. 5.12. The distribution of design variables is listed in Table 5.7 .

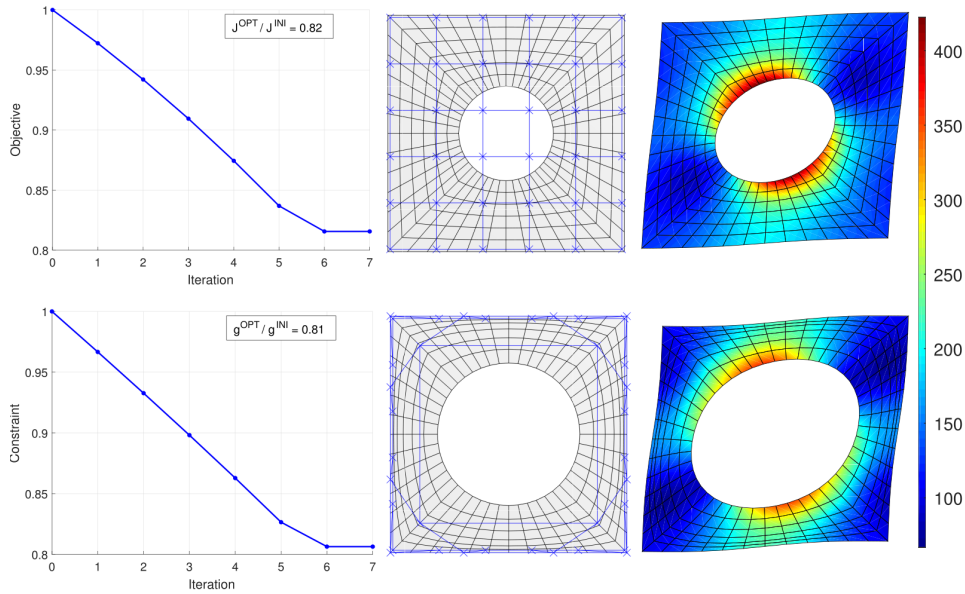

Figure 5.12: RVE-like domains: optimisation results for domain **D.2**: progress of objective and constraint (left), initial and optimised design (middle), von Mises stress disctribution for initial and optimised design (right).

Table 5.7: RVE-like domains: distribution of design variables for domain **D.2**: defined lower and upper design bounds $s^{\mathrm{l}}$and s^{u}, initial and optimised design values $s^{\mathrm{ini}}$and s^{opt}.

Design variable	Direction ($1 = x, 2 = y$)	s^{l}	s^{u}	s^{ini}	s^{opt}
1	1	−0.5000	−0.2000	−0.2940	−0.4999
1	2	−0.5000	−0.2000	−0.2940	−0.4999
2	1	−0.1900	−0.0100	−0.0980	−0.1899
2	2	−0.5000	−0.2000	−0.2940	−0.4999
3	1	0.0100	0.1900	0.0980	0.1899
3	2	−0.5000	−0.2000	−0.2940	−0.4999
4	1	0.2000	0.5000	0.2940	0.4999
4	2	−0.5000	−0.2000	−0.2940	−0.4999
5	1	−0.5000	−0.2000	−0.2940	−0.4999
5	2	−0.1900	−0.0100	−0.0980	−0.1899
6	1	−0.3750	0.1000	−0.0980	−0.3749
6	2	−0.3750	0.1000	−0.0980	−0.3749
7	1	−0.1000	0.3750	0.0980	0.3749
7	2	−0.3750	0.1000	−0.0980	−0.3749
8	1	0.2000	0.5000	0.2940	0.4999
8	2	−0.1900	−0.0100	−0.0980	−0.1899
9	1	−0.5000	−0.2000	−0.2940	−0.4999
9	2	0.0100	0.2000	0.0980	0.1999
10	1	−0.3750	0.1000	−0.0980	−0.3749
10	2	−0.1000	0.3750	0.0980	0.3749
11	1	−0.1000	0.3750	0.0980	0.3749
11	2	−0.1000	0.3750	0.0980	0.3749
12	1	0.2000	0.5000	0.2940	0.4999
12	2	0.0100	0.2000	0.0980	0.1999
13	1	−0.5000	−0.2000	−0.2940	−0.4999
13	2	0.2100	0.5000	0.2940	0.4999
14	1	−0.1900	−0.0100	−0.0980	−0.1899

continued on next page ...

Design variable	Direction ($1 = x, 2 = y$)	s^{l}	s^{u}	s^{ini}	s^{opt}
14	2	0.2100	0.5000	0.2940	0.4999
15	1	0.0100	0.1900	0.0980	0.1899
15	2	0.2100	0.5000	0.2940	0.4999
16	1	0.2000	0.5000	0.2940	0.4999
16	2	0.2100	0.5000	0.2940	0.4999

The optimisation algorithm takes 9 iterations to reduce the volume objective by approximately 28%. Simultaneously, the maximum amplitude of arising reaction forces on the surface of the domain can be reduced by approximately 28%. The reduction of reaction forces has an impact on the maximum value of resulting local von Mises stresses, i.e. the maximum value $\sigma_{\mathsf{eq}}^{\mathrm{ini}} = 422.32$ can be reduced to $\sigma_{\mathsf{eq}}^{\mathrm{opt}} = 358.60$. A similar impact can be observed after evaluation of effective stresses for both states, i.e.

$$\overline{\boldsymbol{P}}_{\mathrm{K,P}}^{\mathrm{ini}} = \begin{bmatrix} 171.37 & 39.45 \\ 33.28 & 120.21 \end{bmatrix} \quad \text{and} \quad \overline{\boldsymbol{P}}_{\mathrm{K,P}}^{\mathrm{opt}} = \begin{bmatrix} 113.52 & 23.54 \\ 20.01 & 75.65 \end{bmatrix}. \tag{5.123}$$

Square domain with a circular inclusion

Here, situation D.3 is considered, i.e. a square domain with a circular inclusion. The parametrisation of the domain is realised using morphing. The evaluation of structural analysis part is based on the Neo-Hookean constitutive law with a Young's modulus $E_{\mathrm{m}} = 1000$ for the matrix and $E_{\mathrm{i}} = 1500$ for the inclusion's material, and a Poisson's ratio $\nu = 0.2$ for both. The thickness of the matrix material is set to $t_{\mathrm{m}} = 0.1$ and for the inclusion to $t_{\mathrm{i}} = 0.3$. This circumstance simulates the worthiness of the inclusion's material, e.g. the inclusion's material might be more expensive. Within volume minimisation, this part of the domain is therefore priorised for design changes. The overall domain is evaluated for a macroscopic deformation gradient as a loading case

$$\overline{\boldsymbol{F}} = \begin{bmatrix} 1.20 & 0.15 \\ 0.15 & 1.20 \end{bmatrix} \tag{5.124}$$

in accordance to numerical homogenisation techniques. A subset of all coordinates of control points of the morphing box is chosen as design space, i.e. inner control points of the morphing box are design variables, and therefore, $n_s = 32$. The optimisation results for D.3 are pictured in Fig. 5.13. The distribution of design variables is listed in Table 5.8.

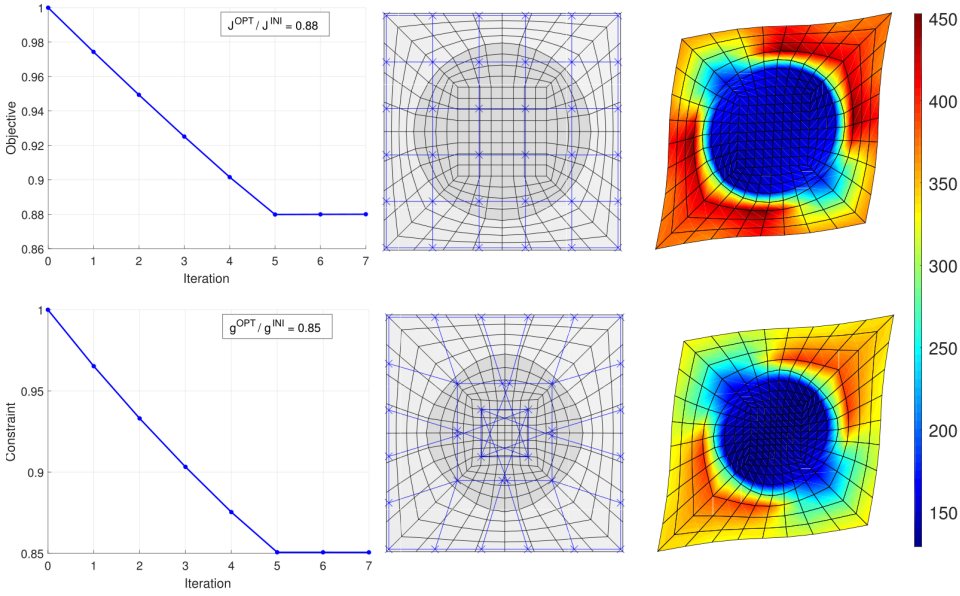

Figure 5.13: RVE-like domains: optimisation results for domain **D.3**: progress of objective and constraint (left), initial and optimised design (middle), von Mises stress disctribution for initial and optimised design (right).

Table 5.8: RVE-like domains: distribution of design variables for domain **D.3**: defined lower and upper design bounds $s^{\mathrm{l}}$and s^{u}, initial and optimised design values $s^{\mathrm{ini}}$and s^{opt}.

Design variable	Direction ($1 = x, 2 = y$)	s^{l}	s^{u}	s^{ini}	s^{opt}
1	1	−0.6000	−0.2000	−0.2940	−0.2000
1	2	−0.6000	−0.2000	−0.2940	−0.2000
2	1	−0.1900	−0.0100	−0.0980	−0.0100
2	2	−0.6000	−0.2000	−0.2940	−0.2000
3	1	0.0100	0.1900	0.0980	0.0100
3	2	−0.6000	−0.2000	−0.2940	−0.2000
4	1	0.2000	0.6000	0.2940	0.2000
4	2	−0.6000	−0.2000	−0.2940	−0.2000
5	1	−0.6000	−0.2000	−0.2940	−0.2000
5	2	−0.1900	−0.0100	−0.0980	−0.0100

continued on next page ...

Design variable	Direction ($1 = x, 2 = y$)	s^{l}	s^{u}	s^{ini}	s^{opt}
6	1	−0.4500	0.1000	−0.0980	0.0999
6	2	−0.4500	0.1000	−0.0980	0.0999
7	1	−0.1000	0.4500	0.0980	−0.0999
7	2	−0.4500	0.1000	−0.0980	0.0999
8	1	0.2000	0.6000	0.2940	0.2000
8	2	−0.1900	−0.0100	−0.0980	−0.0100
9	1	−0.6000	−0.2000	−0.2940	−0.2000
9	2	0.0100	0.2000	0.0980	0.0100
10	1	−0.4500	0.1000	−0.0980	0.0999
10	2	−0.1000	0.4500	0.0980	−0.0999
11	1	−0.1000	0.4500	0.0980	−0.0999
11	2	−0.1000	0.4500	0.0980	−0.0999
12	1	0.2000	0.6000	0.2940	0.2000
12	2	0.0100	0.2000	0.0980	0.0100
13	1	−0.6000	−0.2000	−0.2940	−0.2000
13	2	0.2100	0.6000	0.2940	0.2100
14	1	−0.1900	−0.0100	−0.0980	−0.0100
14	2	0.2100	0.6000	0.2940	0.2100
15	1	0.0100	0.1900	0.0980	0.0196
15	2	0.2100	0.6000	0.2940	0.2100
16	1	0.2000	0.6000	0.2940	0.2000
16	2	0.2100	0.6000	0.2940	0.2100

The optimisation algorithm takes 7 iterations to reduce the volume objective by approximately 12%. Simultaneously, the maximum amplitude of arising reaction forces on the surface of the domain can be reduced by approximately 15%. The reduction of reaction forces has an impact on the maximum value of resulting local von Mises stresses, i.e. the maximum value $\sigma_{\mathsf{eq}}^{\mathrm{ini}} = 452.69$ can be reduced to $\sigma_{\mathsf{eq}}^{\mathrm{opt}} = 400.32$. A similar impact can be observed after the evaluation of effective stresses for both states, i.e.

$$\overline{\boldsymbol{P}}_{\mathsf{K,P}}^{\mathrm{ini}} = \begin{bmatrix} 213.33 & 65.77 \\ 65.77 & 213.33 \end{bmatrix} \quad \text{and} \quad \overline{\boldsymbol{P}}_{\mathsf{K,P}}^{\mathrm{opt}} = \begin{bmatrix} 185.65 & 57.76 \\ 57.73 & 185.86 \end{bmatrix}. \tag{5.125}$$

Square domain with rectangular stripe

The final study for situation D.4 considers a square domain with a lengthy inclusion. The parametrisation of the domain is realised using morphing. The evaluation of structural analysis part is based on the Neo-Hookean constitutive law with a Young's modulus $E_\mathrm{m} = 1000$ for the matrix and $E_\mathrm{i} = 1500$ for the inclusion's material and a Poisson's ratio $\nu = 0.2$ for both. Compared to situation D.3, a similar strategy for the thickness disctribution is utilised to characterise the worthiness of used materials, i.e. the thickness of the matrix material is set to $t_\mathrm{m} = 0.1$ and for the inclusion to $t_\mathrm{i} = 0.3$. Here, the inclusion's material might be more expensive. Within volume minimisation, this part of the domain is therefore priorised for design changes. The overall domain is evaluated for a macroscopic deformation gradient as a loading case

$$\overline{\boldsymbol{F}} = \begin{bmatrix} 1.20 & 0.15 \\ 0.15 & 1.20 \end{bmatrix} \tag{5.126}$$

in accordance to numerical homogenisation techniques. A subset of all coordinates of control points of the morphing box is chosen as design space, i.e. inner control points of the morphing box are design variables, and therefore, $n_s = 10$. The optimisation results for D.4 are pictured in Fig. 5.14. The distribution of design variables is listed in Table 7.9.

Table 5.9: RVE-like domains: distribution of design variables for domain **D.4**: defined lower and upper design bounds $s^\mathrm{l}$and s^u, initial and optimised design values $s^\mathrm{ini}$and s^opt.

Design variable	Direction ($1 = x, 2 = y$)	s^l	s^u	s^ini	s^opt
1	1	−0.6500	−0.0100	−0.2450	−0.6500
1	2	−0.6500	0.1000	−0.2450	0.0999
2	2	−0.6500	0.1000	−0.2450	0.0999
3	1	0.0100	0.6500	0.2450	0.6499
3	2	−0.6500	0.1000	−0.2450	0.0999
4	1	−0.6500	−0.0100	−0.2450	−0.6500
4	2	−0.1000	0.6500	0.2450	−0.0999
5	2	−0.1000	0.6500	0.2450	−0.0999
6	1	0.0100	0.6500	0.2450	0.6499
6	2	−0.1000	0.6500	0.2450	−0.0999

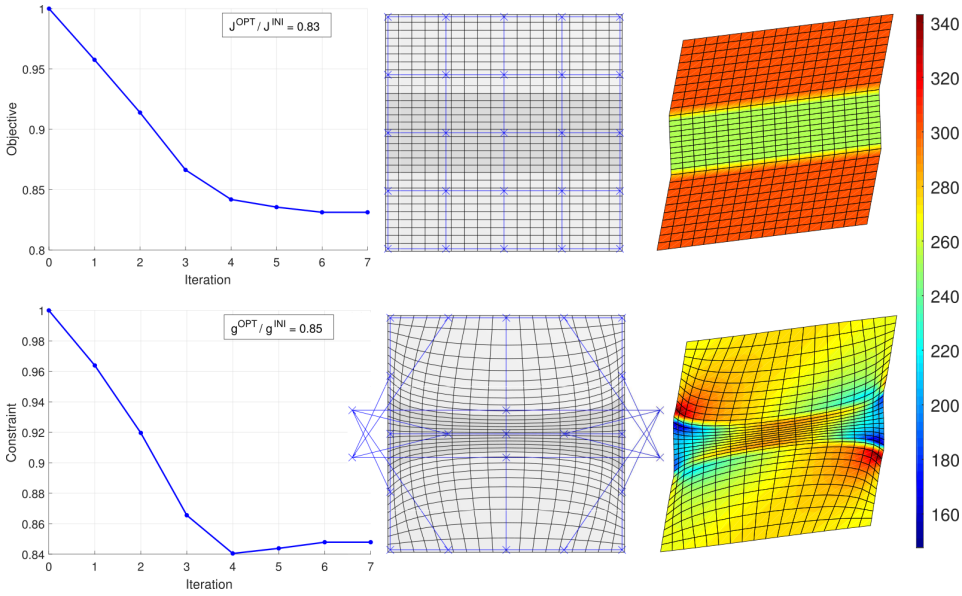

Figure 5.14: RVE-like domains: optimisation results for domain **D.4**: progress of objective and constraint (left), initial and optimised design (middle), von Mises stress disctribution for initial and optimised design (right).

The optimisation algorithm takes 8 iterations to reduce the volume objective by approximately 22%. Simultaneously, the maximum amplitude of arising reaction forces on the surface of the domain can be reduced by approximately 23%. In contrast to prior studies, the reduction of reaction forces has an opposite impact on the maximum value of resulting local von Mises stresses, i.e. the maximum value $\sigma_{\text{eq}}^{\text{ini}} = 302.97$ increases to $\sigma_{\text{eq}}^{\text{opt}} = 342.90$. Finally, it depends on the engineers experience and requirements for useful decisions concerning the material choice. Nevertheless, it can be observed that effective stresses can be decreased, i.e.

$$\underline{\overline{\boldsymbol{P}}}_{\text{K,P}}^{\text{ini}} = \begin{bmatrix} 318.30 & 70.80 \\ 82.67 & 223.24 \end{bmatrix} \quad \text{and} \quad \underline{\overline{\boldsymbol{P}}}_{\text{K,P}}^{\text{opt}} = \begin{bmatrix} 250.52 & 62.04 \\ 68.80 & 196.42 \end{bmatrix}. \tag{5.127}$$

Conclusion

In summary, design sensitivity information of physical reaction forces is used to evaluate constraints within structural optimisation and to control the design process. In each case, the maximum amplitude of resulting reaction forces could be reduced by a certain amount, which directly has an impact on effective and homogenised stresses. These are usually used for structural analysis purposes on the upper scale within numerical homogenisation schemes. Incorporation of physical reaction forces and of their sensitivity information gives the designing engineers the opportunity to adjust the material's behaviour to stated macroscopic problem formulations and to tailor applications to their special requirements.

5.9 Summary and concluding remarks

After an introduction and the outline on the state of the art, basic relations for the variational design sensitivity analysis based on the intrinsic formulation with enhanced kinematics are presented. Several relations known from continuum mechanics are extended by necessary design variations to obtain gradients for optimisation procedures based on first order methods. All continuous relations are transferred to their discrete counterparts and are available for numerical treatment and investigation in the scope of FEM and structural optimisation. The most important quantities and relations in continuous and discrete form, which are frequently used throughout this work, are compiled in Table 5.10 and Table 5.11 and can directly be used for further investigations.

Table 5.10: Overview of continuous and discrete parameters, tangent stiffness and pseudo load as well as sensitivity operators on single scale.

	Continuous	**Discrete**	cf. Eq.
Parameters			
state	$\boldsymbol{v}$	$\boldsymbol{v}$	5.28, 5.46
design (mesh level)	$\boldsymbol{s}, (\boldsymbol{X})$	$\boldsymbol{s}, (\boldsymbol{X})$	5.28, 5.46
state variation	$\delta\boldsymbol{v}$	$\delta\boldsymbol{v}$	5.29, 5.46
design variation (mesh level)	$\delta\boldsymbol{s}, (\delta\boldsymbol{X})$	$\delta\boldsymbol{s}, (\delta\boldsymbol{X})$	5.29, 5.46
Physical residual	$R(\boldsymbol{v}, \boldsymbol{s}; \boldsymbol{\eta})$	$\boldsymbol{R}(\boldsymbol{v}, \boldsymbol{s}; \boldsymbol{\eta})$	5.28, 5.46
Stiffness operator	$k(\boldsymbol{v}, \boldsymbol{s}; \boldsymbol{\eta}, \delta\boldsymbol{v})$	$\boldsymbol{K} = \partial\boldsymbol{R}/\partial\boldsymbol{v}$	5.30, 5.47
Pseudo load operator	$p(\boldsymbol{v}, \boldsymbol{s}; \boldsymbol{\eta}, \delta\boldsymbol{s})$	$\boldsymbol{P} = \partial\boldsymbol{R}/\partial\boldsymbol{X}$	5.31, 5.48
Sensitivity operator	$s(\boldsymbol{v}, \boldsymbol{s}; \delta\boldsymbol{s})$	$\boldsymbol{S} = \mathrm{d}\boldsymbol{v}/\mathrm{d}\boldsymbol{X} = \boldsymbol{K}^{-1}\boldsymbol{P}$	5.32, 5.51

Table 5.11: Summary of discrete sensitivity relations and operators on single scales.

	Discretisation	cf. Eq.
Physical residual		
internal	$\boldsymbol{R}_i^e = \int_{\boldsymbol{\mathcal{K}}^e} \boldsymbol{P}_{\mathsf{K}} \boldsymbol{L}_i \, \mathrm{d}V$	5.89
external	$\boldsymbol{F}_i^e = \int_{\overline{\boldsymbol{\mathcal{K}}}^e} N_i \overline{\boldsymbol{b}} \, \mathrm{d}V$	5.90
Physical stiffness	$\boldsymbol{K}_{ij}^e = \int_{\boldsymbol{\mathcal{K}}^e} \boldsymbol{B}_{vi}^T \boldsymbol{A} \boldsymbol{B}_{vj} \, \mathrm{d}V$	5.91
Pseudo load		
internal	$\boldsymbol{P}_{ij}^e = \int_{\boldsymbol{\mathcal{K}}^e} \boldsymbol{B}_{vi}^T \boldsymbol{A} \boldsymbol{B}_{sj} - \boldsymbol{P}_{\mathsf{K}} \boldsymbol{L}_j \boldsymbol{L}_i^T + \boldsymbol{P}_{\mathsf{K}} \boldsymbol{L}_i \boldsymbol{L}_j^T \, \mathrm{d}V$	5.92
external	$(\overline{\boldsymbol{F}}'_{\overline{X}})_{ij} = \int_{\overline{\boldsymbol{\mathcal{K}}}^e} N_i \, \overline{\boldsymbol{b}} \, \boldsymbol{L}_j^T \, \mathrm{d}V$	5.93

Several studies accentuated possible usage and application of the sensitivity information, especially of the sensitivity information of physical reaction forces. For instance, they are used to control amplitudes of arising physical reaction forces, which interact with foundations of mechanical parts in Section 5.8.1 or within numerical homogenisation schemes to control effective parameters in Section 5.8.2. A brief discussion on performance and accuracy concerning one of the presented model problems can be found in Section 5.8.1.

Chapter 6

Material design based on variational sensitivity information

In this chapter, ideas and several aspects for optimal material design are stated. Formulations for design sensitivity analysis on multiple scales are provided and prepared for the enhancement of frameworks for multiscale structural analysis. Especially variational formulations for sensitivity analysis are focused on and are implemented into an environment for numerical structural optimisation. General multiscale optimisation problems are formulated and accentuated by some proposals for solution strategies.

6.1 Introduction

Understanding multiscale homogenisation techniques and the well-known FE^2 methods gives the opportunity to analyse complex and heterogeneous materials on different length scales. A brief overview on methods and literature is given in Chapter 4. This outstanding and deep insight into the physical behaviour of individual constituents of heterogeneous material compositions comes along with the allure of improvements in terms of the overall performance or adjustments of the physical response. The presented framework for multiscale analysis is predestinated for purposes within structural optimisation, especially due to its variety of possible applications.

One of the objectives of the work at hand is the enhancement of established FE^2 methods with elements from variational sensitivity analysis, presented in Chapter 5, and the usage of obtained formulations within frameworks for structural optimisation. Formulations of BVPs on multiple scales have to be augmented by formulations of problems for structural optimisation with objective functions, constraints and design variables on different scales. Decoupled problem formulations, where the macroscale and the microscale are investigated individually, are possible in general, but these formulations are unrewarding within issues based on complex interactions between referred scales and therefore, they are unrewarding within the presented work. The target is to obtain a closed formulation, which contains the sensitivity information of the overall macroscopic BVP and therefore, the sensitivity information of all underlying microscopic BVPs. Within the setup for multiscale structural analysis problems, the domains $\overline{\boldsymbol{\mathcal{K}}}$ for the macroscale and the domain $\boldsymbol{\mathcal{K}}$ for the microscale are introduced. After the solution of the stated BVP in terms of structural analysis, the

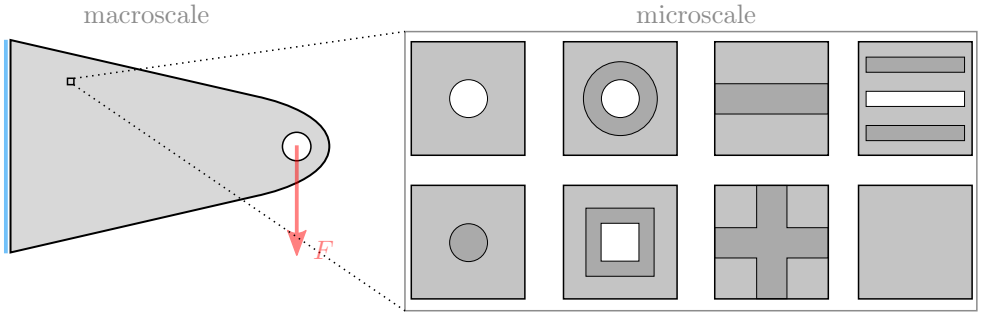

Figure 6.1: Possible model problems for structural optimisation on multiple scales.

subsequently performed design sensitivity analysis gives the opportunity to deal with following three questions and investigations:

- How will physical responses in $\overline{\mathcal{K}}$ react, if design parameters in $\overline{\mathcal{K}}$ change?
- How will physical responses in $\overline{\mathcal{K}}$ react, if design parameters in $\mathcal{K}$ change?
- How will physical responses in $\overline{\mathcal{K}}$ react, if design parameters in $\overline{\mathcal{K}}$ and $\mathcal{K}$ change?

These questions represent a central investigation and are evaluated in Chapter 7 within several numerical examples. Beforehand, some possible model problems are schematically pictured in Fig. 6.1. Each individual microscale RVE can be embedded into the macroscale domain and investigated within several optimisation procedures. A basic selection of objective functions, constraints and design parameters is introduced in Table 3.1 in Chapter 3 and can now be used for several combinations within problem formulations over multiple scales. For instance, on the macroscale, the compliance or the volume of the system, according to classical approaches for structural optimisation, can be chosen as objective function. Design variables can be defined using appropriate degrees of freedom within the underlying geometry description. The overall procedure can be controlled by some constraints, which incorporate boundaries for stresses, strains or displacements. On the microscale, there are only design variables and constraints to choose. Possible design variables are the half-axes, the position or orientation of holes or inclusions, or in general the geometry in an abstract sense. The range of possible design parameters can be supplemented by different material parameters for the inclusion or matrix material. Constraints like volume fractions for matrix material and inclusion or boundaries for displacement or stress measures are also useful within the optimisation setup. The presented range of possible combinations of objective functions, constraints and design parameters, underlines the necessity of a closed form of the optimisation problem with the overall sensitivity information. The behaviour of an introduced macroscopic objective function depends directly on the choice of design parameters on the microscale. The upcoming challenge is characterised by the verification of incorporated FE^2 analysis and FE^2 optimisation methods in mathematical, mechanical and computational sense. The field of optimisation on multiple scales using techniques for numerical homogenisation is investigated by several researchers and groups over the past years. Overall, a broad field of applications is considered intensively but particularly, solution strategies within the

field of topology optimisation methods are the major topics of interest. The authors in [22] give an extensive introduction on topology optimisation methods in general, but they also refer topics on inverse homogenisation methods. They briefly overview methodologies on how to design materials with several target properties like a specific Young's modulus, a specific thermal expansion coefficient or a negative Poisson's ratio. This topics are also part of several works listed below. The goal of most discussed examples is to find solutions for problem formulations based on optimisation of series of individual base cells and not to find one optimal representation for the whole domain. This holds true for several publications on inverse homogenisation problems within procedures for topology optimisation. Most relations are formulated in accordance to the rules of continuum elasticity and effective parameters are obtained using averaging schemes over lower scales, represented by periodic base cells or RVEs within frameworks for numerical homogenisation. The general field of continuum elasticity provides a wide range of possible applications and therefore, several publications propose a variety of formulations for the design of materials, especially for the design of linear elastic materials. The author in [139, 140] explains how to prescribe thermoelastic properties within a stated topology optimisation problem and how to seek for solutions in terms of weight minimisation and manufacturing constraints for truss-like and continuum-like materials. Further problem formulations for the choice of optimal thermoelastic properties with the target of maximum, zero or negative thermal expansion can be found in [141, 142]. Aspects concerning efficient methods for the design of microstructures for heat transfer problems and high-resolution problems with multiscale and multiphysics characteristics are discussed in [1]. The design of periodic linear elastic microstructures of cellular materials in terms of maximisation of weighted sum of equivalent strain energy density or linear combinations of mechanical properties under volume and material symmetry constraints are discussed in [110] as well as for minimisation of mean compliance subject to volume fractions of constituents in an underlying RVE in [55]. Poroelastic materials which act as actuators under mechanical pressure and are modeled in a two-scale fluid-structure interaction approach are introduced in [4].

The key idea of extreme materials is often represented by applications with negative Poisson's ratios. Several authors in [87, 108, 125, 139, 140] tackle optimisation problems and provide results and material representations for this kind of structures, which in general are characterised by their ability for high energy absorption and fracture resistance. Further examples on extremal materials like composites with extremal bulk modulus in two and three dimensions for honeycomb-like structures are reported in [138], combinations of extreme bulk and shear modulus and negative Poisson's ratio are presented in [172] and examples for functionally graded composites with near-zero shear modulus and negative Poisson's ratio are topics in [116]. Two-phase composite materials with targeted properties such as piezoelectric properties in combination with thermoelectric coefficients can be found in [75]. The author in [3] suggests a strategy to obtain an isotropic three-dimensional structure consisting of rods, hinges and springs, which finally results in a Poisson's ratio close to minus one. Composites with extreme thermal expansion coefficients and piezocomposites with optimal hydrophone characteristics subject to elastic symmetry and volume fractions are addressed to in [143]. Inverse homogenisation problems for two-phase viscoelastic properties of composites to obtain improved stiffness or damping characteristics are studied in [177] and for prescribed shear modulus in [36]. Topological

design of multiphase RVEs with respect to minimisation of the sound power radiation from vibrating macrostructures under time-harmonic mechanical loadings is illustrated in [176]. General investigations for multiphase composites and their design process for optimal performance under certain constraints are proposed in [61, 158, 160] and especially in [150] for high stiffness or high strength composites. Procedures which tackle orthotropic materials, thickness of components and especially the optimisation of the angle of material rotation or material orientation in general are derived in [118, 119] and [117]. The authors in [41] introduce a computational model to design bi-material composite laminates to minimise structural compliance with mixed sets of micro and macro design variables. The target is to find optimal composite microstructures and optimal fibre orientation on the macroscale. Material design and application to sandwich-type structures with a reduction of the total number of design variables due to the introduction of design subdomains to simplify applicability and manufacturability is investigated in [42]. Aspects on lightweight materials for non-periodic topologies within minimum and compliant mechanism problems can be found in [91].

Topology optimisation of microstructures with a fixed macroscale based on so-called material test on the lower scale, cf. [156] for details, is stated in [79]. Strategies based on evolutionary optimisation algorithms, like the *bi-directional evolutionary structural optimisation* (BESO), for the concurrent design of material and structures within frameworks for topology optimisation and non-linear FE^2 analysis with design variables on both scales are investigated in [170, 171, 173, 174]. In order to reduce numerical effort, the authors in latter publications also introduce reduced multiscale models in terms of *Proper Orthogonal Decomposition* (POD) or reduced database models affiliated with a priori off-line steps. An improved optimisation scheme for the mentioned BESO algorithm based on the introduction of a damping scheme for sensitivity numbers is proposed by [54, 175]. Furthermore, the authors exchanged the non-linear elastoplastic FE^2 analysis by a *potential-based Reduced Basis Model Order Reduction* (pRBMOR) with GPU acceleration. All mentioned aspects on efficient topology optimisation schemes for the design of multiscale non-linear heterogeneous structures and high performance materials are summarised in [169]. In comparison to previously cited publications, solution strategies for two-scale optimisation problems based on level set and on *extended finite element method* (XFEM) formulations can be found in [164], and in [93] for closed liquid cells materials, with the shape of fluid inclusion as design on the microscale and topology as design on the macroscale. Improved structural performance and improved effective response results from improved underlying lower scale periodic design. The authors in [78] bridge topology and shape optimisation schemes to design three-dimensional microstructured materials with extreme properties using energy-based homogenisation and parameteric level set methods. Patterns for engineered materials in terms of size, shape and layout of inclusion-like phases in continuum domains are obtained in [64].

An extensive introduction on shape optimisation methods using homogenisation techniques is given in [2]. Shape optimisation results for bi-material microstructures are reported in [76] for inelastic materials and in [112] for minimisation of local stress fields by the application of XFEM and a level set representation of the geometry.

In this work special emphasis is given to methods for shape optimisation. The extension of methods for numerical homogenisation by variational sensitivity relations for design modifications in terms of geometrical parameters plays the central role.

6.2 Sensitivity relations for problems on multiple scales

Most relations introduced in Chapter 5 for sensitivity analysis on single scales can be used for investigations on multiple scales. Beside notational modifications, several extensions and conventions are necessary. According to Remark 4.1, also within design sensitivity analysis for multiscale problems, quantities connected to the macroscale are identified by overlines and quantities connected to the microscale are represented without any additional markers. The extension of the classical layout for continuum mechanics for multiscale problems is presented in Fig. 6.2. Beside the macroscopic deformation mapping $\overline{\boldsymbol{\varphi}}(\overline{\boldsymbol{X}}(\overline{s}),t)$,

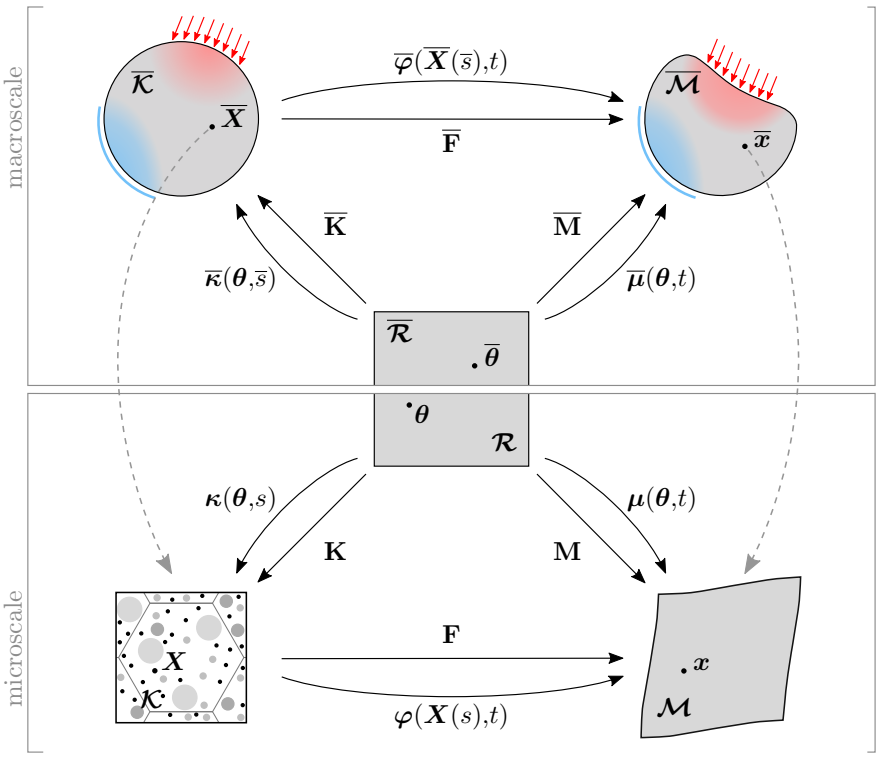

Figure 6.2: Enhanced kinematics within the framework of multiple scales: referential configurations $\overline{\mathcal{K}}$ and $\mathcal{K}$, physical configurations $\overline{\mathcal{M}}$ and $\mathcal{M}$, introduction of a local convective configuration $\overline{\mathcal{R}}$ and $\mathcal{R}$, deformation mappings $\overline{\boldsymbol{\varphi}}$ and $\boldsymbol{\varphi}$, introduction of a local geometry mappings $\overline{\boldsymbol{\kappa}}$ and $\boldsymbol{\kappa}$ and introduction of local motion mappings $\overline{\boldsymbol{\mu}}$ and $\boldsymbol{\mu}$.

which in general depends on the time variable (t) and the macroscopic design $(\overline{s})$, the microscopic deformation mapping $\boldsymbol{\varphi}(\boldsymbol{X}(\boldsymbol{s}),t)$ with the dependence on the microscopic design (s) is introduced. Both mappings can be equivalently decomposed in so-called local geometry and local deformation mappings with the distinction in macroscopic and microscopic contributions, i.e. using mappings $\{\overline{\boldsymbol{\mu}},\overline{\boldsymbol{\kappa}}^{-1}\}$ for the macroscale and mappings $\{\boldsymbol{\mu},\boldsymbol{\kappa}^{-1}\}$ for the microscale one obtains the decompositions

$$\overline{\boldsymbol{\varphi}} = \overline{\boldsymbol{\mu}} \circ \overline{\boldsymbol{\kappa}}^{-1} \qquad \text{and} \qquad \boldsymbol{\varphi} = \boldsymbol{\mu} \circ \boldsymbol{\kappa}^{-1}. \tag{6.1}$$

The full set of point mappings and affiliated tangent mappings in terms of macro- and microscopic notation is summarised in Table 6.1. All introduced tangent mappings can be used to perform pull-back and push-forward operations between the configurations $\overline{\mathcal{K}}, \overline{\mathcal{M}}$ and $\overline{\mathcal{R}}$ on the macroscale and between the configurations $\mathcal{K}, \mathcal{M}$ and $\mathcal{R}$ on the microscale for several variations and several quantities from continuum mechanics. The advantage of the presented approach is, that the methodological procedure for obtaining analytical variations of physical quantities can be proceeded independent of the scale under investigation. All presented relations in Section 5.2 and Section 5.3 are also valid for problems on multiple scales.

Table 6.1: Overview of macro- and microscopic point and tangent mappings.

Description	**Macroscale**	**Microscale**
Deformation mapping	$\overline{\boldsymbol{\varphi}}$	$\boldsymbol{\varphi}$
Local geometry mapping	$\overline{\boldsymbol{\kappa}}$	$\boldsymbol{\kappa}$
Local deformation mapping	$\overline{\boldsymbol{\mu}}$	$\boldsymbol{\mu}$
Deformation gradient	$\overline{\mathbf{F}} = \operatorname{Grad} \overline{\boldsymbol{\varphi}}$	$\mathbf{F} = \operatorname{Grad} \boldsymbol{\varphi}$
Local geometry gradient	$\overline{\mathbf{K}} = \operatorname{GRAD} \overline{\boldsymbol{\kappa}}$	$\mathbf{K} = \operatorname{GRAD} \boldsymbol{\kappa}$
Local deformation gradient	$\overline{\mathbf{M}} = \operatorname{GRAD} \overline{\boldsymbol{\mu}}$	$\mathbf{M} = \operatorname{GRAD} \boldsymbol{\mu}$

6.2.1 Macroscopic weak form of equilibrium and its variation

Special attention has to be paid concerning the weak form of equilibrium and therefore, concerning the physical residual on the macroscale. The dependencies change and the list of arguments is extended by quantities resulting from the microscale. Due to the characteristics of used homogenisation approaches, treatment of stated physical situations on the microscale in terms of structural analysis but also in terms of design sensitivity analysis is similar to problems on single scales, presented in Section 5.3.1. The treatment of stated physical situations on the upper scale depends on effective parameters not only within structural analysis but also within design sensitivity analysis. Furthermore, a design description for the microscale is introduced. All combinations of possible dependencies are summarised in Table 6.2. The full relation for the weak form of equilibrium as the

Table 6.2: Macroscopic physical residual: possible dependencies and situations.

Scope	**Single scale**	**Multiple scales**
Structural analysis	$R(\boldsymbol{v}; \boldsymbol{\eta}) = 0$	$\overline{R}(\overline{\boldsymbol{v}}, \boldsymbol{v}; \overline{\boldsymbol{\eta}}) = 0$
Design sensitivity analysis	$R(\boldsymbol{v}, \boldsymbol{s}; \boldsymbol{\eta}) = 0$	$\overline{R}(\overline{\boldsymbol{v}}, \overline{\boldsymbol{s}}, \boldsymbol{v}, \boldsymbol{s}; \overline{\boldsymbol{\eta}}) = 0$

basis for all upcoming investigations within design sensitivity analysis, and later structural optimisation, reads

$$\overline{R}(\overline{\boldsymbol{v}}, \overline{\boldsymbol{s}}, \boldsymbol{v}, \boldsymbol{s}; \overline{\boldsymbol{\eta}}) = 0. \tag{6.2}$$

Equal to formulations on single scales, any perturbation of state and design parameters on the macro- and the microscale must not violate the equilibrium state of a given mechanical system. Therefore, Eq. (6.2) has to be fulfilled for any perturbation $\delta\overline{\boldsymbol{v}}$ of the state variable $\overline{\boldsymbol{v}}$, both $\{\overline{\boldsymbol{v}}, \delta\overline{\boldsymbol{v}}\} \in \overline{\mathcal{V}}$, any perturbation $\delta\overline{\boldsymbol{s}}$ in the design parameter $\overline{\boldsymbol{s}}$, both $\{\overline{\boldsymbol{s}}, \delta\overline{\boldsymbol{s}}\} \in \overline{\mathcal{S}}$, any perturbation $\delta\boldsymbol{v}$ of the state variable $\boldsymbol{v}$, both $\{\boldsymbol{v}, \delta\boldsymbol{v}\} \in \mathcal{V}$ and for any perturbation $\delta\boldsymbol{s}$ in the design parameter $\boldsymbol{s}$, both $\{\boldsymbol{s}, \delta\boldsymbol{s}\} \in \mathcal{S}$. The consequence from this statement is the possibility for the formulation of several tangent operators. Considering aforementioned dependencies, the total variation of the physical residual reads

$$\begin{aligned}
\overline{R}'(\overline{\boldsymbol{v}}, \overline{\boldsymbol{s}}, \boldsymbol{v}, \boldsymbol{s}; \overline{\boldsymbol{\eta}}, \delta\overline{\boldsymbol{v}}, \delta\overline{\boldsymbol{s}}, \delta\boldsymbol{v}, \delta\boldsymbol{s}) &= \overline{R}'_{\overline{v}}(\overline{\boldsymbol{v}}, \overline{\boldsymbol{s}}, \boldsymbol{v}, \boldsymbol{s}; \overline{\boldsymbol{\eta}}, \delta\overline{\boldsymbol{v}}) + \overline{R}'_{\overline{s}}(\overline{\boldsymbol{v}}, \overline{\boldsymbol{s}}, \boldsymbol{v}, \boldsymbol{s}; \overline{\boldsymbol{\eta}}, \delta\overline{\boldsymbol{s}}) \\
&\quad + \overline{R}'_{v}(\overline{\boldsymbol{v}}, \overline{\boldsymbol{s}}, \boldsymbol{v}, \boldsymbol{s}; \overline{\boldsymbol{\eta}}, \delta\boldsymbol{v}) + \overline{R}'_{s}(\overline{\boldsymbol{v}}, \overline{\boldsymbol{s}}, \boldsymbol{v}, \boldsymbol{s}; \overline{\boldsymbol{\eta}}, \delta\boldsymbol{s}) \\
&= \overline{k}(\overline{\boldsymbol{v}}, \overline{\boldsymbol{s}}, \boldsymbol{v}, \boldsymbol{s}; \overline{\boldsymbol{\eta}}, \delta\overline{\boldsymbol{v}}) + \overline{p}(\overline{\boldsymbol{v}}, \overline{\boldsymbol{s}}, \boldsymbol{v}, \boldsymbol{s}; \overline{\boldsymbol{\eta}}, \delta\overline{\boldsymbol{s}}) \\
&\quad + \widetilde{k}(\overline{\boldsymbol{v}}, \overline{\boldsymbol{s}}, \boldsymbol{v}, \boldsymbol{s}; \overline{\boldsymbol{\eta}}, \delta\boldsymbol{v}) + \widetilde{p}(\overline{\boldsymbol{v}}, \overline{\boldsymbol{s}}, \boldsymbol{v}, \boldsymbol{s}; \overline{\boldsymbol{\eta}}, \delta\boldsymbol{s}) = 0.
\end{aligned} \tag{6.3}$$

Here, the variations of the macroscopic physical residual with respect to state variables $\overline{\boldsymbol{v}}$ and $\boldsymbol{v}$ are introduced by tangent stiffness operators $\overline{k}$ and $\widetilde{k}$ and variations with respect to design parameters $\overline{\boldsymbol{s}}$ and $\boldsymbol{s}$ are introduced by tangent pseudo operators $\overline{p}$ and $\widetilde{p}$, respectively. At this point, it is important to distinguish the tangent operators $\{\widetilde{k}, \widetilde{p}\}$ and explicit microscopic tangent operators $\{k, p\}$, which are derived in Section 6.4.1 in terms of microscopic quantities exclusively. In the following, each tangent operator is stated

$$\begin{aligned}
\overline{k}(\overline{\boldsymbol{v}}, \overline{\boldsymbol{s}}, \boldsymbol{v}, \boldsymbol{s}; \overline{\boldsymbol{\eta}}, \delta\overline{\boldsymbol{v}}) &= \overline{R}'_{\overline{v}}(\overline{\boldsymbol{v}}, \overline{\boldsymbol{s}}, \boldsymbol{v}, \boldsymbol{s}; \overline{\boldsymbol{\eta}}, \delta\overline{\boldsymbol{v}}) && \text{macro physical stiffness operator,} \\
\overline{p}(\overline{\boldsymbol{v}}, \overline{\boldsymbol{s}}, \boldsymbol{v}, \boldsymbol{s}; \overline{\boldsymbol{\eta}}, \delta\overline{\boldsymbol{s}}) &= \overline{R}'_{\overline{s}}(\overline{\boldsymbol{v}}, \overline{\boldsymbol{s}}, \boldsymbol{v}, \boldsymbol{s}; \overline{\boldsymbol{\eta}}, \delta\overline{\boldsymbol{s}}) && \text{macro pseudo load operator,} \\
\widetilde{k}(\overline{\boldsymbol{v}}, \overline{\boldsymbol{s}}, \boldsymbol{v}, \boldsymbol{s}; \overline{\boldsymbol{\eta}}, \delta\boldsymbol{v}) &= \overline{R}'_{v}(\overline{\boldsymbol{v}}, \overline{\boldsymbol{s}}, \boldsymbol{v}, \boldsymbol{s}; \overline{\boldsymbol{\eta}}, \delta\boldsymbol{v}) && \textit{multilevel} \text{ stiffness operator,} \\
\widetilde{p}(\overline{\boldsymbol{v}}, \overline{\boldsymbol{s}}, \boldsymbol{v}, \boldsymbol{s}; \overline{\boldsymbol{\eta}}, \delta\boldsymbol{s}) &= \overline{R}'_{s}(\overline{\boldsymbol{v}}, \overline{\boldsymbol{s}}, \boldsymbol{v}, \boldsymbol{s}; \overline{\boldsymbol{\eta}}, \delta\boldsymbol{s}) && \textit{multilevel} \text{ pseudo load operator.}
\end{aligned} \tag{6.4}$$

Remark 6.1 (Utilisation of the term *multilevel*) *Throughout the entire work, the term "multilevel" indicates variations of the macroscopic residual $\overline{R}$ with respect to parameters related to the microscale, i.e. quantities like the microscopic state and design.*

6.2.2 Sensitivity of the macroscopic physical state

The solution of the sensitivity relation in Eq. (6.3) allows the derivation of an implicit sensitivity relation for the macroscopic state in current equilibrium point $(\overline{\boldsymbol{v}}, \overline{\boldsymbol{s}}, \boldsymbol{v}, \boldsymbol{s})$, i.e.

$$\delta\overline{\boldsymbol{v}} = \widehat{s}\,(\overline{\boldsymbol{v}}, \overline{\boldsymbol{s}}, \boldsymbol{v}, \boldsymbol{s}; \delta\widehat{\boldsymbol{s}}\,) = \overline{s}\,(\overline{\boldsymbol{v}}, \overline{\boldsymbol{s}}, \boldsymbol{v}, \boldsymbol{s}; \delta\overline{\boldsymbol{s}}\,) + \widetilde{s}\,(\overline{\boldsymbol{v}}, \overline{\boldsymbol{s}}, \boldsymbol{v}, \boldsymbol{s}; \delta\boldsymbol{s}) \qquad \text{with} \quad \delta\widehat{\boldsymbol{s}} = \begin{bmatrix} \delta\overline{\boldsymbol{s}} \\ \delta\boldsymbol{s} \end{bmatrix}. \tag{6.5}$$

Here, the sensitivity operator $\widehat{s}$ represents a combination of contributions $\overline{s}$ resulting from the macroscale (red) and of $\widetilde{s}$ resulting from the microscale (blue). The operator $\widehat{s}$ is formulated in terms of the combined vector $\delta\widehat{\boldsymbol{s}}$, which includes design variations in both referred scales. From Eq. (6.5), changes of the macroscopic state $\delta\overline{\boldsymbol{v}}$ induced by

changes of macroscopic (red) and microscopic (blue) design parameters can be deduced, i.e. changes due to $\delta\overline{\boldsymbol{s}}$ and $\delta\boldsymbol{s}$. Introduced sensitivity operators $\widehat{s}$, $\overline{s}$ and $\widetilde{s}$ in Eq. (6.5) and the additional exclusive sensitivity of the microscopic state s are characterised as follows

$$\begin{aligned}
\overline{s}: &\quad \text{sensitivity of macro state (exclusively),}\\
\widetilde{s}: &\quad \text{sensitivity of macro state caused by micro changes (multilevel),}\\
\widehat{s}: &\quad \text{effective sensitivity of macro state caused by macro and micro changes,}\\
s: &\quad \text{sensitivity of micro state (exclusively).}
\end{aligned} \tag{6.6}$$

Discrete relations for sensitivity operators are provided in Section 6.3. Explicit formulations of residual and tangent forms on individual scales as well as formulations of the sensitivity of effective parameters are given in Section 6.4.

6.2.3 Variations of arbitrary macroscopic functionals

Similar to the design variation of an arbitrary functional on a single scale in Section 5.3.3, a design variation of an arbitrary functional formulated on multiple scales can be obtained in terms of the implicit macro- and multilevel sensitivity relation in Eq. (6.5) and the implicit sensitivity relation of the state on one scale from Eq. (5.32), here of the microscale. Dependencies on quantities from two different scales have to be taken into account. For an objective functional or constraint $f(\overline{\boldsymbol{v}}, \overline{\boldsymbol{s}}, \boldsymbol{v}, \boldsymbol{s})$ the total design variation with respect to macroscopic and microscopic design, i.e. with respect to $\overline{\boldsymbol{s}}$ and $\boldsymbol{s}$, reads

$$\begin{aligned}
f' &= f'_{\overline{v}} + f'_{\overline{s}} + f'_{v} + f'_{s} = \frac{\partial f}{\partial \overline{\boldsymbol{v}}}\delta\overline{\boldsymbol{v}} + \frac{\partial f}{\partial \overline{\boldsymbol{s}}}\delta\overline{\boldsymbol{s}} + \frac{\partial f}{\partial \boldsymbol{v}}\delta\boldsymbol{v} + \frac{\partial f}{\partial \boldsymbol{s}}\delta\boldsymbol{s}\\
&= \left[\frac{\partial f}{\partial \overline{\boldsymbol{v}}} \circ \overline{s} + \frac{\partial f}{\partial \overline{\boldsymbol{s}}}\right]\delta\overline{\boldsymbol{s}} + \left[\frac{\partial f}{\partial \overline{\boldsymbol{v}}} \circ \widetilde{s} + \frac{\partial f}{\partial \boldsymbol{v}} \circ s + \frac{\partial f}{\partial \boldsymbol{s}}\right]\delta\boldsymbol{s}.
\end{aligned} \tag{6.7}$$

The first bracket term (red) provides information about changes of the functional f due to changes of macroscopic design parameters $\delta\overline{\boldsymbol{s}}$ and the second bracket term (blue) provides information about changes induced by changes of microscopic design parameters $\delta\boldsymbol{s}$.

6.3 Discrete sensitivity relations for multiscale problems

Established and standard finite element discretisation techniques, based on discrete approximations $\{\overline{\boldsymbol{v}}_h, \boldsymbol{v}_h\}$ for macro- and microscopic state variables and on discrete approximations $\{\overline{\boldsymbol{X}}_h, \boldsymbol{X}_h\}$ for macro- and microscopic design parameters, can be utilised in terms of discrete parameters $\overline{\boldsymbol{v}} \in \mathbb{R}^{\overline{n}_v}$, $\boldsymbol{v} \in \mathbb{R}^{n_v}$, $\overline{\boldsymbol{X}} \in \mathbb{R}^{\overline{n}_X}$ and $\boldsymbol{X} \in \mathbb{R}^{n_X}$ to derive matrix descriptions of continuous tangent forms.

The dimensions are characterised as follows

$$\begin{aligned} \overline{n}_v &: \quad \text{number of discrete macro state variables in } \overline{\mathcal{V}}_h \subset \overline{\mathcal{V}}, \\ n_v &: \quad \text{number of discrete micro state variables in } \mathcal{V}_h \subset \mathcal{V}, \\ \overline{n}_X &: \quad \text{number of discrete macro design parameters in } \overline{\mathcal{S}}_h \subset \overline{\mathcal{S}}, \\ n_X &: \quad \text{number of discrete micro design parameters in } \mathcal{S}_h \subset \mathcal{S}. \end{aligned} \tag{6.8}$$

The variations $\{\delta\overline{\boldsymbol{v}}_h, \delta\overline{\boldsymbol{X}}_h, \delta\boldsymbol{v}_h, \delta\boldsymbol{X}_h\}$ and the test function $\overline{\boldsymbol{\eta}}_h$ are approximated in the same fashion, i.e. $\delta\overline{\boldsymbol{v}} \in \mathbb{R}^{\overline{n}_v}$, $\delta\overline{\boldsymbol{X}} \in \mathbb{R}^{\overline{n}_X}$, $\delta\boldsymbol{v} \in \mathbb{R}^{n_v}$, $\delta\boldsymbol{X} \in \mathbb{R}^{n_X}$ and $\overline{\boldsymbol{\eta}} \in \mathbb{R}^{\overline{n}_v}$.

Remark 6.2 (Choice of design parameters) *In the scope of FEM, design parameters on referred scales are the coordinates of nodes of the finite element meshes, i.e.* $\overline{\boldsymbol{s}} = \overline{\boldsymbol{X}}$ *on the macro- and* $\boldsymbol{s} = \boldsymbol{X}$ *on the microscale. Utilisation of geometry parametrisation techniques for* $\overline{\boldsymbol{s}}$ *and/or* $\boldsymbol{s}$ *induces additional dependencies. Obtained relations and especially the obtained sensitivity information on finite element mesh level has to be transformed to the design space of interest using corresponding design velocity field matrices* $\overline{\boldsymbol{V}}$ *and/or* $\boldsymbol{V}$*, each affiliated to the appropriate scale. This situation is already argued in Section 3.4 and holds true for problem formulations on multiple scales.*

Using introduced finite element approximations, the discrete counterparts of continuous residual in Eq. (6.2) and tangent forms in Eq. (6.4) result to

$$\overline{R}(\overline{\boldsymbol{v}}_h, \overline{\boldsymbol{X}}_h, \boldsymbol{v}_h, \boldsymbol{X}_h; \overline{\boldsymbol{\eta}}_h) = \overline{\boldsymbol{\eta}}^T \overline{\boldsymbol{R}}, \qquad \overline{\boldsymbol{R}} \in \mathbb{R}^{\overline{n}_v}, \tag{6.9}$$

$$\overline{k}(\overline{\boldsymbol{v}}_h, \overline{\boldsymbol{X}}_h, \boldsymbol{v}_h, \boldsymbol{X}_h; \overline{\boldsymbol{\eta}}_h, \delta\overline{\boldsymbol{v}}_h) = \overline{\boldsymbol{\eta}}^T \overline{\boldsymbol{K}} \delta\overline{\boldsymbol{v}}, \qquad \overline{\boldsymbol{K}} \in \mathbb{R}^{\overline{n}_v \times \overline{n}_v}, \tag{6.10}$$

$$\overline{p}(\overline{\boldsymbol{v}}_h, \overline{\boldsymbol{X}}_h, \boldsymbol{v}_h, \boldsymbol{X}_h; \overline{\boldsymbol{\eta}}_h, \delta\overline{\boldsymbol{s}}_h) = \overline{\boldsymbol{\eta}}^T \overline{\boldsymbol{P}} \delta\overline{\boldsymbol{X}}, \qquad \overline{\boldsymbol{P}} \in \mathbb{R}^{\overline{n}_v \times \overline{n}_X}, \tag{6.11}$$

$$\widetilde{k}(\overline{\boldsymbol{v}}_h, \overline{\boldsymbol{X}}_h, \boldsymbol{v}_h, \boldsymbol{X}_h; \overline{\boldsymbol{\eta}}_h, \delta\boldsymbol{v}_h) = \overline{\boldsymbol{\eta}}^T \widetilde{\boldsymbol{K}} \delta\boldsymbol{v}, \qquad \widetilde{\boldsymbol{K}} \in \mathbb{R}^{\overline{n}_v \times n_v}, \tag{6.12}$$

$$\widetilde{p}(\overline{\boldsymbol{v}}_h, \overline{\boldsymbol{X}}_h, \boldsymbol{v}_h, \boldsymbol{X}_h; \overline{\boldsymbol{\eta}}_h, \delta\boldsymbol{s}_h) = \overline{\boldsymbol{\eta}}^T \widetilde{\boldsymbol{P}} \delta\boldsymbol{X}, \qquad \widetilde{\boldsymbol{P}} \in \mathbb{R}^{\overline{n}_v \times n_X}. \tag{6.13}$$

The set above can be used for the evaluation of the discrete form of the variation of the weak form from Eq. (6.3) in $(\overline{\boldsymbol{v}}_h, \overline{\boldsymbol{X}}_h, \boldsymbol{v}_h, \boldsymbol{X}_h)$ and yields

$$\overline{R}' = \overline{\boldsymbol{\eta}}^T \overline{\boldsymbol{R}}' = \overline{\boldsymbol{\eta}}^T \left[\overline{\boldsymbol{K}} \delta\overline{\boldsymbol{v}} + \overline{\boldsymbol{P}} \delta\overline{\boldsymbol{X}} + \widetilde{\boldsymbol{K}} \delta\boldsymbol{v} + \widetilde{\boldsymbol{P}} \delta\boldsymbol{X} \right] = 0, \tag{6.14}$$

and due to the arbitrariness of the test function $\overline{\boldsymbol{\eta}}$ one obtains the discrete counterpart of the total variation of the weak form to

$$\overline{\boldsymbol{R}}' = \overline{\boldsymbol{K}} \delta\overline{\boldsymbol{v}} + \overline{\boldsymbol{P}} \delta\overline{\boldsymbol{X}} + \widetilde{\boldsymbol{K}} \delta\boldsymbol{v} + \widetilde{\boldsymbol{P}} \delta\boldsymbol{X} = \boldsymbol{0}. \tag{6.15}$$

6.3.1 Discrete sensitivity of the macroscopic physical state

The implicitly given sensitivity relation for the macroscopic state parameter in Eq. (6.5) can be evaluated using the discretised form of the variation of the physical residual in Eq. (6.15). To avoid confusion, prior to the evaluation of the sensitivity relation the

following sensitivity operators are introduced

$$\begin{aligned}
\overline{\boldsymbol{S}} &= -\overline{\boldsymbol{K}}^{-1}\overline{\boldsymbol{P}} && \text{sensitivity of macro state (exclusively),}\\
\widetilde{\boldsymbol{S}} &= -\overline{\boldsymbol{K}}^{-1}\breve{\boldsymbol{P}} && \text{sensitivity of macro state due to micro changes (multilevel),}\\
\widehat{\boldsymbol{S}} &= \left[\begin{array}{cc}\overline{\boldsymbol{S}} & \widetilde{\boldsymbol{S}}\end{array}\right] && \text{effective sensitivity of macro state,}\\
\boldsymbol{S} &= -\boldsymbol{K}^{-1}\boldsymbol{P} && \text{sensitivity of micro state (exclusively).}
\end{aligned} \tag{6.16}$$

After a standard discretisation and the solution of the stated macroscopic BVP, each sensitivity matrix can be computed. Both, the macroscopic sensitivity matrix $\overline{\boldsymbol{S}}$ and the *multilevel sensitivity matrix* $\widetilde{\boldsymbol{S}}$ are compiled to a global sensitivity matrix $\widehat{\boldsymbol{S}}$.

According to the list of sensitivity operators in Eq. (6.16), the sensitivity of the macroscopic state parameter reads

$$\begin{aligned}
\delta\overline{\boldsymbol{v}} &= -\overline{\boldsymbol{K}}^{-1}\left[\overline{\boldsymbol{P}}\delta\overline{\boldsymbol{X}} + \widetilde{\boldsymbol{K}}\delta\boldsymbol{v} + \widetilde{\boldsymbol{P}}\delta\boldsymbol{X}\right] = -\overline{\boldsymbol{K}}^{-1}\left[\overline{\boldsymbol{P}}\,\delta\overline{\boldsymbol{X}} + \left(\widetilde{\boldsymbol{K}}\boldsymbol{S} + \widetilde{\boldsymbol{P}}\right)\delta\boldsymbol{X}\right]\\
&= -\overline{\boldsymbol{K}}^{-1}\left[\overline{\boldsymbol{P}}\,\delta\overline{\boldsymbol{X}} + \breve{\boldsymbol{P}}\,\delta\boldsymbol{X}\right] = \overline{\boldsymbol{S}}\,\delta\overline{\boldsymbol{X}} + \widetilde{\boldsymbol{S}}\,\delta\boldsymbol{X} = \left[\begin{array}{cc}\overline{\boldsymbol{S}} & \widetilde{\boldsymbol{S}}\end{array}\right]\begin{bmatrix}\delta\overline{\boldsymbol{X}}\\ \delta\boldsymbol{X}\end{bmatrix} = \widehat{\boldsymbol{S}}\,\delta\widehat{\boldsymbol{X}}.
\end{aligned} \tag{6.17}$$

Here, the sensitivity relation $\delta\boldsymbol{v} = \boldsymbol{S}\delta\boldsymbol{X}$ for the microscopic state variable, which is evaluated in the equilibrium point of each stated microscopic BVP, is used. Furthermore, the multilevel terms are stored in a *total multilevel pseudo load matrix*

$$\breve{\boldsymbol{P}} = \left(\widetilde{\boldsymbol{K}}\,\boldsymbol{S} + \widetilde{\boldsymbol{P}}\right), \tag{6.18}$$

which represents the total derivative of the macroscopic residual with respect to microscopic design parameters, i.e. $\mathrm{d}\overline{\boldsymbol{R}}/\mathrm{d}\boldsymbol{X}$. A complete overview of introduced parameters, tangent and sensitivity operators and the affiliated matrix representations is given in Table 6.3 and in Table 6.4.

6.3.2 Discrete form of the variation of arbitrary functionals

The continuous formulation for the variation of an arbitrary functional formulated on multiple scales from Eq. (6.7) can be transferred to its discrete counterpart using discretised sensitivity relations and sensitivity operators from Eq. (6.17) and Eq. (6.16), respectively. Its final form results to

$$\begin{aligned}
f' &= \frac{\partial f}{\partial\overline{\boldsymbol{v}}}\delta\overline{\boldsymbol{v}} + \frac{\partial f}{\partial\overline{\boldsymbol{s}}}\delta\overline{\boldsymbol{s}} + \frac{\partial f}{\partial\boldsymbol{v}}\delta\boldsymbol{v} + \frac{\partial f}{\partial\boldsymbol{s}}\delta\boldsymbol{s}\\
&= \frac{\partial f}{\partial\overline{\boldsymbol{v}}}\overline{\boldsymbol{S}}\,\delta\overline{\boldsymbol{s}} + \frac{\partial f}{\partial\overline{\boldsymbol{v}}}\widetilde{\boldsymbol{S}}\,\delta\boldsymbol{s} + \frac{\partial f}{\partial\overline{\boldsymbol{s}}}\,\delta\overline{\boldsymbol{s}} + \left(\frac{\partial f}{\partial\boldsymbol{v}}\boldsymbol{S} + \frac{\partial f}{\partial\boldsymbol{s}}\right)\delta\boldsymbol{s}\\
&= \left(\frac{\partial f}{\partial\overline{\boldsymbol{v}}}\overline{\boldsymbol{S}} + \frac{\partial f}{\partial\overline{\boldsymbol{s}}}\right)\delta\overline{\boldsymbol{s}} + \left(\frac{\partial f}{\partial\overline{\boldsymbol{v}}}\widetilde{\boldsymbol{S}} + \frac{\partial f}{\partial\boldsymbol{v}}\boldsymbol{S} + \frac{\partial f}{\partial\boldsymbol{s}}\right)\delta\boldsymbol{s},
\end{aligned} \tag{6.19}$$

and can be used for derivations and evaluations of several objective or constraint functionals on multiple scales, especially of their gradients or general sensitivity information, within frameworks for multiscale structural optimisation.

Table 6.3: Overview of macroscopic and microscopic parameters. Quantities connected to a single scale exclusively are indicated by $(\cdot)^*$ for macro- and by $(\cdot)_*$ for microscopic scale.

	Continuous	**Discrete**	cf. Eq.
Parameters: macro $\overline{(\cdot)}$, micro $(\cdot)$			
state	$\overline{\boldsymbol{v}}, \boldsymbol{v}$	$\overline{\boldsymbol{v}}, \boldsymbol{v}$	6.2, 6.8
design (mesh level)	$\overline{\boldsymbol{s}}, \boldsymbol{s}, (\overline{\boldsymbol{X}}, \boldsymbol{X})$	$\overline{\boldsymbol{s}}, \boldsymbol{s}, (\overline{\boldsymbol{X}}, \boldsymbol{X})$	6.2, 6.8
state variation	$\delta\overline{\boldsymbol{v}}, \delta\boldsymbol{v}$	$\delta\overline{\boldsymbol{v}}, \delta\boldsymbol{v}$	6.2, 6.8
design variation (mesh level)	$\delta\overline{\boldsymbol{s}}, \delta\boldsymbol{s}, (\delta\overline{\boldsymbol{X}}, \delta\boldsymbol{X})$	$\delta\overline{\boldsymbol{s}}, \delta\boldsymbol{s}, (\delta\overline{\boldsymbol{X}}, \delta\boldsymbol{X})$	6.2, 6.8
multilevel design	$\widehat{\boldsymbol{s}} = \begin{bmatrix} \overline{\boldsymbol{s}} \\ \boldsymbol{s} \end{bmatrix}, \widehat{\boldsymbol{X}} = \begin{bmatrix} \overline{\boldsymbol{X}} \\ \boldsymbol{X} \end{bmatrix}$	$\widehat{\boldsymbol{s}} = \begin{bmatrix} \overline{\boldsymbol{s}} \\ \boldsymbol{s} \end{bmatrix}, \widehat{\boldsymbol{X}} = \begin{bmatrix} \overline{\boldsymbol{X}} \\ \boldsymbol{X} \end{bmatrix}$	
multilevel design variation	$\delta\widehat{\boldsymbol{s}} = \begin{bmatrix} \delta\overline{\boldsymbol{s}} \\ \delta\boldsymbol{s} \end{bmatrix}, \delta\widehat{\boldsymbol{X}} = \begin{bmatrix} \delta\overline{\boldsymbol{X}} \\ \delta\boldsymbol{X} \end{bmatrix}$	$\delta\widehat{\boldsymbol{s}} = \begin{bmatrix} \delta\overline{\boldsymbol{s}} \\ \delta\boldsymbol{s} \end{bmatrix}, \delta\widehat{\boldsymbol{X}} = \begin{bmatrix} \delta\overline{\boldsymbol{X}} \\ \delta\boldsymbol{X} \end{bmatrix}$	6.5, 6.17

Table 6.4: Overview of macroscopic and microscopic tangent stiffness and pseudo load as well as sensitivity operators on multiple scales. Quantities connected to a single scale exclusively are indicated by $(\cdot)^*$ for macro- and by $(\cdot)_*$ for microscopic scale.

	Continuous	**Discrete**	cf. Eq.
Physical residual forms			
macro*	$\overline{R}(\overline{\boldsymbol{v}}, \overline{\boldsymbol{s}}, \boldsymbol{v}, \boldsymbol{s}; \overline{\boldsymbol{\eta}})$	$\overline{\boldsymbol{R}}(\overline{\boldsymbol{v}}, \overline{\boldsymbol{s}}, \boldsymbol{v}, \boldsymbol{s}; \overline{\boldsymbol{\eta}})$	6.2, 6.9
micro$_*$	$R(\boldsymbol{v}, \boldsymbol{s}; \boldsymbol{\eta})$	$\boldsymbol{R}(\boldsymbol{v}, \boldsymbol{s}; \boldsymbol{\eta})$	5.28, 5.46
Stiffness operators			
macro*	$\overline{k}(\overline{\boldsymbol{v}}, \overline{\boldsymbol{s}}, \boldsymbol{v}, \boldsymbol{s}; \overline{\boldsymbol{\eta}}, \delta\overline{\boldsymbol{v}})$	$\overline{\boldsymbol{K}} = \partial\overline{\boldsymbol{R}}/\partial\overline{\boldsymbol{v}}$	6.4, 6.10
multilevel	$\widetilde{k}(\overline{\boldsymbol{v}}, \overline{\boldsymbol{s}}, \boldsymbol{v}, \boldsymbol{s}; \overline{\boldsymbol{\eta}}, \delta\boldsymbol{v})$	$\widetilde{\boldsymbol{K}} = \partial\overline{\boldsymbol{R}}/\partial\boldsymbol{v}$	6.4, 6.12
micro$_*$	$k(\boldsymbol{v}, \boldsymbol{s}; \boldsymbol{\eta}, \delta\boldsymbol{v})$	$\boldsymbol{K} = \partial\boldsymbol{R}/\partial\boldsymbol{v}$	5.30, 5.47
Pseudo load operators			
macro*	$\overline{p}(\overline{\boldsymbol{v}}, \overline{\boldsymbol{s}}, \boldsymbol{v}, \boldsymbol{s}; \overline{\boldsymbol{\eta}}, \delta\overline{\boldsymbol{s}})$	$\overline{\boldsymbol{P}} = \partial\overline{\boldsymbol{R}}/\partial\overline{\boldsymbol{X}}$	6.4, 6.11
multilevel (partial)	$\widetilde{p}(\overline{\boldsymbol{v}}, \overline{\boldsymbol{s}}, \boldsymbol{v}, \boldsymbol{s}; \overline{\boldsymbol{\eta}}, \delta\boldsymbol{s})$	$\widetilde{\boldsymbol{P}} = \partial\overline{\boldsymbol{R}}/\partial\boldsymbol{X}$	6.4, 6.13
multilevel (total)	$\breve{p}(\overline{\boldsymbol{v}}, \overline{\boldsymbol{s}}, \boldsymbol{v}, \boldsymbol{s}; \overline{\boldsymbol{\eta}}, \delta\boldsymbol{s})$	$\breve{\boldsymbol{P}} = \mathrm{d}\overline{\boldsymbol{R}}/\mathrm{d}\boldsymbol{X} = \widetilde{\boldsymbol{K}}\boldsymbol{S} + \widetilde{\boldsymbol{P}}$	6.17
effective		$\widehat{\boldsymbol{P}} = \mathrm{d}\overline{\boldsymbol{R}}/\mathrm{d}\widehat{\boldsymbol{X}} = \begin{bmatrix} \overline{\boldsymbol{P}} & \breve{\boldsymbol{P}} \end{bmatrix}$	6.17
micro$_*$	$p(\boldsymbol{v}, \boldsymbol{s}; \boldsymbol{\eta}, \delta\boldsymbol{s})$	$\boldsymbol{P} = \partial\boldsymbol{R}/\partial\boldsymbol{X}$	5.31, 5.48
Sensitivity operators			
macro*	$\overline{s}(\overline{\boldsymbol{v}}, \overline{\boldsymbol{s}}, \boldsymbol{v}, \boldsymbol{s}; \delta\overline{\boldsymbol{s}})$	$\overline{\boldsymbol{S}} = \mathrm{d}\overline{\boldsymbol{v}}/\mathrm{d}\overline{\boldsymbol{X}} = -\overline{\boldsymbol{K}}^{-1}\overline{\boldsymbol{P}}$	6.6, 6.16
multilevel	$\widetilde{s}(\overline{\boldsymbol{v}}, \overline{\boldsymbol{s}}, \boldsymbol{v}, \boldsymbol{s}; \delta\boldsymbol{s})$	$\widetilde{\boldsymbol{S}} = \mathrm{d}\overline{\boldsymbol{v}}/\mathrm{d}\boldsymbol{X} = -\overline{\boldsymbol{K}}^{-1}\widehat{\boldsymbol{P}}$	6.6, 6.16
effective	$\widehat{s}(\overline{\boldsymbol{v}}, \overline{\boldsymbol{s}}, \boldsymbol{v}, \boldsymbol{s}; \delta\widehat{\boldsymbol{s}})$	$\widehat{\boldsymbol{S}} = \mathrm{d}\overline{\boldsymbol{v}}/\mathrm{d}\widehat{\boldsymbol{X}} = \begin{bmatrix} \overline{\boldsymbol{S}} & \widetilde{\boldsymbol{S}} \end{bmatrix}$	6.6, 6.16
micro$_*$	$s(\boldsymbol{v}, \boldsymbol{s}; \delta\boldsymbol{s})$	$\boldsymbol{S} = \mathrm{d}\boldsymbol{v}/\mathrm{d}\boldsymbol{X} = \boldsymbol{K}^{-1}\boldsymbol{P}$	5.32, 5.51

6.4 Explicit formulations for multiscale sensitivity analysis

In this section explicit representations for introduced residual and tangent forms on multiple scales are derived. Relations for sensitivity analysis on the microscale are followed by relations for sensitivity analysis on the macroscale and are completed by sensitivity relations for effective parameters, i.e. for homogenised stresses.

6.4.1 Sensitivity analysis on the microscale

The consequence of the arguments in the introduction of this chapter, which state, that the solution of each microscopic BVP in terms of the physical behaviour contributes to the overall global macroscopic sensitivity information, is the necessity of performance of several sensitivity analyses in discretised sense in each macroscopic integration point p

of each macroscopic element e individually. The required sensitivity analysis for each microscopic BVP is carried out analogously to the procedure for sensitivity analysis on single scales, which is described in Chapter 5 in detail.

The solution of stated microscopic BVPs is based on the solution of the weak form of equilibrium, stated in Eq. (5.28). Therefore, a Newton solution scheme in terms of boundary conditions formulated for the solution of optimisation problem of homogenisation, outlined in Algorithm 4.1, is referred to and requires a consistent linearisation of the physical residual. Following the sequence of steps presented in Section 5.3.1 in the continuous, and especially in Section 5.4.1 in the discrete sense, results in the discretised physical residual vector in Eq. (5.46) and the physical stiffness matrix in Eq. (5.47). Explicit formulations for mentioned residual and stiffness operators are introduced in Section 5.6 and are summarised here to confirm their choice and to avoid confusion. The discretisation of the residual vector in terms of the first Piola-Kirchhoff stress $\mathbf{P}$ and the deformation gradient $\mathbf{F}$ reads

$$R(\boldsymbol{v}_h,\boldsymbol{X}_h;\boldsymbol{\eta}_h) = \bigcup_{e=1}^{n_{el}} \int_{\boldsymbol{\mathcal{K}}^e} \mathbf{P} : \mathbf{F}'_v(\boldsymbol{v}_h^e,\boldsymbol{\eta}_h^e)\, \mathrm{d}V = \bigcup_{e=1}^{n_{el}} \sum_{i=1}^{nn} \boldsymbol{\eta}_i^T \boldsymbol{R}_i^e = \boldsymbol{\eta}^T \boldsymbol{R}, \tag{6.20}$$

with the contribution of the element residual vector

$$\boldsymbol{R}_i^e = \int_{\boldsymbol{\mathcal{K}}^e} \boldsymbol{P}_{\mathsf{K}} \boldsymbol{L}_i \, \mathrm{d}V. \tag{6.21}$$

The principle of scale separation introduced in Fig. 4.1 and the affiliated characteristic of different length scales explained in Section 4.3.1 cause the omission of external contributions in terms of body loads and tractions on the surface. The physical stiffness operator or stiffness matrix, respectively, is obtained from

$$\begin{aligned} k(\boldsymbol{v}_h,\boldsymbol{X}_h;\boldsymbol{\eta}_h,\delta\boldsymbol{v}_h) &= \bigcup_{e=1}^{n_{el}} \int_{\boldsymbol{\mathcal{K}}^e} \mathbf{F}'_v(\boldsymbol{v}_h^e,\boldsymbol{\eta}_h^e) : \mathbb{A} : \mathbf{F}'_v(\boldsymbol{v}_h^e,\delta\boldsymbol{v}_h^e)\, \mathrm{d}V \\ &= \bigcup_{e=1}^{n_{el}} \sum_{i=1}^{nn} \sum_{j=1}^{nn} \boldsymbol{\eta}_i^T \boldsymbol{K}_{ij}^e \delta\boldsymbol{v}_j = \boldsymbol{\eta}^T \boldsymbol{K} \delta\boldsymbol{v}, \end{aligned} \tag{6.22}$$

with its discretised counterpart for the element stiffness matrix

$$\boldsymbol{K}_{ij}^e = \int_{\boldsymbol{\mathcal{K}}^e} \boldsymbol{B}_{vi}^T \boldsymbol{A} \boldsymbol{B}_{vj} \, \mathrm{d}V. \tag{6.23}$$

The last missing part within the presented solution scheme is the specification of used constitutive laws. Beside the hyperelastic St. Venant-Kirchhoff material model, several other Green elastic constitutive models like Ogden- or Mooney-Rivlin-type material can be taken into account. Within the presented work, the Neo-Hookean material formulation is chosen, which is characterised by the following strain energy function

$$W(I_C, J_F) = \frac{1}{2}\mu \left(I_C - n^d - 2\ln J_F\right) + \frac{1}{2}\lambda \left(J_F - 1\right)^2, \tag{6.24}$$

with $I_C = \mathrm{tr}(\mathbf{C}) = \mathrm{tr}(\mathbf{F}^T\mathbf{F})$ being the first invariant of the Cauchy-Green deformation tensor $\mathbf{C}$, the Jacobian of the deformation gradient $J_F = \det \mathbf{F}$, the Lamé constants λ and μ, and the dimension of the problem n^d. Corresponding stresses $\mathbf{P}$ in tensorial and index notation are evaluated from

$$\begin{aligned} \mathbf{P} &= \mu \left(\mathbf{F} - \mathbf{F}^{-T} \right) - \lambda \, J_F \left(J_F - 1 \right) \mathbf{F}^{-T}, \\ P_{ij} &= \mu \left(F_{ij} F_{ji}^{-1} \right) - \lambda \, J_F \left(J_F - 1 \right) F_{ji}^{-1}. \end{aligned} \tag{6.25}$$

The corresponding constitutive tensor $\mathbb{A}$ and its index representation is evaluated from

$$\begin{aligned} \mathbb{A} &= \mu \, \mathbf{I} \otimes \mathbf{I} + \lambda \left(2 \, J_F^2 - J_F \right) \mathbf{F}^{-T} \otimes \mathbf{F}^{-T} + \left[\mu - \lambda \left(J_F^2 - J_F \right) \right] \mathbf{F}^{-T} \otimes \mathbf{F}^{-1}, \\ A_{ijkl} &= \mu \, \delta_{ik} \delta_{jl} + \lambda \left(2 \, J_F^2 - J_F \right) F_{ji}^{-1} F_{lk}^{-1} + \left[\mu - \lambda \left(J_F^2 - J_F \right) \right] F_{li}^{-1} F_{jk}^{-1}. \end{aligned} \tag{6.26}$$

Beside the obtained solution for the state parameter $\boldsymbol{v}$, homogenised or effective parameters are also prerequisites for the solution of the stated BVP and upcoming sensitivity analysis. The design variation of the weak form of the residual leads to the tangent pseudo load operator in Eq. (5.31) or Eq. (5.48) in the discretised sense. The explicit form

$$\begin{aligned} p(\boldsymbol{v}_h, \boldsymbol{X}_h; \boldsymbol{\eta}_h, \delta \boldsymbol{X}_h) = \bigcup_{e=1}^{n_{el}} \int_{\boldsymbol{\mathcal{K}}^e} & \mathbf{P} : \mathbf{F}''_{vs}(\boldsymbol{v}_h^e, \boldsymbol{\eta}_h^e, \delta \boldsymbol{X}_h^e) + \mathbf{F}'_v(\boldsymbol{v}_h^e, \boldsymbol{\eta}_h^e) : \mathbb{A} : \mathbf{F}'_s(\boldsymbol{v}_h^e, \delta \boldsymbol{X}_h^e) \\ & + \mathbf{P} : \mathbf{F}'_v(\boldsymbol{v}_h^e, \boldsymbol{\eta}_h^e) \, \mathrm{Div} \, \delta \boldsymbol{X}_h^e \, \mathrm{d}V \\ = \bigcup_{e=1}^{n_{el}} \sum_{i=1}^{nn} \sum_{j=1}^{nn} & \boldsymbol{\eta}_i^T \boldsymbol{P}_{ij}^e \delta \boldsymbol{X}_j = \boldsymbol{\eta}^T \boldsymbol{P} \delta \boldsymbol{X} \end{aligned} \tag{6.27}$$

has to be evaluated in the current state $\boldsymbol{v}$ for the element pseudo load matrix and reads

$$\boldsymbol{P}_{ij}^e = \int_{\boldsymbol{\mathcal{K}}^e} \boldsymbol{B}_{vi}^T \boldsymbol{A} \boldsymbol{B}_{sj} - \boldsymbol{P}_{\mathsf{K}} \boldsymbol{L}_j \boldsymbol{L}_i^T + \boldsymbol{P}_{\mathsf{K}} \boldsymbol{L}_i \boldsymbol{L}_j^T \, \mathrm{d}V. \tag{6.28}$$

The obtained global tangent operators, i.e. assembled matrices $\boldsymbol{K}$ and $\boldsymbol{P}$, are finally used to evaluate the sensitivity relation in Eq. (5.51) on global microscopic system level and yield the sensitivity of the microscopic state

$$\boldsymbol{S} = -\boldsymbol{K}^{-1} \boldsymbol{P}. \tag{6.29}$$

The resulting matrix $\boldsymbol{S}$ represents the sensitivity matrix with the sensitivity information of the microscopic state parameter in the current integration point p in current element e and contributes to parts of the sensitivity information of the corresponding macroscopic element, i.e. to the total multilevel pseudo load $\check{\boldsymbol{P}}$ from Eq. (6.17) on the upper scale.

Sensitivity of the microscopic physical state for periodic materials

A wide range of common materials used in real world mechanical structures and constructions is characterised by periodical properties. For the class of periodic materials it is possible to find representative subsets, the so-called unit cells or RVEs introduced

in Section 4.3.1, which represent the typical structural properties of the material on average. By definition, the periodicity condition allows to copy the specified unit cell in all spatial directions and to obtain statistically representative material properties in each macroscopic material point. From mechanical point of view, promising results for the analysis of structural behaviour can be obtained by methods, which take the mentioned periodicity properties into account. In the case of computational homogenisation and FE^2 methods this requirement is fulfilled by the application of periodic boundary conditions on the microscale, which reflect the materials response in the most realistic way.

Due to the practical relevance and despite the introduction of three different types of boundary conditions $\mathrm{I} = \{\mathrm{D}, \mathrm{P}, \mathrm{S}\}$ on the microscale in Section 4.3.3 and Section 4.4.2, the focus of following investigations and numerical studies lies on the application of the formulation for periodic boundary conditions (P). Nevertheless, all types are implemented and available in the in-house MATLAB code MANO. The formulations for linear displacements (D) and uniform tractions (S) can be used for the estimation of upper and lower bounds for homogenised effective parameters but are omitted for the design sensitivity analysis and the multiscale optimisation.

Similar to assumptions for multiscale structural analysis in terms of periodic boundary conditions on the microscale, also for the design sensitivity analysis it is important to define pairs of contributions on positive and negative boundaries $\partial\mathcal{K}^+$ and $\partial\mathcal{K}^-$ of the microscopic domain. For each pair, the periodicity condition $[\![\delta \boldsymbol{v}_\mathrm{b}]\!] = \boldsymbol{0}$ with the jump notation $[\![\delta \boldsymbol{v}_\mathrm{b}]\!] = \delta \boldsymbol{v}_\mathrm{b}^+ - \delta \boldsymbol{v}_\mathrm{b}^-$ is required for the proper evaluation of the sensitivity matrix $\boldsymbol{S}$ given in Eq. (6.29).

A methodology for the consideration of the periodicity condition in terms of structural analysis and the *periodic boundary fluctuations model* is introduced in [178] and can be adopted for the design sensitivity analysis. The following discretisation of state and design parameters and of corresponding variations

$$\boldsymbol{v} = \begin{bmatrix} \boldsymbol{v}_\mathrm{i} \\ \boldsymbol{v}_+ \\ \boldsymbol{v}_- \end{bmatrix}, \quad \delta\boldsymbol{v} = \begin{bmatrix} \delta\boldsymbol{v}_\mathrm{i} \\ \delta\boldsymbol{v}_+ \\ \delta\boldsymbol{v}_- \end{bmatrix}, \quad \boldsymbol{X} = \begin{bmatrix} \boldsymbol{X}_\mathrm{i} \\ \boldsymbol{X}_+ \\ \boldsymbol{X}_- \end{bmatrix}, \quad \delta\boldsymbol{X} = \begin{bmatrix} \delta\boldsymbol{X}_\mathrm{i} \\ \delta\boldsymbol{X}_+ \\ \delta\boldsymbol{X}_- \end{bmatrix}, \tag{6.30}$$

refers contribution in the inner domain $(\cdot)_\mathrm{i}$, on the positive boundary $(\cdot)_+$ and the negative boundary $(\cdot)_-$ of the domain. This discretisation affects the representation of the total variation of the microscopic residual in Eq. (5.50) and yields

$$\boldsymbol{R}' = \begin{bmatrix} \boldsymbol{K}_\mathrm{ii} & \boldsymbol{K}_\mathrm{i+} & \boldsymbol{K}_\mathrm{i-} \\ \boldsymbol{K}_\mathrm{+i} & \boldsymbol{K}_\mathrm{++} & \boldsymbol{K}_\mathrm{+-} \\ \boldsymbol{K}_\mathrm{-i} & \boldsymbol{K}_\mathrm{-+} & \boldsymbol{K}_\mathrm{--} \end{bmatrix} \begin{bmatrix} \delta\boldsymbol{v}_\mathrm{i} \\ \delta\boldsymbol{v}_+ \\ \delta\boldsymbol{v}_- \end{bmatrix} + \begin{bmatrix} \boldsymbol{P}_\mathrm{ii} & \boldsymbol{P}_\mathrm{i+} & \boldsymbol{P}_\mathrm{i-} \\ \boldsymbol{P}_\mathrm{+i} & \boldsymbol{P}_\mathrm{++} & \boldsymbol{P}_\mathrm{+-} \\ \boldsymbol{P}_\mathrm{-i} & \boldsymbol{P}_\mathrm{-+} & \boldsymbol{P}_\mathrm{--} \end{bmatrix} \begin{bmatrix} \delta\boldsymbol{X}_\mathrm{i} \\ \delta\boldsymbol{X}_+ \\ \delta\boldsymbol{X}_- \end{bmatrix} = \boldsymbol{0}. \tag{6.31}$$

Due to the square characteristic of RVEs, design modifications on the boundary are not feasible and the variations $\delta\boldsymbol{X}_+$ and $\delta\boldsymbol{X}_-$ vanish. Consequently, the pseudo load matrix $\boldsymbol{P}$ reduces to the first column. Considering the periodicity condition, unknowns are coupled and the final system of equations is reduced to

$$\begin{bmatrix} \boldsymbol{K}_\mathrm{ii} & \boldsymbol{K}_\mathrm{i+} + \boldsymbol{K}_\mathrm{i-} \\ \boldsymbol{K}_\mathrm{+i} + \boldsymbol{K}_\mathrm{-i} & \boldsymbol{K}_\mathrm{++} + \boldsymbol{K}_\mathrm{+-} + \boldsymbol{K}_\mathrm{-+} + \boldsymbol{K}_\mathrm{--} \end{bmatrix} \begin{bmatrix} \delta\boldsymbol{v}_\mathrm{i} \\ \delta\boldsymbol{v}_+ \end{bmatrix} + \begin{bmatrix} \boldsymbol{P}_\mathrm{ii} \\ \boldsymbol{P}_\mathrm{+i} + \boldsymbol{P}_\mathrm{-i} \end{bmatrix} \left[\delta\boldsymbol{X}_\mathrm{i}\right] = \boldsymbol{0}. \tag{6.32}$$

After the solution for the variations on the positive boundary of the microscopic domain $\delta \boldsymbol{v}_+$, the variations in the inner domain $\delta \boldsymbol{v}_\mathrm{i}$ are determined. The aforementioned assumptions provide the variations on the negative boundary, i.e. $\delta \boldsymbol{v}_- = \delta \boldsymbol{v}_+$ and thus, $\boldsymbol{S}_- = \boldsymbol{S}_+$ holds true. The final overall sensitivity relation for the microscopic state parameter solved in terms of periodic boundary conditions reads

$$\begin{bmatrix} \delta \boldsymbol{v}_\mathrm{i} \\ \delta \boldsymbol{v}_+ \\ \delta \boldsymbol{v}_- \end{bmatrix} = \begin{bmatrix} \boldsymbol{S}_\mathrm{i} \\ \boldsymbol{S}_+ \\ \boldsymbol{S}_- \end{bmatrix} \left[\delta \boldsymbol{X}_\mathrm{i} \right] \tag{6.33}$$

with the explicit entries of the sensitivity matrix $\boldsymbol{S}$

$$\boldsymbol{S}_+ = -\left[\boldsymbol{K}_4 - \boldsymbol{K}_2 \boldsymbol{K}_2^{-1} \boldsymbol{K}_3 \right]^{-1} \left[\boldsymbol{P}_2 - \boldsymbol{K}_2 \boldsymbol{K}_1^{-1} \boldsymbol{P}_1 \right], \quad \boldsymbol{S}_\mathrm{i} = -\left[\boldsymbol{K}_1 \right]^{-1} \left[\boldsymbol{K}_3 \, \boldsymbol{S}_+ + \boldsymbol{P}_1 \right]. \tag{6.34}$$

For notational simplicity, the following abbreviations are introduced

$$\begin{aligned} \boldsymbol{K}_1 &= \boldsymbol{K}_\mathrm{ii}, & \boldsymbol{K}_3 &= \boldsymbol{K}_{+\mathrm{i}} + \boldsymbol{K}_{-\mathrm{i}}, \\ \boldsymbol{K}_2 &= \boldsymbol{K}_{\mathrm{i}+} + \boldsymbol{K}_{\mathrm{i}-}, & \boldsymbol{K}_4 &= \boldsymbol{K}_{++} + \boldsymbol{K}_{+-} + \boldsymbol{K}_{-+} + \boldsymbol{K}_{--}, \\ \boldsymbol{P}_1 &= \boldsymbol{P}_\mathrm{ii}, & \boldsymbol{P}_2 &= \boldsymbol{P}_{+\mathrm{i}} + \boldsymbol{P}_{-\mathrm{i}}. \end{aligned} \tag{6.35}$$

The coefficient matrices $\mathcal{S}_1$ and $\mathcal{S}_2$ introduced in Eq. (4.26) for the general form of boundary conditions can be used to obtain the solution of the sensitivity relation for the microscopic state parameter in a similar fashion. The required variation of the microscopic residual can be initiated by

$$\boldsymbol{R}' = \begin{bmatrix} \boldsymbol{K}_\mathrm{aa} & \boldsymbol{K}_\mathrm{ab} \, \mathcal{S}_1^T \\ \mathcal{S}_1 \, \boldsymbol{K}_\mathrm{ba} & \mathcal{S}_1 \, \boldsymbol{K}_\mathrm{bb} \, \mathcal{S}_1^T \end{bmatrix} \begin{bmatrix} \delta \boldsymbol{v}_\mathrm{a} \\ \mathcal{S}_1 \, \delta \boldsymbol{v}_\mathrm{b} \end{bmatrix} + \begin{bmatrix} \boldsymbol{P}_\mathrm{aA} \\ \mathcal{S}_1 \, \boldsymbol{P}_\mathrm{bA} \end{bmatrix} \left[\delta \boldsymbol{X}_\mathrm{A} \right] = \boldsymbol{0}, \tag{6.36}$$

and has to be solved for the state variation on the positive boundary of the domain $\delta \boldsymbol{v}_+ = \mathcal{S}_1 \, \delta \boldsymbol{v}_\mathrm{b}$ and $\delta \boldsymbol{v}_\mathrm{a}$. The individual components can be related to the prior derivation, i.e. $\boldsymbol{K}_1 = \boldsymbol{K}_\mathrm{aa}, \boldsymbol{K}_2 = \mathcal{S}_1 \, \boldsymbol{K}_\mathrm{ba}, \boldsymbol{K}_3 = \boldsymbol{K}_\mathrm{ab} \, \mathcal{S}_1^T, \boldsymbol{K}_4 = \mathcal{S}_1 \, \boldsymbol{K}_\mathrm{bb} \, \mathcal{S}_1^T$ for the stiffness matrix, $\delta \boldsymbol{v}_\mathrm{i} = \delta \boldsymbol{v}_\mathrm{a}$ for the state variation in the inner domain, $\boldsymbol{P}_1 = \boldsymbol{P}_\mathrm{aA}, \boldsymbol{P}_2 = \mathcal{S}_1 \, \boldsymbol{P}_\mathrm{bA}$ for the pseudo load matrix and $\delta \boldsymbol{X}_\mathrm{i} = \delta \boldsymbol{X}_\mathrm{A}$ for the design variation. This representation allows the negligence of the $(+,-)$ notation within the determination of the sensitivity matrix $\boldsymbol{S}$ and suits the notation provided in the presented work.

6.4.2 Sensitivity analysis on the macroscale

Schematically and beside some modifications in terms of micro-macro notation, the methodology for the derivation of sensitivity information on the macroscale is similar to the procedure on the micro scale. Relevant differences are accentuated in the following. The derivation is based on the macroscopic weak form of equilibrium stated in Eq. (6.2) with an extended list of arguments compared to single scales and requires consistent linearisations with respect to state and design parameters affiliated to both referred scales, i.e. with respect to parameters $\{\overline{\boldsymbol{v}}, \overline{\boldsymbol{X}}, \boldsymbol{v}, \boldsymbol{X}\}$. Continuous derivations are already presented in Section 6.2.1 and the discrete counterparts can be referred to in Section 6.3. The explicit

discretisation of the macroscopic residual vector in terms of the macroscopic deformation gradient $\overline{\mathbf{F}}$ and now, in terms of effective or homogenised stresses $\overline{\mathbf{P}}_{\mathrm{I}} = \dfrac{1}{V}\displaystyle\int_{\boldsymbol{\mathcal{K}}} \mathbf{P}\ \mathrm{d}V$ according to statements and relations for numerical homogenisation techniques presented in Section 4.3, reads

$$\begin{aligned}\overline{R}(\overline{\boldsymbol{v}}_h,\overline{\boldsymbol{X}}_h,\boldsymbol{v}_h,\boldsymbol{X}_h;\overline{\boldsymbol{\eta}}_h) &= \bigcup_{e=1}^{\overline{n}_{el}} \int_{\overline{\boldsymbol{\mathcal{K}}}^e} \overline{\mathbf{P}}_{\mathrm{I}} : \overline{\mathbf{F}}'_{\overline{v}}(\overline{\boldsymbol{v}}_h^e,\overline{\boldsymbol{\eta}}_h^e)\ \mathrm{d}V - \overline{F}(\overline{\boldsymbol{X}}_h^e,\overline{\boldsymbol{\eta}}_h^e) \\ &= \bigcup_{e=1}^{\overline{n}_{el}} \sum_{i=1}^{nn} \overline{\boldsymbol{\eta}}_i^T\ \overline{\boldsymbol{R}}_i^e = \overline{\boldsymbol{\eta}}^T\ \overline{\boldsymbol{R}}.\end{aligned} \tag{6.37}$$

The relation in Eq. (6.37) contains the contribution of the element residual vector

$$\overline{\boldsymbol{R}}_i^e = \int_{\overline{\boldsymbol{\mathcal{K}}}^e} \overline{\boldsymbol{P}_{\mathsf{K},\mathrm{I}}}\ \boldsymbol{L}_i\ \mathrm{d}V - \overline{\boldsymbol{F}}_i^e(\overline{\boldsymbol{X}}), \tag{6.38}$$

and $\overline{F}(\overline{\boldsymbol{X}}_h^e,\overline{\boldsymbol{\eta}}_h^e)$ or $\overline{\boldsymbol{F}}_i^e(\overline{\boldsymbol{X}})$, which both represent the contribution of external loads on the macroscale. The discretisation of external contributions is realised using the relation introduced in Eq. (5.90) and adapted for macroscopic notation, i.e.

$$\overline{\boldsymbol{F}}_i^e(\overline{\boldsymbol{X}}) = \int_{\overline{\boldsymbol{\mathcal{K}}}^e} N_i \overline{\boldsymbol{b}}\ \mathrm{d}V. \tag{6.39}$$

The design sensitivity analysis is based on the solution of the stated macroscopic BVP obtained from the application of the Newton-type method presented in Algorithm 6.2.

The total variation of the residual form in Eq. (6.2) contains partial variations with respect to all introduced parameters in the argument list, i.e. with respect to $\{\overline{\boldsymbol{v}}, \overline{\boldsymbol{X}}, \boldsymbol{v}, \boldsymbol{X}\}$ and therefore, it reads $\overline{R}' = \overline{R}'_{\overline{v}} + \overline{R}'_{\overline{s}} + \overline{R}'_{v} + \overline{R}'_{s}$. All four contributions can be extracted from the total variation of Eq. (6.37)

$$\begin{aligned}\delta\overline{R}(\overline{\boldsymbol{v}},\overline{\boldsymbol{X}},\boldsymbol{v},\boldsymbol{X};\overline{\boldsymbol{\eta}}) &= \delta \int_{\overline{\boldsymbol{\mathcal{K}}}} \overline{\mathbf{P}}_{\mathrm{I}} : \overline{\mathbf{F}}'_{\overline{v}}(\overline{\boldsymbol{v}},\overline{\boldsymbol{\eta}})\ \mathrm{d}V - \overline{F}'_X(\overline{\boldsymbol{X}};\overline{\boldsymbol{\eta}},\delta\boldsymbol{X}) \\ &= \int_{\boldsymbol{\mathcal{R}}} \delta\left[\overline{\mathbf{P}}_{\mathrm{I}} : \overline{\mathbf{F}}'_{\overline{v}}(\overline{\boldsymbol{v}},\overline{\boldsymbol{\eta}})\ J_{\overline{K}}\right]\ \mathrm{d}V_\theta - \overline{F}'_X(\overline{\boldsymbol{X}};\overline{\boldsymbol{\eta}},\delta\boldsymbol{X}) \\ &= \int_{\boldsymbol{\mathcal{R}}} \left[\left(\delta\overline{\mathbf{P}}_{\mathrm{I}} : \overline{\mathbf{F}}'_{\overline{v}} + \overline{\mathbf{P}}_{\mathrm{I}} : \delta\overline{\mathbf{F}}'_{\overline{v}}\right)\ J_{\overline{K}} + \overline{\mathbf{P}}_{\mathrm{I}} : \overline{\mathbf{F}}'_{\overline{v}}(\overline{\boldsymbol{v}},\overline{\boldsymbol{\eta}})\,\delta J_{\overline{K}}\right]\ \mathrm{d}V_\theta \\ &\qquad - \overline{F}'_X(\overline{\boldsymbol{X}};\overline{\boldsymbol{\eta}},\delta\boldsymbol{X}).\end{aligned} \tag{6.40}$$

Here, the total variation (or mixed variation) of the variation of the deformation gradient $\delta\overline{\mathbf{F}}'_{\overline{v}}$ as well as the variation of the Jacobian $\delta J_{\overline{K}}$ are provided from sensitivity analysis on single scales.

Algorithm 6.2 Newton-type method: solution procedure for nonlinear equations.

procedure SOLVE NONLINEAR EQUATION
  set $\{\overline{\boldsymbol{v}}, \boldsymbol{v}\} \leftarrow \boldsymbol{0}$ ▷ set or compute appropriate initial values
  for $i_L \leftarrow 1, n_L$ **do** ▷ loop over macroscopic load steps
    get $\lambda_L = i_L \cdot \dfrac{1}{n_L}$ ▷ get macroscopic load scale
    set $it = 0$, convergence = `false` ▷ start Newton iteration
    while convergence = `false` and $it < it_{\max}$ **do**
      // *Assemble vector of internal forces and tangent of discretised RVE*
      $\{\overline{\boldsymbol{R}}^{\,\mathrm{int}}, \overline{\boldsymbol{K}}\} \leftarrow$ `assemble`$(\overline{\boldsymbol{v}}_{it}, \boldsymbol{v}_{it}, \lambda_L)$ ▷ in terms of $\{\underline{\overline{\boldsymbol{P}}}_{\mathrm{K}}, \overline{\boldsymbol{A}}\}$
      // *Compute overall residual for current load step*
      $\overline{\boldsymbol{R}} = \overline{\boldsymbol{R}}^{\,\mathrm{int}} - \lambda_L \overline{\boldsymbol{F}}$
      // *Compute increment*
      $\overline{\boldsymbol{K}}\, \Delta\overline{\boldsymbol{v}}_{it} = -\overline{\boldsymbol{R}}$ ▷ solve linear system of global equations
      // *Update state variable*
      $\overline{\boldsymbol{v}}_{it+1} = \overline{\boldsymbol{v}}_{it} + \Delta\overline{\boldsymbol{v}}_{it}$
      // *Check convergence*
      $|| \overline{\boldsymbol{R}}^{\,\mathrm{int}}(\overline{\boldsymbol{v}}_{it+1}) - \lambda_L \overline{\boldsymbol{F}} ||_{L_2}$ $\begin{cases} \texttt{if} \ > TOL_v \ \ \texttt{than} \ it \leftarrow it + 1 \\ \texttt{if} \ \leq TOL_v \ \ \texttt{than} \ \text{conv} = \texttt{true} \end{cases}$
    end while ▷ end Newton iteration
  end for ▷ loop over macroscopic load steps
end procedure

From Eq. (5.16) and Remark 5.2 one obtains

$$\begin{aligned} \delta\overline{\mathbf{F}}'_{\overline{v}} &= \overline{\mathbf{F}}''_{\overline{v}\,\overline{s}} = -\operatorname{Grad}\delta\overline{\boldsymbol{v}} \operatorname{Grad}\delta\overline{\boldsymbol{X}} \quad \text{and} \\ \delta J_{\overline{K}} &= J_{\overline{K}}\, \overline{\mathbf{K}}^{-T} : \operatorname{GRAD}\delta\boldsymbol{X} = J_{\overline{K}} \operatorname{Div}\delta\boldsymbol{X}, \end{aligned} \tag{6.41}$$

where the rule $\mathbf{A} : \mathbf{B} = \mathbf{B}^T\mathbf{A} : \mathbf{I}$ for the transformation of the divergence operator is used, i.e. $\operatorname{Div}\delta\overline{\boldsymbol{X}} = \operatorname{GRAD}\delta\overline{\boldsymbol{X}}\, \overline{\mathbf{K}}^{-1} : \mathbf{I} = \overline{\mathbf{K}}^{-T} : \operatorname{GRAD}\delta\overline{\boldsymbol{X}}$. The major difference in comparison to sensitivity analysis on single scales is the total variation of stresses, especially here of the homogenised stresses $\overline{\mathbf{P}}_{\mathrm{I}}$, which contains following partial variations

$$\delta\overline{\mathbf{P}}_{\mathrm{I}} = (\overline{\mathbf{P}}_{\mathrm{I}})'_{\overline{v}} + (\overline{\mathbf{P}}_{\mathrm{I}})'_{\overline{s}} + (\overline{\mathbf{P}}_{\mathrm{I}})'_{v} + (\overline{\mathbf{P}}_{\mathrm{I}})'_{s} = \frac{\partial\overline{\mathbf{P}}_{\mathrm{I}}}{\partial\overline{\boldsymbol{v}}}\delta\overline{\boldsymbol{v}} + \frac{\partial\overline{\mathbf{P}}_{\mathrm{I}}}{\partial\overline{\boldsymbol{X}}}\delta\overline{\boldsymbol{X}} + \frac{\partial\overline{\mathbf{P}}_{\mathrm{I}}}{\partial\boldsymbol{v}}\delta\boldsymbol{v} + \frac{\partial\overline{\mathbf{P}}_{\mathrm{I}}}{\partial\boldsymbol{X}}\delta\boldsymbol{X}. \tag{6.42}$$

Inserting the obtained relations in Eq. (6.40), an appropriate rearranging leads to

$$\begin{aligned}\delta\overline{R}(\overline{\boldsymbol{v}},\overline{\boldsymbol{X}},\boldsymbol{v},\boldsymbol{X};\overline{\boldsymbol{\eta}}) = &\int_{\overline{\mathcal{K}}} (\overline{\mathbf{P}}_{\mathrm{I}})'_{\overline{v}} : \overline{\mathbf{F}}'_{\overline{v}}\,\mathrm{d}V \\ &+ \int_{\overline{\mathcal{K}}} (\overline{\mathbf{P}}_{\mathrm{I}})'_{\overline{s}} : \overline{\mathbf{F}}'_{\overline{v}} + \overline{\mathbf{P}}_{\mathrm{I}} : \overline{\mathbf{F}}''_{\overline{v}\,\overline{s}} + \overline{\mathbf{P}}_{\mathrm{I}} : \overline{\mathbf{F}}'_{\overline{v}}\,\mathrm{Div}\,\delta\boldsymbol{X}\,\mathrm{d}V - \overline{F}'_{X} \\ &+ \int_{\overline{\mathcal{K}}} (\overline{\mathbf{P}}_{\mathrm{I}})'_{v} : \overline{\mathbf{F}}'_{\overline{v}}\,\mathrm{d}V \\ &+ \int_{\overline{\mathcal{K}}} (\overline{\mathbf{P}}_{\mathrm{I}})'_{s} : \overline{\mathbf{F}}'_{\overline{v}}\,\mathrm{d}V.\end{aligned} \tag{6.43}$$

The physical stiffness operator or stiffness matrix, respectively, which is necessary for the solution of the stated non-linear equation for equilibrium using a Newton-type method presented in Algorithm 6.2 is obtained from the variation of the physical residual with respect to the macroscopic state $\overline{\boldsymbol{v}}$. The first integral in Eq. (6.43) in terms of the variation of stresses $(\overline{\mathbf{P}}_{\mathrm{I}})'_{\overline{v}} = \overline{\mathbb{A}}_{\mathrm{I}} : \overline{\mathbf{F}}'_{\overline{v}}(\overline{\boldsymbol{v}}^e_h, \delta\overline{\boldsymbol{v}}^e_h)$ with respect to the macroscopic state can be identified as the macroscopic tangent stiffness operator $\overline{k}$ from Eq. (6.4) and reads

$$\begin{aligned}\overline{k}(\overline{\boldsymbol{v}}_h,\overline{\boldsymbol{X}}_h,\boldsymbol{v}_h,\boldsymbol{X}_h;\overline{\boldsymbol{\eta}}_h,\delta\overline{\boldsymbol{v}}_h) &= \bigcup_{e=1}^{\overline{n}_{el}} \int_{\overline{\mathcal{K}}^e} \overline{\mathbf{F}}'_{\overline{v}}(\overline{\boldsymbol{v}}^e_h,\overline{\boldsymbol{\eta}}^e_h) : \overline{\mathbb{A}}_{\mathrm{I}} : \overline{\mathbf{F}}'_{\overline{v}}(\overline{\boldsymbol{v}}^e_h,\delta\overline{\boldsymbol{v}}^e_h)\,\mathrm{d}V \\ &= \bigcup_{e=1}^{\overline{n}_{el}} \sum_{i=1}^{nn}\sum_{j=1}^{nn} \overline{\boldsymbol{\eta}}_i^T\,\overline{\boldsymbol{K}}^e_{ij}\,\delta\overline{\boldsymbol{v}}_j = \overline{\boldsymbol{\eta}}^T\,\overline{\boldsymbol{K}}\delta\overline{\boldsymbol{v}},\end{aligned} \tag{6.44}$$

with its discretised counterpart for the element stiffness matrix

$$\overline{\boldsymbol{K}}^e_{ij} = \int_{\overline{\mathcal{K}}^e} \boldsymbol{B}^T_{\overline{v}i}\,\overline{\boldsymbol{A}}_{\mathrm{I}}\,\boldsymbol{B}_{\overline{v}j}\,\mathrm{d}V. \tag{6.45}$$

Incorporated material properties in terms of $\overline{\mathbb{A}}_{\mathrm{I}}$ or $\overline{\boldsymbol{A}}_{\mathrm{I}}$ are obtained according to homogenisation principles presented in Section 4.3 and therefore, $\overline{\mathbb{A}}_{\mathrm{I}} = \partial_{\overline{\mathbf{F}}}\,\overline{\mathbf{P}}_{\mathrm{I}}$ or $\overline{\boldsymbol{A}}_{\mathrm{I}} = \partial_{\overline{\mathbf{F}}}\,\overline{\underline{\boldsymbol{P}}_{\mathrm{K,I}}}$, cf. Eq. (4.12) and Eq. (4.31), respectively, and replace the evaluation of a classical constitutive law formulated for single scale problems.

The second integral can be directly connected to the macroscopic tangent pseudo load operator $\overline{p}$ from Eq. (6.4) and has a similar structure to the pseudo load operator within

the sensitivity analysis on single scales, cf. Eq. (5.87), i.e.

$$\begin{aligned}\overline{p}(\overline{\boldsymbol{v}}_h, \overline{\boldsymbol{X}}_h, \boldsymbol{v}_h, \boldsymbol{X}_h; \overline{\boldsymbol{\eta}}_h, \delta\overline{\boldsymbol{X}}_h) = \bigcup_{e=1}^{\overline{n}_{el}} \int_{\overline{\mathcal{K}}^e} \Big[& \overline{\mathbf{P}}_{\mathrm{I}} : \overline{\mathbf{F}}''_{\overline{v}\,\overline{s}}(\overline{\boldsymbol{v}}_h^e, \overline{\boldsymbol{\eta}}_h^e, \delta\overline{\boldsymbol{X}}_h^e) \\ & + \overline{\mathbf{F}}'_{\overline{v}}(\overline{\boldsymbol{v}}_h^e, \overline{\boldsymbol{\eta}}_h^e) : \overline{\mathbb{A}}_{\mathrm{I}} : \overline{\mathbf{F}}'_{\overline{s}}(\overline{\boldsymbol{v}}_h^e, \delta\overline{\boldsymbol{X}}_h^e) \\ & + \overline{\mathbf{P}}_{\mathrm{I}} : \overline{\mathbf{F}}'_{\overline{v}}(\overline{\boldsymbol{v}}_h^e, \overline{\boldsymbol{\eta}}_h^e)\, \mathrm{Div}\, \delta\overline{\boldsymbol{X}}_h^e \Big]\, \mathrm{d}V \\ & - \overline{F}'_{\overline{s}}(\overline{\boldsymbol{X}}_h^e; \overline{\boldsymbol{\eta}}_h^e, \delta\overline{\boldsymbol{X}}_h^e) \\ = \bigcup_{e=1}^{\overline{n}_{el}} \sum_{i=1}^{nn} \sum_{j=1}^{nn} & \overline{\boldsymbol{\eta}}_i^T\, \overline{\boldsymbol{P}}_{ij}^e\, \delta\overline{\boldsymbol{X}}_j = \overline{\boldsymbol{\eta}}^T\, \overline{\boldsymbol{P}}\, \delta\overline{\boldsymbol{X}}.\end{aligned} \tag{6.46}$$

The discretised counterpart for the element pseudo load matrix is evaluated from

$$\overline{\boldsymbol{P}}_{ij}^e = \int_{\overline{\mathcal{K}}^e} \boldsymbol{B}_{\overline{v}i}^T \overline{\boldsymbol{A}}_{\mathrm{I}} \boldsymbol{B}_{\overline{s}j} - \overline{\boldsymbol{P}_{\mathrm{KI}}} \boldsymbol{L}_j \boldsymbol{L}_i^T + \overline{\boldsymbol{P}_{\mathrm{KI}}} \boldsymbol{L}_i \boldsymbol{L}_j^T\, \mathrm{d}V - (\overline{\boldsymbol{F}}'_{\overline{X}})_{ij}(\overline{\boldsymbol{X}}). \tag{6.47}$$

The approximation of $(\overline{\boldsymbol{F}}'_{\overline{X}})_{ij}$, i.e. the approximation for divergence operators, yields

$$(\overline{\boldsymbol{F}}'_{\overline{X}})_{ij}(\overline{\boldsymbol{X}}) = \int_{\overline{\mathcal{K}}^e} N_i\, \overline{\boldsymbol{b}}\, \boldsymbol{L}_j^T\, \mathrm{d}V. \tag{6.48}$$

The last two terms in Eq. (6.43) contain partial variations of the macroscopic physical residual with respect to microscopic state and design parameters, i.e. with respect to $\boldsymbol{v}$ and $\boldsymbol{X}$ and can be identified with the multilevel stiffness operator $\widetilde{k}$ and the multilevel tangent pseudo load operator $\widetilde{p}$, both introduced in Eq. (6.4). The corresponding assembly procedure for the multilevel stiffness operator yields

$$\begin{aligned}\widetilde{k}(\overline{\boldsymbol{v}}_h, \overline{\boldsymbol{X}}_h, \boldsymbol{v}_h, \boldsymbol{X}_h; \overline{\boldsymbol{\eta}}_h, \delta\boldsymbol{v}_h) &= \bigcup_{e=1}^{\overline{n}_{el}} \int_{\overline{\mathcal{K}}^e} (\overline{\mathbf{P}}_{\mathrm{I}})'_v : \overline{\mathbf{F}}'_{\overline{v}}(\overline{\boldsymbol{v}}_h^e, \overline{\boldsymbol{\eta}}_h^e)\, \mathrm{d}V \\ &= \bigcup_{e=1}^{\overline{n}_{el}} \sum_{i=1}^{nn} \sum_{j=1}^{nn} \overline{\boldsymbol{\eta}}_i^T\, \widetilde{\boldsymbol{K}}_{ij}^e\, \delta\overline{\boldsymbol{X}}_j = \overline{\boldsymbol{\eta}}^T\, \widetilde{\boldsymbol{K}}\, \delta\overline{\boldsymbol{X}}\end{aligned} \tag{6.49}$$

with its element contribution

$$\widetilde{\boldsymbol{K}}_{ij}^e = \int_{\overline{\mathcal{K}}^e} \boldsymbol{B}_{\overline{v}i}^T (\overline{\boldsymbol{P}_{\mathrm{KI}}})'_v\, \mathrm{d}V \tag{6.50}$$

and for the multilevel pseudo load operator

$$\begin{aligned}\widetilde{p}(\overline{\boldsymbol{v}}_h, \overline{\boldsymbol{X}}_h, \boldsymbol{v}_h, \boldsymbol{X}_h; \overline{\boldsymbol{\eta}}_h, \delta\boldsymbol{X}_h) &= \bigcup_{e=1}^{\overline{n}_{el}} \int_{\overline{\mathcal{K}}^e} (\overline{\mathbf{P}}_{\mathrm{I}})'_X : \overline{\mathbf{F}}'_{\overline{v}}(\overline{\boldsymbol{v}}_h^e, \overline{\boldsymbol{\eta}}_h^e)\, \mathrm{d}V \\ &= \bigcup_{e=1}^{\overline{n}_{el}} \sum_{i=1}^{nn} \sum_{j=1}^{nn} \overline{\boldsymbol{\eta}}_i^T\, \widetilde{\boldsymbol{P}}_{ij}^e\, \delta\overline{\boldsymbol{X}}_j = \overline{\boldsymbol{\eta}}^T\, \widetilde{\boldsymbol{P}}\, \delta\overline{\boldsymbol{X}}\end{aligned} \tag{6.51}$$

with its element contribution

$$\widetilde{\boldsymbol{P}}_{ij}^e = \int_{\overline{\mathcal{K}}^e} \boldsymbol{B}_{\overline{v}i}^T\, (\overline{\boldsymbol{P}_{\mathrm{KI}}})'_X\, \mathrm{d}V. \tag{6.52}$$

Necessary variations of effective stresses, i.e. variations of homogenised stresses in vector notation $(\overline{\boldsymbol{P}_{\mathrm{KI}}})'_v$ and $(\overline{\boldsymbol{P}_{\mathrm{KI}}})'_X$, can be connected to the sensitivity of the micro-macro coupling scheme within homogenisation and are derived in the following section.

6.4.3 Sensitivity analysis of effective parameters

To obtain the full formulation of the total variation of the macroscopic weak form of equilibrium from Section 6.4.2, variations of homogenised stresses are required and are derived in this section. In the following, variations with respect to all microscopic parameters are also indicated by the compact notation using the index mic, i.e. $(\cdot)'_{\mathsf{mic}} = (\cdot)'_v + (\cdot)'_s$, and therefore, the partial variations are also expressed by

$$\overline{R}'_{\mathsf{mic}} = \overline{R}'_v + \overline{R}'_s = \int_{\overline{\mathcal{K}}} \left[(\overline{\mathbf{P}}_{\mathrm{I}})'_v + (\overline{\mathbf{P}}_{\mathrm{I}})'_s\right] : \overline{\mathbf{F}}'_{\overline{v}}(\overline{\boldsymbol{v}}, \overline{\boldsymbol{\eta}})\, \mathrm{d}V = \int_{\overline{\mathcal{K}}} (\overline{\mathbf{P}}_{\mathrm{I}})'_{\mathsf{mic}} : \overline{\mathbf{F}}'_{\overline{v}}(\overline{\boldsymbol{v}}, \overline{\boldsymbol{\eta}})\, \mathrm{d}V. \tag{6.53}$$

In accordance to the minimisation problem of homogenisation, presented in Eq. (4.9) in terms of the Lagrange formalism and deduced homogenised stresses in Eq. (4.13), effective stresses $\overline{\mathbf{P}}_{\mathrm{I}}$ explicitly depend on the Lagrange multiplier $\boldsymbol{\lambda}_{\mathrm{I}}$ and their variation reads

$$(\overline{\mathbf{P}}_{\mathrm{I}})'_{\mathsf{mic}}(\boldsymbol{\lambda}_{\mathrm{I}}) = \frac{\partial \overline{\mathbf{P}}_{\mathrm{I}}}{\partial \boldsymbol{\lambda}_{\mathrm{I}}} (\boldsymbol{\lambda}_{\mathrm{I}})'_{\mathsf{mic}} = \frac{\partial \overline{\mathbf{P}}_{\mathrm{I}}}{\partial \boldsymbol{\lambda}_{\mathrm{I}}} \left[(\boldsymbol{\lambda}_{\mathrm{I}})'_v + (\boldsymbol{\lambda}_{\mathrm{I}})'_s\right]. \tag{6.54}$$

This relation can be connected to the sensitivity of the micro-macro coupling condition. The sensitivity of the Lagrange multiplier $\boldsymbol{\lambda}_{\mathrm{I}}$ has to be investigated. Referring the solution scheme on the lower scale and corresponding Euler-Lagrange equations in Eq. (4.28), in the solution point of stated microscopic BVP the obtained Lagrange multiplier $\boldsymbol{\lambda}_{\mathrm{I}}$, especially directly in the case of linear displacements (D) for boundary conditions, corresponds to resulting reaction forces or the external part of the residual on the surface of the underlying RVE scaled by the value of the microscopic volume. For different types of boundary conditions, like periodic displacements (P) or uniform tractions (S), the resulting sensitivity relations have to be adapted. As a consequence, the following relation holds true

$$V \mathcal{S}_1^T \boldsymbol{\lambda}_{\mathrm{I}} = \boldsymbol{R}_{\mathrm{b}}^{\mathsf{ext}} = \boldsymbol{R}_{\mathrm{b}}^{\mathsf{int}}. \tag{6.55}$$

Correct results for reaction forces and therefore, for their sensitivity information can only be guaranteed for an equilibrium state obtained with respect to a required and sufficient precision. The total variation with respect to microscopic parameters yield, due to constant volume V and constant boundary conditions matrix $\mathcal{S}_1$, the statement

$$V\mathcal{S}_1^T(\boldsymbol{\lambda}_\mathrm{I})'_{\mathsf{mic}} = (\boldsymbol{R}_\mathrm{b}^{\mathsf{ext}})'_{\mathsf{mic}} = (\boldsymbol{R}_\mathrm{b}^{\mathsf{int}})'_{\mathsf{mic}} = (\boldsymbol{R}_\mathrm{b}^{\mathsf{int}})'_v + (\boldsymbol{R}_\mathrm{b}^{\mathsf{int}})'_s. \tag{6.56}$$

It is sufficient to consider variations of the internal part of the physical residual $\boldsymbol{R}^{\mathsf{int}}$ on the surface or boundary of the RVE and to connect them with variations of the external part of the residual $\boldsymbol{R}^{\mathsf{ext}}$ or directly with the sensitivity of the Lagrange multiplier $\boldsymbol{\lambda}_\mathrm{I}$. The required total variation in terms of reaction forces is introduced in Section 5.7.3, especially in Eq. (5.117), and reads

$$\left(\boldsymbol{R}_\mathrm{b}^{\mathsf{ext}}\right)'_{\mathsf{mic}} = (\boldsymbol{R}_\mathrm{b}^{\mathsf{int}})'_v + (\boldsymbol{R}_\mathrm{b}^{\mathsf{int}})'_s = \boldsymbol{K}_{\mathrm{ba}}^{\mathsf{int}}\, \delta\boldsymbol{v}_\mathrm{a} + \boldsymbol{P}_\mathrm{b}^{\mathsf{int}}\, \delta\boldsymbol{X}, \tag{6.57}$$

or in terms of the total variation with respect to the design parameters

$$\left(\boldsymbol{R}_\mathrm{b}^{\mathsf{ext}}\right)' = \left[\boldsymbol{K}_{\mathrm{ba}}^{\mathsf{int}}\, \boldsymbol{S}_\mathrm{a} + \boldsymbol{P}_\mathrm{b}^{\mathsf{int}}\right] \delta\boldsymbol{X}. \tag{6.58}$$

Partial variations can be identified with

$$(\boldsymbol{R}_\mathrm{b}^{\mathsf{int}})'_v = \frac{\partial(\boldsymbol{R}_\mathrm{b}^{\mathsf{int}})}{\partial\boldsymbol{v}}\delta\boldsymbol{v} = \boldsymbol{K}_{\mathrm{ba}}^{\mathsf{int}}\, \delta\boldsymbol{v}_\mathrm{a} \qquad \text{and} \qquad (\boldsymbol{R}_\mathrm{b}^{\mathsf{int}})'_s = \frac{\partial(\boldsymbol{R}_\mathrm{b}^{\mathsf{int}})}{\partial\boldsymbol{X}}\delta\boldsymbol{X} = \boldsymbol{P}_\mathrm{b}^{\mathsf{int}}\delta\boldsymbol{X}. \tag{6.59}$$

Finally, the total design variation of the Lagrange multiplier for alternative boundary conditions $\mathrm{I} = \{\mathrm{D}, \mathrm{P}, \mathrm{S}\}$ is obtained from

$$V\mathcal{S}_1^T(\boldsymbol{\lambda}_\mathrm{I})' = \left[\boldsymbol{K}_{\mathrm{ba}}^{\mathsf{int}}\, \boldsymbol{S}_\mathrm{a} + \boldsymbol{P}_\mathrm{b}^{\mathsf{int}}\right] \delta\boldsymbol{X}. \tag{6.60}$$

The chosen homogenisation approach requires the incorporation of the obtained sensitivity information into the context of homogenised stresses in Eq. (4.31) and formulated boundary conditions presented in Section 4.3.3 and Section 4.4.2. The variation of effective stresses directly is presented in Eq. (6.54). In the computational sense, they are adapted for different boundary conditions and are computed using the general formulation of the boundary conditions matrix $\mathcal{S}_2$, i.e. $\overline{\underline{\boldsymbol{P}}}_{\mathrm{K,I}}(\boldsymbol{\lambda}_\mathrm{I}) = \mathcal{S}_2^T\boldsymbol{\lambda}_\mathrm{I}$. In comparison to Eq. (6.54), the boundary conditions matrix $\mathcal{S}_2$ can be identified with the partial derivative of effective stresses with respect to the Lagrange multiplier $\boldsymbol{\lambda}_\mathrm{I}$. Due to the fact that $\mathcal{S}_2$ is constant for all introduced types of boundary conditions, the variation of homogenised stresses contains only the variation of $\boldsymbol{\lambda}_\mathrm{I}$ and therefore, its final form result to

$$(\overline{\underline{\boldsymbol{P}}}_{\mathrm{K,I}})'_{\mathsf{mic}} = \mathcal{S}_2(\boldsymbol{\lambda}_\mathrm{I})' = \frac{1}{V}\,\mathcal{S}_2\,\mathcal{S}_1^{-T}\left[\boldsymbol{K}_{\mathrm{ba}}^{\mathsf{int}}\, \boldsymbol{S}_\mathrm{a} + \boldsymbol{P}_\mathrm{b}^{\mathsf{int}}\right] \delta\boldsymbol{X}. \tag{6.61}$$

The introduced notation using the index $(\cdot)'_{\mathsf{mic}}$ allows the formulation of the total multilevel

pseudo load operator from Eq. (6.17)

$$\begin{aligned}\breve{p}(\overline{\boldsymbol{v}}_h, \overline{\boldsymbol{X}}_h, \boldsymbol{v}_h, \boldsymbol{X}_h; \overline{\boldsymbol{\eta}}_h, \delta\boldsymbol{X}_h) &= \bigcup_{e=1}^{\overline{n}_{el}} \int_{\overline{\mathcal{K}}^e} (\overline{\mathbf{P}}_{\mathrm{I}})'_{\mathsf{mic}} : \overline{\mathbf{F}}'_{\overline{v}}(\overline{\boldsymbol{v}}_h^e, \overline{\boldsymbol{\eta}}_h^e)\, \mathrm{d}V \\ &= \bigcup_{e=1}^{\overline{n}_{el}} \sum_{i=1}^{nn} \sum_{j=1}^{nn} \overline{\boldsymbol{\eta}}_i^T\, \breve{\boldsymbol{P}}_{ij}^e\, \delta\overline{\boldsymbol{X}}_j = \overline{\boldsymbol{\eta}}^T\, \breve{\boldsymbol{P}}\, \delta\overline{\boldsymbol{X}}.\end{aligned} \tag{6.62}$$

An appropriate discretisation yields the contribution on element level

$$\breve{\boldsymbol{P}}_{ij}^e = \int_{\overline{\mathcal{K}}^e} \boldsymbol{B}_{\overline{v}i}^T\, (\overline{\boldsymbol{P}_{\mathsf{KI}}})'\, \mathrm{d}V. \tag{6.63}$$

The following Table 6.5 summarises all relevant discrete relations for the sensitivity analysis on multiple scales.

Table 6.5: Summary of discrete sensitivity relations and operators on multiple scales. Quantities connected to a single scale exclusively are indicated by $(\cdot)^*$ for the macroscopic and by $(\cdot)_*$ for the microscopic scale.

	Discretisation	cf. Eq.
Physical residual		
micro$_*$	$\boldsymbol{R}_i^e = \int_{\mathcal{K}^e} \boldsymbol{P}_{\mathsf{K}} \boldsymbol{L}_i\, \mathrm{d}V$	6.21
macro*	$\overline{\boldsymbol{R}}_i^e = \int_{\overline{\mathcal{K}}^e} \overline{\boldsymbol{P}_{\mathsf{K,I}}}\, \boldsymbol{L}_i\, \mathrm{d}V$	6.38
macro* (external)	$\overline{\boldsymbol{F}}_i^e = \int_{\overline{\mathcal{K}}^e} N_i \overline{\boldsymbol{b}}\, \mathrm{d}V$	6.39
Physical stiffness		
micro$_*$	$\boldsymbol{K}_{ij}^e = \int_{\mathcal{K}^e} \boldsymbol{B}_{vi}^T \boldsymbol{A} \boldsymbol{B}_{vj}\, \mathrm{d}V$	6.23
macro*	$\overline{\boldsymbol{K}}_{ij}^e = \int_{\overline{\mathcal{K}}^e} \boldsymbol{B}_{\overline{v}i}^T\, \overline{\boldsymbol{A}}_{\mathrm{I}}\, \boldsymbol{B}_{\overline{v}j}\, \mathrm{d}V$	6.45
multilevel	$\widetilde{\boldsymbol{K}}_{ij}^e = \int_{\overline{\mathcal{K}}^e} \boldsymbol{B}_{\overline{v}i}^T (\overline{\boldsymbol{P}_{\mathsf{KI}}})'_v\, \mathrm{d}V$	6.50
Pseudo load		
micro$_*$	$\boldsymbol{P}_{ij}^e = \int_{\mathcal{K}^e} \boldsymbol{B}_{vi}^T \boldsymbol{A} \boldsymbol{B}_{sj} - \boldsymbol{P}_{\mathsf{K}} \boldsymbol{L}_j \boldsymbol{L}_i^T + \boldsymbol{P}_{\mathsf{K}} \boldsymbol{L}_i \boldsymbol{L}_j^T\, \mathrm{d}V$	6.28
macro*	$\overline{\boldsymbol{P}}_{ij}^e = \int_{\overline{\mathcal{K}}^e} \boldsymbol{B}_{\overline{v}i}^T \overline{\boldsymbol{A}}_{\mathrm{I}} \boldsymbol{B}_{\overline{s}j} - \overline{\boldsymbol{P}_{\mathsf{KI}}} \boldsymbol{L}_j \boldsymbol{L}_i^T + \overline{\boldsymbol{P}_{\mathsf{KI}}} \boldsymbol{L}_i \boldsymbol{L}_j^T\, \mathrm{d}V$	6.47
multilevel	$\widetilde{\boldsymbol{P}}_{ij}^e = \int_{\overline{\mathcal{K}}^e} \boldsymbol{B}_{\overline{v}i}^T\, (\overline{\boldsymbol{P}_{\mathsf{KI}}})'_X\, \mathrm{d}V$	6.52
multilevel (total)	$\breve{\boldsymbol{P}}_{ij}^e = \int_{\overline{\mathcal{K}}^e} \boldsymbol{B}_{\overline{v}i}^T\, (\overline{\boldsymbol{P}_{\mathsf{KI}}})'_{\mathsf{mic}}\, \mathrm{d}V$	6.63
macro* (external)	$(\overline{\boldsymbol{F}}'_{\overline{X}})_{ij} = \int_{\overline{\mathcal{K}}^e} N_i\, \overline{\boldsymbol{b}}\, \boldsymbol{L}_j^T\, \mathrm{d}V$	6.48
Effective parameters		
Lagrange multiplier	$V \mathcal{S}_1^T (\boldsymbol{\lambda}_{\mathrm{I}})' = \left[\boldsymbol{K}_{\mathrm{ba}}^{\mathsf{int}}\, \boldsymbol{S}_{\mathrm{a}} + \boldsymbol{P}_{\mathrm{b}}^{\mathsf{int}}\right] \delta\boldsymbol{X}$	6.60
homogenised stresses	$(\overline{\boldsymbol{P}_{\mathsf{K,I}}})'_{\mathsf{mic}} = \frac{1}{V}\, \mathcal{S}_2\, \mathcal{S}_1^{-T} \left[\boldsymbol{K}_{\mathrm{ba}}^{\mathsf{int}}\, \boldsymbol{S}_{\mathrm{a}} + \boldsymbol{P}_{\mathrm{b}}^{\mathsf{int}}\right] \delta\boldsymbol{X}$	6.61

6.5 Optimisation setup for problems on multiple scales

In this section a general setup for optimisation problems on multiple scales in terms of their continuous and discrete representation as well as of their numerical realisation is outlined. Modifications of notation and adaptations of formulations for single scale optimisation problems are performed to obtain closed formulations for FE^2 optimisation frameworks.

6.5.1 General formulation of the optimisation problem

The general optimisation problem with an arbitrary macroscopic objective functional J, various equality and inequality constraints $(\overline{\boldsymbol{h}}, \overline{\boldsymbol{g}})$ on the macroscale and $(\boldsymbol{h}, \boldsymbol{g})$ on the microscale, several lower and upper side constraints $\overline{\boldsymbol{s}}^{\mathrm{l}}, \overline{\boldsymbol{s}}^{\mathrm{u}}$ on the macroscale and $\boldsymbol{s}^{\mathrm{l}}, \boldsymbol{s}^{\mathrm{u}}$ on the microscale for design parameters can be introduced in the following abstract way.

Problem 6.1 (General multiscale optimisation problem) *Find* $\{\overline{\boldsymbol{v}}, \overline{\boldsymbol{s}}, \boldsymbol{v}, \boldsymbol{s}\} \in \overline{\mathcal{V}} \times \overline{\mathcal{S}} \times \mathcal{V} \times \mathcal{S}$ *of the macroscopic objective functional* $J : \overline{\mathcal{V}} \times \overline{\mathcal{S}} \times \mathcal{V} \times \mathcal{S} \to \mathbb{R}$ *such that*

$$\min_{\overline{\boldsymbol{v}}, \overline{\boldsymbol{s}}, \boldsymbol{v}, \boldsymbol{s} \in \overline{\mathcal{V}} \times \overline{\mathcal{S}} \times \mathcal{V} \times \mathcal{S}} J(\overline{\boldsymbol{v}}, \overline{\boldsymbol{s}}, \boldsymbol{v}, \boldsymbol{s}) \tag{6.64}$$

subject to the constraints

$$\begin{aligned} &\overline{\boldsymbol{h}}(\overline{\boldsymbol{v}}, \overline{\boldsymbol{s}}, \boldsymbol{v}, \boldsymbol{s}) = \boldsymbol{0}, && \overline{\boldsymbol{g}}(\overline{\boldsymbol{v}}, \overline{\boldsymbol{s}}, \boldsymbol{v}, \boldsymbol{s}) \leq \boldsymbol{0}, && \overline{\boldsymbol{s}}^{l} \leq \overline{\boldsymbol{s}} \leq \overline{\boldsymbol{s}}^{u}, \\ &\boldsymbol{h}(\boldsymbol{v}, \boldsymbol{s}) = \boldsymbol{0}, && \boldsymbol{g}(\boldsymbol{v}, \boldsymbol{s}) \leq \boldsymbol{0}, && \boldsymbol{s}^{l} \leq \boldsymbol{s} \leq \boldsymbol{s}^{u}. \end{aligned} \tag{6.65}$$

Here, the following vector notations are introduced: $\overline{\boldsymbol{h}}(\overline{\boldsymbol{v}}, \overline{\boldsymbol{s}}, \boldsymbol{v}, \boldsymbol{s})$ *for introduced macroscopic equality constraints* $\overline{h}_i(\overline{\boldsymbol{v}}, \overline{\boldsymbol{s}}, \boldsymbol{v}, \boldsymbol{s}) = 0$, $i \in \overline{\mathcal{E}}$, *the vector notation* $\overline{\boldsymbol{g}}(\boldsymbol{v}, \boldsymbol{s})$ *for introduced macroscopic inequality constraints* $\overline{g}_j(\boldsymbol{v}, \boldsymbol{s}) \leq 0$, $j \in \overline{\mathcal{I}}$, *the vector notation* $\boldsymbol{h}(\boldsymbol{v}, \boldsymbol{s})$ *for introduced microscopic equality constraints* $h_i(\boldsymbol{v}, \boldsymbol{s}) = 0$, $i \in \mathcal{E}$, *and also the vector notation* $\boldsymbol{g}(\boldsymbol{v}, \boldsymbol{s})$ *for introduced microscopic inequality constraints* $g_j(\boldsymbol{v}, \boldsymbol{s}) \leq 0$, $j \in \mathcal{I}$. *The sets of indices for equality and inequality constraints are denoted by* $\overline{\mathcal{E}}, \mathcal{E}, \overline{\mathcal{I}}$ *and* $\mathcal{I}$.

6.5.2 Discrete form of the optimisation problem

Within numerical frameworks, it is necessary to formulate accurate matrix representations of continuous relations. According to the continuous formulation of the general multiscale optimisation Problem 6.1, the discrete form can be obtained by using discretised values for objectives, macro- and microscopic constraints and design parameters.

Problem 6.2 (Discrete multiscale optimisation problem) *Find* $\{\overline{\boldsymbol{v}}, \overline{\boldsymbol{s}}, \boldsymbol{v}, \boldsymbol{s}\} \in \overline{\mathcal{V}}_h \times \overline{\mathcal{S}}_h \times \mathcal{V}_h \times \mathcal{S}_h$ *of the discrete macroscopic objective functional* $J : \overline{\mathcal{V}}_h \times \overline{\mathcal{S}}_h \times \mathcal{V}_h \times \mathcal{S}_h \to \mathbb{R}$ *such that*

$$\min_{\overline{\boldsymbol{v}}, \overline{\boldsymbol{s}}, \boldsymbol{v}, \boldsymbol{s} \in \overline{\mathcal{V}}_h \times \overline{\mathcal{S}}_h \times \mathcal{V}_h \times \mathcal{S}_h} J(\overline{\boldsymbol{v}}, \overline{\boldsymbol{s}}, \boldsymbol{v}, \boldsymbol{s}) \tag{6.66}$$

subject to the constraints

$$\begin{aligned} &\overline{\boldsymbol{h}}(\overline{\boldsymbol{v}},\overline{\boldsymbol{s}},\boldsymbol{v},\boldsymbol{s})=\boldsymbol{0}, && \overline{\boldsymbol{g}}(\overline{\boldsymbol{v}},\overline{\boldsymbol{s}},\boldsymbol{v},\boldsymbol{s})\leq\boldsymbol{0}, && \overline{\boldsymbol{s}}^{l}\leq\overline{\boldsymbol{s}}\leq\overline{\boldsymbol{s}}^{u},\\ &\boldsymbol{h}(\boldsymbol{v},\boldsymbol{s})=\boldsymbol{0}, && \boldsymbol{g}(\boldsymbol{v},\boldsymbol{s})\leq\boldsymbol{0}, && \boldsymbol{s}^{l}\leq\boldsymbol{s}\leq\boldsymbol{s}^{u}. \end{aligned} \tag{6.67}$$

Here, the following matrix notations are introduced: a matrix notation $\overline{\boldsymbol{h}}(\overline{\boldsymbol{v}},\overline{\boldsymbol{s}},\boldsymbol{v},\boldsymbol{s})$ *of introduced macroscopic equality constraints* $\overline{h}_i(\overline{\boldsymbol{v}},\overline{\boldsymbol{s}},\boldsymbol{v},\boldsymbol{s})=0$, $i\in\overline{\mathcal{E}}_h$, *a matrix representation* $\overline{\boldsymbol{g}}(\overline{\boldsymbol{v}},\overline{\boldsymbol{s}},\boldsymbol{v},\boldsymbol{s})$ *of introduced macroscopic inequality constraints* $\overline{g}_j(\overline{\boldsymbol{v}},\overline{\boldsymbol{s}},\boldsymbol{v},\boldsymbol{s})\leq 0$, $j\in\overline{\mathcal{I}}_h$, *a matrix notation* $\boldsymbol{h}(\boldsymbol{v},\boldsymbol{s})$ *of introduced microscopic equality constraints* $h_i(\boldsymbol{v},\boldsymbol{s})=0$, $i\in\mathcal{E}_h$, *and a matrix representation* $\boldsymbol{g}(\boldsymbol{v},\boldsymbol{s})$ *of introduced microscopic inequality constraints* $g_j(\boldsymbol{v},\boldsymbol{s})\leq 0$, $j\in\mathcal{I}_h$. *The sets of indices for equality and inequality constraints are denoted by* $\overline{\mathcal{E}}_h,\mathcal{E}_h,\overline{\mathcal{I}}_h$ *and* $\mathcal{I}_h$.

The application of the general SQP method as a solver for the stated optimisation problem, which guarantees solutions in feasible regions with respect to the stated constraints, requires a compact and summarising representation of all introduced macro- and microscopic constraints and design parameters. Therefore, the following representation is introduced

$$\begin{aligned} \text{Equality constraints:}\quad & \widehat{\boldsymbol{h}}\,(\overline{\boldsymbol{v}},\overline{\boldsymbol{s}},\boldsymbol{v},\boldsymbol{s})=\begin{bmatrix}\overline{\boldsymbol{h}}\\ \boldsymbol{h}\end{bmatrix},\\ \text{Inequality constraints:}\quad & \widehat{\boldsymbol{g}}\,(\overline{\boldsymbol{v}},\overline{\boldsymbol{s}},\boldsymbol{v},\boldsymbol{s})=\begin{bmatrix}\overline{\boldsymbol{g}}\\ \boldsymbol{g}\end{bmatrix},\\ \text{Design parameters:}\quad & \widehat{\boldsymbol{s}}=\begin{bmatrix}\overline{\boldsymbol{s}}\\ \boldsymbol{s}\end{bmatrix}. \end{aligned} \tag{6.68}$$

The Lagrange function introduced in Problem 3.3 and used within SQP as well as its gradient are modified to

$$\mathcal{L}(\widehat{\boldsymbol{s}},\widehat{\boldsymbol{\lambda}},\widehat{\boldsymbol{\mu}})=J(\widehat{\boldsymbol{s}})+\widehat{\boldsymbol{\lambda}}^{T}\,\widehat{\boldsymbol{h}}\,(\widehat{\boldsymbol{s}})+\widehat{\boldsymbol{\mu}}^{T}\,\widehat{\boldsymbol{g}}\,(\widehat{\boldsymbol{s}})\qquad\text{and}\qquad\nabla\mathcal{L}(\widehat{\boldsymbol{s}},\widehat{\boldsymbol{\lambda}},\widehat{\boldsymbol{\mu}})=\boldsymbol{0}. \tag{6.69}$$

For the solution of the optimality criteria using the SQP method, a sequential solution of quadratic subproblems with a quadratic approximation of the objective functional $J(\overline{\boldsymbol{v}},\overline{\boldsymbol{s}},\boldsymbol{v},\boldsymbol{s})$ and the linearisation of equality $\widehat{\boldsymbol{h}}\,(\overline{\boldsymbol{v}},\overline{\boldsymbol{s}},\boldsymbol{v},\boldsymbol{s})$ and inequality constraints $\widehat{\boldsymbol{g}}\,(\overline{\boldsymbol{v}},\overline{\boldsymbol{s}},\boldsymbol{v},\boldsymbol{s})$ is required. This principle procedure in terms of the formulation of quadratic subproblems and linearisation of constraints is also described in Problem 3.3.

6.5.3 Numerical environment for optimisation on multiple scales

The numerical iterative solution process of Problem 6.1 or Problem 6.2, respectively, with essential and recurring steps is outlined in Fig. 6.3. The first step includes the definition of initial structural designs on both referred scales in terms of physical models with appropriate boundary conditions on individual scales, affiliated geometry and/or CAE-FEM models, the definition of the mathematical optimisation model, which includes the definition of an macroscopic objective function J, equality and/or inequality constraints $(\overline{\boldsymbol{h}},\overline{\boldsymbol{g}})$ on macro- and of $(\boldsymbol{h},\boldsymbol{g})$ on microscale, some side constraints $(\overline{\boldsymbol{s}}^{\mathrm{l}},\overline{\boldsymbol{s}}^{\mathrm{u}})$ on macro- and side constraints $(\boldsymbol{s}^{\mathrm{l}},\boldsymbol{s}^{\mathrm{u}})$ on microscale and basically macro- and microscopic design parameters $\overline{\boldsymbol{s}}$ and $\boldsymbol{s}$.

This basic definition is followed by the first and initial structural analysis on multiple scales in terms of numerical homogenisation or FE^2 techniques. The results obtained for the equilibrium state can be used for the evaluation of required design responses, in terms of objective functions and constraints, and the design sensitivity analysis (DSA) for the stated optimisation problem. The provided sensitivity information and therefore all available gradient information serve as inputs for algorithms for mathematical optimisation and *non-linear programming* (NLP) and are essential quantities to seek for a new and updated design description. Final optimisation results can be provided as drafts to the responsible designers and design engineers. The kernel task within the presented framework for multiscale optimisation pictured in Fig. 6.3 is the integrated design sensitivity analysis. Therefore, macro- and microscopic models $\{\mathsf{M}, \mathsf{m}\}$ as well as solution states $\{\overline{\boldsymbol{v}}, \boldsymbol{v}\}$ on both scales are required. Based on this information the tangents $\{\overline{\boldsymbol{K}}, \overline{\boldsymbol{P}}, \breve{\boldsymbol{P}}\}$ are assembled. This assembly procedure is performed on the macroscopic element level. The sequence of necessary steps is outlined in Algorithm 6.3 in detail. Element contributions of mentioned tangent forms are provided within two loops, i.e. within a loop over macroscopic elements and loop over affiliated macroscopic integration points. It has to be mentioned that the design sensitivity analysis depends on effective and homogenised parameters in terms of FE^2. These parameters have to be solved within the integration point loop or can alternatively be provided from stored data. In the last step obtained element contributions have to be assembled to matrices on global level according to techniques known from standard FEM assembly techniques.

6.5.4 Design parameters and possible combinations

The multiscale optimisation framework requires a definition of an optimisation model with an objective function, equality and inequality constraints and design parameters. Possible choices are already outlined in Chapter 3 and summarised in Table 3.1. Special attention has to be paid concerning the definition of the objective function namely, the objective function under investigation has to be formulated on the present macroscale but in terms of macroscopic and microscopic parameters, where the formulation of equality and inequality constraints and of design parameters is allowed on both scales. Cases and problem formulations which deal with objective functions on the microscale exclusively do not need the overhead of an upper scale and can be treated as optimisation problems on single scales in terms of a macroscopic deformation as the loading case. In summary, mandatory (X) definitions and optional combinations (✓) are outlined in Table 6.6.

Table 6.6: Mandatory definitions and optional combinations in FE^2 optimisation model.

	Goals	**Restrictions**	**Design parameters**
Macroscale	X	✓	✓
Microscale		✓	✓

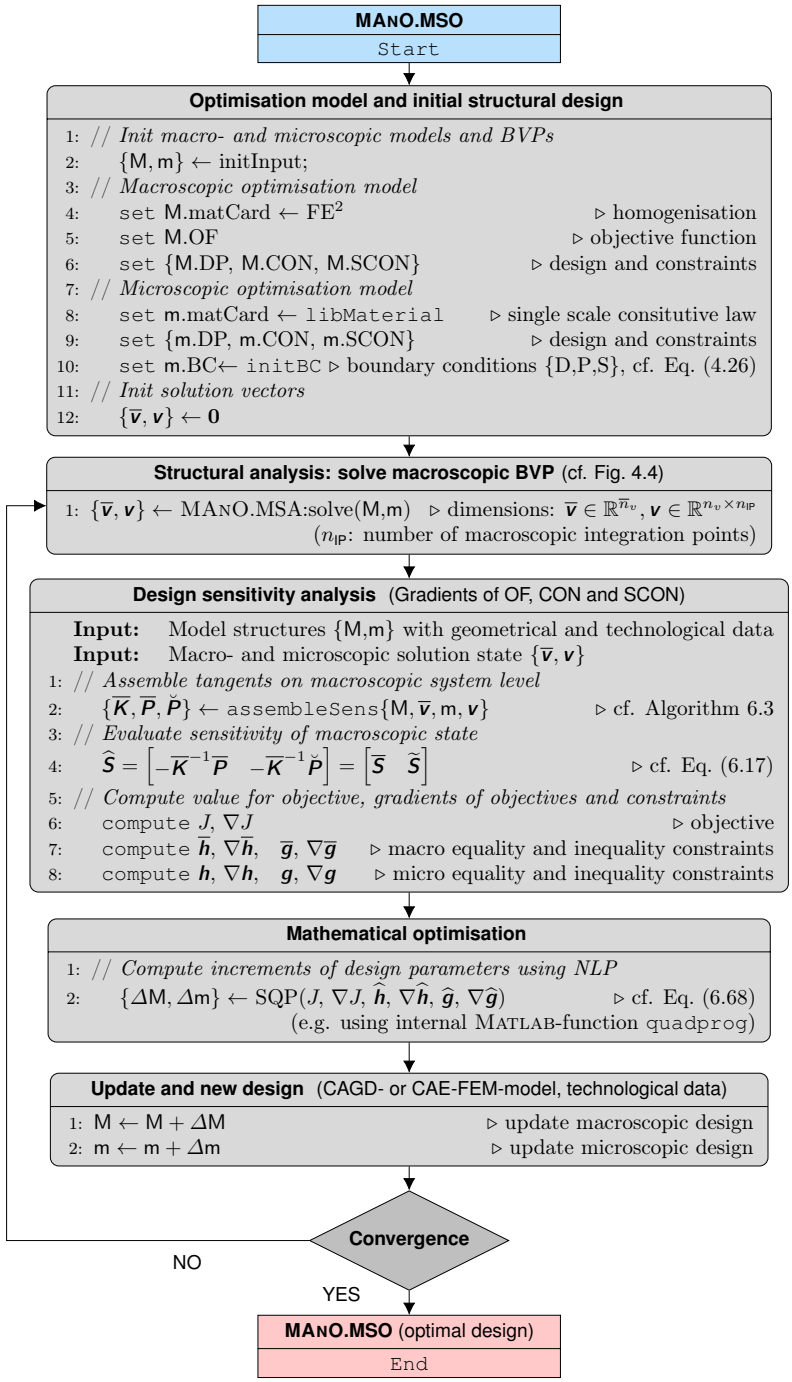

Figure 6.3: Principle framework for multiscale structural optimisation (MANO.MSO).

Algorithm 6.3 Procedure for design sensitivity analysis on macroscopic element level. Contributions of integration points $(\cdot)_p^e$ are summarised in contributions $(\cdot)^e$ on element level. Element contributions are assembled to contributions on global system level $(\cdot)$.

Input: Model structures $\{\mathsf{M},\mathsf{m}\}$ with geometrical and technological data
Input: Macroscopic and microscopic solution state $\{\overline{\boldsymbol{v}}, \boldsymbol{v}\}$
Output: Global stiffness tangent $\overline{\boldsymbol{K}}$ and global pseudo load tangents $\overline{\boldsymbol{P}}$, $\breve{\boldsymbol{P}}$

procedure ASSEMBLE ELEMENT DESIGN SENSITIVITY INFORMATION($\mathsf{M}, \overline{\boldsymbol{v}}, \mathsf{m}, \boldsymbol{v}$)
  for $i_e \leftarrow 1,n_{el}$ **do** ▷ loop over macroscopic elements
    for $i_p \leftarrow 1,n_{\mathsf{IP}}$ **do** ▷ loop over macroscopic element integration points
      // *Get homogenised parameters*
      $\{\overline{\underline{\boldsymbol{P}}}_{\mathrm{K,I}}, \overline{\boldsymbol{A}}_{\mathrm{I}}\} \leftarrow$ `get` MANO.MSA:solve($\mathsf{M}, \overline{\boldsymbol{v}}, \mathsf{m}, \boldsymbol{v}$) ▷ cf. Algorithm 4.1 (or read results from file)
      // *Compute contributions of macroscopic tangents*
      $\overline{\boldsymbol{K}}^e \leftarrow \overline{\boldsymbol{K}}^e_{i_p}(\overline{\underline{\boldsymbol{P}}}_{\mathrm{K,I}}, \overline{\boldsymbol{A}}_{\mathrm{I}})$ ▷ cf. Eq. (6.44)
      $\overline{\boldsymbol{P}}^e \leftarrow \overline{\boldsymbol{P}}^e_{i_p}(\overline{\underline{\boldsymbol{P}}}_{\mathrm{K,I}}, \overline{\boldsymbol{A}}_{\mathrm{I}})$ ▷ cf. Eq. (6.46)
      // *Compute contributions of microscopic tangents*
      $\{\boldsymbol{K}, \boldsymbol{P}\} \leftarrow$ `assemble` RVE(m,$\boldsymbol{v}$) ▷ overall stiffness and pseudo load cf. Eq. (6.22) and Eq. (6.27)
      // *Evaluate sensitivity of microscopic state*
      $\boldsymbol{S} = -\boldsymbol{K}^{-1}\boldsymbol{P}$ ▷ cf. Eq. (6.29)
      // *Compute sensitivity of Lagrange multiplier*
      $\{\boldsymbol{\lambda}'_{\mathrm{I}}, (\boldsymbol{\lambda}_{\mathrm{I}})'_v, (\boldsymbol{\lambda}_{\mathrm{I}})'_s\} \leftarrow$ `eval` $(\boldsymbol{K}, \boldsymbol{P}, \boldsymbol{S})$ ▷ cf. Eq. (6.60)
      // *Compute sensitivity of effective stresses*
      $(\overline{\underline{\boldsymbol{P}}}_{\mathrm{K,I}})'_v \leftarrow \dfrac{\partial \overline{\underline{\boldsymbol{P}}}_{\mathrm{K,I}}}{\partial \boldsymbol{\lambda}_{\mathrm{I}}}(\boldsymbol{\lambda}_{\mathrm{I}})'_v$ ▷ cf. Eq. (6.61)
      $(\overline{\underline{\boldsymbol{P}}}_{\mathrm{K,I}})'_s \leftarrow \dfrac{\partial \overline{\underline{\boldsymbol{P}}}_{\mathrm{K,I}}}{\partial \boldsymbol{\lambda}_{\mathrm{I}}}(\boldsymbol{\lambda}_{\mathrm{I}})'_s$ ▷ cf. Eq. (6.61)
      // *Compute contributions of multilevel tangents*
      $\widetilde{\boldsymbol{K}}^e \leftarrow \widetilde{\boldsymbol{K}}^e_{i_p}((\overline{\underline{\boldsymbol{P}}}_{\mathrm{K,I}})'_v)$ ▷ cf. Eq. (6.49)
      $\widetilde{\boldsymbol{P}}^e \leftarrow \widetilde{\boldsymbol{P}}^e_{i_p}((\overline{\underline{\boldsymbol{P}}}_{\mathrm{K,I}})'_s)$ ▷ cf. Eq. (6.51)
      // *Compute contributions of overall multilevel tangent*
      $\breve{\boldsymbol{P}}^e \leftarrow \breve{\boldsymbol{P}}^e_{i_p}(\widetilde{\boldsymbol{K}}, \widetilde{\boldsymbol{P}}, \boldsymbol{S})$ ▷ cf. Eq. (6.62)
    end for ▷ loop over macroscopic integration points
  end for ▷ loop over macroscopic elements
  // *Assemble tangents on macroscopic system level*
  $\overline{\boldsymbol{K}} \leftarrow \overline{\boldsymbol{K}}^e, \quad \overline{\boldsymbol{P}} \leftarrow \overline{\boldsymbol{P}}^e, \quad \breve{\boldsymbol{P}} \leftarrow \breve{\boldsymbol{P}}^e$
end procedure

6.6 Summary and concluding remarks

This chapter provides the essential steps for the material design based on variational sensitivity. A review on the state of the art and results from literature motivate the major topic of the presented work and emphasises the relevance.

Required sensitivity relations in continuous form are derived and formulated based on the enhanced layout of kinematics, which is adapted with respect to the microscale representation. The connection of sensitivity relations on the micro- and the macroscale takes the aforementioned results for physical reaction forces and their sensitivity information introduced in Chapter 5 into account. The Lagrange multiplier within applied FE^2 techniques can be related to reaction forces on the boundary of the RVE in an appropriate sense. As a consequence, the design sensitivity of the reaction forces can be related to the design sensitivity of the Lagrange multiplier and allows the formulation of a sensitivity relation for the homogenisation condition. Together with effective parameters the latter formulation bridges both individual scales in general, but also in the case of design sensitivity analysis. The explicit discrete representations are composed for the implementation into the in-house MATLAB code MANO.

In the last part of the chapter, the abstract setting for structural optimisation problems on single scales is extended and arranged for the general layout of multiscale optimisation problems with objective functions, constraints and design parameters on both scales. A flow chart illustrates the final framework for numerical structural optimisation on multiple scales. It contains the FE^2 method for structural analysis, the aforementioned design sensitivity analysis on multiple scales as well as the SQP method for mathematical optimisation and is fully implemented in MANO.

Chapter 7

Numerical investigations

So far, previous chapters deliver theoretical foundations for the overall framework of computational material design. The compilation comprises formulations for structural analysis in terms of computational homogenisation and for design sensitivity analysis based on the variational approach, which are both combined with algorithms for mathematical optimisation. The presented structural optimisation environment is used for an automatic generation of designs with maximum stiffness under certain constraints.

In the following, three examples with different design parametrisation setups illustrate the applicability of the formulated sensitivity relations and corresponding numerical aspects from previous chapters. The stated optimisation problems focus on the minimisation of the overall macroscopic compliance, which is directly related to the maximisation of the overall macroscopic stiffness. In addition to some constraints for defined design parameters, volume constraints on both scales are incorporated into the optimisation process.

The first example in Section 7.1 demonstrates a shape optimisation process based on two different kinds of design parameters, i.e. CAGD parameters on the macroscale and diameters of a void on the microscale. This study contains three different evaluations, i.e. optimisation only on the macroscale, optimisation only on the microscale and optimisation with constraints and design parameters distributed on both scales. In the second example in Section 7.2, the macroscopic domain is fixed and evaluated for two different load case scenarios. The design parametrisations for four different microscale representations are realised using morphing based parametrisation techniques. In the third example in Section 7.3 morphing based design parametrisation on the macro- and the microscale is used to perform shape optimisation on both scales simultaneously.

The introduction of different design parameters establishes the flexibility of the proposed formulation and incorporated necessary design velocity field matrices and corresponding transformations into the presented examples. Due to the wide range of applicability and practical relevance, all examples are evaluated using the formulation for periodic boundary conditions (P) on the microscale.

The iterative solutions in terms of structural analysis are provided by the application of the Newton's method on the macro- and the microscale. The computations are based on the hyperelastic Neo-Hookean material law for the constituents on the microscale and

are stopped after the criterion of $TOL_v = 10^{-8}$ for the residuals is reached. The iterative solutions within the structural optimisation are carried out by the SQP method. The change in the objective function is defined as stop criterion and is set to $TOL_s = 10^{-4}$. Details on theoretical, numerical and algorithmic aspects of used solution methods are compiled in Chapter 3, Chapter 4 and Chapter 6.

Remark 7.1 (Verification of sensitivity information in numerical studies)
Prior to the discussion on numerical examples and obtained optimisation results, it is mentioned that all analytically obtained quantities and values within the design sensitivity analysis are verified using the finite difference method introduced and explained in Section 3.3. These numerical tests guarantee correct gradient information and therefore, they guarantee an efficient optimisation process. The verifications are performed in accordance to the appropriate quantity either on the element (e.g. pseudo load matrices), on the global system level (e.g. sensitivities of the state) or after the transformation with the design velocity field matrices (e.g. final objectives and constraints).

7.1 Macroscopic tension test

In the following, three different structural optimisation setups for the macroscopic tension test pictured in Fig. 7.1 are investigated and compared. The target is to figure out the influence of the underlying microscale on the optimisation results and to determine the amount of possible improvement of the overall macroscopic behaviour. Within the performed tests, modifications of the macroscale $\overline{\mathcal{K}}$, of the microscale $\mathcal{K}$ and of both scales simultaneously are considered. For better clarity, the tests are identified as follows:

- **T.1**: design parameters and optimisation **only on macroscale**,
- **T.2**: design parameters and optimisation **only on microscale**,
- **T.3**: design parameters and optimisation **on macro- and microscale**.

The mechanical system is presented in Fig. 7.1. Due to symmetry, only a quarter of the macroscopic system is modeled within the finite element analysis and structural optimisation procedure. It is fixed on the left-hand and bottom side and loaded on the right-hand side. The illustrated microscale representation is connected with each macroscopic integration point and allows the computation of effective stress and material parameters in terms of computational homogenisation. Characteristic system parameters for both scales, like dimensions and material properties, are compiled in Table 7.1. The solution of the non-linear problem on each microscale is carried out by the iterative Newton scheme introduced in Algorithm 4.1 with the evaluation of the Neo-Hookean constitutive law. The sequence of microscopic solution steps is nested into the solution procedure for non-linear equations on the macroscale outlined in Algorithm 6.2.

The optimisation model with all available design parameters on the macro- and the microscale is set up according to Fig. 7.2. On the macroscale the coordinates of control points of the Bézier patch of the upper edge of the system (indicated by numbers 1-7 in Fig. 7.2) are chosen as design parameters. On the microscale, half-axes $\boldsymbol{a} = \begin{bmatrix} a & b \end{bmatrix}$ of the

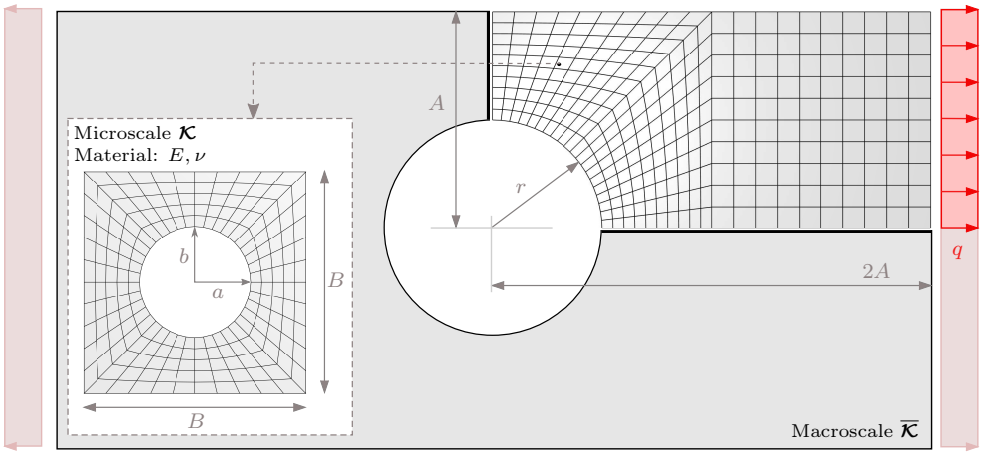

Figure 7.1: Macroscopic tension test: mechanical system and initial design.

circular void are the design variables. Their choice determines the position of the CAGD parameters of the Bézier geometry description. Overall, following dependencies hold true

$$\text{macroscale: } \overline{(\cdot)}(\overline{\boldsymbol{v}}(\overline{\boldsymbol{X}}(\overline{\boldsymbol{C}})), \overline{\boldsymbol{X}}(\overline{\boldsymbol{C}})) \quad \text{and} \quad \text{microscale: } (\cdot)(\boldsymbol{v}(\boldsymbol{X}(\boldsymbol{C}(\boldsymbol{a}))), \boldsymbol{X}(\boldsymbol{C}(\boldsymbol{a}))) \tag{7.1}$$

with $(\overline{\boldsymbol{v}}, \boldsymbol{v})$ being the macro- and microscopic state, $(\overline{\boldsymbol{X}}, \boldsymbol{X})$ being the macro- and the microscopic coordinates of the FE mesh and $(\overline{\boldsymbol{C}}, \boldsymbol{C})$ being the coordinates of the macro- and the microscopic CAGD parameters. The stated optimisation problem introduced in Problem 3.2 in Chapter 3 contains the minimisation of an objective, which is the macroscopic compliance $\overline{C}$. Its minimisation is performed with respect to constant volume constraints ($\overline{V}$, V) and lower and upper bounds (s_i^{l}, s_i^{u}) for the design parameters on

Table 7.1: Macroscopic tension test: model parameters.

Parameter	**Macroscale**		**Microscale**	
length	A	10.0	B	1.0
radius	r	5.0	a	0.25
			b	0.25
thickness	$\bar{t}$	0.1	t	0.1
load	q	1.0		
Young's modulus			E	10000
Poisson's ratio			ν	0.2
number degrees of freedom	$\overline{n}_v$	682	n_v	480

both scales. The solution is obtained by the application of the SQP method discussed in Chapter 3. Due to the choice of design parameters, i.e. control points of the Bézier patch and radii of the void, the sensitivity information calculated with respect to nodal coordinates of the FE mesh, i.e. $\partial(\cdot)/\partial\overline{\boldsymbol{X}}$ on the macro- and $\partial(\cdot)/\partial\boldsymbol{X}$ on the microscale, has to be transformed using design velocity fields matrices introduced in Section 3.4. The final sensitivity information for arbitrary functionals $\overline{f}$ on the macroscale and f on the microscale are obtained from

$$\overline{f}' = \left(\frac{\partial\overline{f}}{\partial\overline{\boldsymbol{v}}}\,\widetilde{\boldsymbol{S}} + \frac{\partial\overline{f}}{\partial\overline{\boldsymbol{X}}}\right)\frac{\partial\overline{\boldsymbol{X}}}{\partial\overline{\boldsymbol{C}}}\delta\overline{\boldsymbol{C}} = \left(\frac{\partial\overline{f}}{\partial\overline{\boldsymbol{v}}}\,\widetilde{\boldsymbol{S}} + \frac{\partial\overline{f}}{\partial\overline{\boldsymbol{X}}}\right)\overline{\boldsymbol{V}}\delta\overline{\boldsymbol{C}} \tag{7.2}$$

for the macroscale and from

$$f' = \left(\frac{\partial f}{\partial\boldsymbol{v}}\,\boldsymbol{S} + \frac{\partial f}{\partial\boldsymbol{X}}\right)\frac{\partial\boldsymbol{X}}{\partial\boldsymbol{C}}\frac{\partial\boldsymbol{C}}{\partial\boldsymbol{a}}\delta\boldsymbol{a} = \left(\frac{\partial f}{\partial\boldsymbol{v}}\,\boldsymbol{S} + \frac{\partial f}{\partial\boldsymbol{X}}\right)\boldsymbol{V}\delta\boldsymbol{a}, \tag{7.3}$$

for the microscale, both using the appropriate sensitivity matrix $\widetilde{\boldsymbol{S}}$ for the macro- and $\boldsymbol{S}$ for the microscale.

The optimisation results for all three tests can be observed in Fig. 7.3. The objectives are minimised in each scenario and the volume constraints are fulfilled in each case. The optimisation algorithm takes 6 iterations for test T.1, 6 iterations for test T.2 and 4 iterations for test T.3 to find a solution. The final values for the macroscopic compliance $\overline{C}_{\text{T.2}}$ (modifications on microscale only) and $\overline{C}_{\text{T.3}}$ (modifications on both scales) are approximately equal ($\overline{C}_{\text{T.3}}$ / $\overline{C}_{\text{T.2}} = 0.99 \approx 1$). Comparison with the curve for $\overline{C}_{\text{T.1}}$, which represents the optimisation with modifications only on the macroscale, shows that the overall macroscopic stiffness can be increased by $\approx 10\%$ compared to its initial shape and design ($\overline{C}_{\text{T.2}}$ / $\overline{C}_{\text{T.1}} = 0.9046$ and $\overline{C}_{\text{T.3}}$ / $\overline{C}_{\text{T.1}} = 0.9045$) by the incorporation of the underlying microscale structure into the optimisation process.

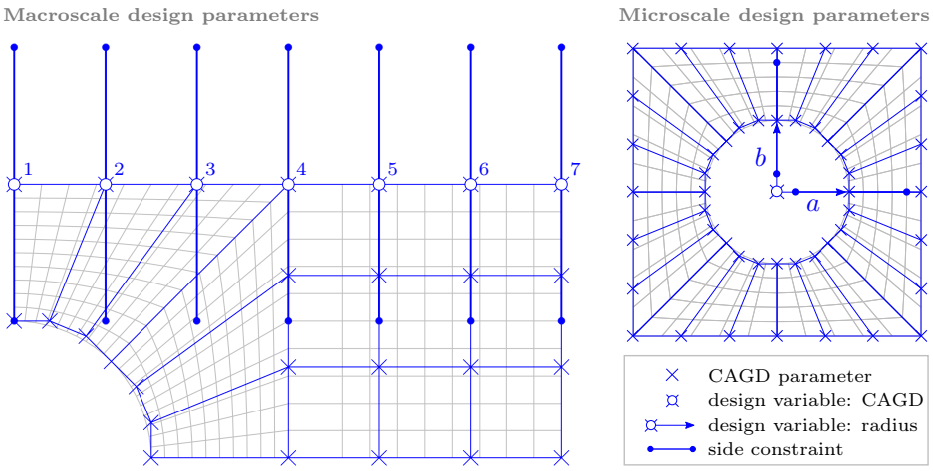

Figure 7.2: Macroscopic tension test: optimisation model and design parameters.

Due to the fact that the macrostructure is nearly optimal for the defined load case q (due to the low complexity of the presented macroscopic tension test), the final macroscopic shape for test T.1 and test T.3 differs only little from its initial design. For the same reason it can be observed in Fig. 7.3, that the macroscale does not have a significant influence on the optimisation results compared to the influence of the microscale. The comprehensible optimised shape of the microscale structure is pictured in Fig. 7.4. The distribution of design parameters on the macro- and microscale for the initial and optimised shape are plotted for the investigated systems in Fig. 7.4 for all three tests T.1, T.2 and T.3. Additionally, the exact coordinates of geometrical points on the macroscale as well as for the radii a and b, both before and after optimisation, are listed in Table 7.2. For comparison, the lower and upper bounds $(s_i^{\mathrm{l}}, s_i^{\mathrm{u}})$ for selected design parameters are listed too. All design parameters fulfill their constraints and lie in the feasible domain.

As evident from Fig. 7.3, consideration of the underlying microscale is essential for creating improved designs and mechanical structures. The results prove the eminent importance and influence of the microscale representation on macroscopic objectives, constraints and quantities of interest. Only in the two cases with design parameters on the microscale, i.e. for the test T.2 and T.3, the objectives can be reduced significantly. Whenever possible, multiscale optimisation techniques and results should be investigated within the overall design process to take advantage of its huge potential for improvements.

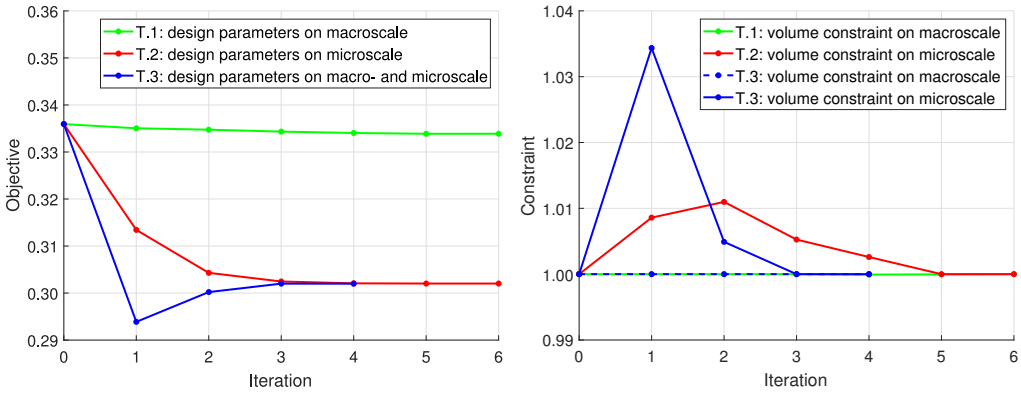

Figure 7.3: Macroscopic tension test: objectives (left) correspond to macroscopic compliance $\overline{C}$ and constraints (right) correspond to volume constraints $(\overline{V}, V)$ on both scales. Comparison of initial and optimised values of objectives for performed examples results to: **T.1**: $\overline{C}^{\,\mathrm{opt}} \,/\, \overline{C}^{\,\mathrm{ini}} = 0.3339 \,/\, 0.3359 = 0.9940$, **T.2**: $\overline{C}^{\,\mathrm{opt}} \,/\, \overline{C}^{\,\mathrm{ini}} = 0.3020 \,/\, 0.3359 = 0.8991$, **T.3**: $\overline{C}^{\,\mathrm{opt}} \,/\, \overline{C}^{\,\mathrm{ini}} = 0.3020 \,/\, 0.3359 = 0.8991$. The volume of the referred domain remains constant, i.e. $\overline{V}^{\,\mathrm{ini}} \,/\, \overline{V}^{\,\mathrm{opt}} = V^{\,\mathrm{ini}} \,/\, V^{\,\mathrm{opt}} = 1$ depending on incorporated scale.

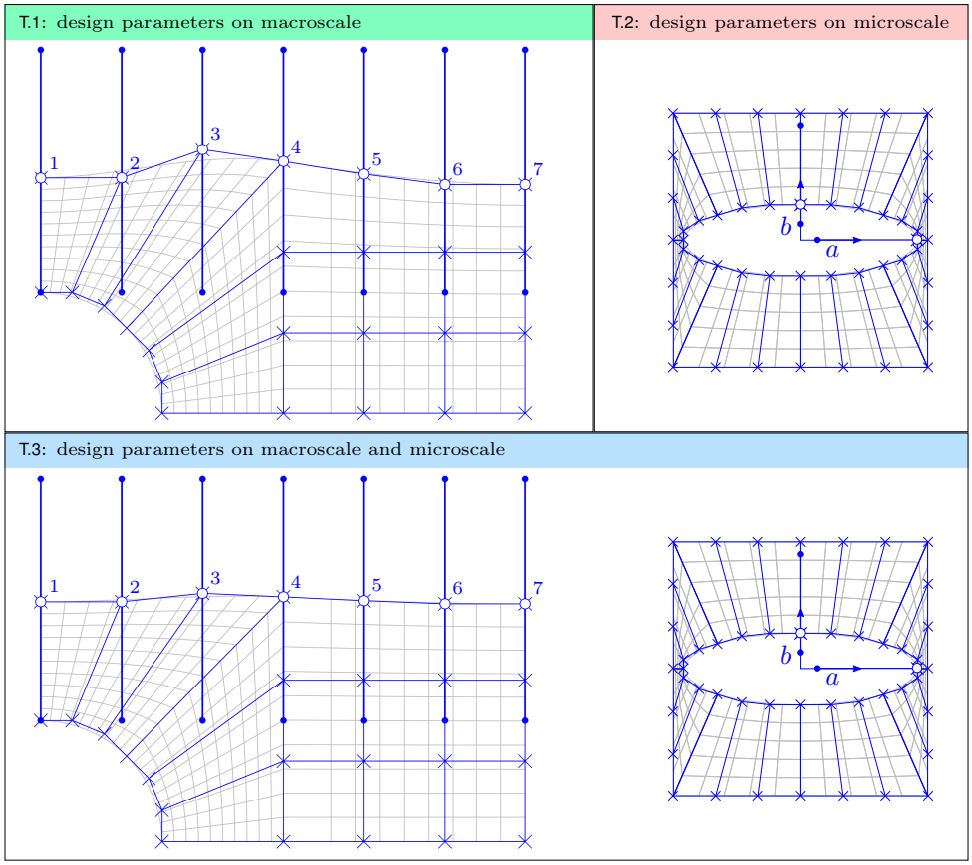

Figure 7.4: Macroscopic tension test: distribution of design parameters on macro- and microscale for initial and optimised shape. **T.1**: design parameters on macroscale, **T.2**: design parameters on microscale, **T.3**: design parameters on macroscale and microscale. Design parameters (1-7) correspond to coordinates of macroscopic CAGD control points in vertical (y-) direction, design parameters (a, b) correspond to the radii of the void on the microscale.

Table 7.2: Macroscopic tension test: distribution of design parameters on macro- and microscale for initial and optimised shape. **T.1**: design parameters on macroscale, **T.2**: design parameters on microscale, **T.3**: design parameters on macro- and microscale. Design parameters (1-7) correspond to coordinates of macroscopic CAGD control points in vertical (y-) direction, design parameters (a, b) correspond to the radii of the void on the microscale. Parameters (s_i^{l}, s_i^{u}) define lower and upper bounds for design.

Design parameter	**Initial value**	**T.1**	**T.2**	**T.3**	s_i^{l}	s_i^{u}
1	10.0000	10.4118		10.1235	5.0	15.0
2	10.0000	10.9034		10.2710	5.0	15.0
3	10.0000	9.7388		9.9216	5.0	15.0
4	10.0000	9.7274		9.9182	5.0	15.0
5	10.0000	9.8900		9.9670	5.0	15.0
6	10.0000	9.4533		9.8360	5.0	15.0
7	10.0000	9.4537		9.8361	5.0	15.0
a	0.25		0.45	0.45	0.05	0.45
b	0.25		0.15	0.15	0.05	0.45

7.2 Multiscale application for the design of microstructures using morphing based design parametrisation

The aim of the following investigations is the demonstration of the versatility of morphing based parametrisation methods within the overall optimisation process in combination with analytically derived sensitivity relations for multiscale problems. A huge advantage of morphing techniques is the handling of arbitrary finite element meshes and mesh topologies. The finite element mesh can be generated in standalone programs and has to be included into the optimisation environment by importing the nodes with corresponding coordinates and the element connectivity list. The defined morphing box and the underlying algorithm establishes the connectivity between the finite element mesh and the geometry parametrisation and can be used for optimisation purposes. Details are given in Section 3.4. This chapter tackles a multiscale optimisation problem with a fixed macroscopic domain $\overline{\mathcal{K}}$, which is evaluated for two different load cases, i.e. L.1 and L.2. The microscale domain $\mathcal{K}$ is represented by four different domains, i.e. m.1, m.2, m.3 and m.4, which are investigated in four distinct optimisation runs. The design parametrisation of all microscale structures is realised by the morphing technique. An overview on the described situation is given in Fig. 7.6.

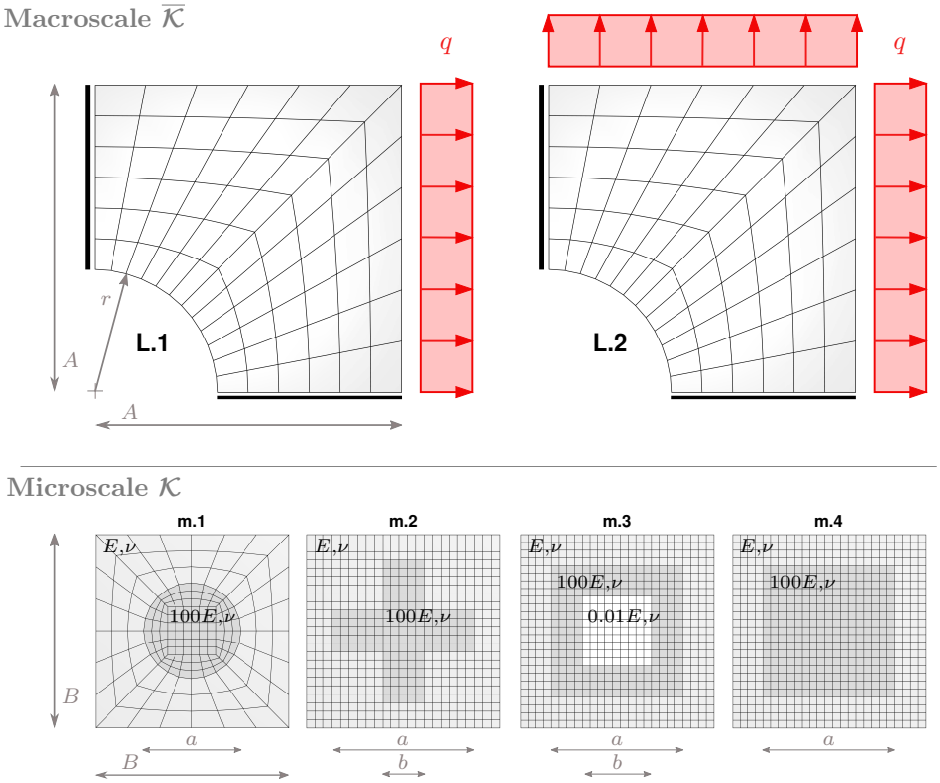

Figure 7.5: Microscale design: macroscopic mechanical system with two load cases **L.1**, **L.2** and four different microscale representations **m.1**, **m.2**, **m.3** and **m.4** for initial design.

The macroscopic system is fixed on the left-hand and bottom side. Depending on the load case, it is loaded on the right-hand side for L.1 and on the right-hand and top side for load case L.2. The microscopic representations are individually connected with each macroscopic integration point and allow the computation of effective stress and material parameters in terms of computational homogenisation. Each domain consists of a soft matrix material with a Young's modulus E and a stiffer kernel material. Additionally, the microscale m.3 contains a third material domain, which is even softer than the matrix material. Characteristic system parameters for both scales, like dimensions and material parameters are listed in Table 7.3 and complete the descriptive data from Fig. 7.6. The solution of the non-linear problem on each microscale is carried out by the iterative Newton scheme introduced in Algorithm 4.1 with the evaluation of the Neo-Hookean constitutive law. The sequence of microscopic solution steps is nested into the solution procedure for non-linear equations on the macroscale outlined in Algorithm 6.2.

Table 7.3: Microscale design: model parameters.

Parameter	**Macroscale**		**Microscale**	**m.1**	**m.2**	**m.3**	**m.4**
length	A	10.0	B	1.0	1.0	1.0	1.0
			a	0.5	0.74	0.68	0.68
			b		0.22	0.36	
radius	r	4.0					
thickness	$\bar{t}$	0.1	t	0.1	0.1	0.25	0.10
load	q	0.6					
Young's modulus			E	10000	10000	10000	10000
Poisson's ratio			ν	0.2	0.2	0.2	0.2
num. degrees of freedom	$\overline{n}_v$	182	n_v	386	1152	1352	1352

The optimisation model with all available design parameters on the microscale is set up according to Fig. 7.6. Here, the grey background serves as a dummy domain, which can be exchanged by any of the introduced microscale representations m.1, m.2, m.3 and m.4. The coordinates of the inner control points of the morphing box (indicated by numbers 1-8 in Fig. 7.6) are chosen as design variables. They can move nearly to the defined boundary of the domain. The control point in the center of the domain is neglected as design variable due to symmetry of the system. Basically, this choice for design parameters is tackled in a similar way as control points of a Bézier patch, i.e. following dependencies hold true

$$\text{microscale: } (\cdot)(\boldsymbol{v}(\boldsymbol{X}(\boldsymbol{C})), \boldsymbol{X}(\boldsymbol{C})), \tag{7.4}$$

with $\boldsymbol{v}$ being the microscopic state, $\boldsymbol{X}$ being the microscopic coordinates of the FE mesh and $\boldsymbol{C}$ being the coordinates of the microscopic CAGD parameters. Therefore, the following

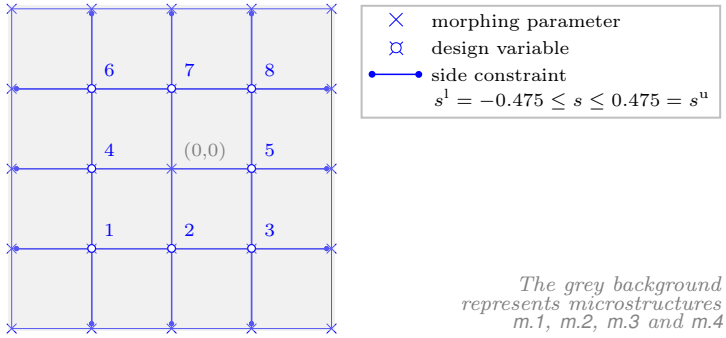

Figure 7.6: Microscale design: optimisation model and design parameters. Design parameters correspond to the coordinates of the control points of the defined morphing box.

transformation of sensitivity information for an arbitrary functional f is necessary

$$f' = \left(\frac{\partial f}{\partial \boldsymbol{v}} \boldsymbol{S} + \frac{\partial f}{\partial \boldsymbol{X}} \right) \frac{\partial \boldsymbol{X}}{\partial \boldsymbol{C}} \delta \boldsymbol{C} = \left(\frac{\partial f}{\partial \boldsymbol{v}} \boldsymbol{S} + \frac{\partial f}{\partial \boldsymbol{X}} \right) \boldsymbol{V} \delta \boldsymbol{C} \tag{7.5}$$

using the appropriate sensitivity matrix $\boldsymbol{S}$ on the microscale. Eq. (7.5) provides the transformation of sensitivity information calculated with respect to nodal coordinates of the finite element mesh, i.e. of $\partial(\cdot)/\partial \boldsymbol{X}$, into the design space of interest.

The stated optimisation problem introduced in Problem 3.2 in Chapter 3 contains the minimisation of an objective, which is here the macroscopic compliance $\overline{C}$. Its minimisation is performed with respect to constant volume constraints V and lower and upper bounds $(s_i^{\mathrm{l}},\ s_i^{\mathrm{u}})$ for the design parameters on the microscale. The solution is obtained by the application of the SQP method discussed in Chapter 3. As discussed in Remark 3.1, it is necessary to define weight factors for each microscopic constituent within the accumulation of volume constraints to provide a well posed optimisation problem. Otherwise, difficulties during the evaluation of the constraints and of their derivatives arise. The weights for the matrix material of all microscale domains are set to $w_1 = 1.0$, for the stiffer kernel material to $w_2 = 2.0$ and for the soft inclusion in m.3 to $w_3 = 0.5$.

In the following two sections, multiscale optimisation for previously described problems is performed for introduced load case scenarios L.1 and L.2. The results are evaluated, compared and possible improvements in terms of performance of the obtained designs are outlined. Choosing the macroscopic compliance as objective attributes the optimisation problem having a deformation driven characteristic. Therefore in some cases, the maximum resulting displacements of the optimised mechanical macroscale structure are expected to be less compared to the initial design and confirm the minimisation of the macroscopic compliance $\overline{C}$. This statement is not necessarily true for the resulting distribution of local von Mises stresses and will be accentuated by the evaluation of microscale problems in individual integration points.

7.2.1 Evaluation of load case L.1: uniaxial tension

The optimisation results for all investigated microscale representations and the load case L.1 are pictured in Fig. 7.7. The objectives (macroscopic compliance) are minimised in each scenario and the microscopic volume constraint is fulfilled. The volume of each microscale remains constant in each optimisation run. The optimisation algorithm takes 18 iterations for m.1, 21 iterations for m.2, 28 iterations for m.3 and 18 iterations for m.4 to find a solution. The final values for the macroscopic compliance can be reduced in a range between $\approx 10-30\%$. In the opposite sense, this means, that the macroscopic stiffness can be increased by $\approx 10-30\%$ depending on the underlying microscale representation.

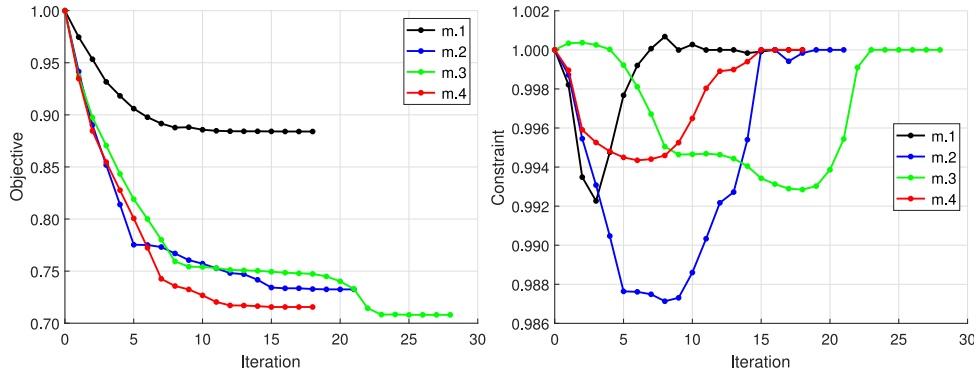

Figure 7.7: Microscale design: (**L.1**) objectives (left) correspond to macroscopic compliance $\overline{C}$ and constraints (right) correspond to volume constraints V on the microscale. Comparison of initial and optimised values of objectives for performed examples results to: **m.1**: $\overline{C}^{\,\mathrm{opt}}/\,\overline{C}^{\,\mathrm{ini}} = 5.5480\ /\ 6.2761 = 0.8840$, **m.2**: $\overline{C}^{\,\mathrm{opt}}/\,\overline{C}^{\,\mathrm{ini}} = 2.5240\ /\ 3.4459 = 0.7325$, **m.3**: $\overline{C}^{\,\mathrm{opt}}/\,\overline{C}^{\,\mathrm{ini}} = 1.8626\ /\ 2.6307 = 0.7080$, **m.4**: $\overline{C}^{\,\mathrm{opt}}/\,\overline{C}^{\,\mathrm{ini}} = 2.1316\ /\ 2.9789 = 0.7156$. The volume of the referred domain remains constant, i.e. $V^{\,\mathrm{ini}}/V^{\,\mathrm{opt}} = 1$.

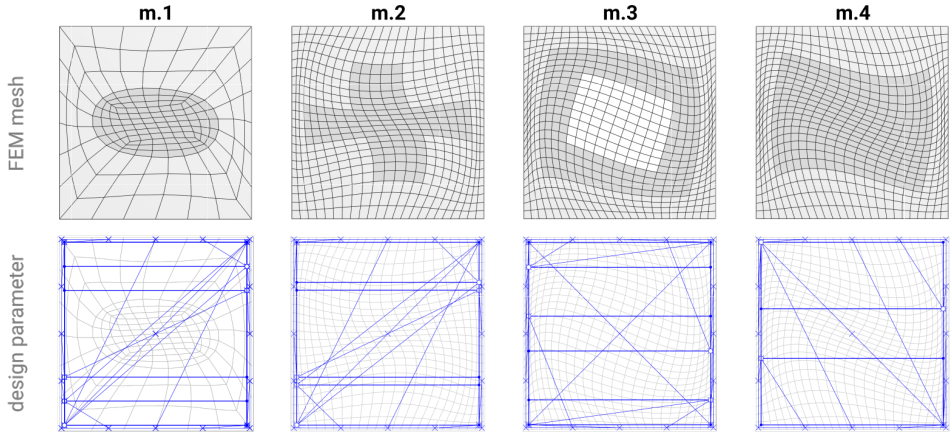

Figure 7.8: Microscale design: FEM mesh (top) and distribution of design parameters (bottom) after optimisation for load case **L.1** for microscale representations **m.1**, **m.2**, **m.3** and **m.4**. Design parameters are the coordinates of control points of defined morphing box.

The distribution of design parameters and the corresponding finite element meshes for all microscale domains m.1, m.2, m.3 and m.4 after optimisation can be found in Fig. 7.8. It is difficult to obtain the exact positions of design parameters from the graphical illustration and therefore, the distribution of design parameters with all coordinates is listed in Table 7.4. For comparison, the initial values for selected design parameters are listed as well. All design parameters fulfill their constraints and lie in the feasible domain.

Table 7.4: Microscale design: distribution of design parameters after optimisation for load case **L.1** for microscale representations **m.1**, **m.2**, **m.3** and **m.4**. Design parameters are the coordinates in x and y direction of control points of defined morphing box.

	Initial coordinates		**m.1**		**m.2**		**m.3**		**m.4**	
#	x	y	x	y	x	y	x	y	x	y
1	-0.245	-0.245	-0.475	-0.349	-0.475	-0.266	-0.475	0.090	-0.475	-0.129
2	0.000	-0.245	0.475	0.475	0.475	0.475	-0.475	-0.475	-0.475	0.475
3	0.245	-0.245	0.475	-0.475	0.475	-0.475	0.475	-0.345	0.475	-0.475
4	-0.245	0.000	-0.475	-0.225	-0.475	-0.226	-0.475	0.475	-0.475	0.475
5	0.245	0.000	0.475	0.225	0.475	0.226	0.475	-0.475	0.475	-0.475
6	-0.245	0.245	-0.475	0.475	-0.475	0.475	-0.475	0.345	-0.475	0.475
7	0.000	0.245	-0.475	-0.475	-0.475	-0.475	0.475	0.475	0.475	-0.475
8	0.245	0.245	0.475	0.349	0.475	0.266	0.475	-0.090	0.475	0.129

The plots in Fig. 7.9 to 7.12 outline the results for each optimisation run for load case L.1 and all introduced microscale representations m.1, m.2, m.3 and m.4. The compilations include macroscopic displacements and the distribution of local von Mises stresses on the microscale, both for the initial and optimised design. The pictured microscale results are obtained in three selected macroscopic integration points indicated by the numbers (1-3) in all plots. The maximum values for macroscopic displacements and microscopic von Mises stresses for each investigation are compiled and compared in Table 7.5. In each scenario, the resulting displacements of the macrostructure are reduced for the optimised design. This results fulfill the expectations and prove the maximisation of the overall macroscopic stiffness. When it comes to the local distribution of von Mises stresses, it is up to the designing engineer to estimate the situation and to decide whether the workload can be handled by the present material distribution or material choice or not. Nevertheless, the optimisation task is accomplished satisfactorily.

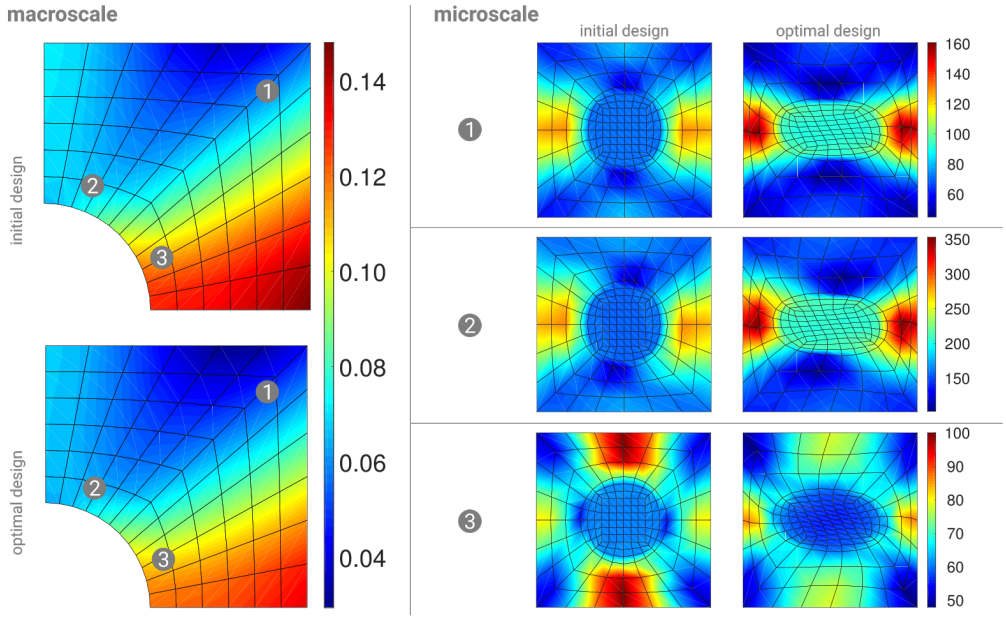

Figure 7.9: Microscale design: (**L.1-m.1**) macroscopic displacements (left) for initial and optimised designs, and microscopic von Mises stress distribution in selected macroscopic integration points (1-3) for initial (middle) and optimised (right) design.

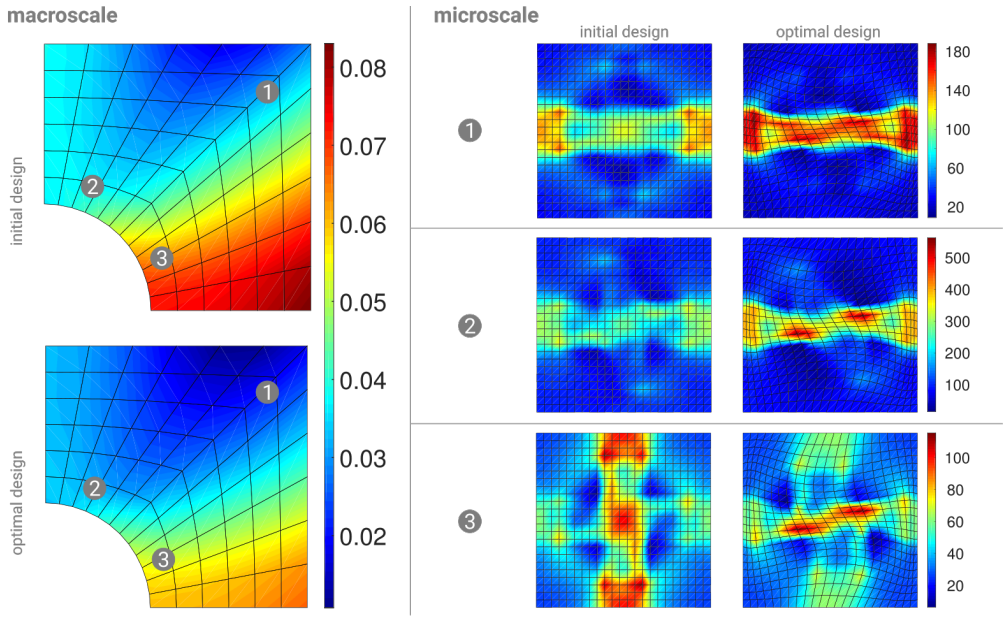

Figure 7.10: Microscale design: (**L.1-m.2**) macroscopic displacements (left) for initial and optimised designs, and microscopic von Mises stress distribution in selected macroscopic integration points (1-3) for initial (middle) and optimised (right) design.

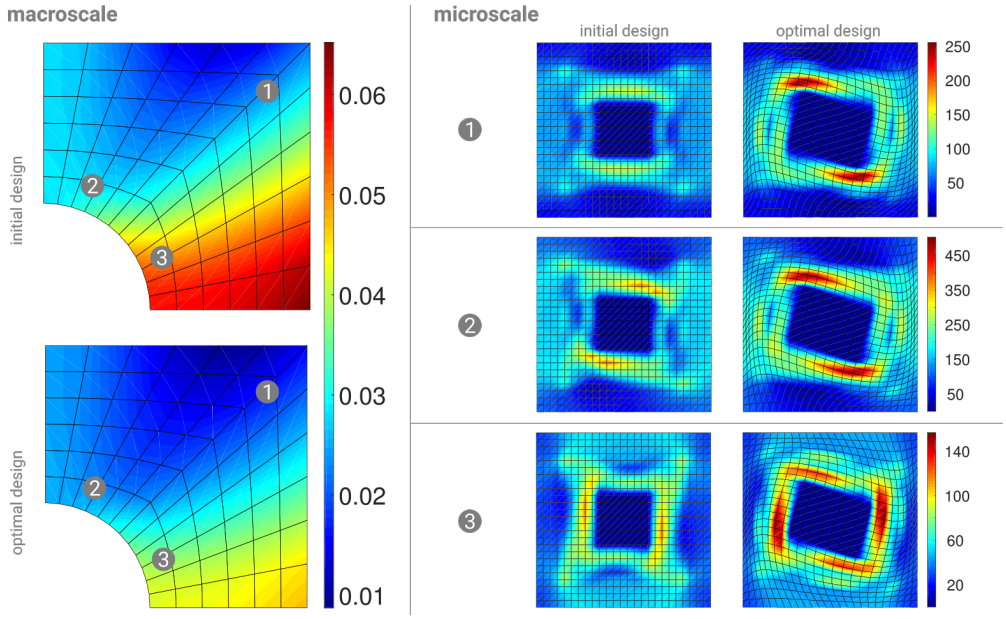

Figure 7.11: Microscale design: (**L.1-m.3**) macroscopic displacements (left) for initial and optimised designs, and microscopic von Mises stress distribution in selected macroscopic integration points (1-3) for initial (middle) and optimised (right) design.

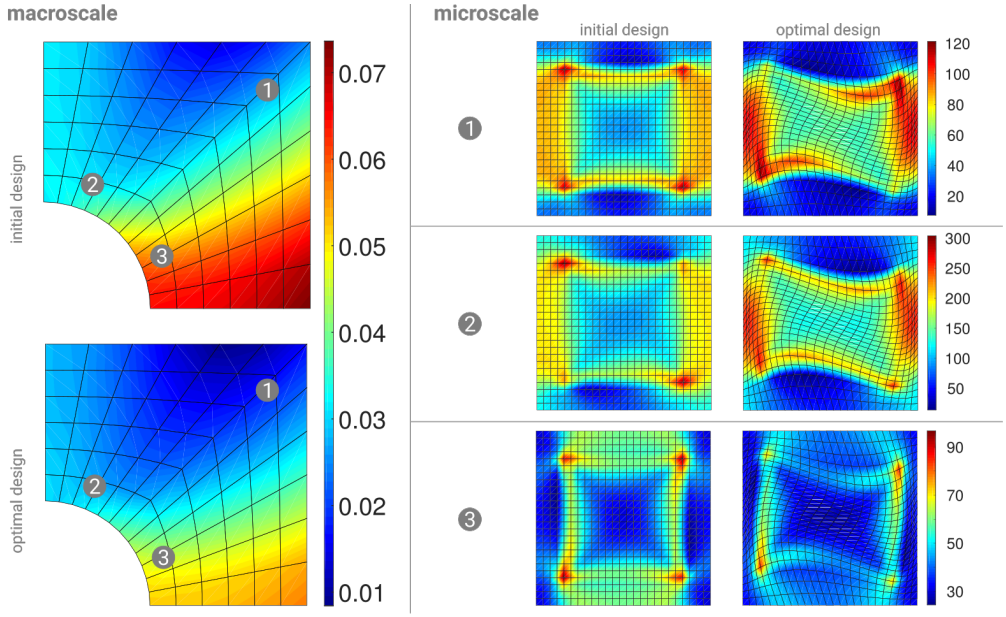

Figure 7.12: Microscale design: (**L.1-m.4**) macroscopic displacements (left) for initial and optimised designs, and microscopic von Mises stress distribution in selected macroscopic integration points (1-3) for initial (middle) and optimised (right) design.

Table 7.5: Comparison of results for load case **L.1**. Maximum value for macroscopic displacements $v_{\max}$ for initial and optimised designs, maximum value for microscopic von Mises stress $\sigma_{\text{eq}}^{\text{IP}}$ in selected macroscopic integration points (1-3) for initial and optimised design.

		$(\cdot)^{\text{ini}}$	$(\cdot)^{\text{opt}}$	$(\cdot)^{\text{opt}}/(\cdot)^{\text{ini}}$
macroscale	$v_{\max}$	0.1480	0.1345	0.9088
m.1	σ_{eq}^{1}	129.41	160.71	1.2419
	σ_{eq}^{2}	287.21	353.03	1.2292
	σ_{eq}^{3}	100.01	86.51	0.8650
macroscale	$v_{\max}$	0.0830	0.0667	0.8036
m.2	σ_{eq}^{1}	153.08	188.23	1.2296
	σ_{eq}^{2}	350.99	562.92	1.6038
	σ_{eq}^{3}	113.32	115.40	1.0184
macroscale	$v_{\max}$	0.0652	0.0473	0.7255
m.3	σ_{eq}^{1}	149.50	255.66	1.7101
	σ_{eq}^{2}	385.35	502.92	1.3129
	σ_{eq}^{3}	115.50	156.84	1.3579
macroscale	$v_{\max}$	0.0736	0.0572	0.7772
m.4	σ_{eq}^{1}	121.35	121.29	0.9995
	σ_{eq}^{2}	303.86	267.11	0.8791
	σ_{eq}^{3}	96.72	85.46	0.8836

7.2.2 Evaluation of load case L.2: biaxial tension

The optimisation results for all investigated microscale representations and the load case L.2 are pictured in Fig. 7.13. The objectives (macroscopic compliance) are minimised in each scenario and the microscopic volume constraint is fulfilled. The volume of each microscale remains constant in each optimisation run. The optimisation algorithm takes 9 iterations for m.1, 13 iterations for m.2, 10 iterations for m.3 and 14 iterations for m.4 to find a solution. The final values for the macroscopic compliance can be reduced in a range between $\approx 5-10\%$. In the opposite sense, this means, that the macroscopic stiffness can be increased by $\approx 5-10\%$ depending on the underlying microscale representation.

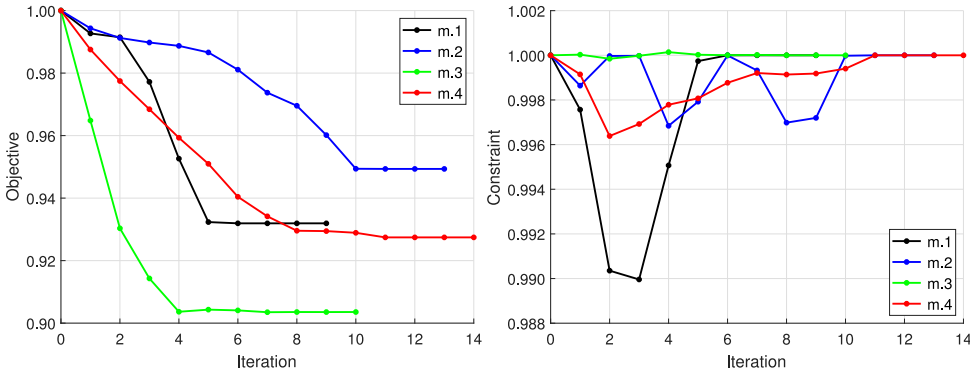

Figure 7.13: Microscale design: (**L.2**) objectives (left) correspond to macroscopic compliance $\overline{C}$ and constraints (right) correspond to volume constraints V on the microscale. Comparison of initial and optimised values of objectives for performed examples results to: **m.1**: $\overline{C}^{\,\mathrm{opt}}/\,\overline{C}^{\,\mathrm{ini}} = 7.7616\ /\ 8.3286 = 0.9319$, **m.2**: $\overline{C}^{\,\mathrm{opt}}/\,\overline{C}^{\,\mathrm{ini}} = 4.5767\ /\ 4.8209 = 0.9493$, **m.3**: $\overline{C}^{\,\mathrm{opt}}/\,\overline{C}^{\,\mathrm{ini}} = 3.4573\ /\ 3.8263 = 0.9036$, **m.4**: $\overline{C}^{\,\mathrm{opt}}/\,\overline{C}^{\,\mathrm{ini}} = 4.0320\ /\ 4.3475 = 0.9274$. The volume of the referred domain remains constant, i.e. $V^{\,\mathrm{ini}}/V^{\,\mathrm{opt}} = 1$.

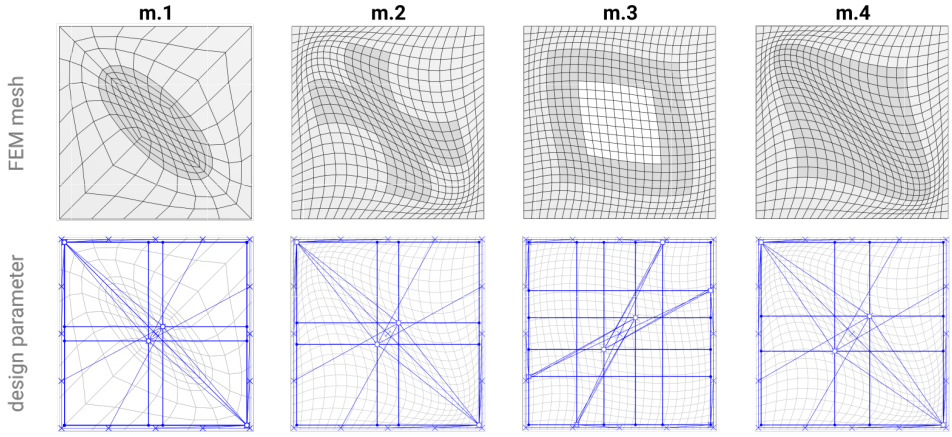

Figure 7.14: Microscale design: FEM mesh (top) and distribution of design parameters (bottom) after optimisation for load case **L.2** for microscale representations **m.1**, **m.2**, **m.3** and **m.4**. Design parameters are the coordinates of control points of defined morphing box.

The distribution of design parameters and the corresponding finite element meshes for all microscale domains m.1, m.2, m.3 and m.4 after optimisation can be found in Fig. 7.14. It is difficult to obtain the exact positions of design parameters from the graphical illustration and therefore, the distribution of design parameters with all coordinates is listed in Table 7.6. For comparison, the initial values for selected design parameters are listed too. All design parameters fulfill their constraints and lie in the feasible domain.

Table 7.6: Microscale design: distribution of design parameters after optimisation for load case **L.2** for microscale representations **m.1**, **m.2**, **m.3** and **m.4**. Design parameters are the coordinates in x and y direction of control points of defined morphing box.

	Initial coordinates		**m.1**		**m.2**		**m.3**		**m.4**	
#	x	y	x	y	x	y	x	y	x	y
1	-0.245	-0.245	0.037	0.037	0.056	0.056	0.082	0.082	0.091	0.091
2	0.000	-0.245	0.475	-0.475	0.475	-0.475	-0.224	-0.475	0.475	-0.475
3	0.245	-0.245	0.475	-0.475	0.475	-0.475	0.475	-0.475	0.475	-0.475
4	-0.245	0.000	-0.475	0.475	-0.475	0.475	-0.475	-0.224	-0.475	0.475
5	0.245	0.000	0.475	-0.475	0.475	-0.475	0.475	0.224	0.475	-0.475
6	-0.245	0.245	-0.475	0.475	-0.475	0.475	-0.475	0.475	-0.475	0.475
7	0.000	0.245	-0.475	0.475	-0.475	0.475	0.224	0.475	-0.475	0.475
8	0.245	0.245	-0.037	-0.037	-0.056	-0.056	-0.082	-0.082	-0.091	-0.091

The plots in Fig. 7.15 to 7.18 outline results for each optimisation run for load case L.2 and all introduced microscale representations m.1, m.2, m.3 and m.4. The compilations include macroscopic displacements and the distribution of local von Mises stresses on the microscale both for the initial and optimised design. The pictured microscale results are obtained in three selected macroscopic integration points indicated by the numbers (1-3) in all plots. The maximum values for macroscopic displacements and microscopic von Mises stresses for each investigation are compiled and compared in Table 7.7. The optimisation task is accomplished satisfactorily.

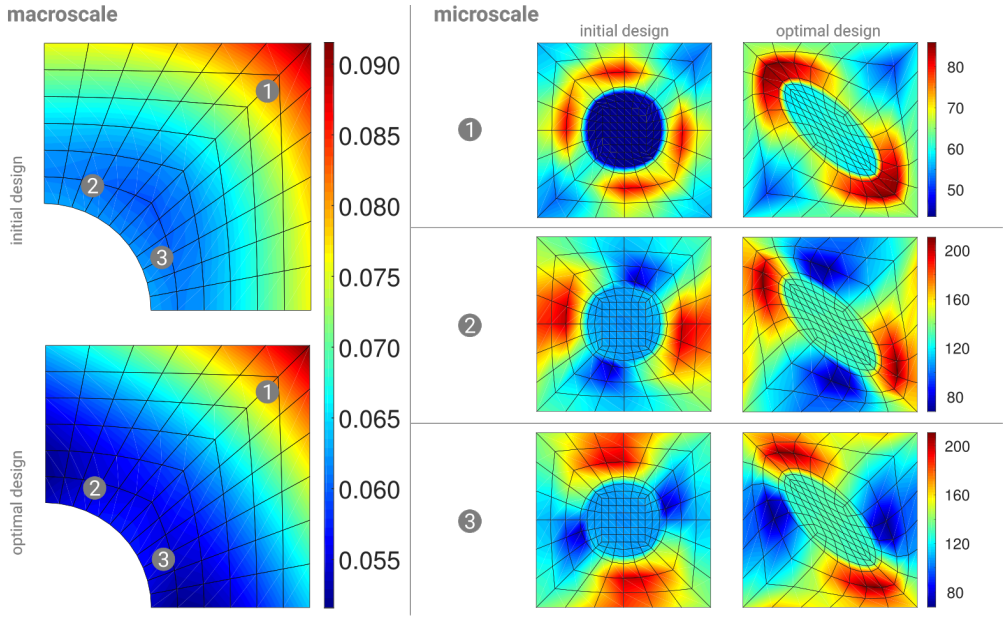

Figure 7.15: Microscale design: (**L.2-m.1**) macroscopic displacements (left) for initial and optimised designs, and microscopic von Mises stress distribution in selected macroscopic integration points (1-3) for initial (middle) and optimised (right) design.

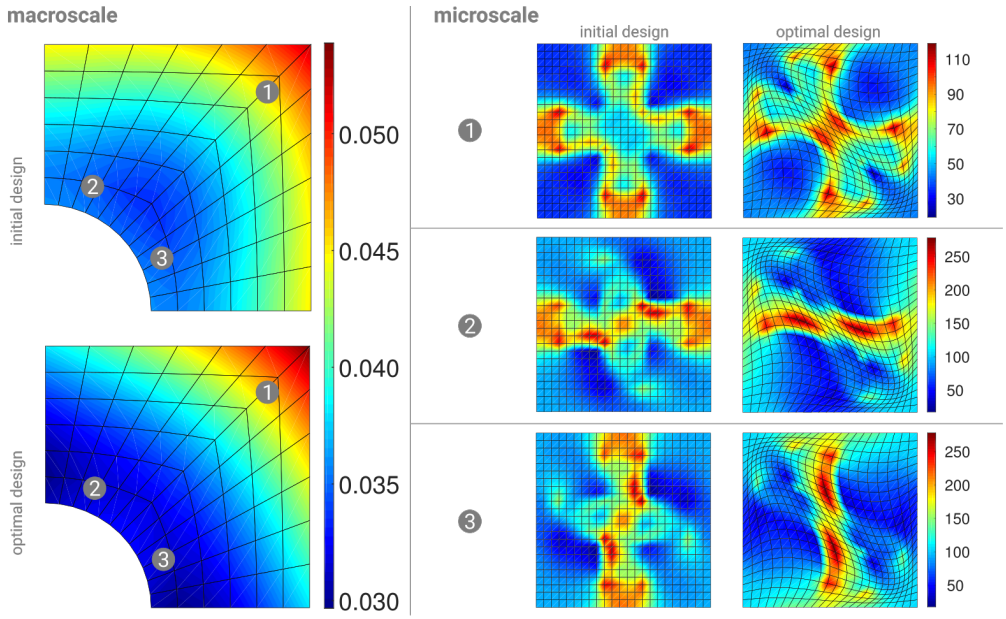

Figure 7.16: Microscale design: (**L.2-m.2**) macroscopic displacements (left) for initial and optimised designs, and microscopic von Mises stress distribution in selected macroscopic integration points (1-3) for initial (middle) and optimised (right) design.

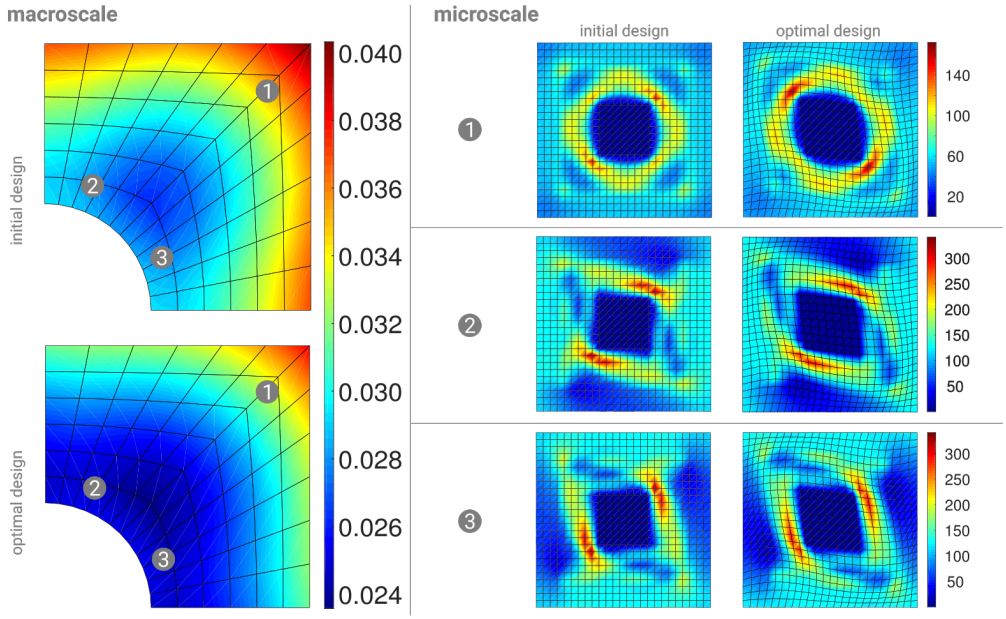

Figure 7.17: Microscale design: (**L.2-m.3**) macroscopic displacements (left) for initial and optimised designs, and microscopic von Mises stress distribution in selected macroscopic integration points (1-3) for initial (middle) and optimised (right) design.

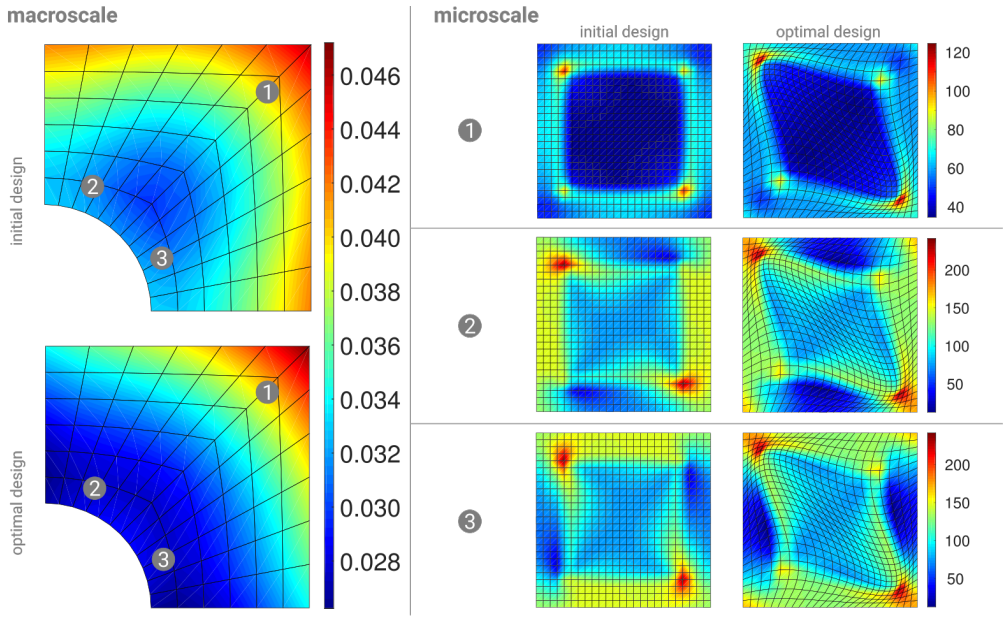

Figure 7.18: Microscale design: (**L.2-m.4**) macroscopic displacements (left) for initial and optimised designs, and microscopic von Mises stress distribution in selected macroscopic integration points (1-3) for initial (middle) and optimised (right) design.

Table 7.7: Comparison of results for load case **L.2**. Maximum value for macroscopic displacements $v_{\max}$ for initial and optimised designs, maximum value for microscopic von Mises stress $\sigma_{\mathsf{eq}}^{\mathsf{IP}}$ in selected macroscopic integration points (1-3) for initial and optimised design.

		$(\cdot)^{\text{ini}}$	$(\cdot)^{\text{opt}}$	$(\cdot)^{\text{opt}}/(\cdot)^{\text{ini}}$
macroscale	$v_{\max}$	0.0912	0.0915	1.0033
m.1	σ_{eq}^{1}	81.76	85.96	1.0514
	σ_{eq}^{2}	200.85	210.92	1.0501
	σ_{eq}^{3}	200.85	210.92	1.0501
macroscale	$v_{\max}$	0.0521	0.0539	1.0345
m.2	σ_{eq}^{1}	114.54	119.22	1.0409
	σ_{eq}^{2}	270.30	277.99	1.0284
	σ_{eq}^{3}	270.30	277.99	1.0284
macroscale	$v_{\max}$	0.0403	0.0383	0.9504
m.3	σ_{eq}^{1}	154.34	172.43	1.1172
	σ_{eq}^{2}	341.39	297.67	0.8719
	σ_{eq}^{3}	341.39	297.67	0.8719
macroscale	$v_{\max}$	0.0460	0.0472	1.0261
m.4	σ_{eq}^{1}	111.58	124.70	1.1176
	σ_{eq}^{2}	239.94	241.72	1.0074
	σ_{eq}^{3}	239.94	241.72	1.0074

7.3 Multiscale optimisation of a bracket

This example demonstrates the applicability of the morphing based design parametrisation on both scales, i.e. on the macroscale $\overline{\mathcal{K}}$ and the microscale $\mathcal{K}$. For the finite element analysis a half of a bracket on the macroscale with main dimensions A and B and a microscale with the main dimension a consisting of a stiff matrix and a softer kernel material is modeled, cf. Fig. 7.19. The illustrated microscale representation is connected with each macroscopic integration point and allows the computation of effective stress and material parameters in terms of computational homogenisation. Characteristic system parameters for both scales, like dimensions and material properties, are compiled in Table 7.8. The solution of the non-linear problem on each microscale is carried out by the iterative Newton scheme introduced in Algorithm 4.1 with the evaluation of the Neo-Hookean constitutive law. The sequence of microscopic solution steps is nested into the solution procedure for non-linear equations on the macroscale outlined in Algorithm 6.2. The optimisation setup with all design parameters on the macro- and the microscale also can be found in Fig. 7.19. On both scales selected coordinates of control points of defined morphing boxes are chosen as design parameters.

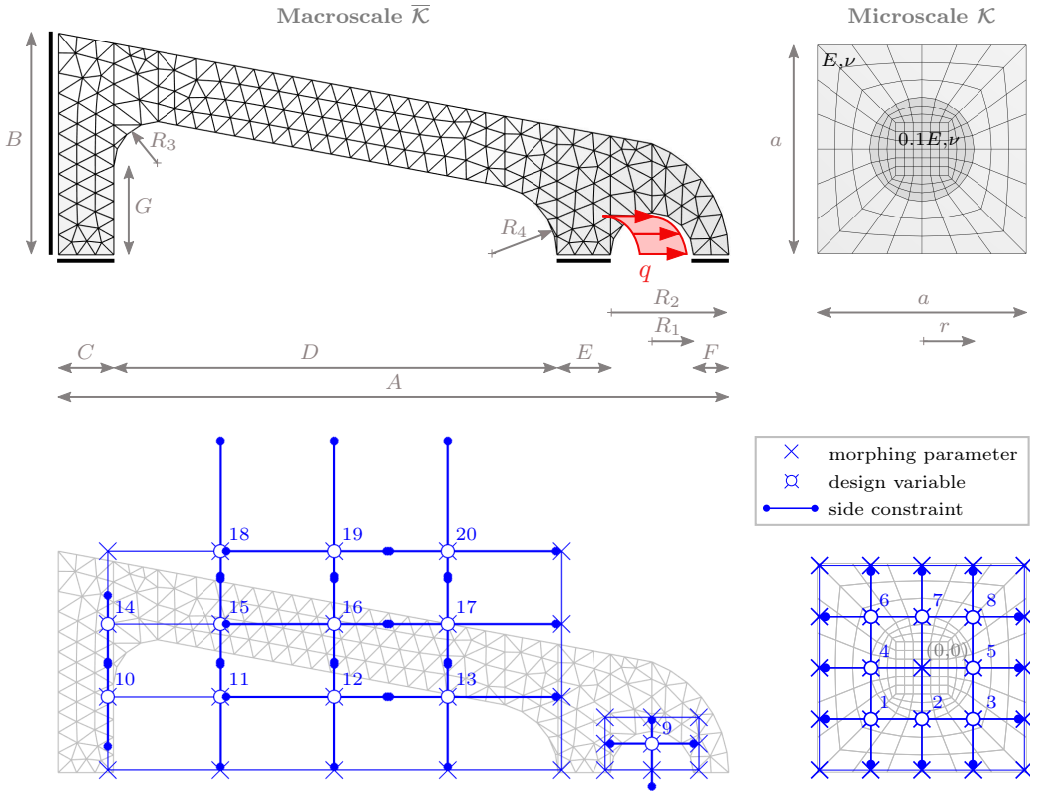

Figure 7.19: Multiscale optimisation of a bracket: mechanical system and FE mesh for the macro- and microscopic initial design (top line). Optimisation model for macroscale with two morphing boxes and for microscale with one morphing box (bottom line).

Table 7.8: Multiscale optimisation of a bracket: model parameters.

Parameter	**Macroscale**		**Microscale**	
length	A	10.0	a	1.0
	B	4.0		
	C	1.0		
	D	8.0		
	E	1.0		
	F	0.64		
	G	1.6		
radius	R_1	0.75	r	0.25
	R_2	2.14		
	R_3	0.8		
	R_4	2.0		
thickness	$\bar{t}$	0.1	t	0.1
load	q	5.1		
Young's modulus			E	10000
Poisson's ratio			ν	0.2
number degrees of freedom	$\overline{n}_v$	464	n_v	386

On the microscale one morphing box with 25 control points is defined. The coordinates of the inner control points of the morphing box (indicated by numbers 1-8 in Fig. 7.19) are chosen as design variables. They can move nearly to the defined boundary of the domain. The control point in the center of the domain is neglected as design due to symmetry properties of the system. On the macroscale two morphing boxes are defined. The first one is around the loading area and consists of 9 control points. Here, coordinates of only one control point are chosen as design variable (indicated by number 9 in Fig. 7.19). The second morphing box is defined over the main and regular part of the system. It contains 20 control points. For this morphing box, coordinates of 11 control points (indicated by the numbers 10-20 in Fig. 7.19) are chosen as design parameters within the optimisation procedure. Due to the characteristics of morphing based design parametrisation, the following dependencies hold true

$$\text{macroscale: } \overline{(\cdot)}(\overline{\boldsymbol{v}}(\overline{\boldsymbol{X}}(\overline{\boldsymbol{C}})), \overline{\boldsymbol{X}}(\overline{\boldsymbol{C}})) \quad \text{and} \quad \text{microscale: } (\cdot)(\boldsymbol{v}(\boldsymbol{X}(\boldsymbol{C})), \boldsymbol{X}(\boldsymbol{C})) \tag{7.6}$$

with $(\overline{\boldsymbol{v}}, \boldsymbol{v})$ being the macro- and microscopic state, $(\overline{\boldsymbol{X}}, \boldsymbol{X})$ being the macro- and the microscopic coordinates of the FE mesh and $(\overline{\boldsymbol{C}}, \boldsymbol{C})$ being the coordinates of the macro- and the microscopic CAGD parameters. Therefore, the following transformations of sensitivity information for arbitrary functionals $\overline{f}$ on the macroscale and f on the microscale are

necessary

$$\overline{f}' = \left(\frac{\partial \overline{f}}{\partial \overline{\boldsymbol{v}}} \, \widetilde{\boldsymbol{S}} + \frac{\partial \overline{f}}{\partial \overline{\boldsymbol{X}}} \right) \frac{\partial \overline{\boldsymbol{X}}}{\partial \overline{\boldsymbol{C}}} \delta \overline{\boldsymbol{C}} = \left(\frac{\partial \overline{f}}{\partial \overline{\boldsymbol{v}}} \, \widetilde{\boldsymbol{S}} + \frac{\partial \overline{f}}{\partial \overline{\boldsymbol{X}}} \right) \overline{\boldsymbol{V}} \delta \overline{\boldsymbol{C}} \tag{7.7}$$

for the macroscale and for the microscale

$$f' = \left(\frac{\partial f}{\partial \boldsymbol{v}} \, \boldsymbol{S} + \frac{\partial f}{\partial \boldsymbol{X}} \right) \frac{\partial \boldsymbol{X}}{\partial \boldsymbol{C}} \delta \boldsymbol{C} = \left(\frac{\partial f}{\partial \boldsymbol{v}} \, \boldsymbol{S} + \frac{\partial f}{\partial \boldsymbol{X}} \right) \boldsymbol{V} \delta \boldsymbol{C}. \tag{7.8}$$

In both cases the appropriate sensitivity matrix $\widetilde{\boldsymbol{S}}$ for the macro- and $\boldsymbol{S}$ for the microscale is required. Eq. (7.8) provides the transformation of sensitivity information calculated with respect to nodal coordinates of the finite element mesh, i.e. of $\partial(\cdot)/\partial \overline{\boldsymbol{X}}$ on the macro- or $\partial(\cdot)/\partial \boldsymbol{X}$ on the microscale, into the design space of interest. The stated optimisation problem introduced in Problem 3.2 in Chapter 3 contains the minimisation of an objective, which is here the macroscopic compliance $\overline{C}$. Its minimisation is performed with respect to constant volume constraints $(\overline{V}, V)$ and lower and upper bounds $(s_i^{\mathrm{l}}, s_i^{\mathrm{u}})$ for the design parameters on the macro- and the microscale. The solution is obtained by the application of the SQP method discussed in Chapter 3. As discussed in Remark 3.1, it is necessary to define weight factors for each microscopic constituent within the accumulation of volume constraints to provide a well posed optimisation problem. Otherwise, difficulties during the evaluation of the constraints and of their derivatives arise. The weight for the matrix material is set to $w_1 = 2.0$ and for the softer kernel material to $w_2 = 1.0$

The optimisation results for this multiscale optimisation problem of a macroscopic bracket with a heterogeneous microstructure are plotted in Fig. 7.20. The objective can be minimised to a value that is 17% lower than the initial value and the volume constraints on both scales are fulfilled. This means that the overall volume on the macroscale as well as the overall volume on the microscale remain constant. The optimisation algorithm takes 23 iterations to find a feasible solution.

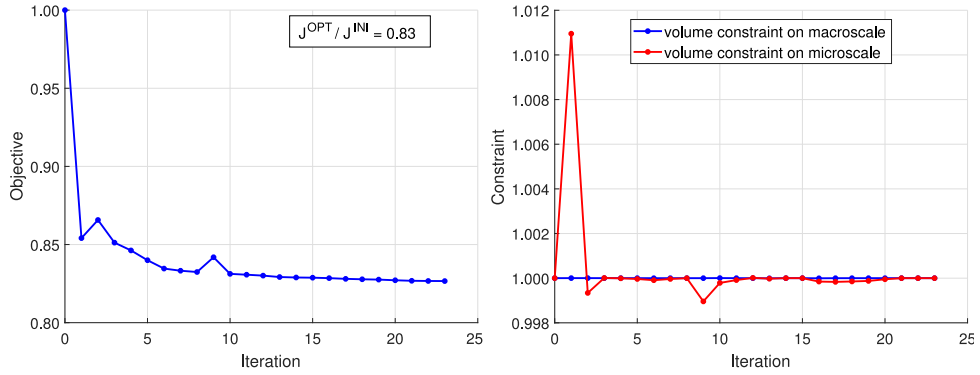

Figure 7.20: Multiscale optimisation of a bracket: objective (left) corresponds to macroscopic compliance $\overline{C}$ and constraints (right) correspond to volume constraints $\overline{V}$,V on the macro- and the microscale. Comparison of initial and optimised values of objectives for performed example results to: $\overline{C}^{\,\mathrm{opt}} / \overline{C}^{\,\mathrm{ini}} = 0.329 \,/\, 0.398 = 0.83$. The volumes of referred domains remain constant, i.e. $\overline{V}^{\,\mathrm{ini}} / \overline{V}^{\,\mathrm{opt}} = V^{\,\mathrm{ini}} / V^{\,\mathrm{opt}} = 1$.

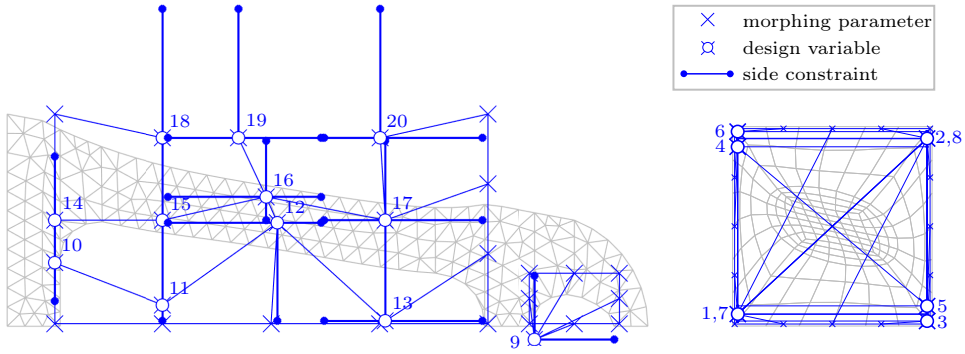

Figure 7.21: Multiscale optimisation of a bracket: distribution of final design parameters for the macroscopic optimisation model with two morphing boxes (left) and the microscopic optimisation model with one morphing box (right).

The distribution of design parameters on both scales for the initial and optimised shape can be found in Fig. 7.21. Additionally for a better overview, the exact coordinates of geometrical points on the macroscale as well as on the microscale, both before and after optimisation, are listed in Table 7.2. For comparison, the lower and upper bounds (s_i^{l}, s_i^{u}) for selected design parameters are listed too. All design parameters fulfill their constraints and lie in the feasible domain. The comparison of the initial and optimised designs in terms of overall performance is illustrated in Fig. 7.22. The results obtained one half of the system can be mirrored due symmetry properties to design the overall system. It is shown that minimisation of the macroscopic compliance leads to a lower maximum value of the macroscopic displacements, i.e. $\overline{\boldsymbol{v}}_{\max}^{\mathrm{opt}} \,/\, \overline{\boldsymbol{v}}_{\max}^{\mathrm{ini}} = 0.0593 \,/\, 0.0733 = 0.81$, which is in the range of the reduction of overall compliance. Concurrently, this means, that the overall macroscopic stiffness can be increased by $\approx 19\%$. Furthermore, the design of the obtained microscale representation leads to a lower distribution of von Mises stresses in the selected macroscopic integration points. This example proves the applicability of the presented relations for the sensitivity analysis over multiple scales and that it comes along with a large gain in terms of overall behaviour of investigated systems.

Table 7.9: Multiscale optimisation of a bracket: distribution of design parameters for macro- and microscopic domain: defined lower and upper design bounds $s^{\mathrm{l}}$and s^{u}, initial and optimised design values $s^{\mathrm{ini}}$and s^{opt}.

Design parameter	Direction ($1 = x, 2 = y$)	s^{l}	s^{u}	s^{ini}	s^{opt}
1	1	−0.4750	0.4750	−0.2450	−0.4749
1	2	−0.4750	0.4750	−0.2450	−0.4415
2	1	−0.4750	0.4750	0.0000	0.4749
2	2	−0.4750	0.4750	−0.2450	0.4391

continued on next page ...

Design parameter	Direction ($1 = x, 2 = y$)	s^{l}	s^{u}	s^{ini}	s^{opt}
3	1	−0.4750	0.4750	0.2450	0.4749
3	2	−0.4750	0.4750	−0.2450	−0.4749
4	1	−0.4750	0.4750	−0.2450	−0.4749
4	2	−0.4750	0.4750	0.0000	0.3989
5	1	−0.4750	0.4750	0.2450	0.4749
5	2	−0.4750	0.4750	0.0000	−0.3989
6	1	−0.4750	0.4750	−0.2450	−0.4749
6	2	−0.4750	0.4750	0.2450	0.4749
7	1	−0.4750	0.4750	0.0000	−0.4749
7	2	−0.4750	0.4750	0.2450	−0.4391
8	1	−0.4750	0.4750	0.2450	0.4749
8	2	−0.4750	0.4750	0.2450	0.4415
9	1	10.0000	11.5000	10.7500	10.0000
9	2	−0.2500	0.9500	0.5250	−0.2499
10	2	0.4800	1.9500	1.3666	1.1950
11	2	0.1000	1.9500	1.3666	0.4014
12	1	3.0500	5.9500	5.0000	5.1214
12	2	0.1000	1.9500	1.3666	1.9499
13	1	6.0000	9.0000	7.0500	7.1610
13	2	0.1000	1.9500	1.3666	0.1000
14	2	2.0000	3.2000	2.6833	2.0000
15	2	2.0000	3.5000	2.6833	2.0000
16	1	3.0500	5.9500	5.0000	4.9055
16	2	2.0000	3.5000	2.6833	2.4402
17	1	6.0000	9.0000	7.0500	7.1600
17	2	2.0000	3.5000	2.6833	2.0000
18	2	3.5500	6.0000	4.0000	3.5500
19	1	3.0500	5.9500	5.0000	4.3834
19	2	3.5500	6.0000	4.0000	3.5500
20	1	6.0000	9.0000	7.0500	7.0664
20	2	3.5500	6.0000	4.0000	3.5504

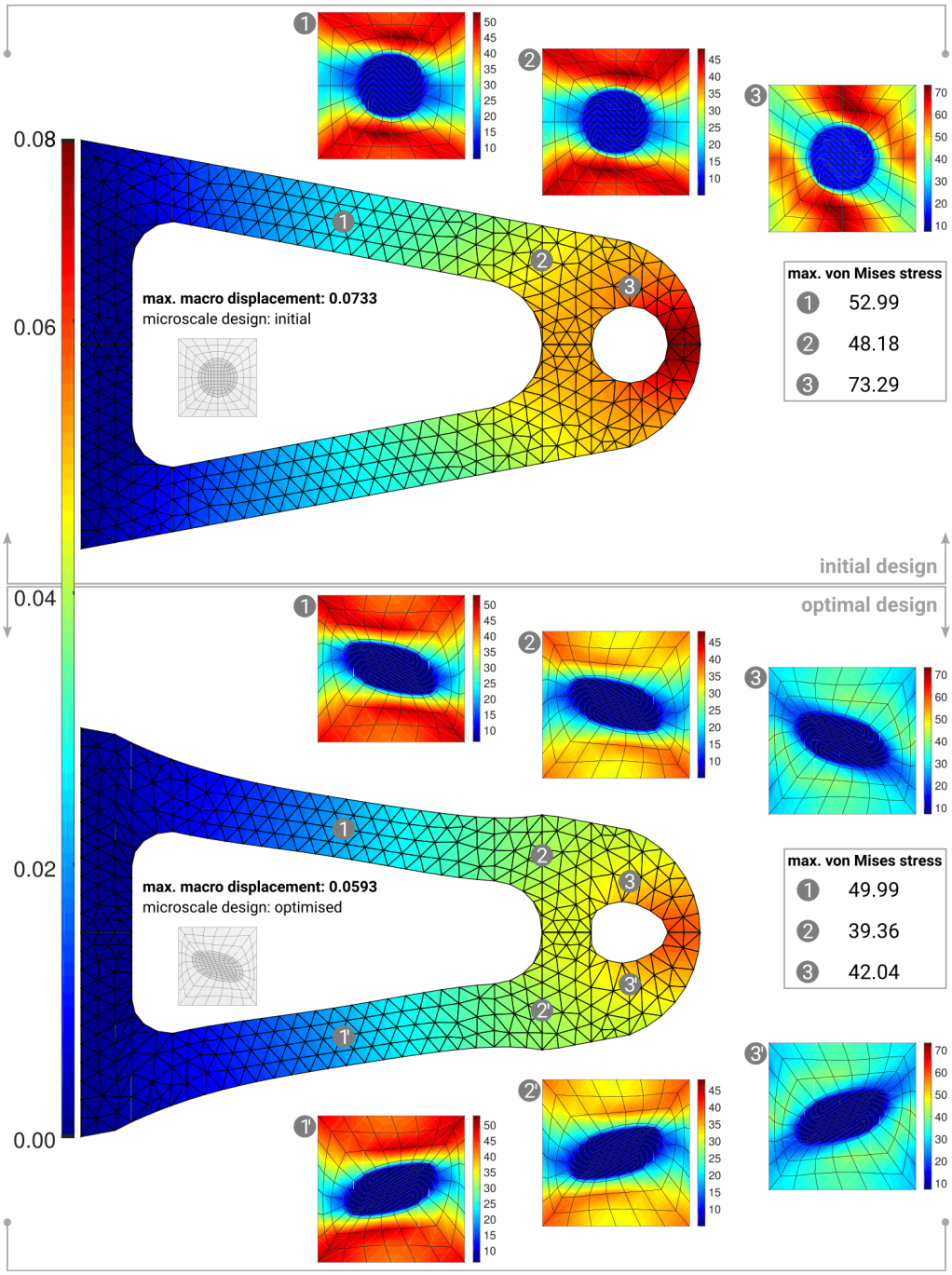

Figure 7.22: Multiscale optimisation of a bracket: macroscopic displacements (large) for initial and optimised supplemented designs. Microscopic von Mises stress distribution in selected macroscopic integration points (1-3) for initial and optimised design. Due to symmetry properties, microstructures in points (1-3) can be copied to design the full system.

7.4 Observations concerning numerical behaviour

The final remark in the scope of presented numerical investigations refers the time consumption of presented numerical investigations. The computation times ${}^{\mathrm{d}}t_{\mathrm{o}}$ for the solution of each individual overall optimisation problem and the number of required optimisation steps n_{IT} are listed in Table 7.10 for all examples. The optimisation results are carried out on the desktop workstation introduced in Table 2.4 in Chapter 2. Additionally, the values in the brackets summarise some basic details about the investigated examples and give a brief insight concerning the complexity in terms of the mesh and the number of degrees of freedom on the macro- and the microscale as well as the overall number of macroscopic integration points, which is related to the number of microscopic BVPs to be solved.

Concerning the results in Table 7.10 the numerical performance of methods for design sensitivity based on the variational approach is emphasised. Despite existing *semi-analytical methods*, which are also wide-spread and investigated intensively for several years, the comparison focuses on the numerical optimisation with numerical gradients of objectives, constraints and of quantities on element level in terms of FDM. Although no complete numerical multiscale structural optimisation is carried out, the *expected results* can be extrapolated with regard to the results and the numerical performance of aforementioned examples.

As reference, the optimisation problem with the lowest *complexity* and therefore, with the lowest computation time per iteration step ${}^{\mathrm{d}}t_{\mathrm{o}} \;/\; n_{\mathsf{IT}} = 3.4$ minutes is chosen, i.e. the *microscale design* example from Section 7.2.2 for the load case L.2 and the microstructure m.1. The time per iteration is split into ${}^{\mathrm{d}}t_{\mathrm{a}} \approx 0.5 \cdot {}^{\mathrm{d}}t_{\mathrm{o}} = 1.7$ minutes for one multiscale analysis, ${}^{\mathrm{d}}t_{\mathrm{s}} \approx 0.4 \cdot {}^{\mathrm{d}}t_{\mathrm{o}} = 1.36$ minutes for one design sensitivity analysis and $\approx 0.1 \cdot {}^{\mathrm{d}}t_{\mathrm{o}} = 0.34$ minutes for one incremental SQP update. The time consumption of one sensitivity analysis is in the range of one structural analysis.

The corresponding design parameters are the coordinates of eight control points of the morphing box on the microscale. Due to the dimension $n^d = 2$ of the problem, the final number of design parameters is $n_s = 16$. Gradients have to be computed with respect to these design variables. The overall optimisation procedure takes 9 iterations to find a feasible solution and lasts about ${}^{\mathrm{d}}t_{\mathrm{o}} = 30.6$ minutes.

The following consideration allows a rough estimation of the time consumption for one optimisation step performed using numerical gradients. The effort for the multiscale structural analysis and the incremental design update by the SQP method remains the same. The evaluation of the design sensitivity analysis using numerical difference quotients in terms of FDM requires $n_{\mathrm{F}}^{\mathrm{f,b}} = n_s + 1 = 17$ for a forward/backward difference quotient and $n_{\mathrm{F}}^{\mathrm{c}} = 2 \cdot n_s = 32$ evaluations of the function for the multiscale structural analysis. Therefore, the computation times can be assumed to

$$
\begin{aligned}
{}^{\mathrm{d}}t_{\mathrm{s,num}}^{\mathrm{f,b}} &= n_{\mathrm{F}}^{\mathrm{f,b}} \cdot {}^{\mathrm{d}}t_{\mathrm{a}} &&= 17 \cdot 1.7 = 28.9 \text{ min.} && \text{for the forward/backward FDM scheme,} \\
{}^{\mathrm{d}}t_{\mathrm{s,num}}^{\mathrm{c}} &= n_{\mathrm{F}}^{\mathrm{c}} \cdot {}^{\mathrm{d}}t_{\mathrm{a}} &&= 32 \cdot 1.7 = 54.4 \text{ min.} && \text{for the central FDM scheme.}
\end{aligned}
$$

The projection to one optimisation iteration yields 31 minutes for the forward/backward and 56 minutes for the central FDM scheme. Due to the fact, that the gradients are equal with respect to a numerical error and precision, the optimisation algorithm will

Table 7.10: Comparison of computation times for numerical investigations for the *macroscopic tension test*, *design of microstructures using morphing based parametrisation* and *multiscale optimisation of a bracket*. The presented time consumption ${}^{\mathrm{d}}t_{\mathrm{o}}$ for one overall optimisation and the corresponding number of iterations n_{IT} refers computations on the desktop workstation listed in Table 2.4. Some basic numerical details of affiliated examples are listed in the brackets for an overview, i.e. the number of: macroscopic integration points $\overline{n}_{\mathsf{IP}}$, macroscopic elements $\overline{n}_{el}$, macroscopic degrees of freedom $\overline{n}_{v}$, microscopic elements n_{el} and microscopic degrees of freedom n_{v}.

Section	Example		$(\overline{n}_{\mathsf{IP}}, \overline{n}_{el}, \overline{n}_{v}, n_{el}, n_{v})$	Number of iterations n_{IT}	Time ${}^{\mathrm{d}}t_{\mathrm{o}}$ (min.)	${}^{\mathrm{d}}t_{\mathrm{o}}$ / n_{IT}
7.1	**Tension test**					
		T.1	(1200, 300, 682, 200, 480)	6	89.5	14.9
		T.2	(1200, 300, 682, 200, 480)	6	92.5	15.4
		T.3	(1200, 300, 682, 200, 480)	4	67.0	16.8
7.2	**Microscale design**					
7.2.1	L.1	m.1	(288, 72, 182, 180, 386)	18	61.0	3.4
		m.2	(288, 72, 182, 539, 1152)	21	263.7	12.6
		m.3	(288, 72, 182, 625, 1352)	28	454.5	16.2
		m.4	(288, 72, 182, 625, 1352)	18	289.0	16.1
7.2.2	L.2	m.1	(288, 72, 182, 180, 386)	9	30.6	3.4
		m.2	(288, 72, 182, 539, 1152)	13	153.9	11.8
		m.3	(288, 72, 182, 625, 1352)	10	157.1	15.7
		m.4	(288, 72, 182, 625, 1352)	14	200.6	14.3
7.3	**Bracket optimisation**					
			(1089, 363, 464, 180, 386)	23	245.5	10.7

find a solution within $n_{\mathsf{IT}} = 9$ iteration steps. The overall numerical multiscale design optimisation procedure will last

$$
\begin{aligned}
{}^{\mathrm{d}}t_{\mathrm{o,num}} &= n_{\mathsf{IT}} \cdot {}^{\mathrm{d}}t^{\mathrm{f,b}}_{\mathrm{s,num}} &&= 279 \text{ min.} \quad \text{for the forward/backward FDM scheme and} \\
{}^{\mathrm{d}}t_{\mathrm{o,num}} &= n_{\mathsf{IT}} \cdot {}^{\mathrm{d}}t^{\mathrm{c}}_{\mathrm{s,num}} &&= 504 \text{ min.} \quad \text{for the central FDM scheme.}
\end{aligned}
$$

The final comparison of computation times for numerical multiscale optimisation and multiscale optimisation based on the variational approach for design sensitivity analysis

presented in this work leads the following ratios

$$^{\mathrm{d}}t_{\mathrm{o}} \;/\; ^{\mathrm{d}}t_{\mathrm{o,num}} = 30.6 \;/\; 279 \approx 0.11 \quad \text{for the forward/backward FDM scheme and}$$
$$^{\mathrm{d}}t_{\mathrm{o}} \;/\; ^{\mathrm{d}}t_{\mathrm{o,num}} = 30.6 \;/\; 504 \approx 0.06 \quad \text{for the central FDM scheme.}$$

The required computation effort by means of time can be estimated in the range between 6 and 11 percent compared to the numerical multiscale optimisation procedure. The overall speed-up of approximately 10 to 15 proves that it is worthwhile to investigate in methods, witch are overly theoretical but efficient by nature.

7.5 Summary and concluding remarks

The intention of the investigations in this chapter is to emphasize the applicability of formulated sensitivity relations for multiscale design optimisation. The generation of optimal material designs is an automatical process based on mathematical optimisation algorithms with defined objectives and constraints. In the presented case studies, the target is to find macroscopic structures with maximum macroscopic stiffness based on a constant amount of material on both scales. The translation of the mentioned goals into the corresponding optimisation problem contains the definition of the overall macroscopic compliance as objective and of equality constraints for the volume on both scales.

Based on different parametrisation techniques for the design, i.e. for geometrical measures like diameters or angles, for control points of geometrical nodes in terms of CAGD or for control points of defined morphing boxes, the mathematical optimisation algorithm provides minimum values for the objective and fulfils the constraints in each case. It can be shown that the incorporation of the microscopic structure into the overall optimisation and design process comes along with a significant improvement of the overall macroscopic quantity of interest. The maximum stiffness of the presented macroscopic structures can be increased in the range of approximately 5 to 30 percent. Furthermore, the studies in Section 7.4 prove the added value of the variational approach for design sensitivity by an approximate speed-up of 10 to 15 compared to numerical optimisation based on the numerical determination of required gradient information.

Chapter 8

Summary and outlook

This final chapter highlights the main goals and achieved results of the presented work. A brief summary of discussed topics, comments on obtained numerical results as well as inspirations for future research are given.

8.1 Summary

The presented doctoral thesis provides an overall structural optimisation framework for optimal material design based on variational sensitivity analysis. The major goal

> *"Formulate a method for the determination of optimal design layouts of macroscopic structures and microscopic materials!"*

is achieved by accomplishing the following three sub-targets:

1. Obtaining a method for the solution of structural analysis (SA) problems on multiple scales in terms of computational homogenisation and FE^2 techniques.
2. Formulating variational relations for the design sensitivity analysis (DSA) of the mechanical system under investigation and revealing predictions for the structural behaviour with respect to modifications of design parameters.
3. Assembling SA and DSA in such a way, that a formulation of the overall multiscale design optimisation task using mathematical optimisation algorithms (NLP) with objective functions, constraints and design parameters on different scales is possible.

After a general introduction and motivation for the entire work in Chapter 1 and a compilation of frequently used mathematical operations and notations in Chapter 2, the attainment of articulated targets is organised as follows.

Realisation of target 1. In the first part of the work, the established method for computational homogenisation in the scope of multiscale structural analysis and the solution of corresponding microscopic BVPs is presented and complemented with relevant publications in Chapter 4. Based on the definition of effective field variables and remarks on the choice of appropriate RVEs, the minimisation problem of homogenisation is formulated as a

Lagrange functional, which incorporates different boundary conditions on the microscale. The boundary conditions are enforced by the corresponding Lagrange multiplier. Each nonlinear microscopic BVP with hyperelastic constitutive behaviour is driven by the macroscopic deformation gradient of the corresponding macroscopic integration point and solved by the iterative Newton scheme. The sequence of microscopic solution steps in distinctive macroscopic integration points is nested into the global macroscopic Newton solution scheme, in which each microscopic solution serves for the evaluation of homogenised macroscopic material properties on the element level. The FE^2 method is implemented and tested in the in-house MATLAB code MANO. Furthermore, it is construed for an efficient solution of SA problems within the iterative solution process of stated optimisation problems.

Realisation of target 2. The second part of the work at hand addresses the derivation and formulation of required sensitivity relations in continuous form and the evaluation of sensitivity information in discrete form. This target is characterised by two consecutive viewpoints: (a) DSA on single scales and (b) DSA on multiple scales.

Based on the variational approach for DSA and the concept of an enhanced layout of kinematics, which contains the introduction of a local convective configuration, relevant physical and mechanical quantities and especially their continuous variations are outlined in Chapter 5 and utilised for DSA on single scales. The presented compilation is augmented by the design sensitivity relation for physical reaction forces on the boundary of investigated domains. Discussed solutions of different structural optimisation problems on single scales act as illustrative examples for the demonstration of the applicability of reaction forces and of their sensitivities as constraints.

Essential relations for DSA on multiple scales are motivated, derived and formulated in Chapter 6. The concept of the enhanced layout of kinematics is adapted with respect to the microscale representation. The formulation of sensitivity relations for DSA on the microscale is followed by the formulation of sensitivity relations for DSA on the macroscale. The association of obtained sensitivity formulations on both individual scales takes into account the aforementioned results for physical reaction forces from Chapter 5 and enables the formulation of the sensitivity relation for the homogenisation condition and effective parameters, which in general, but also in the case of DSA, bridge the scales. The Lagrange multiplier within the applied FE^2 technique is related to reaction forces on the boundary of the RVE in an appropriate sense. As a consequence, the design sensitivity of reaction forces is related to the design sensitivity of the Lagrange multiplier. It plays a central role for the formulation of multiscale design sensitivity relations and couples the scales within the selected solution strategie for structural multiscale problems.

Realisation of target 3. Beside the introduction of possible objective functions, constraints, design parameters and different parametrisation techniques for the geometry of investigated mechanical systems and domains, the abstract setting of a general non-linear structural optimisation problem on single scales is introduced in Chapter 3. The extension to an abstract setting of continuous and discrete multiscale structural optimisation problems is provided in Section 6.5. Multiscale methods for SA and DSA together with methods for non-linear mathematical optimisation in terms of NLP are combined into an overall

numerical framework for structural optimisation on multiple scales, i.e. all components are implemented into the in-house MATLAB code MAnO. Remarks on the numerical realisation as well as on the choice of design parameters and possible combinations of objective functions and constraints are pointed out and accomplish the modelling of the computational material design task.

Examples and numerical investigations. Chapter 7 emphasizes the potential for improvements of macroscopic mechanical structures by the incorporation of the microscale representation into the overall structural design optimisation process by means of three different examples. The examples contain different design parametrisation setups and demonstrate the applicability of the presented sensitivity formulations. The first example with two different kinds of design parameters on the macro- and the microscale comprises the following situations: (i) design parameters and optimisation only on the macroscale, (ii) design parameters and optimisation only on the microscale and (iii) design parameters and optimisation on both scales simultaneously. In the second example a fixed macroscale domain with two different load cases is investigated in order to design four different independant microscale representations based on the morphing parametrisation technique for the present geometry model. The last example demonstrates a multiscale structural optimisation process with morphing based design parametrisation on both scales. The major purpose of this investigation is to design the macroscopic shape of the structure and the microscopic material representation simultaneously.

In addition to the fact, that investigated examples serve as a *proof of concept*, it is evident that the variational approach for the integrated DSA is an efficient and performant strategie to provide required sensitivity information within multiscale design optimisation problems. Compared to other approaches for DSA, especially DSA based on FDM and the numerical determination of gradients at the extreme, the variational approach comes along with the overhead on theory and analytical calculus, but after all, it also comes along with a significant gain of reduced and convenient computation times. Some observations concerning the numerical behaviour are outlined in Section 7.4. Based on the variational approach for DSA, numerical simulations and design optimisation procedures can be organised efficiently.

8.2 Future work

Although much effort and time has been investigated into the presented work and especially into the development of the simulation software MAnO, there are some limitations. In the following, few motivational aspects and inspirational ideas for future work and activities in the presented field of research are pointed out.

Inelastic materials and coupled problems. The extension to inelastic materials with time and history dependent effects seems to be natural. Essential steps for the treatment of DSA for problems with elastoplastic deformations are introduced in [89, 90, 165] and [14]. For a more versatile, interdisciplinary cooperation and research, the presented multiscale formulation can be extended for the analysis and optimisation of several coupled problem

formulations for investigations of applications with thermo-mechanical, electro-mechanical or magneto-electro-mechanical coupling effects, see [52, 131] or [132] for further reading.

Extensions for shape and topology optimisation. Especially when it comes to structural optimisation, there are some interesting questions to be answered. For instance, the cooperation between MSE, CMMS and SMO could figure out, which kinds of objective functions, constraints or design parameters can be used best for the determination of optimal material designs. At the same time, the definition and investigation of new and/or not-common objectives and constraints could be beneficial. Within the presented geometry parametrisation techniques, which are implemented in MAnO, some limitations occur due to several technical characteristics of CAGD. Restrictions concerning the number, shape and position of voids and inclusions are present and especially during the optimisation process the design modifications have to be observed and checked for feasibility. In this scope, established and well-known *level set* and *extended finite element methods* (XFEM) or even the *modified extended finite element method* (also labelled YFEM) are assumed to be an elegant way for the treatment of one or more inclusions and/or voids on the microscale, cf. [17, 126] or [15] for further details on the latter approach. In combination with *topological derivatives* the appearance and disappearance of voids and inclusions can be realised and controlled. In general, it might be interesting to combine methods from different disciplines on structural optimisation, i.e. methods, which provide shape and topological design changes. One possibility could be the application of shape optimisation on the macroscale for the generation of optimal layouts of macroscopic structures and the application of topology optimisation methods on the microscale to obtain completely freeform microscale representations and microscopic topologies without restrictions on number, size and position of heterogeneities.

Efficient computations and numerical performance. The last major topic of interest is the question on *efficient* methods for DSA and on the general overall numerical performance of the solution procedure for stated multiscale optimisation problems. This question can be put into the context of hardware environment and programing skills on one hand, and into the context of theoretical and methodological approaches for the improvements of used formulations on the other hand.

So far, a MATLAB R2018a implementation on mentioned hardware environments (cf. Table 2.4) is available. In the next step a complete translation of the code to *high performance* programming languages like C++ or FORTRAN could provide first interesting insights and time consumptions for comparison. Several HPC techniques like MPI, OpenMP or even GPU acceleration using CUDA could be implemented to push forward the numerical behaviour. The performance evaluation in terms of computation times of proposed implementations could be tested and compared on mobile and desktop workstations with available computation power or even on HPC clusters. In all mentioned points, advices from experienced programmers and computer scientist are useful and established standards in their research fields should be taken into account.

The second aspect concerning the improvement of performance is more of theoretical fashion. Observation of obtained results in Chapter 7, especially of the local distribution of von Mises stresses on the microscale, let assume, that principal stresses are the driving force

for the incremental design modification provided by mathematical optimisation methods. As a consequence, this statement can be projected to the macroscopic deformation gradients in corresponding macroscopic integration points. It is obvious, that within the deformation driven context for numerical homogenisation, the deformation gradient is the driving force. In several macroscopic regions the amplitude of the deformation can be assumed to be in a similar range and therefore, the following questions arises: "Is it necessary to perform DSA in each individual macroscopic integration point or is it possible to subdivide the overall macroscopic domain in regions with *similar* deformation states and to evaluate DSA only in this characteristic sub-domains?" This kind of approach is common in different research fields, like machine learning, image processing or pattern recognition. It is based on statistical data analysis and often termed *cluster analysis* or *clustering*. Determination of clusters could be based on the question on how many information is required or how much deviation is acceptable to obtain sufficient results for DSA and SO with respect to a predefined precision.

Methods termed *design exploration*, especially methods that are based on the *singular value decomposition* (SVD) are applied to single scale structural optimisation problems in [59] or [14] and can employed for an investigation of the presented multiscale sensitivity information. These methods are useful for figuring out important or significant design parameters with major influence on objectives and constraints by the investigation of corresponding sensitivity data like the pseudo load or sensitivity matrix. The overall optimisation model can be reduced by a systematical reselection of design parameter sets using mathematical methods. The presented framework for multiscale design optimisation is predestinated for the design exploration process due to the large number of BVPs to be solved and the corresponding and resulting large amount of sensitivity information with pseudo load and sensitivity operators on different scales. Further improvements can be deduced from so-called *reanalysis methods*, which allow predictions of state parameters due to design modifications based on function evaluations in terms of available data only. A brief introduction on this topic can be found in [98] among others.

List of Figures

1.1 Examples for microstructures 2
1.2 Computational Material Design (CMD) 3

3.1 Principle framework for structural optimisation. 17
3.2 Design parametrisation techniques 22
3.3 Design parametrisation based on CAGD model 23
3.4 Design parametrisation based on morphing 24

4.1 Principle of scale separation: macro-, meso- and microscale. 26
4.2 Basic homogenisation scheme. 28
4.3 Separation of nodes on boundary 34
4.4 Framework for multiscale structural analysis (MAnO.MSA) 39

5.1 Concept of enhanced kinematics 43
5.2 Partitioning of nodes 53
5.3 Cube of multi-material: mechanical system and optimisation model . . 67
5.4 Cube of multi-material: optimisation results for material parameters γ 70
5.5 Cube of multi-material: optimal design for material parameters γ . . . 71
5.6 Cube of multi-material: objective (compliance) and constraint 72
5.7 Cube of multi-material: compliance minimisation - optimal design . . 72
5.8 Cube of multi-material: objective (volume) and constraint 73
5.9 Cube of multi-material: volume minimisation - optimal design 74
5.10 RVE-like domains: selection of samples for numerical investigations . . 76
5.11 RVE-like domains: optimisation results for domain D.1 78
5.12 RVE-like domains: optimisation results for domain D.2 79
5.13 RVE-like domains: optimisation results for domain D.3 82
5.14 RVE-like domains: optimisation results for domain D.4 85

6.1 Model problems for structural optimisation on multiple scales 90
6.2 Enhanced kinematics within the framework of multiple scales 93
6.3 Framework for multiscale structural optimisation (MAnO.MSO) . . . 115

7.1 Macroscopic tension test: mechanical system and initial design 121
7.2 Macroscopic tension test: optimisation model and design parameters . 122
7.3 Macroscopic tension test: objectives and constraints 123
7.4 Macroscopic tension test: distribution of design parameters 124
7.5 Microscale design: mechanical system and initial design 126
7.6 Microscale design: optimisation model and design parameters 128

7.7 Microscale design: objectives and constraints for load case L.1 129
7.8 Microscale design: mesh and distribution of design parameters (L.1) . 129
7.9 Microscale design: macro displacements and micro stresses (L.1-m.1) . 131
7.10 Microscale design: macro displacements and micro stresses (L.1-m.2) . 131
7.11 Microscale design: macro displacements and micro stresses (L.1-m.3) . 132
7.12 Microscale design: macro displacements and micro stresses (L.1-m.4) . 132
7.13 Microscale design: objectives and constraints for load case L.2 134
7.14 Microscale design: mesh and distribution of design parameters (L.2) . 134
7.15 Microscale design: macro displacements and micro stresses (L.2-m.1) . 136
7.16 Microscale design: macro displacements and micro stresses (L.2-m.2) . 136
7.17 Microscale design: macro displacements and micro stresses (L.2-m.3) . 137
7.18 Microscale design: macro displacements and micro stresses (L.2-m.4) . 137
7.19 Optimisation of a bracket: mechanical system and optimisation model 139
7.20 Optimisation of a bracket: objective and constraint 141
7.21 Optimisation of a bracket: distribution of design parameters 142
7.22 Optimisation of a bracket: macro displacements and micro stresses . . 144

List of Algorithms

4.1 Solution procedure for minimisation problem of homogenisation 38

6.2 Newton-type method: solution procedure for nonlinear equations. . . . 106
6.3 Procedure for design sensitivity analysis on macroscopic element level . 116

List of Tables

2.1 Notation and topography. 8
2.2 Mathematical operations and tensorial products. 8
2.3 List of utilised MATLAB R2018a toolboxes. 12
2.4 Hardware environments and labels for numerical investigations. 13

3.1 Possible sets for objectives, constraints and design parameters. 20

5.1 Cube of multi-material: model parameters 68
5.2 Cube of multi-material: optimisation results for material parameters γ 69
5.3 Numerical effort for optimisation based on numerical gradients (FDM). 75
5.4 Cube of multi-material: accuracy of derived gradients 75
5.5 RVE-like domains: model dimensions for numerical investigations . . . 77
5.6 RVE-like domains: distribution of design variables for domain D.1 . . . 79
5.7 RVE-like domains: distribution of design variables for domain D.2 . . . 80
5.8 RVE-like domains: distribution of design variables for domain D.3 . . . 82
5.9 RVE-like domains: distribution of design variables for domain D.4 . . . 84
5.10 Overview of parameters and tangent operators on single scale 86
5.11 Summary of discrete sensitivity relations and operators 86

6.1 Overview of macro- and microscopic point and tangent mappings . . . 94
6.2 Macroscopic physical residual: possible dependencies and situations . . 94
6.3 Overview of macro- and microscopic parameters 99
6.4 Overview of macro- and microscopic tangent operators 100
6.5 Summary of discrete sensitivity relations and operators on multiple scales 111
6.6 Mandatory definitions and optional combinations in FE^2 optimisation 114

7.1 Macroscopic tension test: model parameters 121
7.2 Macroscopic tension test: design parameters on macro- and microscale 125
7.3 Microscale design: model parameters 127
7.4 Microscale design: distribution of design parameters for load case L.1 . 130
7.5 Microscale design: comparison of results for load case L.1 133
7.6 Microscale design: distribution of design parameters for load case L.2 . 135
7.7 Microscale design: comparison of results for load case L.2 138
7.8 Optimisation of a bracket: model parameters 140
7.9 Optimisation of a bracket: distribution of design parameters 142
7.10 Comparison of computation times for numerical investigations 146

List of Problems

3.1 Problem (General optimisation problem) 16
3.2 Problem (Discrete form of the optimisation problem) 16
3.3 Problem (Lagrange formalism in the scope of SQP) 17

6.1 Problem (General multiscale optimisation problem) 112
6.2 Problem (Discrete multiscale optimisation problem) 112

List of Remarks

2.1 Remark (Definition of parameters) 9
2.2 Remark (Gâteaux or directional derivative) 9
2.3 Remark (Type of arguments) 10
2.4 Remark (Structure of argument list) 11
2.5 Remark (Element library and controls on element level) 13

3.1 Remark (Multiobjective optimisation) 18

4.1 Remark (Macro and micro notation) 28
4.2 Remark (Contribution of external loads to microscopic energy) 33

5.1 Remark (Gradient and divergence operators) 44
5.2 Remark (Variation of determinants) 44
5.3 Remark (Variation of inverse tensors) 44
5.4 Remark (Transformation of gradients) 45
5.5 Remark (Nomination of sets for state parameters) 53
5.6 Remark (Structure of stiffness and pseudo load operator) 60

6.1 Remark (Utilisation of the term *multilevel*) 95
6.2 Remark (Choice of design parameters) 97

7.1 Remark (Verification of sensitivity information in numerical studies) . 120

Bibliography

[1] Alexandersen, J.: Efficient topology optimisation of multiscale and multiphysics problems. PhD Thesis. Technical University of Denmark (DTU), 2016.

[2] Allaire, G.: *Shape Optimization by the Homogenization Method*. Springer, 2002.

[3] Almgren, R.F.: An isotropic three-dimensional structure with Poisson's ratio $= -1$. *Journal of Elasticity* (1985), vol. (4): pp. 427–430.

[4] Andreasen, C.S. and O. Sigmund: Multiscale modeling and topology optimization of poroelastic actuators. *Smart Materials and Structures* (2012), vol. 21(6): p. 065005.

[5] ANSYS, Inc.: *ANSYS*. Version 18.2. 2017. URL: `http://www.ansys.com`.

[6] Arora, J.S.: An exposition of the material derivative approach for structural shape sensitivity analysis. *Computer Methods in Applied Mechanics and Engineering* (1993), vol. 105(1): pp. 41–62.

[7] Baier, H., C. Seesselberg, and B. Specht: *Optimierung in der Strukturmechanik*. Vieweg & Sohn Verlagsgesellschaft mbH, Braunschweig/Wiesbaden, 1994.

[8] Balzani, D., D. Brands, J. Schröder, and C. Carstensen: Sensitivity analysis of statistical measures for the reconstruction of microstructures based on the minimization of generalized least–square functionals. *Technische Mechanik* (2009), vol. 30: pp. 297–315.

[9] Balzani, D., L. Scheunemann, D. Brands, and J. Schröder: Construction of two- and three-dimensional statistically similar RVEs for coupled micro-macro simulations. *Computational Mechanics* (2014), vol. 54: pp. 1269–1284.

[10] Barthold, F.-J.: Remarks on variational shape sensitivity analysis based on local coordinates. *Engineering Analysis with Boundary Elements* (2008), vol. 32(11): pp. 971–985.

[11] Barthold, F.-J.: Theorie und Numerik zur Berechnung und Optimierung von Strukturen aus isotropen, hyperelastischen Materialien. PhD Thesis. Institut für Baumechanik und Numerische Mechanik, Universität Hannover, 1993. URL: `http://hdl.handle.net/2003/24388`.

[12] Barthold, F.-J.: Zur Kontinuumsmechanik inverser Geometrieprobleme. Habilitation. Braunschweiger Schriften zur Mechanik 44-2002, TU Braunschweig, 2002. URL: http://hdl.handle.net/2003/23095.

[13] Barthold, F.-J., N. Gerzen, W. Kijanski, and D. Materna: Efficient Variational Design Sensitivity Analysis. *Mathematical Modeling and Optimization of Complex Structures*. Ed. by Neittaanmäki, Pekka, Sergey Repin, and Tero Tuovinen. Springer International Publishing, 2016: pp. 229–257.

[14] Barthold, F.-J. and J. Liedmann: Remarks on variational sensitivity analysis of elastoplastic deformations. *AIP Conference Proceedings* (2017), vol. 1896(1): p. 100007.

[15] Barthold, F.-J. and D. Materna: A modified extended finite element method approach for design sensitivity analysis. *International Journal for Numerical Methods in Engineering* (2015), vol. 104(3): pp. 209–234.

[16] Barthold, F.-J. and D. Materna: Remarks on different strategies for variational design sensitivity analysis. *Proc. 7th World Congress on Structural and Multidisciplinary Optimization*. 2007: pp. 1348–1357.

[17] Barthold, F.-J. and D. Materna: Shape sensitivity analysis in the extended finite element method. *Proc. Appl. Math. Mech.* (2012), vol. 12(1): pp. 693–694.

[18] Barthold, F.J. and E. Stein: A continuum mechanical-based formulation of the variational sensitivity analysis in structural optimization. Part I: analysis. *Structural Optimization* (1996), vol. 11(1): pp. 29–42.

[19] Basar, Y. and D. Weichert: *Nonlinear Continuum Mechanics of Solids: Fundamental Mathematical and Physical Concepts*. Applied Mechanics. Springer Berlin Heidelberg, 2000.

[20] Bathe, K.-J.: *Finite Element Procedures*. Prentice-Hall, 1996.

[21] Bayreuther, C.: Mehrskalenmodelle in der Festkörpermechanik und Kopplung von Mehrgittermethoden mit Homogenisierungsverfahren. PhD Thesis. Institut für Mechanik (Bauwesen) Lehrstuhl I, Stuttgart, 2005.

[22] Bendsøe, M.P. and O. Sigmund: *Topology Optimization*. Springer Verlag Berlin Heidelberg New York, 2003.

[23] Blanchard, P. and E. Brüning: *Direkte Methoden der Variationsrechnung: ein Lehrbuch*. Springer, 1982.

[24] Bletzinger, K.-U., M. Firl, J. Linhard, and R. Wüchner: Optimal shapes of mechanically motivated surfaces. *Computer Methods in Applied Mechanics and Engineering* (2010), vol. 199(5-8): pp. 324–333.

[25] Boggs, P. T. and J. W. Tolle: Sequential Quadratic Programming. *Acta Numerica* (1996), vol. 4: pp. 1–51.

[26] Bojczuk, D. and Z. Mróz: Determination of optimal actuator forces and positions in smart structures using adjoint method. *Structural and Multidisciplinary Optimization* (2005), vol. 30(4): pp. 308–319.

[27] Bojczuk, D. and Z. Mróz: On optimal design of supports in beam and frame structures. *Structural Optimization* (1998), vol. 16(1): pp. 47–57.

[28] Bonet, J. and R.D. Wood: *Nonlinear Continuum Mechanics for Finite Element Analysis*. Cambridge University Press, 1997.

[29] Boor, C. de: *A practical guide to splines*. Springer-Verlag, 1978.

[30] Broyden, C. G.: The convergence of a class of double-rank minimization algorithms 1. General considerations. *IMA Journal of Applied Mathematics* (1970), vol. 6(1): pp. 76–90.

[31] Bruns, T.E. and D.A. Tortorelli: Topology optimization of non-linear elastic structures and compliant mechanisms. *Computer Methods in Applied Mechanics and Engineering* (2001), vol. 190(26): pp. 3443–3459.

[32] Buhl, T.: Simultaneous topology optimization of structure and supports. *Structural and Multidisciplinary Optimization* (2002), vol. 23(5): pp. 336–346.

[33] Buhl, T., C.B.W. Pedersen, and O. Sigmund: Stiffness design of geometrically nonlinear structures using topology optimization. *Structural and Multidisciplinary Optimization* (2000), vol. 19(2): pp. 93–104.

[34] Cardoso, J.B. and J.S. Arora: Variational method for design sensitivity analysis in nonlinear structural mechanics. *AIAA Journal* (1988), vol. 26(5): pp. 595–603.

[35] Chen, W.-H. and C.-R. Ou: Shape optimization in contact problems with desired contact traction distribution on the specified contact surface. *Computational Mechanics* (1995), vol. 15(6): pp. 534–545.

[36] Chen, W. and S. Liu: Topology optimization of microstructures of viscoelastic damping materials for a prescribed shear modulus. *Structural and Multidisciplinary Optimization* (2014), vol. 50(2): pp. 287–296.

[37] Chiandussi, G., M. Codegone, S. Ferrero, and F.E. Varesio: Comparison of multi-objective optimization methodologies for engineering applications. *Computers and Mathematics with Applications* (2012), vol. 63(5): pp. 912–942.

[38] Choi, K.-K. and N.-H. Kim: *Structural sensitivity analysis and optimization 1 - Linear systems*. Mechanical Engineering Series. Springer, 2005.

[39] Choi, K.-K. and N.-H. Kim: *Structural sensitivity analysis and optimization 2 - Nonlinear systems and applications*. Mechanical Engineering Series. Springer, 2005.

[40] Christensen, P. W. and A. Klabring: *An Introduction to Structural Optimisation*. Springer Science and Business Media B. V., 2009.

[41] Coelho, P.G., J.M. Guedes, and H.C. Rodrigues: Multiscale topology optimization of bi-material laminated composite structures. *Composite Structures* (2015), vol. 132: pp. 495–505.

[42] Coelho, P.G. and H.C. Rodrigues: Hierarchical topology optimization addressing material design constraints and application to sandwich-type structures. *Structural and Multidisciplinary Optimization* (2015), vol. 52(1): pp. 91–104.

[43] COMSOL: *COMSOL Multiphysics*. Version 5.3. 2017. URL: `https://www.comsol.de`.

[44] Dassault Systémes: *Abaqus*. Version 2017. 2017. URL: `https://www.3ds.com`.

[45] de Boer, R.: *Vektor- und Tensorrechnung für Ingenieure*. Springer, 1982.

[46] Deb, K.: *Multi-Objective Optimization Using Evolutionary Algorithms*. New York, USA: John Wiley & Sons, Inc., 2001.

[47] Edelsbrunner, H.: *Geometry and Topology for Mesh Generation*. Cambridge Monographs on Applied and Computational Mathematics. Cambridge University Press, 2001.

[48] Ehrgott, M.: *Multicriteria Optimization*. Berlin, Heidelberg: Springer-Verlag, 2005.

[49] Farin, G.: *Curves and Surfaces for CAGD: A Practical Guide*. The Morgan Kaufmann Series in Computer Graphics. Morgan Kaufmann, 2002.

[50] Fletcher, R.: A new approach to variable metric algorithms. *The Computer Journal* (1970), vol. 13(3): pp. 317–322.

[51] Frey, P.J. and P.-L. George: *Mesh Generation: Application to Finite Elements*. ISTE, 2010.

[52] Fritzen, F.: Microstructural modeling and computational homogenization of the physically linear and nonlinear constitutive behaviour of micro-heterogeneous materials. PhD Thesis. Karlsruher Institut für Technologie, 2011.

[53] Fritzen, F. and M. Leuschner: Nonlinear reduced order homogenization of materials including cohesive interfaces. *Computational Mechanics* (2015), vol. 56(1): pp. 131–151.

[54] Fritzen, F., L. Xia, M. Leuschner, and P. Breitkopf: Topology optimization of multiscale elastoviscoplastic structures. *International Journal for Numerical Methods in Engineering* (2015), vol. 106(6): pp. 430–453.

[55] Fujii, D., B. C. Chen, and N. Kikuchi: Composite material design of two-dimensional structures using the homogenization design method. *International Journal for Numerical Methods in Engineering* (2001), vol. 50(9): pp. 2031–2051.

[56] Gea, H. C. and J. Luo: Topology optimization of structures with geometrical nonlinearities. *Computers and Structures* (2001), vol. 79(20): pp. 1977–1985.

[57] Geers, M.G.D., V.G. Kouznetsova, and W.A.M. Brekelmans: Multi-scale computational homogenization: Trends and challenges. *Journal of Computational and Applied Mathematics* (2010), vol. 234(7). Fourth Int. Conference on Advanced Computational Methods in Engineering (ACOMEN 2008): pp. 2175–2182.

[58] Gelfand, I.M., S.V. Fomin, and R.A. Silverman: *Calculus of Variations*. Dover Books on Mathematics. Dover Publications, 2000.

[59] Gerzen, N.: Analysis and applications of variational sensitivity information in structural optimisation. PhD Thesis. Dortmund University of Technology, 2014. URL: http://hdl.handle.net/2003/33191.

[60] Gerzen, N., D. Materna, and F.-J. Barthold: The inner structure of sensitivities in nodal based shape optimisation. *Computational Mechanics* (3 2012), vol. 49: pp. 379–396.

[61] Gibiansky, L.V. and O. Sigmund: Multiphase composites with extremal bulk modulus. *Journal of Mechanics and Physics of Solids* (2000), vol. 48(3): pp. 461–498.

[62] Goldfarb, D.: A family of variable-metric methods derived by variational means. *Mathematics of Computation* (1970), vol. 24(1): pp. 23–26.

[63] Gould, N., D. Orban, and P. Toint: Numerical methods for large-scale nonlinear optimization. *Acta Numerica* (2005), vol. 14: pp. 299–361.

[64] Ha, S.-H. and J.K. Guest: Optimizing inclusion shapes and patterns in periodic materials using Discrete Object Projection. *Structural and Multidisciplinary Optimization* (2014), vol. 50(1): pp. 65–80.

[65] Haber, R.B.: A New Variational Approach to Structural Shape Design Sensitivity Analysis. *Computer Aided Optimal Design: Structural and Mechanical Systems*. Ed. by Mota Soares and A. Carlos. Vol. 27. NATO ASI Series. Springer Berlin Heidelberg, 1987: pp. 573–587.

[66] Haftka, R.T. and R.V. Grandhi: Structural shape optimization - a survey. *Computer Methods in Appl. Mechanics and Engineering* (1986), vol. 57: pp. 91–106.

[67] Harzheim, L.: *Strukturoptimierung: Grundlagen und Anwendungen.* Wissenschaftlicher Verlag Harri Deutsch GmbH, 2008.

[68] Hibbitt, H.D., P.V. Marcal, and J.R. Rice: A finite element formulation for problems of large strain and large displacements. *International Journal of Solids and Structures* (1970), vol. 6(8): pp. 1069–1086.

[69] Hill, R.: A self-consistent mechanics of composite materials. *Journal of the Mechanics and Physics of Solids* (1965), vol. 13(4): pp. 213–222.

[70] Hill, R.: Elastic properties of reinforced solids: Some theoretical principles. *Journal of the Mechanics and Physics of Solids* (1963), vol. 11(5): pp. 357–372.

[71] Hill, R.: Theory of mechanical properties of fibre-strengthened materials: I. Elastic behaviour. *Journal of the Mechanics and Physics of Solids* (1964), vol. 12(4): pp. 199–212.

[72] Hill, R.: Theory of mechanical properties of fibre-strengthened materials: II. Inelastic behaviour. *Journal of the Mechanics and Physics of Solids* (1964), vol. 12(4): pp. 213–218.

[73] Hill, R.: Theory of mechanical properties of fibre-strengthened materials: III. self-consistent model. *Journal of the Mechanics and Physics of Solids* (1965), vol. 13(4): pp. 189–198.

[74] Holzapfel, G. A.: *Nonlinear Solid Mechanics - A Continuum Approach for Engineering.* John Wiley & Sons, 2000.

[75] Hyun, S. and S. Torquato A: Designing composite microstructures with targeted properties. *J. Mater. Res* (2001), vol. 16: pp. 280–285.

[76] Ibrahimbegović, A., I. Grešovnik, D. Markovič, S. Melnyk, and T. Rodič: Shape optimization of two-phase inelastic material with microstructure. *Engineering Computations* (2005), vol. 22(5/6): pp. 605–645.

[77] Itskov, M.: *Tensor Algebra and Tensor Analysis for Engineers: With Applications to Continuum Mechanics.* Springer Berlin Heidelberg, 2009.

[78] Jie, G., L. Hao, G. Liang, and X. Mi: Topological shape optimization of 3D micro-structured materials using energy-based homogenization method. *Advances in Engineering Software* (2018), vol. 116: pp. 89–102.

[79] Kato, J., D. Yachi, K. Terada, and T. Kyoya: Topology optimization of microstructure for composites applying a decoupling multi-scale analysis. *Structural and Multidisciplinary Optimization* (2014), vol. 49(4): pp. 595–608.

[80] Kitware: *ParaView.* Version 5.4.1. 2017. url: `https://www.paraview.org`.

[81] Klarbring, A. and N. Strömberg: Topology optimization of hyperelastic bodies including non-zero prescribed displacements. *Structural and Multidisciplinary Optimization* (2013), vol. 47(1): pp. 37–48.

[82] Klinge, S.: Inverse analysis for multiphase nonlinear composites with random microstructure. *International Journal for Multiscale Computational Engineering* (2012), vol. 10(4): pp. 361–373.

[83] Klinge, S. and K. Hackl: Application of the multiscale FEM to the modeling of nonlinear composites with a random microstructure. *International Journal for Multiscale Computational Engineering* (2012), vol. 10(3): pp. 213–227.

[84] Klinge, S. and P. Steinmann: Inverse analysis for heterogeneous materials and its application to viscoelastic curing polymers. *Computational Mechanics* (2015), vol. 55(3): pp. 603–615.

[85] Komkov, V., K.K. Choi, and E.J. Haug: *Design sensitivity analysis of structural systems*. Vol. 177. Academic press, 1986.

[86] Kouznetsova, V., W. A. M. Brekelmans, and F. P. T. Baaijens: An approach to micro-macro modeling of heterogeneous materials. *Computational Mechanics* (2001), vol. 27(1): pp. 37–48.

[87] Lakes, R.: Foam structures with a negative Poisson's ratio. *Science* (1987), vol. 235(4792): pp. 1038–1040.

[88] Le, C., T. Bruns, and D. Tortorelli: A gradient-based, parameter-free approach to shape optimization. *Computer Methods in Applied Mechanics and Engineering* (2011), vol. 200(9–12): pp. 985–996.

[89] Liedmann, J. and F.-J. Barthold: Exploration of internal response sensitivities of materially nonlinear structures. *Proc. Appl. Math. Mech.* (2017), vol. 17(1): pp. 745–746.

[90] Liedmann, J. and F.-J. Barthold: Optimisation of structures with inelastic deformations. *Proc. Appl. Math. Mech.* (2016), vol. 16(1): pp. 703–704.

[91] Liu, K. and A. Tovar: Multiscale topology optimization of structures and periodic cellular materials. *Proc. 10th World Congress on Structural and Multidisciplinary Optimization*. 2013.

[92] Lovelock, D. and H. Rund: *Tensors, Differential Forms, and Variational Principles*. Dover Books on Mathematics Series. Dover Publications, 1989.

[93] Lv, J., H. W. Zhang, and B. S. Chen: Shape and topology optimization for closed liquid cell materials using extended multiscale finite element method. *Structural and Multidisciplinary Optimization* (2013), vol. 49(3): pp. 367–385.

[94] Materna, D. and F.-J. Barthold: On variational sensitivity analysis and configurational mechanics. *Computational Mechanics* (2008), vol. 41(5): pp. 661–681.

[95] Materna, D. and F.-J. Barthold: Relations between structural optimization and configurational mechanics with applications to mesh optimization. *Proc. 6th ASMO-UK/ISSMO Conf. on Engineering Design Optimization*. University of Leeds, UK, 2006: pp. 173–181.

[96] Materna, D. and F.-J. Barthold: Theoretical aspects and applications of variational sensitivity analysis in the physical and material space. *Computational Optimization: New Research Developments*. Ed. by Linton, Richard F. and Thomas B. Carroll. Nova Science Publishers, 2010: pp. 397–444.

[97] Materna, D. and F.-J. Barthold: Variational design sensitivity analysis in the context of structural optimization and configurational mechanics. *Int. J. Fract.* (2007), vol. 147(1-4): pp. 133–155.

[98] Materna, D. and V.K. Kalpakides: Nonlinear reanalysis for structural modifications based on residual increment approximations. *Computational Mechanics* (2015), vol. 57(1): pp. 1–18.

[99] Materna, Daniel: Structural and Sensitivity Analysis for the Primal and Dual Problems in the Physical and Material Spaces. PhD Thesis. Dortmund University of Technology, 2009. url: `http://hdl.handle.net/2003/26542`.

[100] Michel, J.C., H. Moulinec, and P. Suquet: Effective properties of composite materials with periodic microstructure: a computational approach. *Computer Methods in Applied Mechanics and Engineering* (1999), vol. 172(1–4): pp. 109–143.

[101] Miehe, C.: Computational micro-to-macro transitions for discretized microstructures of heterogeneous materials at finite strains based on the minimization of averaged incremental energy. *Computer Methods in Applied Mechanics and Engineering* (2003), vol. 192(5–6): pp. 559–591.

[102] Miehe, C.: Strain-driven homogenization of inelastic microstructures and composites based on an incremental variational formulation. *International Journal for Numerical Methods in Engineering* (2002), vol. 55(11): pp. 1285–1322.

[103] Miehe, C. and C.G. Bayreuther: On multiscale FE analyses of heterogeneous structures: from homogenization to multigrid solvers. *International Journal for Numerical Methods in Engineering* (2007), vol. 71(10): pp. 1135–1180.

[104] Miehe, C. and A. Koch: Computational micro-to-macro transitions of discretized microstructures undergoing small strains. *Archive of Applied Mechanics* (2002), vol. 72(4-5): pp. 300–317.

[105] Miehe, C., J. Schotte, and M. Lambrecht: Homogenization of inelastic solid materials at finite strains based on incremental minimization principles. Application to the texture analysis of polycrystals. *Journal of the Mechanics and Physics of Solids* (2002), vol. 50(10): pp. 2123–2167.

[106] Miehe, C., J. Schotte, and J. Schröder: Computational micro–macro transitions and overall moduli in the analysis of polycrystals at large strains. *Computational Materials Science* (1999), vol. 16(1–4): pp. 372–382.

[107] Miehe, C., J. Schröder, and J. Schotte: Computational homogenization analysis in finite plasticity Simulation of texture development in polycrystalline materials. *Computer Methods in Applied Mechanics and Engineering* (1999), vol. 171(3–4): pp. 387–418.

[108] Milton, G. W.: Composite materials with Poisson's ratios close to -1. *Journal of the Mechanics and Physics of Solids* (1992), vol. 40(5): pp. 1105–1137.

[109] Nemat-Nasser, S. and M. Hori: *Micromechanics: Overall Properties of Heterogeneous Materials*. Applied Mathematics and Mechanics Series. North-Holland, 1993.

[110] Neves, M.M., H. Rodrigues, and J.M. Guedes: Optimal design of periodic linear elastic microstructures. *Computers and Structures* (2000), vol. 76(1): pp. 421–429.

[111] Nocedal, J. and S. Wright: *Numerical optimization*. Springer Science and Business Media, 2006.

[112] Noël, L. and P. Duysinx: Shape optimization of microstructural designs subject to local stress constraints within an XFEM-level set framework. *Structural and Multidisciplinary Optimization* (2016), vol.: pp. 1–16.

[113] Noll, W.: A new mathematical theory of simple materials. *Archive for Rational Mechanics and Analysis* (1972), vol. 48(1): pp. 1–50.

[114] Oden, J.T.: Discussion on "Finite element analysis of non-linear structures". *By R.H. Mallett and P.V. Marcal, Proceedings of the American Society of Civil Engineers* (1969), vol. 95: pp. 1376–1381.

[115] Olhoff, N. and B. Åkesson: Minimum stiffness of optimally located supports for maximum value of column buckling loads. *Structural Optimization* (1991), vol. 3(3): pp. 163–175.

[116] Paulino, G. H., E. C. N. Silva, and Chau H. Le: Optimal design of periodic functionally graded composites with prescribed properties. *Structural and Multidisciplinary Optimization* (2008), vol. 38(5): pp. 469–489.

[117] Pedersen, P.: Material Optimizations — An Engineering View. *Advances in Structural Optimization*. Ed. by Herskovits, José. Dordrecht: Springer Netherlands, 1995: pp. 223–261.

[118] Pedersen, P.: On optimal orientation of orthotropic materials. *Structural Optimization* (June 1989), vol. 1(2): pp. 101–106.

[119] Pedersen, P.: On thickness and orientational design with orthotropic materials. *Structural Optimization* (June 1991), vol. 3(2): pp. 69–78.

[120] Perić, D., E. A. de Souza Neto, R. A. Feijóo, M. Partovi, and A.J.C. Molina: On micro-to-macro transitions for multi-scale analysis of non-linear heterogeneous materials: unified variational basis and finite element implementation. *Int. Journal for Numerical Methods in Engineering* (2011), vol. 87(1-5): pp. 149–170.

[121] Perry, E., R. Balling, and M. Landon: A new morphing method for shape optimization. *American Institute of Aeronautics and Astronautics, Inc.* (1998), vol. 4907: pp. 1510–1519.

[122] Phelan, D.G. and R.B. Haber: Sensitivity analysis of linear elastic systems using domain parameterization and a mixed mutual energy principle. *Computer Methods in Applied Mechanics and Engineering* (1989), vol. 77(1): pp. 31–59.

[123] Piegl, L. and W. Tiller: *The NURBS Book*. Springer-Verlag Berlin Heidelberg, 1997.

[124] Reuss, A.: Berechnung der Fließgrenze von Mischkristallen auf Grund der Plastizitätsbedingung für Einkristalle. *ZAMM - Journal of Applied Mathematics and Mechanics / Zeitschrift für Angewandte Mathematik und Mechanik* (1929), vol. 9(1): pp. 49–58.

[125] Rothenburg, L., AI. Berlin, and R.J. Bathurst: Microstructure of isotropic materials with negative Poisson's ratio. *Nature* (1991), vol. 354: pp. 470–472.

[126] Rotthaus, M. and F.-J. Barthold: Aspects of sensitivity analysis using the level set method in structural optimization. *Proc. Appl. Math. Mech.* (2007), vol. 7(1): pp. 4040041–4040042.

[127] Scherer, M., R. Denzer, and P. Steinmann: A fictitious energy approach for shape optimization. *International Journal for Numerical Methods in Engineering* (2010), vol. 82(3): pp. 269–302.

[128] Schittkowski, K.: NLPQL: A Fortran subroutine solving constrained nonlinear programming problems. *Annals of Operations Research* (1985), vol. 5: pp. 485–500.

[129] Schittkowski, K.: On the convergence of a sequential quadratic programming method with an augmented Lagrangian line search function. *Optimization, Mathematische Operationsforschung und Statistik* (1983), vol. 14: pp. 197–216.

[130] Schröder, J.: A numerical two-scale homogenization scheme: the FE^2-method. *Plasticity and Beyond*. Ed. by Schröder, J. and K. Hackl. Vol. 550. CISM Int. Centre for Mechanical Sciences. Springer Vienna, 2014: pp. 1–64.

[131] Schröder, J. and M.-A. Keip: Two-scale homogenization of electromechanically coupled boundary value problems. *Computational Mechanics* (2012), vol. 50(2): pp. 229–244.

[132] Schröder, J., M. Labusch, and M.-A. Keip: Algorithmic two-scale transition for magneto-electro-mechanically coupled problems: FE^2-scheme: Localization and homogenization. *Computer Methods in Applied Mechanics and Engineering* (2016), vol. 302: pp. 253–280.

[133] Schumacher, A.: *Optimierung mechanischer Strukturen*. Springer-Verlag Berlin Heidelberg, 2005.

[134] Schweizerhof, K.: Nichtlineare Berechnungen von Tragwerken unter verformungsabhängiger Belastung mit Finiten Elementen. PhD Thesis. Institut für Baustatik, Universität Stuttgart, 1982.

[135] Schweizerhof, K. and E. Ramm: Displacement dependent pressure loads in nonlinear finite element analyses. *Computers and Structures* (1984), vol. 18(6): pp. 1099–1114.

[136] Shanno, D. F.: Conditioning of quasi-Newton methods for function minimization. *Mathematics of Computation* (1970), vol. 24(1): pp. 647–656.

[137] Sienkiewicz, Z. and B. Wilczyński: Shape optimization of a dynamically loaded machine foundation coupled to a semi-infinite inelastic medium. *Structural Optimization* (1996), vol. 12(1): pp. 29–34.

[138] Sigmund, O.: A new class of extremal composites. *Journal of the Mechanics and Physics of Solids* (2000), vol. 48(2): pp. 397–428.

[139] Sigmund, O.: Design of Material Structures using Topology Optimization. PhD Thesis. Technical University of Denmark, 1994.

[140] Sigmund, O.: Tailoring materials with prescribed elastic properties. *Mechanics of Materials* (1995), vol. 20(4): pp. 351–368.

[141] Sigmund, O. and S. Torquato: Composites with extremal thermal expansion coefficients. *Applied Physics Letters* (1996), vol. 69(21): pp. 3203–3205.

[142] Sigmund, O. and S. Torquato: Design of materials with extreme thermal expansion using a three-phase topology optimization method. *Journal of the Mechanics and Physics of Solids* (1997), vol. 45(6): pp. 1037–1067.

[143] Sigmund, O. and S. Torquato: Design of smart composite materials using topology optimization. *Smart Materials and Structures* (1999), vol. 8(3): p. 365.

[144] Simo, J.C., R.L. Taylor, and P. Wriggers: A note on finite element implementation of pressure boundary loading. *Communications in Applied Numerical Methods* (1991), vol. 7(7): pp. 513–525.

[145] Sluis, O. van der, P.J.G. Schreurs, W.A.M. Brekelmans, and H.E.H. Meijer: Overall behaviour of heterogeneous elastoviscoplastic materials: effect of microstructural modelling. *Mechanics of Materials* (2000), vol. 32(8): pp. 449–462.

[146] Sompagdee, P.: *Survey of morphing*. Department of Computer Science, Thammasat University, 2000.

[147] Son, J.H. and B.M. Kwak: Optimization of boundary conditions for maximum fundamental frequency of vibrating structures. *American Institute of Aeronautics and Astronautics* (1993), vol. 31(12): pp. 2351–2357.

[148] Sridhar, A., M.-A. Keip, and C. Miehe: Homogenization in micro-magneto-mechanics. *Computational Mechanics* (2016), vol.: pp. 1–19.

[149] Suquet, P. M.: Elements of homogenization for inelastic solid mechanics. *Homogenization Techniques for Composite Media*. Ed. by Sanchez-Palencia, Enrique and André Zaoui. Vol. 272. Lecture Notes in Physics. Springer Berlin Heidelberg, 1987: pp. 193–278.

[150] Swan, C. C. and J. S. Arora: Topology design of material layout in structured composites of high stiffness and strength. *Structural Optimization* (Feb. 1997), vol. 13(1): pp. 45–59.

[151] Tartar, L.: *The General Theory of Homogenization: A Personalized Introduction*. Lecture Notes of the Unione Matematica Italiana. Springer Berlin Heidelberg, 2009.

[152] Taylor, R. L. and S. Govindjee: *FEAP - A Finite Element Analysis Program*. Version 8.5. 2017. url: `http://projects.ce.berkeley.edu/feap`.

[153] Temizer, İ. and P. Wriggers: On the computation of the macroscopic tangent for multiscale volumetric homogenization problems. *Computer Methods in Applied Mechanics and Engineering* (2008), vol. 198(3–4): pp. 495–510.

[154] Temizer, I. and T.I. Zohdi: A numerical method for homogenization in non-linear elasticity. *Computational Mechanics* (2007), vol. 40(2): pp. 281–298.

[155] Terada, K., M. Hori, T. Kyoya, and N. Kikuchi: Simulation of the multi-scale convergence in computational homogenization approaches. *International Journal of Solids and Structures* (2000), vol. 37(16): pp. 2285–2311.

[156] Terada, K., J. Kato, N. Hirayama, T. Inugai, and K. Yamamoto: A method of two-scale analysis with micro-macro decoupling scheme: application to hyperelastic composite materials. *Computational Mechanics* (2013), vol. 52(5): pp. 1199–1219.

[157] Terada, K. and N. Kikuchi: A class of general algorithms for multi-scale analyses of heterogeneous media. *Computer Methods in Applied Mechanics and Engineering* (2001), vol. 190(40–41): pp. 5427–5464.

[158] Terada, K. and N. Kikuchi: Microstructural design of composites using the homogenization method and digital images. *Material Science Research International* (1996), vol. 2(2): pp. 65–72.

[159] Terada, K., I. Saiki, K. Matsui, and Y. Yamakawa: Two-scale kinematics and linearization for simultaneous two-scale analysis of periodic heterogeneous solids at finite strain. *Computer Methods in Applied Mechanics and Engineering* (2003), vol. 192(31–32): pp. 3531–3563.

[160] Theocaris, P.S. and G.E. Stavroulakis: Optimal material design in composites: An iterative approach based on homogenized cells. *Computer Methods in Applied Mechanics and Engineering* (1999), vol. 169(1): pp. 31–42.

[161] Tortorelli, D.A. and Z. Wang: A systematic approach to shape sensitivity analysis. *Int. Journal of Solids and Structures* (1993), vol. 30(9): pp. 1181–1212.

[162] Voigt, W.: *Lehrbuch der Kristalphysik*. Teubner, 1910.

[163] Wang, D.: Sensitivity analysis of structural response to position of external applied load: in plane stress condition. *Structural and Multidisciplinary Optimization* (2014), vol. 50(4): pp. 605–622.

[164] Wang, Y., M.Y. Wang, and F. Chen: Structure-material integrated design by level sets. *Structural and Multidisciplinary Optimization* (2016), vol.: pp. 1–12.

[165] Wiechmann, K.: Theorie und Numerik zur Berechnung und Optimierung von Strukturen mit elastoplastischen Deformationen. PhD Thesis. Institut für Baumechanik und Numerische Mechanik, Universität Hannover, 2000.

[166] Wolberg, G.: Image morphing: a survey. *The Visual Computer* (1998), vol. 14: pp. 360–372.

[167] Wolberg, G.: Recent advances in image morphing. *Proceedings of Computer Graphics International*. 1996: pp. 64–71.

[168] Wriggers, P.: *Nonlinear Finite Element Methods*. Springer, 2008.

[169] Xia, L.: Towards optimal design of multiscale nonlinear structures: reduced-order modeling approaches. PhD Thesis. Université de Technologie de Compiègne, 2015.

[170] Xia, L. and P. Breitkopf: A reduced multiscale model for nonlinear structural topology optimization. *Computer Methods in Applied Mechanics and Engineering* (2014), vol. 280: pp. 117–134.

[171] Xia, L. and P. Breitkopf: Concurrent topology optimization design of material and structure within nonlinear multiscale analysis framework. *Computer Methods in Applied Mechanics and Engineering* (2014), vol. 278: pp. 524–542.

[172] Xia, L. and P. Breitkopf: Design of materials using topology optimization and energy-based homogenization approach in Matlab. *Structural and Multidisciplinary Optimization* (2015), vol. 52(6): pp. 1229–1241.

[173] Xia, L. and P. Breitkopf: Multiscale structural topology optimization. *Proc. 11th World Congress on Structural and Multidisciplinary Optimization*. 2015.

[174] Xia, L. and P. Breitkopf: Multiscale structural topology optimization with an approximate constitutive model for local material microstructure. *Computer Methods in Applied Mechanics and Engineering* (2015), vol. 286: pp. 147–167.

[175] Xia, L., F. Fritzen, and P. Breitkopf: Evolutionary topology optimization of elastoplastic structures. *Structural and Multidisciplinary Optimization* (2017), vol. 55(2): pp. 569–581.

[176] Yang, R. and J. Du: Microstructural topology optimization with respect to sound power radiation. *Structural and Multidisciplinary Optimization* (2013), vol. 47(2): pp. 191–206.

[177] Yi, Y.-M., S.-H. Park, and S.-K. Youn: Design of microstructures of viscoelastic composites for optimal damping characteristics. *International Journal of Solids and Structures* (2000), vol. 37(35): pp. 4791–4810.

[178] Zakhari, M.: Computational Homogenization of Heterogeneous Hyperelastic Materials. PhD Thesis. Swansea University, 2013.

[179] Zhao, Z.: Shape design sensitivity analysis of kinematical boundaries. *Structural Optimization* (1993), vol. 5(3): pp. 190–196.

[180] Zhu, J.H. and W.H. Zhang: Integrated layout design of supports and structures. *Computer Methods in Applied Mechanics and Engineering* (2010), vol. 199(9–12): pp. 557–569.

[181] Zienkiewicz, O.C. and R.L. Taylor: *The Finite Element Method: Solid mechanics*. Butterworth-Heinemann, 2000.

[182] Zienkiewicz, O.C. and R.L. Taylor: *The Finite Element Method: The basis*. Butterworth-Heinemann, 2000.

[183] Zohdi, T.I. and P. Wriggers: *Introduction to Computational Micromechanics*. Lecture Notes. Springer, 2005.